TARGETING DES1: SYNTHESES OF CERAMIDE ANALOGUES WITH A RIGID SCAFFOLD, INHIBITORY ASSAYS, AND AF2-ASSISTED STRUCTURAL INSIGHTS REVEAL PR280 AS A POTENT INHIBITOR

Pablo Rivero Prieto

UNIVERSITAT ROVIRA i VIRGILI

Targeting Des1: Syntheses of ceramide analogues with a rigid scaffold, inhibitory assays, and AF2-assisted structural insights reveal PR280 as a potent inhibitor

Pablo Rivero Prieto

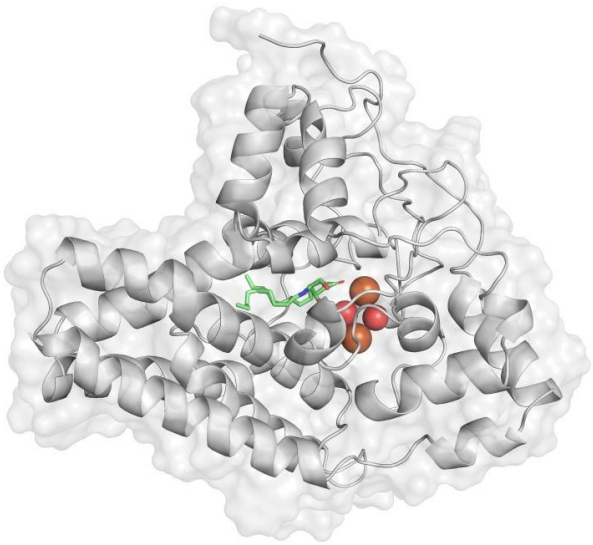

DOCTORAL THESIS
2024

UNIVERSITAT ROVIRA I VIRGILI
TARGETING DES1: SYNTHESES OF CERAMIDE ANALOGUES WITH A RIGID SCAFFOLD, INHIBITORY ASSAYS, AND AF2-ASSISTED STRUCTURAL INSIGHTS REVEAL PR280 AS A POTENT INHIBITOR
Pablo Rivero Prieto

UNIVERSITAT ROVIRA I VIRGILI
TARGETING DES1: SYNTHESES OF CERAMIDE ANALOGUES WITH A RIGID SCAFFOLD, INHIBITORY ASSAYS, AND AF2-ASSISTED STRUCTURAL INSIGHTS REVEAL PR280 AS A POTENT INHIBITOR
Pablo Rivero Prieto

UNIVERSITAT ROVIRA I VIRGILI
TARGETING DES1: SYNTHESES OF CERAMIDE ANALOGUES WITH A RIGID SCAFFOLD, INHIBITORY ASSAYS, AND AF2-ASSISTED STRUCTURAL INSIGHTS REVEAL PR280 AS A POTENT INHIBITOR
Pablo Rivero Prieto

Pablo Rivero Prieto

Targeting Des1: Syntheses of ceramide analogues with a rigid scaffold, inhibitory assays, and AF2-assisted structural insights reveal PR280 as a potent inhibitor

DOCTORAL THESIS

Supervised by

Prof. María Isabel Matheu Malpartida

Dr. Yolanda Díaz Giménez

UNIVERSITAT ROVIRA I VIRGILI

Department of Analytical Chemistry and Organic Chemistry

Tarragona 2024

UNIVERSITAT ROVIRA I VIRGILI
TARGETING DES1: SYNTHESES OF CERAMIDE ANALOGUES WITH A RIGID SCAFFOLD, INHIBITORY ASSAYS, AND AF2-ASSISTED STRUCTURAL INSIGHTS REVEAL PR280 AS A POTENT INHIBITOR
Pablo Rivero Prieto

UNIVERSITAT ROVIRA I VIRGILI

Departament de Química Analítica i Química Orgànica

C/ Marcel·lí Domingo, 1

Campus Sescelades

43007, Tarragona

Prof. María Isabel Matheu Malpartida and Dr. Yolanda Díaz Giménez from the Department of Analytical Chemistry and Organic Chemistry at the University Rovira i Virgili,

WE STATE that the present study, entitled "**Targeting Des1: Syntheses of ceramide analogues with a rigid scaffold, inhibitory assays, and AF2-assisted structural insights reveal PR280 as a potent inhibitor**", presented by Pablo Rivero Prieto for the award of the degree of Doctor and European Mention, has been carried out under our supervision at the Department of Analytical Chemistry and Organic Chemistry of this University.

Tarragona, 23th February 2024

María Isabel Matheu Malpartida - DNI 39682609L (TCAT)
Firmado digitalmente por María Isabel Matheu Malpartida - DNI 39682609L (TCAT)
Fecha: 2024.02.23 12:25:47 +01'00'

DIAZ GIMENEZ MARIA YOLANDA - 39687039X
Firmado digitalmente por DIAZ GIMENEZ MARIA YOLANDA - 39687039X
Fecha: 2024.02.23 12:33:04 +01'00'

Prof. María Isabel Matheu Malpartida

Dr. Yolanda Díaz Giménez

UNIVERSITAT ROVIRA I VIRGILI
TARGETING DES1: SYNTHESES OF CERAMIDE ANALOGUES WITH A RIGID SCAFFOLD, INHIBITORY ASSAYS, AND AF2-ASSISTED STRUCTURAL INSIGHTS REVEAL PR280 AS A POTENT INHIBITOR
Pablo Rivero Prieto

The work performed in the present Doctoral Thesis has been possible thanks to the Martí i Franquès Research Fellowship Program (2019PMF-PIPF-36), and the FI fellowship (Personal investigador predoctoral en formació, FI2021/B00241) founded by the European union.

This thesis has been carried out thanks to the funding of the research project: Targeting new modulators of sphingolipids metabolism for therapeutic cancer intervention (SPHYNGO, reference: CTQ2017-89750-R) funded by the Ministerio de Economía, Industria y Competitividad (MINECO), and Agencia Estatal de Investigación (AEI); and Synthetic approaches to stereodefined amino-alcohol scaffolds for targeting lesser-known enzymes of the sphingolipid metabolism SphK2 and Des1 (SYNTHAMOL, reference: PID2021-125923OB-I00), funded by the Ministerio de Ciencia e Innovación (MCIN) and Agencia Estatal de Investigación (AEI) and by European Regional Development Fund (ERDF) "a way of making Europe".

UNIVERSITAT ROVIRA I VIRGILI
TARGETING DES1: SYNTHESES OF CERAMIDE ANALOGUES WITH A RIGID SCAFFOLD, INHIBITORY ASSAYS, AND AF2-ASSISTED STRUCTURAL INSIGHTS REVEAL PR280 AS A POTENT INHIBITOR
Pablo Rivero Prieto

Acknowledgements

I would like to express my heartfelt gratitude to all those who have supported me throughout this journey of pursuing my Ph.D. I am indebted to all individuals who have contributed to the successful completion of this thesis.

In the first place, I extend my appreciation to Maribel for giving me the opportunity to grow as a scientist in her lab. I also must thank Yolanda, Sergio and Omar for their invaluable contributions in making our research group a collaborative and productive environment. From my Ph.D. placement in Dortmund, I am deeply grateful to Andreas for welcoming me into his lab and providing an encouraging environment for me to learn in a new field.

I would like to also express my gratitude to all my labmates from SintCarb Albert, Miguel, Jordi, Isa, Adrià, Javi, Eric, Paula, Will, Lauren and from the Andrea's research group, specially to Avinash, Elena, and Lorenzo. I am also in debt with all my friend for sharing good moments in this way. Specials thanks to Marina whose unconditional support and love have accompanied me through the best and most joyous moments with warmth and laughter.

Finally, I extend my deepest acknowledgements to my family for their unwavering support throughout this journey. I am incredibly fortunate to have you all by my side. I dedicate this thesis to my parents and my sister, pillars of support and boundless love, who have believed in me and stood by my side through every path I chose to tread.

UNIVERSITAT ROVIRA I VIRGILI
TARGETING DES1: SYNTHESES OF CERAMIDE ANALOGUES WITH A RIGID SCAFFOLD, INHIBITORY ASSAYS, AND AF2-ASSISTED STRUCTURAL INSIGHTS REVEAL PR280 AS A POTENT INHIBITOR
Pablo Rivero Prieto

Table of contents

Chapter VII: General conclusions

Chapter VIII: Experimental section

A	**AAC**	azide-alkyne 1,3-cycloaddition
	ACN	Acetonitrile
	Ac	Acetyl
	AF	AlfaFold
	AGMO	Alkylglycerol monooxygenase
	AI	Artificial intelligence
	Aq.	Aqueous
	app	Apparent
	Ar	Aryl
B	**BB**	Building block
	Boc	*tert*-butyloxycarbonyl
	BQ	1,4-Benzoquinone
	bs	Broad singlet
	Bu	Butil
C	**˚C**	Celsius degrees
	CASP	Critical Assessment of Structure Prediction
	CCDC	
	CDase	Ceramidases
	Cer	Ceramide
	CerC6NBD	6-[*N*-(7-nitro-2,1,3-benzoxadiazol-4-yl)amino]hexanoylsphingosine
	CerS	Ceramide synthases
	COD	Cycloocta-1,5-diene
	COSY	Proton homonuclear correlation spectroscopy
	Cp	cyclopenta-1,3-diene
	Cp*	1,2,3,4,5-pentamethylcyclopenta-1,3-diene
	CPBA	chloroperoxybenzoic acid
	CPG	Controlled pore glass
	CuAAC	Copper-catalysed azide-alkyne 1,3-cycloaddition
	CYB5R	Cytochrome b5 reductase

2. Abbreviations and acronyms

	Cyt b5	Cytochrome b5
D	**2D**	Two dimensional
	3D	Three dimensional
	D	Debye
	DA	1,2-diphenylethane-1,2-diamine derivative of 3rd generation Grubbs catalyst
	Da	Dalton
	d	Doublet
	dd	Doublet of doublets
	ddd	Doublet of doublet of doublets
	DECL	DNA-encoded chemical library
	DEGS1	Drosophila degenerative spermatocyte 1
	Des1	Dihydroceramide desaturase 1
	DFT	Density functional theory
	dhCer	Dihydroceramide
	dhCerC6NBD	6-[*N*-(7-nitro-2,1,3-benzoxadiazol-4-yl)amino]hexanoylsphinganine
	dhSM	Dihydrosphingomyelin
	DIPEA	*N*,*N*-Diisopropylethylamine
	DMF	*N*,*N*-Dimethylformamide
	DMSO	Dimethyl sulfoxide
	DNA	Deoxyribonucleic acid
E	***et al.***	*Et* alia, "and others"
	EBI	European Bioinformatics Institute
	EDC	*N*-(3-dimetilaminopropilo)-*N*′-etilcarbodiimida
	EM	Electron microscopy
	EMBL	European Molecular Biology Laboratory
	eq.	Equivalents
	Et	Ethyl
F	**FD**	Fluorimetric detector

	FDA	U. S. Food and Drug Administration
G	**g**	Gram(s)
	GDTS	Global-Distance-Test-Score
	G-III	3rd Generation Grubbs catalyst
H	**h.**	Hour(s)
	HIV-1	Human immunodeficiency virus 1
	HATU	Hexafluorophosphate Azabenzotriazole Tetramethyl Uronium
	H-bond	Hydrogen Bond
	HCC	Hepatocellular carcinoma
	HG-II	2nd generation Hoveyda-Grubbs catalyst
	HMBC	Heteronuclear Multiple Bond Correlation
	HMPA	Hexamethylphosphoramide
	HOBt	1-Hydroxybenzotriazole
	HPLC	High-performance liquid chromatography
	HRMS	High-resolution Mass spectrometry
	Hz	Hertz
I	**IC_{50}**	Half maximal inhibitory concentration
	ICREA	Catalan Institution for Research and Advanced Studies
	Int	Intermediate
	IQAC	Instituto de Química Avanzada de Cataluña
	IR	Infrared
J	***J***	Coupling constant
K	**KDSR**	3-ketodihydrosphingosine reductase
	K_i	Inhibitory constant
	K_m	Michaelis constant
	KTP	tris(3,5-dimethyl-1-pyrazolyl)borate
L	**L**	Ligand
	LC	Liquid chromatography

4. Abbreviations and acronyms

	lDDT	local distance difference test
	LR	Lawesson's reagent
M	**M**	Molar
	m	Multiplet
	Me	Methyl
	m.p.	Melting Point
	m/z	Mass-to-charge ratio
	MALDI	Matrix-assisted laser desorption/ionization
	Me	Methyl
	min.	Minute(s)
	MOE	Molecular Operating Environment
	MS	Mass spectrometry
N	**NADH**	Nicotinamide adenine dinucleotide
	NADPH	Nicotinamide adenine dinucleotide phosphate
	NBD	Norbornadiene
	NiAAC	Nickel-catalysed azide-alkyne 1,3-cycloaddition
	NMR	Nuclear Magnetic Resonance
	NOE	Nuclear Overhauser effect
	n.r.	No reaction
	ns	Not significant
	Nu	Nucleophile
P	**Ph**	Phenyl
	PCR	Polymerase Chain Reaction
	PDB	Protein Data Bank
	PEMT	Phosphatidylethanolamine *N*-methyltransferase
	pLDDT	Predicted Local Distance Difference Test
	PPI	Protein-Protein Interaction
	ppm	Parts per million
	PTMs	Posttranslational modifications
Q	**q**	Quartet

	quint	Quintet
R	**R**	Carbon substituent
	RCM	Ring Closin Metathesis
	r.t	Room temperature
	R_f	Retardation factor
	RNA	Ribonucleic acid
	RoF	Lipinski's Rule of Five
	RP	Reverse Phase
	RuAAC	Ruthenium-catalysed azide-alkyne 1,3-cycloaddition
	RUBAM	Research Unit on BioActive Molecules
S	**SAR**	Structure-Activity Relationship (studies)
	SARS-CoV-2	Severe acute respiratory syndrome coronavirus 2
	SIK2	Salt-inducible kinase 2
	SK	Sphinosine kinase
	SMase	Sphingomyelinases
	SPL	Sphingosine-1-phosphate lyase
	SPT	Serine palmitoyl-CoA transferase
	Sph	Sphingosine
	SphK	Sphingosine kinase
	S1P	Sphingosine-1-phosphate
T	**t**	Triplet
	TBAF	*N*-Tetrabutylammonium fluoride
	TCA	Trichloroacetic acid
	Temp.	Temperature
	TEMPO	2,2,6,6-Tetramethylpiperidine 1-oxyl
	TFA	Trifluoroacetic acid
	THC	Δ^9-tetrahydrocannabinol
	THF	Tetrahydrofuran
	TLC	Thin layer chromatography

6. Abbreviations and acronyms

	TMS	Trimethylsilyl
	TMSOTf	Trimethylsilyl trifluoromethanesulfonate
	TOF	Time-of-Fly
	TS	Transition State
	TU	Technische Universität
U	**UV**	Ultraviolet
V	***vs***	Versus

Summary[1]

Dihydroceramide desaturase 1 (Des1) is the last enzyme involved in the *de novo* synthesis of ceramide, playing a crucial role in the intricate regulation of the dihydroceramide/ceramide (dhCer/Cer) rheostat. This regulatory mechanism is gaining prominence, with Des1 emerging as a therapeutic target, particularly in the realms of cancer and HIV-1 infection. However, Des1 is a challenging target, given that neither the X-ray crystal structure of the enzyme nor that of any closely related homologue has ever been reported. This lack of structural information hampers the understanding of its mode of action and the design of active site directed inhibitors.

Although examples of active site directed Des1 inhibitors are scarce, potent ceramide analogue inhibitors like **GT11** or **XM462** have already been reported (Figure 1). Moreover, crucial structure-activity relationship studies showed that the natural 2*S*, 3*R* stereochemistry of ceramide, the presence of a hydroxyl group at C-1, and the secondary amide functionality are essential for the enzyme inhibition.

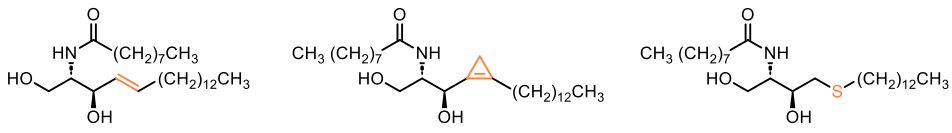

Figure 1. Structure of Ceramide and and Des1 inhibitors **GT11** and **XM462**.

[1] In this summary, the numbering of products has been consistently maintained to align with the enumeration used in the chapters of the thesis. In Chapter VI, the numbered products refer to DNA-conjugates, distinct from the products discussed in the rest of the thesis. Consequently, the product enumeration is restarted to facilitate readability.

In this context, the objective of this thesis is to design ceramide analogueues as potential Des1 inhibitors by replacing the ceramide double bond with a structurally rigid motif that could enhance ligand-protein interactions. The biological evaluation of these ceramide analogues, each incorporating different structural rigid motifs, aims to elucidate the molecular events that take place in enzyme's inhibition and enhance the structural understanding of the enzyme.

As first approach, ceramide analogues containing 1,4- or 1,5-disubstituted 1,2,3-triazoles, and 2,4-disubstituted furan heterocycles were proposed as Des1 inhibitors candidates. These moieties would allow stablishing additional favourable interactions with the enzyme via π-stacking or H-bond interactions.

Ceramide analogues containing 1,4- and 1,5-disubstituted triazoles as the central core were successfully synthetized through analogueous 4-step synthesis with yields ranging from 27 to 30 % (Scheme 1, **1**-**2**, respectively). The key steps were: a) a common stereoselective ethylination of (*S*)-Garner's aldehyde under kinetic control to obtain the desired configuration at positions 2 and 3, and b) a Cu(I)- or Ru-catalyzed azyde-alkyne-1,3-cycloaddition (AAC) reaction to get the corresponding 1,4- or 1,5-disubsituted triazole moieties respectively.

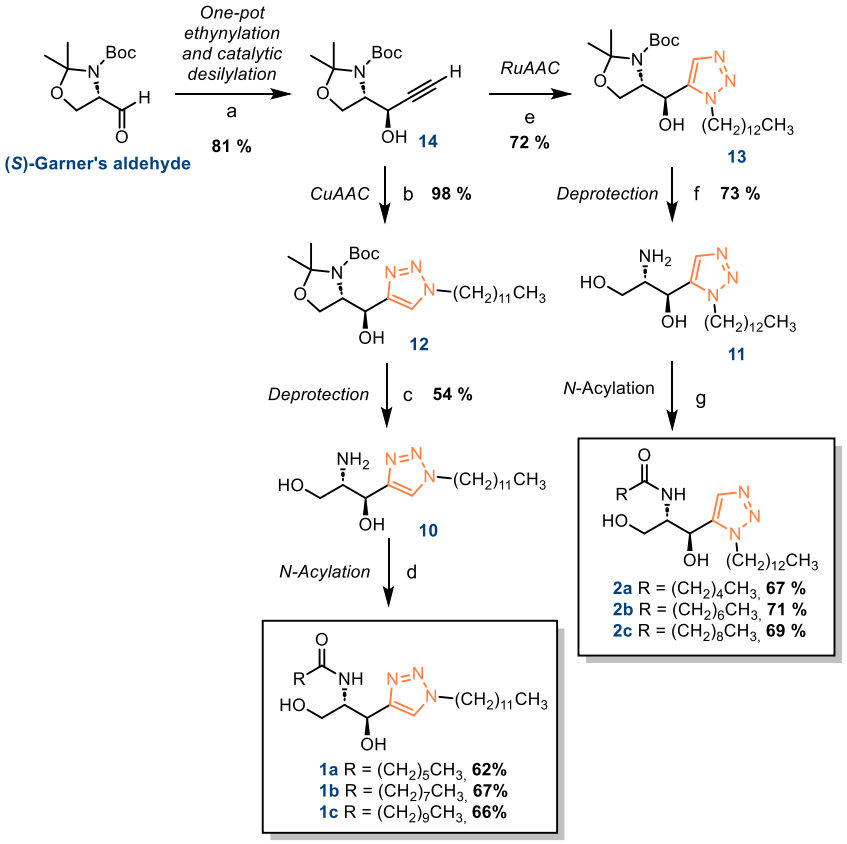

Scheme 1. Synthesis of 1,4- and 1,5-disubstituted-1,2,3-triazole ceramide analogues (**1a-c, 2a-c**). Reagents and conditions: (a) 1. trimethylsilylacetylide, BuLi, HMPA / THF, -55 °C, 18h. 2. TBAF (0.1 eq.)/ THF, 0 °C-r.t. (b) $N_3(CH_2)_{11}CH_3$, $CuSO_4{\cdot}H_2O$ (5.5 % mol), sodium ascorbate, H_2O/CH_2Cl_2, r.t., 48h (c) TFA/H_2O (10:1), r.t. 1h 45 min. (d) RCOOH, EDC·HCl, HOBt, CH_2Cl_2, r.t., overnight (e) $N_3(CH_2)_{12}CH_3$, Cp*RuCl(COD) (5 mol %), Toluene, r.t. (f) TFA/H_2O (10:1), 1h 45 min. (g) RCOOH, EDC·HCl, HOBt, CH_2Cl_2, r.t., overnight.

Ceramide analogues containing a 2,5-disubstituted furan ring as central core were successfully synthesized through a 5-step synthesis, involving a key 2-dodecylfuran diastereoselective addition to (*S*)-Garner's aldehyde and a non-obvious hydrolysis of protecting groups. The total yields ranged from 47 to 57 % (Scheme 2).

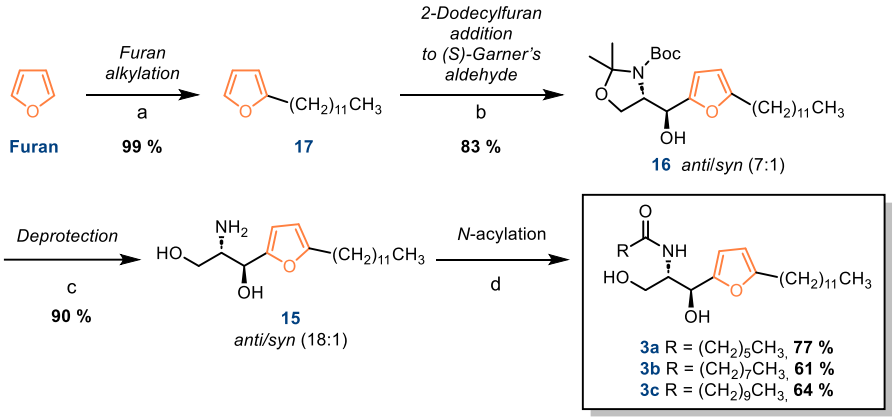

Scheme 2. Synthesis of 2,5-disubstituted furan ceramide analogues (**3a-c**). Reagents and conditions: (a) 1. BuLi, THF, 0 °C, 2h 2. $CH_3(CH_2)_{11}Br$, THF, r.t., overnight. (b) 1. BuLi, HMPA, THF, 0 °C. 2. (*S*)-Garner's aldehyde, THF, -55 °C. (c) 1. TMSOTf, Et_3N, CH_2Cl_2, 0 °C, 30 min. 2. TBAF (1M), THF, r.t., overnight. (d) RCOOH, HOBt, EDC, CH_2Cl_2, r.t., overnight.

In collaboration with Prof. Gemma Fabriàs and Dr. Josefina Casas (RUBAM, Institute for Advanced Chemistry of Catalonia), the synthetized ceramide analogues were evaluated as Des1 inhibitors in intact T98 cells and in T98 cell lysates using fluorescent **dhCerC6NBD** as substrate. Triazole and furan ceramide analogues showed moderate to low inhibition of Des1 activity (10-50%) when evaluated in intact T98 cells, but no significant inhibition was observed in T98 cell lysates. These results suggest that these ceramide analogues do not inhibit Des1 activity by a direct interaction with the enzyme, as no inhibition was observed in cell lysates.

In the course of this investigation, AlphaFold2 (AF2) appeared as a powerful tool for the prediction of the 3D structure of proteins based on their amino acid sequences. In the case of Des1, the 3D structure predicted by AF2 presented a very high confidence level. Working in collaboration with Xavier Barril (ICREA Research Professor, University of Barcelona) a complete holoprotein structure was constructed by rationally placing the inorganic species Fe_2O_2 into a precise location of the AF2 predicted structure. This species is known to participate in the catalytic activity of the enzyme, and it was positioned at the end of a well-defined deep pocked, so that one iron atom could coordinate to five histidine residues, and the second one to four histidine residues and a glutamic acid residue located in this part of the enzyme (Figure 2).

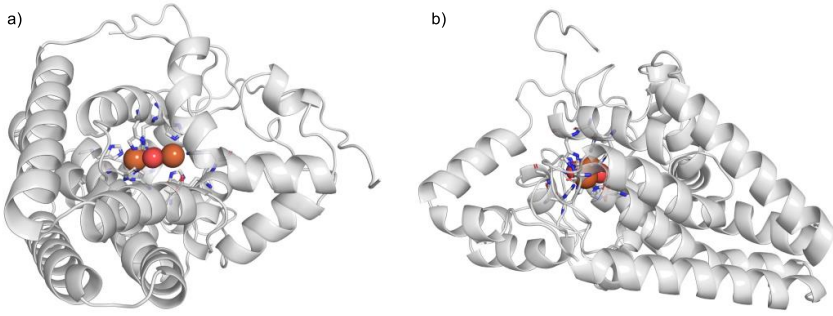

Figure 2. Front (a) and lateral (b) view of Fe_2O_2-Des1 system 3D model.

The constructed Fe_2O_2-Des1 system was used to perform docking calculations of reference Des1 inhibitors (**GT11** and **XM462**). Four common molecular events were observed in both cases:

a) A folded conformation of the ligand hydrophobic chains in the Des1 active site.
b) Close proximity of positions 4 or 5 of ceramide to the Fe_2O_2 cluster.
c) An OH-3 hydrogen bond with one of the oxygen atoms of the dioxo-diiron specie.
d) Involvement of the primary hydroxyl group in a hydrogen bond interaction with a residue of the enzyme.

12. Summary

Docking calculations with previously synthetized triazole and furan ceramide analogues revealed that the bulkiness of the ring causes a distortion of the binding mode of the ligand in the active site, losing most of the favourable ligand-protein interactions previously observed in the docking of Des1 inhibitors.These results suggest that the ligand-enzyme interactions observed in **GT11** and **XM462** are crucial for the inhibition of the enzyme. Moreover, they offer a plausible explanation for the lack of inhibitory capacity of triazole and furan ceramide analogues when evaluated in cell lysates.

As incorporation of bulky 5-member rings showed detrimental for Des1 inhibition, a ceramide analogue that incorporates a cyclopropenone ring as a rigid scaffold was proposed as potential Des1 inhibitor. Docking calculations showed that the smaller 3-member ring promotes a proper arrangement in the active site, and crucial interactions previously observed for the reference inhibitors were also identified for this compound. Thus, cyclopropenone ceramide analogue was considered as a promising Des1 inhibitor candidate.

Cyclopropenone ceramide analogues were successfully synthetized through a 6-step synthesis with total yields ranging from 26 to 29 % (Scheme 3). The syntheses involved: a) the obtaining of the cyclopropenone **58** via difluorocarbene addition to 1-pentadecine and subsequent hydrolysis, and b) stereoselective addition of a cyclopropenone acetal derivative **57** to (*S*)-Garner's aldehyde, as a key steps.

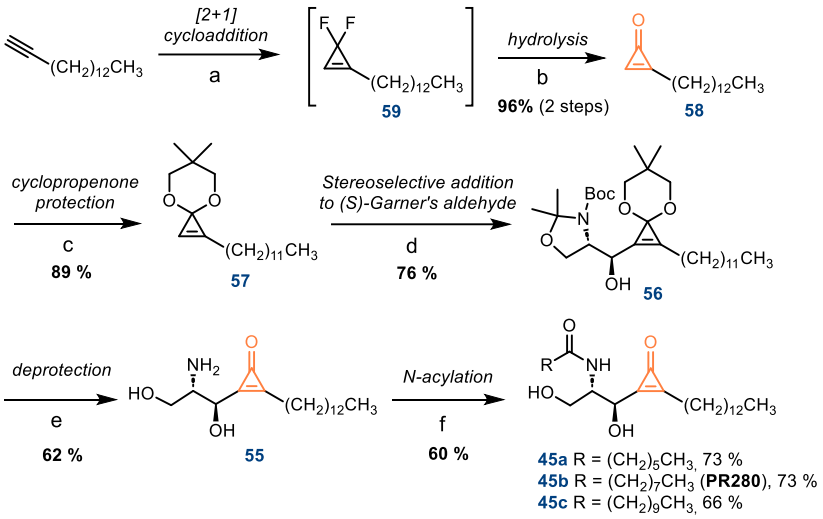

Scheme 3. Synthesis of cyclopropenone ceramide analogues. Reagents and conditions: (a) NaI, $TMSCF_3$, dry THF, 110 °C, 16 h. (b) Silica, Hexane/AcOH (aq. sol.) (99:1), r.t., 16h. (c) Neopentylglycol, $BF_4{\cdot}OEt_3$, dry CH_2Cl_2, dry Et_3N, r.t., overnight. (d) 1. BuLi, HMPA, dry THF, -55 °C, 30 min. 2. (*S*)-Garner's aldehyde, dry THF, -55 °C, overnight. (e) HCl (2 M in Et_2O), H_2O, r.t., 2 h. purification in CH_2Cl_2/MeOH/NH_4OH (9:1:0.1), r.t. (f) RCOOH, HOBt, EDC,dry CH_2Cl_2, r.t. overnight.

PR280 inhibited 86 % of Des1 activity when evaluated in intact T98-cells, and 92% in T98 cell lysates, suggesting a direct interaction with the enzyme active site as the cause of inhibition. The Des1 inhibition induced by **PR280** is dose-dependent with an IC_{50} value of 0.7 μM (*in vitro* evaluation using T98 cell lysates); which is lower than the showed for the reference inhibitors **GT11** (20 μM) and **XM462** (8.2 μM) evaluated in rat liver microsomes.

To assess whether the inclusion of a sulphur atom could enhance enzyme inhibition through its interaction with the iron within the oxodiiron species, the synthesis of ceramides containing thiocyclopropenone and 1,2-thiole-3-one moieties was explored. However, the synthesis failed for the former, and while an efficient synthesis was accomplished for the latter, the compound obtained did not behave as a direct Des1 inhibitor (27 % inhibition in intact cells, no inhibition in cell lysates).

To the best of our knowledge, this work provides the first reported example of the use of AlphaFold2 in the prediction of the 3D structure of Des1 to identify key ligand-protein interactions in well-known ceramide Des1 inhibitors, previous construction of the full Fe_2O_2-Des1 model. Although it should be noted that the protein structure provided by AlphaFold2 is an unrefined and static model and that the position of the Fe_2O_2 complex is estimated, the present study may pave the way to gaining greater knowledge on Des1 inhibition. To this end, docking studies of a large library of cyclopropenone-based inhibitors have already started in this thesis. This work will be completed in the future covering all diversity sites of **PR280**, in order to gain insight into the inhibition mode of this enzyme, and will be coupled with a systematic synthetic plan of those with better predicted inhibition profile. Eventually, inhibition assays will enable to validate the constructed Alphafold2-based model.

Chapter VI of the present PhD work describes the research carried out during a stay at Dortmund Technical University (TU) under the supervision of Prof. Andreas Brunschweiger. The objective of the work was to develop a ring closing metathesis (RCM) methodology on controlled pore glass (CPG) solid phase coupled DNA for the synthesis of a DNA-encoded macrocyclic library.

The procedure designed showed efficient for the on-DNA synthesis of macrocycles. This includes the setting up of the reaction inside a glove bag, with 10 equivalents of **DA** catalyst (1,2-diphenylethane-1,2-diamine derivative of 3rd generation Grubbs catalyst) in degassed and dry toluene for 30 minutes at room temperature. The work-up of the reaction consists of an operationally simple filtration, with an extra incubation step with potassium tris(3,5-dimethyl-1-pyrazolyl)borate (KTP) and a final filtration to remove ruthenium. The optimized procedure allowed the synthesis of a small set of macrocycles (Figure 3) that could be identified by MALDI-TOF-MS, purified

and isolated through semi-preparative ion pair RP-HPLC, proving the effectiveness of the designed strategy.

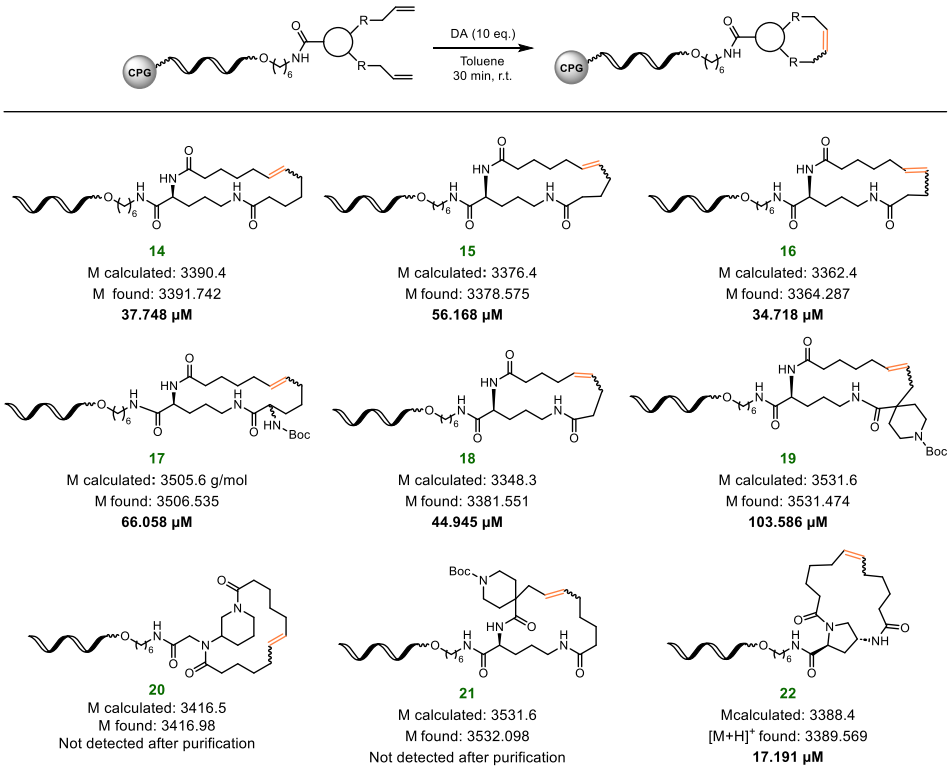

Figure 3. DNA macrocyclic conjugates synthetized by RCM on CPG-coupled DNA. The final concentration after purification is shown in bold.

UNIVERSITAT ROVIRA I VIRGILI
TARGETING DES1: SYNTHESES OF CERAMIDE ANALOGUES WITH A RIGID SCAFFOLD, INHIBITORY ASSAYS, AND AF2-ASSISTED STRUCTURAL INSIGHTS REVEAL PR280 AS A POTENT INHIBITOR
Pablo Rivero Prieto

CHAPTER I

General Introduction

UNIVERSITAT ROVIRA I VIRGILI
TARGETING DES1: SYNTHESES OF CERAMIDE ANALOGUES WITH A RIGID SCAFFOLD, INHIBITORY ASSAYS, AND AF2-ASSISTED STRUCTURAL INSIGHTS REVEAL PR280 AS A POTENT INHIBITOR
Pablo Rivero Prieto

1.1 Bioactive sphingolipids

Research on bioactive lipids has been significantly intensified in recent decades, revealing an unprecedented and unanticipated complexity of the lipidome and its many functions. Bioactive lipids are functionally defined as lipid species, whose levels respond to the action of specific cellular stimuli. These lipids then regulate specific downstream effectors and targets. They have a diverse array of functions related to cell survival, membrane integrity, metabolic regulation, and general adaptations to cellular stressors.[1]

Sphingolipids represent one of the major classes of eukaryotic lipids. The first sphingolipids were isolated from the brain in the late 19th century by Thudicum, who introduced the name *sphingosin* after the Greek mythical creature, the Sphinx, in reference to "the many enigmas which it presented to the inquirer".[2] Sphingolipids are a class of amphipathic lipids which share a sphingoid base backbone, consisting of a long alkyl chain, usually 16 to 20 carbon atoms, with a 2-amino-1,3-diol functionality which can contain a *trans*-double bond located at C-4 (Figure 1.1). Dihydrosphingolipids differ from sphingolipids by the absence of an unsaturation in the sphingoid base. The acylation of the amino functionality with a long-chain fatty acid results in the generation of ceramides, and through phosphorylation or glycosylation on the primary hydroxyl group, more complex sphingolipid derivatives may be obtained.[3]

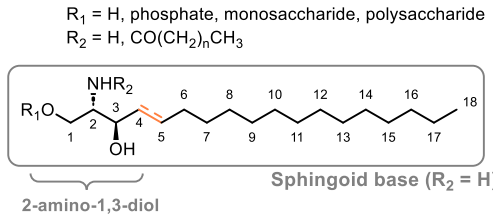

Figure 1.1. General structure of sphingolipids.

[1] Hannun, Y., Obeid, L. *Nat. Rev. Mol. Cell. Biol.* **2018**, *19*, 175-191.

[2] Thudichum, J. L. W. *A Treatise on the Chemical Constitution of the Brain*; Archon Books: 1962.

[3] Quinville, B.M.; Deschenes, N.M.; Ryckman, A.E.; Walia, J.S. *Int. J. Mol. Sci.* **2021**, *22*, 5793.

Among the various sphingolipid species, ceramide (**Cer**) is considered as the central intermediate of sphingolipid metabolism. Ceramide can be generated by *de novo* synthesis, the hydrolysis of complex sphingolipids, or acylation of sphingosine (Scheme 1.1).

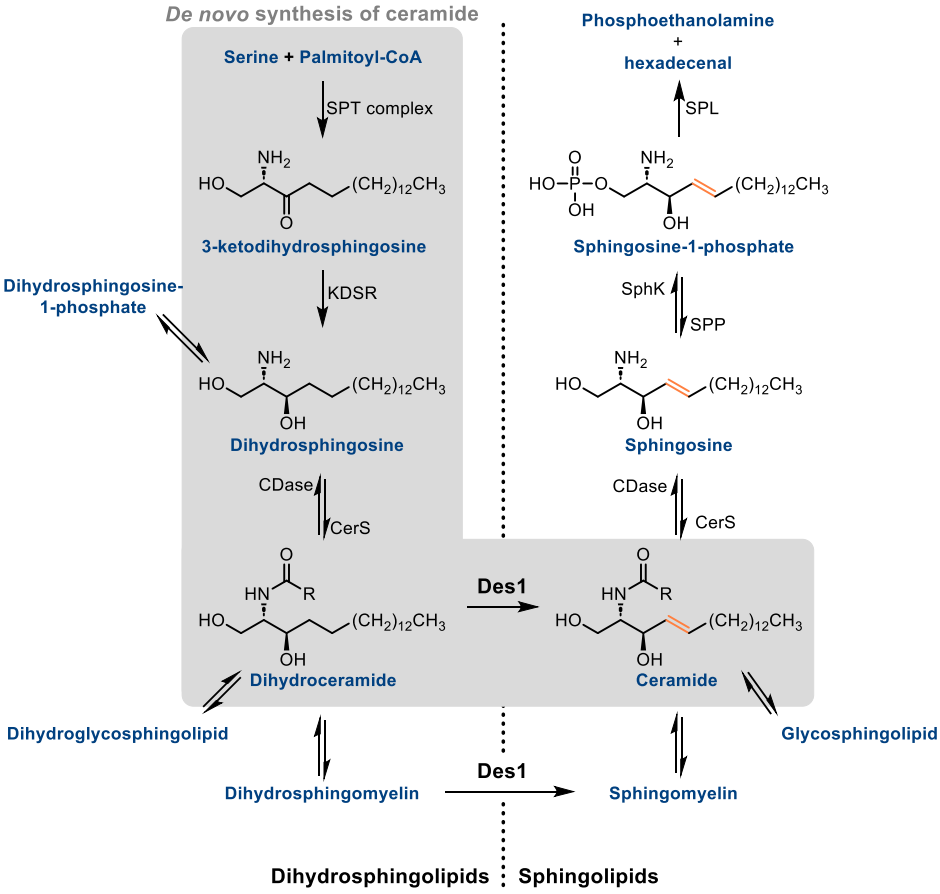

Scheme 1.1. Biosynthesis of (dihydro)sphingolipids. Abbreviations: serine palmitoyl-CoA transferase, SPT; 3-ketodihydrosphingosine reductase, KDSR; ceramide synthases, CerS; dihydroceramide desaturase 1, Des1; ceramidases, CDase; sphingosine kinase, SphK; sphingosine kinase, SphK; sphingosine-1-phosphate phosphatases, SPP; sphingosine-1-phosphate lyase, SPL.

The *de novo* synthesis of Cer typically starts with the condensation of serine and palmitoyl-CoA by the serine palmitoyl-CoA transferase (SPT) complex (Scheme 1.1). This results in the formation of3-ketodihydrosphingosine, which is reduced by the 3-ketodihydrosphingosine reductase (KDSR) to dihydrosphingosine (also known as sphinganine). Next, the *N*-acylation of dihydrosphingosine is carried out by ceramide synthases (CerS), yielding dihydroceramide (dhCer). The final step of the *de novo* synthesis of ceramide is the conversion of dhCer to Cer by dihydroceramide desaturase 1 (Des1). The *de novo* synthesis of ceramide represents the exclusive entry point into the sphingolipid metabolism.

Ceramide can also be generated through the hydrolysis of complex sphingolipids, mainly sphingomyelin by the action of sphingomyelinases (SMase), which is known as the salvage pathway. Additionally, the *N*-acylation of sphingosine by ceramide synthase (CerS) also increases ceramide levels.

Ceramide is a well-known sphingolipid involved in an important biological rheostat with sphingosine and sphingosine-1-phosphate (S1P). Ceramide undergoes deacylation by ceramidases (CDase), resulting in the formation of sphingosine (Sph), which is subsequently converted to sphingosine-1-phosphate by sphingosine kinase (SphK) (Scheme 1.1). These three bioactive sphingolipids maintain a dynamic equilibrium that dictates cell fate, attracting significant attention for its central role in cancer regulation.[4] In this context, ceramide emerges as a tumor-suppressing lipid,

[4] a) Morad, S. A.; Cabot, M. C. *Nat. Rev. Cancer* **2013**, *13*, 51−65. b) Orr Gandy, K. A.; Obeid, L. M. *Biochim. Biophys. Acta* **2013**, *1*, 157−166. c) Chalfant, C. E.; Spiegel, S. *J. Cell Sci.* **2005**, *118*, 4605−4612. d) Airola, M.; Hannun, Y.A. *Handb. Exp. Pharmacol.* **2013**, *215*, 57−76. e) Pyne, S.; Pyne, N.J. *Biochem. J.* **2000**, *349*, 385-402.

demonstrating its capacity to induce apoptosis,[5] quiescence[6] and senescence.[7] On the other hand, S1P[8] is recognized to function as a tumor-promoting lipid through the stimulation of angiogenesis[9] and anti-apoptotic pathways.[10] In fact, one common survival strategy employed by cancer cells is the synthesis of S1P by SphK, promoting in this way their growth, survival, and metastasis.[11]

In the case of dihydroceramide, it serves as a precursor for complex dihydrosphingolipids, giving rise to two closely related yet distinct classes of complex sphingolipids. Unlike ceramides, dihydroceramides are less abundant, with cellular levels maintained at concentrations approximately 20-30-fold lower than that of ceramides.[12] The double bond that distinguishes dihydroceramides from ceramides (or dihydrosphingolipids and sphingolipids in general) markedly alters the biophysical properties of the molecules, modifying their elastic property and their packing behaviour.[13]

---

[5] Obeid, L.M.; Linardic, C.M.; Karolak, L.A.; Hannun, Y.A. *Science* **1993**, *259*, 1769-1771.

[6] Dbaibo, G.; Pushkareva, M.; Jayadev, S.; Schwarz, J.; Horowitz, J.; Obeid, L.; Hannun, Y. *Proc. Nat. Acad. Sci. USA* **1995**, *92*, 1347-1351.

[7] a) Venable, M.; Lee, J.; Smyth, M.; Bielawska, A.; Obeid, L. *J. Biol. Chem.* **1995**, *270*, 30701-30708. b) Young, M. M.; Kester, M.; Wang, H. G. *J. Lipid Res.* **2013**, *54*, 5-19. c) Maceyka, M.; Harikumar, K. B.; Milstien, S.; Spiegel, S. *Trends Cell Biol.* **2012**, *22*, 50-60.

[8] Pulkoski-Gross, M. J.; Donaldson, J. C.; Obedi, L. M. *Crit. Rev. Biochem. Mol. Biol*. **2015**, *50*, 298-313.

[9] Kimura, T.; Watanabe, T.; Sato, K.; Kon, J.; Tomura, H.; Tamama, K.; Kuwabara, A.; Kanda, T.; Kobayashi, I.; Ohta, H.; Ui, M.; Okajima, F. *Biochem. J.* **2000**, *348*, 71-76.

[10] a) Cuvillier, O.; Pirianov, G.; Kleuser, B.; Vanek, P.; Coso, O.; Gutkind, J.; Spiegel, S. *Nature* **1996**, *381*, 800-803. b) Pyne, N. J.; Pyne, S. *Nature Rev*. **2010**, *10*, 489-503. c) Ponnusamy, S.; Meyers-Needham, M.; Senkal, C. E.; Saddoughi, S. A.; Sentelle, D.; Selvam, S. P.; Salas, A.; Ogretmen, B. *Future Oncol*. **2010**, *6*, 1603–1624. d) Jiang, W.; Ogretmen,B. *Biochim. Biophys. Acta Mol. Cell Biol. Lip.* **2014**, *1841*, 783–792. e) Maceyka, M.; Spiegel, S. *Nature* **2014**, *510*, 58-67. f) Pyne, S.; Adams, D.; Pyne, N. *Prog. Lipid Res.* **2016**, *62*, 93-106.

[11] a) Zheng, X.; Li, W.; Ren, L.; Liu, J.; Pang, X.; Chen, X.; Kang, D.; Wang, J.; Du, G. *Pharmacol. Ther.* **2019**, *195*, 85–99. b) Ogretmen, B. *Nature Rev. Cancer* **2018**, *18*, 33–50. c) Adan-Gokbulut, A.; Kartal-Yandim, M.; Iskender, G.; Baran, Y. *Curr. Med. Chem.* **2013**, *20*, 108–122.

[12] a) Apostolopoulou, M.; Gordillo, R.; Gancheva, S.; Strassburger, K.; Herder, C.; Esposito, I.; Schlensak, M.; Scherer, P. M.; Roden, M. *BMJ Open Diabetes Res. Care* **2020,** *8*, e001860. b) Dasgupta, S.; Ray, S. K. *J. Neurol. Psychol.* **2018**, *5*, 1-7.

[13] Brockman, H. L.; Momsen, M. M.; Brown, R. E.; He, L.; Chun, J.; Byun, H. S.; Bittman, R. *Biophys. J.* **2004**, *87*, 1722-1731.

Numerous articles published over the years asserted that dihydroceramides are inactive or ineffective lipid mediators in various biological responses, leading to the dogma that dhCer are biologically inactive counterparts of Cer. This perception originated from studies conducted in the early 1990's using *N*-short-chain analogues of dhCer and Cer, C2-dhCer and C2-Cer, respectively. In these investigations, C2-dhCer was shown to be incapable of inhibiting growth and stimulating ceramide-activated protein phosphatase, a primary target enzyme for Cer, in yeast[14] and in HL-60 cells.[15] Another study demonstrated that C2-Cer induced ADP-induced platelet aggregation and changes in platelet morphology, while C2-dhCer did not exhibited such effects.[16] Furthermore, C2-dhCer failed to mimic the C2-Cer-induced expression of interleukin-1-responsive α 1-acid glycoprotein mRNA in rat hepatocytes.[17] Numerous additional examples supported these findings; for instance, C2-Cer was found to stimulate autophagy in breast cancer,[18] decrease protein kinase B activity in oligodentrocytes,[19] promote rapid fragmentation of the mitochondrial network in rat cardiomyocytes,[20] and impair energy metabolism and insulin or insulin-like growth factor signalling in human neuronal cells.[21] In all these cases, C2-dhCer was unable to replicate the effects induced by C2-Cer.

---

[14] Fishbein, J. D.; Dobrowsky, R. T.; Bielawska, A.; Garrett, S.; Hannun, Y. A. *J. Biol. Chem.* **1993**, *268*, 9255-9261.

[15] a) Bielawska, A.; Crane, H. M.; Liotta, D.; Obeid, L. M.; Hannun, Y. A. *J. Biol. Chem.* **1993**, *268*, 26226-26232. b) Merrill, A. H. *J. Biol. Chem.* **2002**, *277*, 25843-25846.

[16] Simon Jr., C. G.; Gear, A. R. *Biochemistry* **1998**, *37*, 2059-2069.

[17] Chen, J.; Nikolova-Karakashian, M.; Merrill, A. H.; Morgan, E. T. *J. Biol. Chem.* **1995**, *270*, 25233-25238.

[18] Scarlatti, F.; Bauvy, C.; Ventruti, A.; Sala, G.; Cluzeaud, F.; Vandewalle, A.; Ghidoni, R.; Codogno, P. *J. Biol. Chem.* **2004**, *279*, 18384-18391.

[19] Lu, F. G.; Wong, C. S. *Int. J. Radiat. Biol.* **2004**, *80*, 39–51.

[20] Parra, V.; Eisner, V.; Chiong, M.; Criollo, A.; Moraga, F.; Garcia, A.; Härtel, S.; Jaimovich, E.; Zorzano, A.; Hidalgo, C.; Lavander, S. *Cardiovasc. Res.* **2007**, *77*, 387–97.

[21] Tong, M.; de la Monte, S. M. *J. Alzheimers Dis.* **2009**, *16*, 705-714.

The perception of dihydroceramides began to evolve following the publication of two crucial studies. Stiban *et al.*[22] demonstrated the ability of long and short *N*-acyl chain dhCer to inhibit channel formation induced by ceramides in mitochondria, consequently impeding the release of apoptogenic molecules and apoptotic cell death. Their findings prompted the authors to propose that dihydroceramides might attenuate the apoptotic effects of ceramides, and apoptogenic activity of ceramide may thus depend on the Cer/dhCer ratio.

Simultaneously, the development of liquid chromatography coupled with mass spectrometry techniques played a crucial role in uncovering the biological activities of dhCers, as it enabled the differentiation between ceramides and dihydroceramides. In a seminal study, Merrill's group profiled the sphingolipid composition of human prostate cancer cells treated with the anticancer drug fenretinide (4-HPR).[23] Fenretinide has been widely studied, being in clinical trials for the treatment of various cancer pathologies.[24] Initially, it was believed to elevate ceramide levels, leading to cell growth arrest and apoptosis, thus impeding tumour growth as a part of its mechanism of action. However, the application of refined mass spectroscopic techniques revealed that it was in fact the precursor dihydroceramide and other dihydrosphingolipids levels which were increased. In fact, ceramide-derived sphingolipids levels were unchanged or reduced. Further studies with fenretinide revealed that it inhibits Des1, provoking dhCer accumulation. Moreover, Merrill laboratory identified a likely role of dhCer in the induction of autophagy.

It is important to note that the effects observed by Merrill and coworkers were produced by a natural accumulation of endogenous dihydroceramides

---

[22] Stiban, J.; Fistere, D.; Colombini, M. *Apoptosis* **2006**, *11*, 773-780.

[23] Zheng, W.; Kollmeyer, J.; Symolon, H.; Momin, A.; Munter, E.; Wang, E.; Kelly, S.; Allegood, J. C.; Liu, Y.; Peng, Q.; Ramaraju, H.; Sullards, M. C.; Cabot, M.; Merrill, A. H. *Biochim. Biophys. Acta* **2006**, *1758*, 1864-1884.

[24] Potenaza, R. L.; Lodeserto, P.; Orientini, I. *Int. J. Mol. Sci.* **2022**, *23*, 7426.

provoked by Des1 inhibition, whereas the inertness of dihydroceramides was observed in the treatment of cells with exogenous *N*-short-chain dihydroceramides. Differences in the behaviour of short-chain synthetic ceramides as opposed as to natural long-chain ceramides have been well documented.[23]

This new vision of dihydroceramides inspired several groups to evaluate the role of dihydroceramides in cellular responses, and these sphingolipids are now recognized to be implicated in a diverse array of biological processes. Since then, their role in autophagy, hypoxia, and cellular proliferation, as well as their implication in the ethology, diagnosis or treatment of diabetes, cancer, neurodegenerative diseases, and ischemia injury have been described.[1, 25]

In this context, dihydroceramide desaturase 1 (Des1) stands out as the key enzyme in determining the ratio of dihydrosphingolipids to sphingolipids. Des1 catalyses the formation of the 4,5-*trans*-double bond in the sphingoid base in the *de novo* synthesis of ceramide (Scheme 1.1). Moreover, dihydrosphingomyelin (dhSM) also revealed as a relatively good Des1 substrate (20 % activity) (Scheme 1.1), according to enzyme activity assays with rat liver microsomes.[26]

1.2 Dihydroceramide desaturase 1

The gene encoding Des1 was initially cloned in 1996 from *Drosophila melanogaster* and designated as "drosophila degenerative spermatocyte 1" or DEGS1.[27] The gene product was then identified as a membrane bound

[25] Siddique, M.; Li, Y.; Chaurasia, B.; Kaddai, V.; Summers, S. *J. Biol. Chem.* **2015**, *290*, 15371-15379 (and the references listed there in).

[26] Michel, C.; van Echten-Deckert, G.; Rother, J.; Sandhoff, K.; Wang, E.; Merrill, A. H. *J. Biol. Chem.* **1997**, *276*, 22432-22437.

[27] Endo, K.; Akiyama, T.; Kobayashi, S.; Okada, M. *Mol. Gen. Genet.* **1996**, *253*, 157-165.

desaturase.[28] As previously commented, Des1 presents a dihydroceramide C4-desaturase activity being ubiquitously distributed in all human tissues. A Des 1 homologue was also identified in mouse and human, named Des2, which exhibits bifunctional sphingolipid C-4 hydroxylase and, to a lesser extent, C4-desaturase activity (Scheme 1.2).[29] Des2 is preferentially expressed in the small intestine, skin and kidney, where the production of phytoceramides is essential.[30]

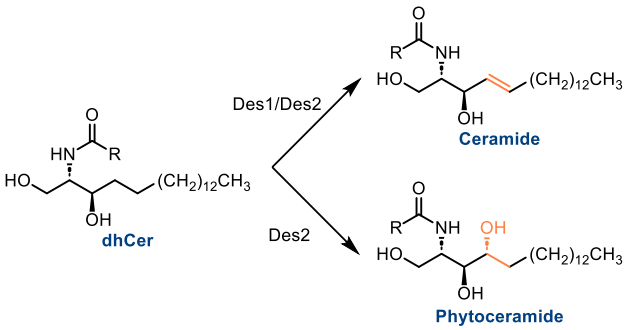

Scheme 1.2. Des1 and Des2 differential activity.

Ternes *et al.* compared several dihydroceramide desaturase sequences from different organisms and found that all of them contained three histidine motifs essential for the catalytic activity.[31] These motifs are characteristic and present in membrane fatty acid desaturases and membrane hydrocarbon hydroxylases.[32]

From the biochemical point of view, Des1 requires either NADPH or NADH as electron donor and oxygen as electron acceptor. The enzyme is part of a larger enzymatic complex (Scheme 1.3), forming an electron transport chain. In this chain, the electron provided by NAD(P)H is sequentially

[28] Cadena, D. L.; Kurten, R. C.; Gill, G. N. *Biochemistry* **1997**, *36*, 6960-6967.

[29] Ternes, P.; Franke, S.; Zahringer, U.; Sperling, P.; Heinz, E. *J. Biol. Chem.* **2002**, *277*, 25512-25518.

[30] a) Omae, F.; Miyazaki, M.; Enomoto, A.; Suzuki, A. *FEBS Lett.* **2004**, *576*, 63-67. b) Omae, F.; Miyazaki, M.; Enomoto, A.; Suzuki, A. *Biochem. J.* **2004**, *379*, 687-695.

[31] Ternes, P.; Franke, S.; Zahringer, U.; Sperling, P.; Heinz, E *J. Biol. Chem.* **2002**, 277, 25512-25518.

[32] Shanklin, J.; Cahoon, E. B. *Annu. Rev. Plant. Physiol. Plant. Mol. Biol.* **1998**, *49*, 611–641.

transported from the cofactor to NADH-cytochrome b5 reductase (CYB5R), cytochrome b5 (Cyt b_5), and the terminal desaturase Des1, which reduces oxygen to water and oxidizes dhCer to Cer.[33,34]

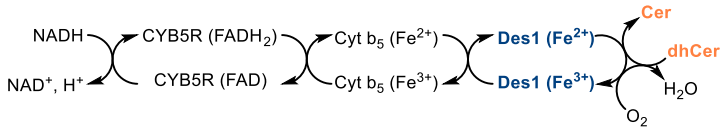

Scheme 1.3. Dihydroceramide desaturase enzymatic complex.

Mechanistically, the desaturation reaction catalysed by Des1 is presumably initiated by an enzyme-bound diiron-dioxo species that abstracts specifically the C-4 hydrogen atom from the substrate (Scheme 1.4).[35] This is a highly energetically demanding C–H cleavage associated with a large kinetic isotope effect. This first oxidation is followed by the fast, isotopically insensitive elimination of the hydrogen atom at C-5. [36]

Stoffel *et al.* performed *in vivo* experiments with rats using tritium-labeled dihydrosphingosine, which was *in situ* converted to dihydroceramide and subsequently desaturated. Product isolation and analysis of the isotopic ratio showed that desaturation of dihydroceramides occurs by abstraction of the *pro*-(*R*) and *pro*-(*S*) hydrogen atoms at C-4 and C-5, respectively (Scheme 1.4), resulting in an overall *syn*-elimination reaction.[37]

These results were confirmed in a study using stereospecifically labelled (2*R*,3*S*)-[2,3,4,4-$^2H_4$]-palmitic acid as a metabolic probe, the first precursor in the *de novo* synthesis of ceramide. Mass spectrometric analysis of the labelled

---

[33] a) Geeraert, L.; Mannaerts, G. P.; van Veldhoven, P. P. *Biochem.* **1997**, *327*, 125–132. b) Michel, C.; van Echten-Deckert, G.; Rother, J.; Sandhoff, K.; Wang, E.; Merrill, A.H. *J. Biol. Chem.* **1997**, *272*, 22432-22437.

[34] Casasampere, M.; Ordoñez, Y. F.; Pou, A.; Casas, J. *Chem. Phys. Lipids.* **2016**, *197*, 33-44.

[35] Buist, P.H. *Nat. Prod. Rep.* **2004**, *21*, 249–262.

[36] a) Beckmann, C.; Rattke, J.; Sperling, P.; Heinz, E.; Boland, W. *Org. Biomol. Chem.* **2003**, *1*, 2448-2454. b) Savile, C. K.; Fabriàs, G.; Buist, P.H. *J. Am. Chem. Soc.* **2001**, *123*, 4382-4385.

[37] Stoffel, W.; Assmann, G.; Bister, K. *Hoppe Seylers Z. Physiol. Chem.* **1971**, *352*, 1531-1544.

products revealed elimination of a single deuterium atom from C-4 (corresponding to the C4-H(*R*)) along with a hydrogen atom from C-5 (corresponding to the C5-H(*S*)). [36a]

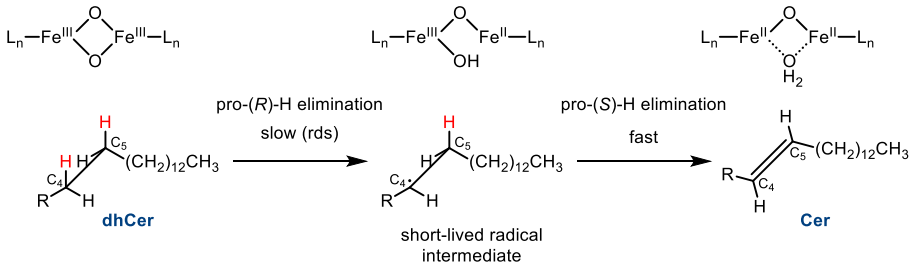

Scheme 1.4. Mechanism of dihydroceramide desaturation by Des1. rds: rate-determining step

Des1 activity is significantly influenced by the stereochemistry of the substrate; desaturation of the D-*erythro*-isomer occurs much more rapidly than that of the L or D-*threo*-isomers.[38] Additionally, the activity is also impacted by the length of the alkyl chain of the amide-linked fatty acid. The *in vitro* activity, tested in rat liver microsomes, decreased as the length of the chain was increased.[33b] However, in fetal rat skin and liver homogenates, C14-dhCer showed as a better substrate than dhCer analogues containing fatty acids with 18, 10, 6, or 2 carbon atoms.[39]

1.3 Des1 inhibitors

The identification of Des1 inhibitors and their use as pharmacological tools has significantly contributed to unrevealing the involvement of dihydroceramide in diverse biological processes. In these investigations, inhibition of Des1 results in an accumulation of dihydroceramide, which

[38] Fabriàs, G.; Muñoz-Olaya, J.; Cingolani, F.; Signorelli, P.; Casas, J.; Gagliostro, V.; Ghidoni, R. *Prog. Lipid Res.* **2012**, *51*, 82-94.

[39] Schulze, H.; Michel, C.; van Echten-Deckert, G. *Meth. Enzymol.* **2000**, *311*, 22–30.

leads to different outcomes depending on the cell line, degree of inhibition, and experimental context.

Only a limited number of Des1 inhibitors, designed with a rational approach and featuring a structure analogueous to sphingolipids, have been documented. Besides, various non-sphingolipid drugs and natural products have exhibited inhibitory effect on Des1. The latter feature redox-sensitive units that can affect the enzyme activity by modifying the redox status of the cell, thus affecting Des1 electron transport chain.

1.3.1 Non-sphingolipid Des1 inhibitors

Phenolic compounds, along with other non-sphingolipid analogueues like fenretidine, resveratrol, celecoxib, γ-tocopherol, γ-tocotrienol, Δ^9-tetrahydrocannabinol, curcumin, SKI II and ABC294640 are among the drugs and natural products known to function as Des1 inhibitors. (Figure 1.2).

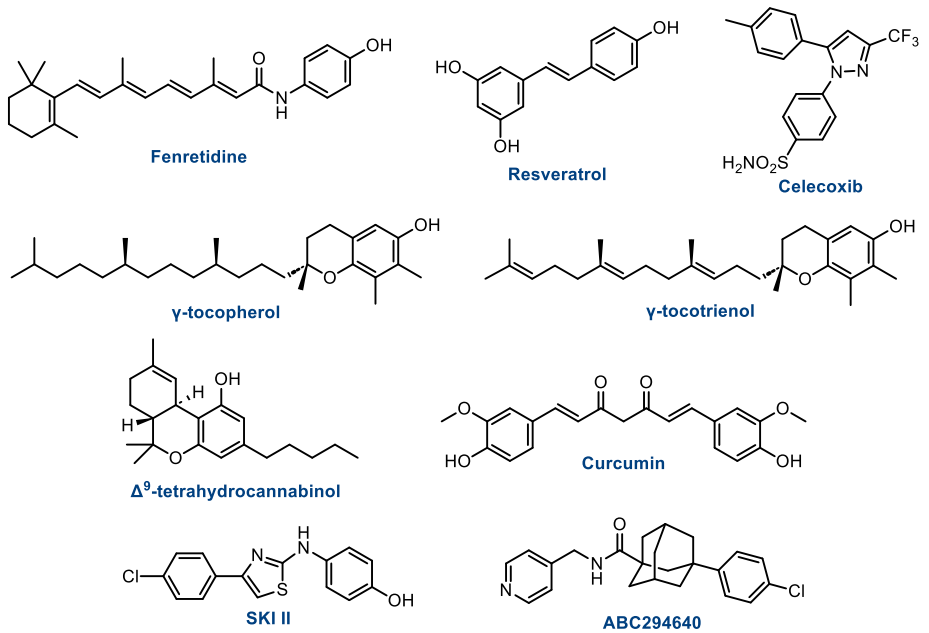

Figure 1.2. Non-sphingolipid Des1 inhibitors.

Fenretidine (4-HPR), a synthetic derivative of retinoic acid, which is a metabolite of vitamin A,[40] has been reported to induce apoptotic cell death and to repress cell proliferation, therefore being useful to stop tumour growth.[41] 4-HPR increases reactive oxygen species levels,[42] which may inhibit Des1 activity by disrupting the electron transport chain.[43] However, in 2011 Rahmaniyan *et al.*[44] showed that Des1 is a direct *in vitro* target for 4-HPR (IC_{50} = 2.32 μM). Regardless of the type of inhibition, 4-HPR promotes an increase in dhCer levels, which seems to be partly responsible for the drug activity. Moreover, Merrill and co-workers described that the induction of autophagy by 4-HPR occurs via dhCer accumulation.[23]

Resveratrol is a widely studied dietary polyphenol reported to have anti-inflammatory and antifibrotic effects, antitumor activities, protection in renal disease and neurodegeneration, activity against obesity, diabetes, stroke, hepatic steatosis, and cardiovascular diseases.[45] Signorelli and co-workers demonstrated that resveratrol induces autophagy in HGC-27 cells via an accumulation of dihydroceramides by inhibition of Des1.[46] Dihydroceramide desaturase was inhibited by resveratrol *in vitro* (IC_{50} = 85 μM at 10 μM substrate concentration in rat liver microsomes), indicating a direct inhibitory Des1 activity of the compound.

---

[40] Rodriguez-Cuenca, S.; Barbarroja, N.; Vidal-Puig, A. *Biochim. Biophys. Acta, Mol. Cell Biol. Lipids* **2015**, *1851*, 40-50.

[41] Hail, N.; Kim, H. J.; Lotan, R. *Apoptosis* **2006**, *11*, 1677-1694.

[42] Oridate, N.; Suzuki, S.; Higuchi, M.; Mitchell, M. F.; Hong, W. K.; Lotan, R. *J. Natl. Cancer Inst.* **1997**, *89*, 1191–1198.

[43] Idkowiak-Baldys, J.; Apraiz, A.; Li, L.; Rahmaniyan, M.; Clarke, C. J.; Kraveka, J. M.; Asumendi, A.; Hannun, Y. A. *Biochem. J.* **2010**, *427*, 265-274.

[44] Rahmaniyan, M.; Curley, R. W.; Obeid, L. M.; Hannun, Y. A.; Kraveka, J. M. *J. Biol. Chem.* **2011**, *286*, 24754-24764.

[45] Salehi, B.; Mishra, A. P.; Nigam, M.; Sener, B.; Kilic, M.; Sharifi-Rad, M.; Fokou, P. V. T.; Martins, N.; Sharifi-Rad, J. *Biomedicines* **2018**, *6*, 91.

[46] Signorelli, P.; Muñoz-Olaya, J. M.; Gagliostro, V.; Casas, J.; Ghidoni, R.; Fabriàs, G. *Cancer Lett.* **2009**, *282*, 238-243.

Celecoxib has been tested in the prevention and treatment of pancreatic, breast, ovarian, non-small cell lung cancer and other advanced human epithelial cancers.[47] Moreover, it has been reported to inhibit Des1 in intact cells with an IC_{50} of 80 μM. Authors describe that Des1 inhibition contribute to the anti-proliferative effects of celecoxib. [48]

γ-Tocopherol and γ-tocotrienol are natural components of vitamin E with well-known antioxidant properties. Moreover, both compounds have been successfully employed in cancer therapies.[49] Some reports relate these anticancer properties with the induction of apoptosis and autophagy provoked by a dhCer and dihydrosphingosine (dhSo) accumulation caused by Des1 inhibition.[50] In this regard, Merrill's group observed a 60% reduction of Des1 activity when incubating γ-tocopherol with prostate cancer cells for 36 h.[23]

Δ^9-tetrahydrocannabinol (THC) efficiently activates autophagy and apoptosis and inhibits tumor growth in mice by inhibition of Des1 activity. THC increases the dhCer/Cer ratio in the endoplasmic reticulum of glioma cells, and this alteration is directed to autophagosomes and autolysosomes to promote lysosomal membrane permeabilization, cathepsin release and the subsequent activation of apoptotic cell death (autophagy-mediated cancer cell death).[51]

---

[47] Jendrossek, V. *Cancer Lett.* **2013**, *332*, 313-324.

[48] Schiffmann, S.; Sandner, J.; Schmidt, R.; Birod, K.; Wobst, I.; Schmidt, H., Angioni, C.; Geisslinger, G.; Grösch, S. *J. Lipid Res.* **2009**, *50*, 32-40.

[49] a) Gopalan, A.; Yu, W.; Jiang, Q.; Jang, Y.; Sanders, B. G.; Kline, K. *Mol. Nutr. Food Res.* **2012**, *56*, 1803-1811. b) Tiwari, R. V.; Parajuli, P.; Sylvester, P. W. *Mol. Cell. Biochem.* **2015**, *408*, 123-137.

[50] a) Jiang, Q.; Rao, X.; Kim, C. Y.; Freiser, H.; Zhang, Q.; Jiang, Z.; Li, G. *Int. J. Cancer* **2012**, *130*, 685-693. b) Jiang, Q.; Wong, J.; Fyrst, H.; Saba, J. D.; Ames, B. N. *Proc. Natl. Acad. Sci. U.S.A.* **2004**, *101*, 17825-17830.

[51] Hernández-Tiedra, S.; Fabriàs, G.; Dávila, D.; Salanueva Í. J.; Casas, J.; Montes, L. R.; Antón, Z.; García-Taboada, E.; Salazar-Roa, M.; Lorente, M.; Nylandsted, J.; Armstrong, J.; López-Valero, I.; McKee, C. S.; Serrano-Puebla, A.; García-López, R.; González-Martínez, J.; Abad, J. L.; Hanada, K.;

Curcumin has shown to cause a 28% of Des1 activity inhibition in human gastric adenocarcinoma HGC-27 cell lysates at 10 μM.[38] As a phenolic compound, authors speculate that the inhibition is indirect, by affecting the electron transport chain or by altering the redox status of the cell. This inhibition has not been related to any specific biological process.

SKI II is a dual sphinosine kinase (SphK) 1 and 2 inhibitor that also showed Des1 inhibitory activity.[52] Molecular modeling studies supported that the SKI II-induced decrease in Des1 activity could result from inhibition of NADH-cytochrome b5 reductase. An effect of SKI II on the cell cycle and autophagy was also observed, which was attributed to Des1 inhibition rather than SK inhibition. Similarly, the dual SphK1 and SphK 2 inhibitor ABC294640 also shows Des1 inhibitory capacity as off-target effect. McNaughton and colleagues demonstrated that both ABC294640 and SKI II induce cell growth arrest in prostate cancer cells.[53]

From the apoptotic-inducing fenretinide to the autophagy-triggering resveratrol, the anti-proliferative effects of celecoxib, autophagy-mediated cancer cell death by THC, the effects SKI II on the cell cycle and autophagy, ABC294640 and SKI II induced cell growth arrest, each compound demonstrates different implications of Des1 activity inhibition. This helped to reveal the importance of dihydroceramides and contributed to the understanding of potential therapeutic interventions focused on Des1.

Nonetheless, the majority of Des1 inhibitors within this category are constituted by phenolic compounds or those containing redox-sensitive units. These compounds appear to exert their influence on Des1 activity by

---

Boya, P.; Goñi, F.; Guzmán, M.; Lovat, P.; Jäättelä, M.; Alonso, A.; Velasco, G. *Autophagy* **2016**, *12*, 2213-2229.

[52] Cingolani, F.; Casasampere, M.; Sanllehi, P.; Casas, J.; Bujons, J.; Fabriàs, G. *J. Lipid Res.* **2014**, *55*, 1711-1720.

[53] McNaughton, M.; Pitman, M.; Pitson, S.; Pyne, N.; Pyne, S. *Oncotarget*. **2016**, *7*, 16663-16675.

modulating the cellular redox state or disrupting the electron transport chain of the enzyme. Employing potential active site-directed inhibitors would offer more precise insights into the effects of specifically inhibiting Des1, thereby avoiding interference with other cellular mechanisms.

1.3.2 Sphingolipid analogues Des1 inhibitors

Although little information about Des1 active site is available, several rationally designed active site directed inhibitors of Des1 have been reported.

GT11 was the first sphingolipid analogue Des1 inhibitor (Figure 1.3) reported.[54] With little information available about the enzyme's active site, the authors rationally designed this ceramide based on studies demonstrating the inhibitory effect of cyclopropene fatty acids on different acyl-CoA desaturases.[55] Consequently, they envisioned the incorporation of a cyclopropene unit to replace the double bond in the ceramide structure. The cyclopropene-containing Des1 inhibitor, **GT11**, exhibited a dose-dependent inhibition of dihydroceramide desaturase 1, with an IC_{50} of 20 μM when it was evaluated in rat liver microsomes,[54] being a competitive inhibitor of Des1, exhibiting a K_i value of 6 μM.[56] The inhibition was postulated to involve a nucleophilic attack of a cysteine residue located in the Des1 active site to the cyclopropene ring, although this event was not confirmed.

A study performed with a **GT11** derivative revealed that Des1 inhibition led to an accumulation of dihydrosphingomielin in the cellular membrane,

[54] a) Triola, G.; Fabriàs, G.; Llebaria, A. *Angew. Chem.* **2001**, *113*, 2014–2016; b) Triola, G.; Fabriàs, G.; Llebaria, A. *Angew. Chem. Int. Ed.* **2001**, *40*, 1960–1962.

[55] Quintana, J.; Barrot, M.; Fabrias, G.; Camps, F. *Tetrahedron* **1998**, *54*, 10187-10198 (and references therein).

[56] Triola, G.; Fabriàs, G.; Casas, J.; Llebaria, A. *J. Org. Chem.* **2003**, *68*, 9924-9932.

altering its composition and reducing HIV-1 infection. These results identified Des1 as a potential therapeutic target against HIV-1 infection.[57]

With the knowledge that **GT11** is metabolized at the amido linkage and the hydroxyl group at C1,[58] G. Triola and coworkers synthesized a collection of **GT11** analogueues, evaluating the impact of each structural modification on Des1 inhibition (Figure 1.3).[56,59] The authors observed that removal, methylation, or replacement with fluorine of the primary hydroxyl group of **GT11** resulted in inactive compounds (**GT11-(a-c)**). None of the different stereoisomers of **GT11** exhibited activity, and substituting the cyclopropene ring with a *Z*-double bond or triple bond also yielded inactive analogues (**GT11-(d,e)**). As far as the amide functionality is concerned, loss of inhibition occurs with *N*-methyl substitution or replacement of the amide by a carbamate functionality (**GT11-(f,g)**). Conversely, urea, thiourea and α-ketoamide analogues maintained the inhibitory activity of **GT11**, although with lower potency (ranging from 40 to 70%) (**GT11-(h-l)**). Authors also assessed the effect of different *N*-acyl chain lengths (**GT11-(m-q)**); only the *N*-hexanoyl- (**GT11-o**) and *N*-decanoyl (**GT11-p**) analogueues retained inhibitory activity, with IC_{50} values of 31 and 13 μM respectively.

These revealing structure-activity relationship studies showed that the natural 2*S*, 3*R* stereochemistry of ceramide, a hydroxyl group at C-1, and the secondary amide functionality are mandatory for the enzyme inhibition. These studies paved the way for the design of ceramide analogues as active-site-directed Des1 inhibitors.

---

[57] Vieira, C. R.; Muñoz-Olaya, J. M.; Sot, J.; Jiménez-Baranda, S.; Izquierdo-Useros, N.; Abad, J. L.; Apellániz, B.; Delgado, R.; Martinez-Picado, J.; Alonso, A.; Casas, J.; Nieva, J. L.; Fabriàs, G.; Mañes, S.; Goñi, F. M. *Chem. Biol.* **2010**, *17*, 766-775.

[58] Triola, G.; Fabriàs, G.; Dragusin, M.; Niederhausen, L.; Broere, R.; Llebaria, A.; Van Echten-Deckert, G. *Mol. Pharmacol.* **2004**, *66*, 1671-1678.

[59] Bedia, C.; Triola, G.; Casas, J.; Llebaria, A.; Fabriàs, G. *Org. Biomol. Chem.* **2005**, *3*, 3707-3712.

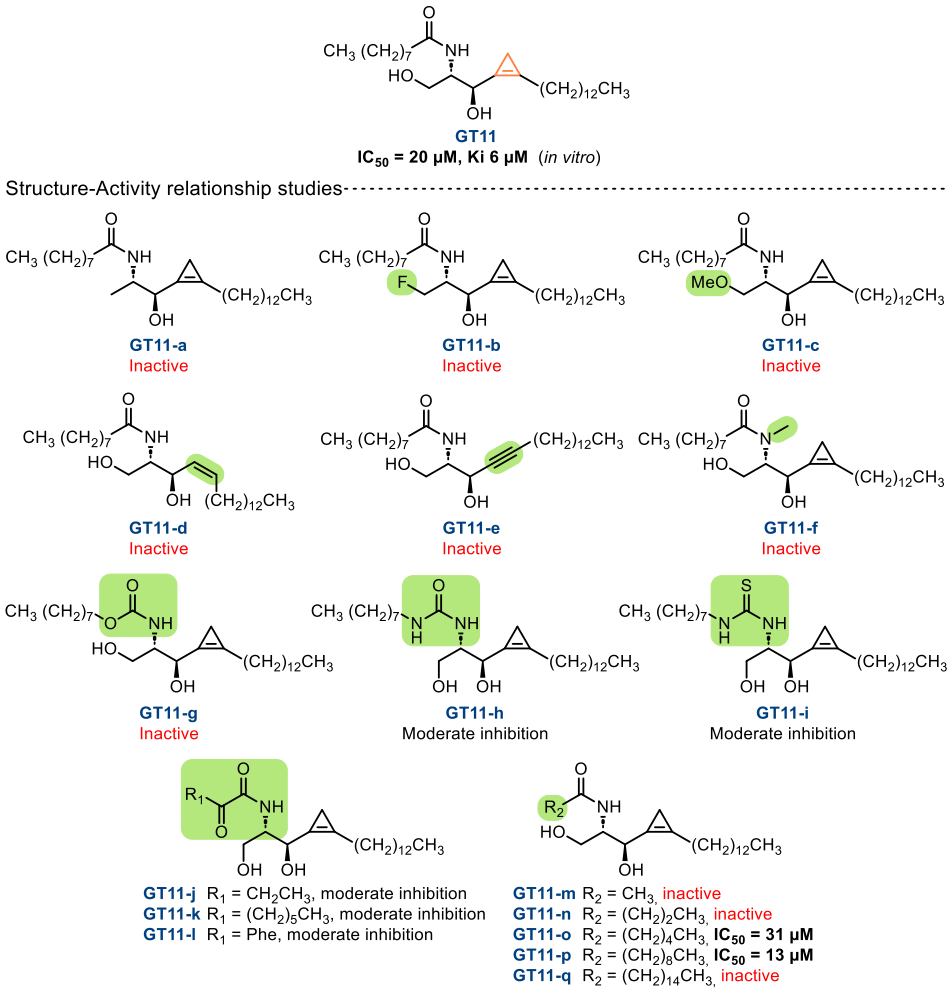

Figure 1.3. GT11 structure and compounds evaluated in structure-activity relationship studies.

J. M. Muñoz-Olaya reported an inhibitor in which the C5-methylene group in ceramide was replaced by a sulphur atom, **XM462** (Figure 1.4,a).[60] Des1 inhibition occurred both *in vitro* (in rat liver microsomes) with a IC_{50} 8.2 µM, and in Jurkat A3 human leukaemia cultured cells with IC_{50} 0.78 µM. *In vitro* experiments showed that **XM462** produced a mixed-type inhibition (Ki=

[60] Muñoz-Olaya, J. M.; Matabosch, X.; Bedia, C.; Egido-Gabas, M.; Casas, J.; Llebaria, A.; Delgado, A.; Fabriàs, G. *ChemMedChem* **2008**, *3*, 946-953.

2 μM, α= 0.83). Authors explain that **XM462** was designed taking into account previous reports on the activity of thiafatty acids as fatty acyl-CoA desaturases inhibitors.[61] Moreover, this sphingolipid analogue maintained the structural features identified as essential in SAR studies performed with **GT11**. Further research on differently *N*-acylated **XM462** analogueues, **RBM2-1(a-c)** (Figure 1.4, b) showed that these compounds inhibited Des1 in intact cells with different potencies, the most active analogue being the one bearing the same acyl chain as the that in the reference product, **RBM2-1a,** with an IC_{50} of 18 μM.

XM462 was used as a pharmacological tool to show the role of dhCer as inducer of autophagy in human gastric cancer cell line HGC27 with no signs of cell death.[62]

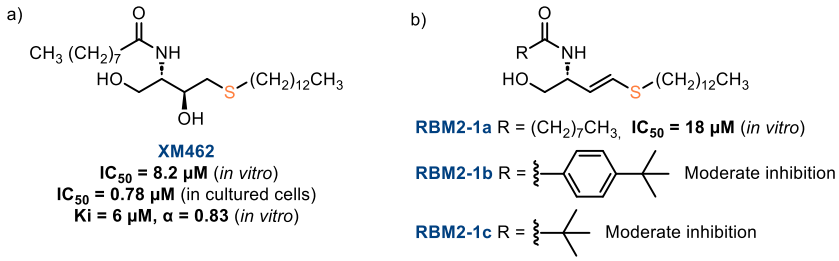

Figure 1.4. a) Structure of **XM462**. b) Structure of **XM462** analogues.

According to Des1 desaturation mechanism, authors postulate that enzyme inhibition caused by **XM462** could involve the generation of the intermediate carbon centred radical species **I**, in equilibrium with the sulphur radical **II** (Scheme 1.5). Inhibition could arise from coordination of the intermediate(s) to the diirondioxo complex or interaction with the disulfide bond(s) proposed to be present in the active site.[60]

---

[61] a) Buist, P. H.; Dallmann, H. G.; R. R. Rymerson, P. M. Seigel, P. Skala, *Tetrahedron Lett.* **1988**, *29*, 435-438. b) K. E. Høvik, Ø. S. Spydevold, J. Bremer, *Biochim. Biophys. Acta Lipids Lipid Metab.* **1997**, *1349*, 251-256.

[62] Gagliostro, V.; Casas, J.; Caretti, A.; Abad, J. L.; Tagliavacca, L.; Ghidoni, R.; Fabriàs, G.; Signorelli, P. *Int. J. Biochem. Cell Biol.* **2012**, *44*, 2135-2143.

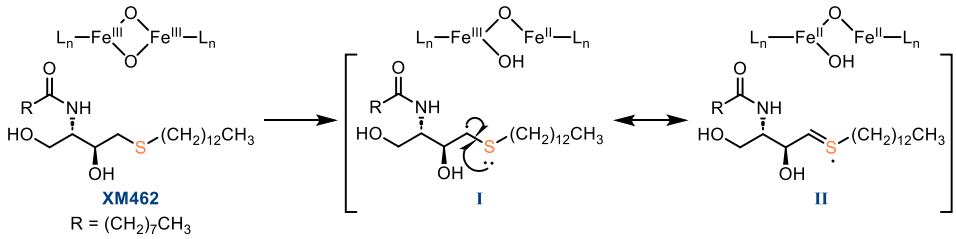

Scheme 1.5. Postulated Des1 inhibition mechanism by **XM462**.

Several reports demonstrate that *Z* and *E*-monoenoic fatty acids are good substrates of acyl-CoA desaturases, furnishing the corresponding conjugated dienes by introduction of an additional double bond. A. Pou and coworkers studied this event in the case of Des1, revealing another sphingolipd analogue Des1 inhibitor.[63] In this case, the introduction of a C6-C7 (*E*)-double bond into dihydroceramide structure furnished a potent Des1 inhibitor (Figure 1.5). Compound **III** inhibits Des1 activity in T98 and U87 cells with an IC_{50} of 0.155 μM. Authors described that dihydroceramide analogue **III** is a non-competitive reversible inhibitor with a K_i value of 111.4 nM. Interestingly, the Z isomer was a suitable Des1 substrate, and the corresponding $\Delta^{4,6}$ diene was detected after the enzymatic reaction.

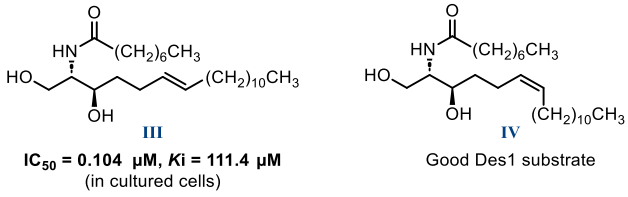

Figure 1.5. Structure of isomeric Δ^7-unsaturated dihydroceramide analogues.

A C12-dihydroceramide analogueue with a cyclopropane ring at C-5 and C-6 provoked a moderate inhibition of Des1 in cultured keratinocytes (Figure

[63] Pou, A.; Abad, J. L.; Ordóñez, Y. F.; Garrido, M.; Casas, J.; Fabriàs, G.; Delgado, A. *Chem. Commun.* **2017**, *53*, 4394-4397.

1.6, a).[64] This analogue was designed based on the oxidation mechanism of Des1. Authors postulated that the enzyme-catalysed homolytic cleavage of the C4-H bond within the sphingoid scaffold of **V** and subsequent opening of the cyclopropyl ring should lead to a delocalized radical intermediate that might covalently bind to the enzyme, provoking its inactivation. The inhibition mechanism of the analogue was not addressed during the report.

Finally, two dhCer analogueues with a fluorine atom replacing 3-hydroxyl group have been reported (Figure 1.6, b).[65] Compounds **VI** and **VII** showed a slight inhibition of Des1 activity, 9 % and 27 % respectively, when were evaluated in rat liver microsomes.

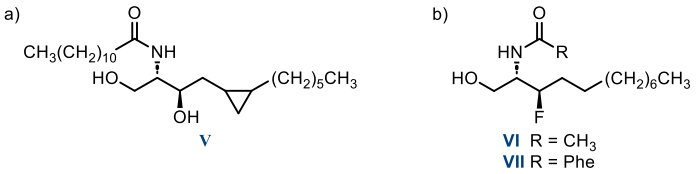

Figure 1.6. a) Structure of cyclopropane-containing dihydroceramide analogue **V**. b) Structure of fluorinated dihydroceramide analogues **VI** and **VII**.

Although examples of active-site directed Des1 inhibitors are scarce, potent inhibitors such as **GT11** or **XM462** have already been reported. Moreover, crucial structure-activity relationship studies had revealed important structural features that must be considered when designing new inhibitors. However, most of the Des1 inhibitors reported to the date were designed based on studies on acyl-CoA desaturases, as information about the Des1's active site is limited. While the previous strategy has proven successful, the synthesis and evaluation of ceramide analogues incorporating different structural features would enhance the understanding of the enzyme inhibition, hopefully contributing to the creation of new guidelines for the design of novel Des1 inhibitors.

---

[64] Brodesser, S.; Kolter, T. *J. Lipids.* **2011**, 724015.

[65] Jonghe, S.; Overmeire, I.; Calenbergh, S.; Hendrix, C.; Busson, R.; Keukeleire, D.; Herdewijn, P. *Eur. J. Org. Chem.* **2000**, 3177-3183.

1.4 Des1 as therapeutic target

Des1 stands as a pivotal catalyst in the conversion of dihydroceramide to ceramide, playing a crucial role in the intricate regulation of the dhCer/Cer rheostat. This regulatory mechanism is gaining prominence as a therapeutic target, particularly in the realms of cancer and HIV-1 infection.

Reports showing that dhCers are involved in cell cycle arrest,[53] apoptosis,[24, 49, 51] autophagy,[23, 46, 49, 51, 62] and oxidative stress underscore the interest of Des1 target for cancer therapy. Moreover, Des1 inhibition was related with clinically used drugs for cancer treatment.[23, 43, 44] The effects of these drugs, initially attributed to Cer, are now believed to involve dhCer. Notably, these drugs contain redox-sensitive units, suggesting that Des1 inhibition results from their ability to modify cellular redox status, a factor known to diminish Des1 activity. As for HIV infection, it has been reported that genetic and pharmacological blockade of Des1 induced a replacement of SM with dhSM in lipid rafts and inhibited cell infection by replication-competent and deficient HIV-1.[57]

The consequences of Des1 inhibition in the fluidity of plasma membrane microdomains holds significance in diseases where lipid rafts' integrity is vital, such as infectivity associated to cystic fibrosis[66] and Alzheimer's disease.[38] Furthermore, dihydrosphingolipids play an essential role in the development and maintenance of the nervous system, presumably due to modification of membrane biophysical properties.[67]

Lastly, Des1's involvement in cell cycle control during spermatogenesis hints at potential applications in addressing male infertility.[68]

---

[66] Zaidi, T.; Bajmoczi, M.; Golan, D. E.; Pier, G. B. *Investig. Ophthalmol. Vis. Sci.* **2008**, *49*, 1000-1009.

[67] Tzou, F. Y.; Hornemann, T.; Yeh, J. Y.; Huang, S. Y. *Prog. Lipid Res.* **2023**, *91*, 101236.

[68] a) Endo, K.; Akiyama, T.; Kobayashi, S.; Okada, M. *Mol. Genet. Genom.* **1996**, *253*, 157-165. b) Endo, K.; Matsuda, Y.; Kobayashi, S. *Dev. Growth Differ.* **1997**, *39*, 399-403.

In this context, Des1 stands out as a relevant therapeutic target. However, it presents a great challenge, as the X-ray crystal structure of the enzyme or any close homologue has never been reported, thus hampering the understanding of its mode of action and the design of active-site directed inhibitors. Moreover, the scarce number of Des1 inhibitors reported so far also complicates the task, as it is challenging to discern the key ligand-enzyme interactions involved in Des1 inhibition.

CHAPTER II

General Objectives

UNIVERSITAT ROVIRA I VIRGILI
TARGETING DES1: SYNTHESES OF CERAMIDE ANALOGUES WITH A RIGID SCAFFOLD, INHIBITORY ASSAYS, AND AF2-ASSISTED STRUCTURAL INSIGHTS REVEAL PR280 AS A POTENT INHIBITOR
Pablo Rivero Prieto

2.1 General Objectives

The scarcity of Des1 inhibitors reported in the literature, coupled with the lack of the enzyme's crystalline structure or any closely related homolog, has impeded a detailed understanding of its inhibition mechanism, thus complicating the design of novel Des1 inhibitors.

The objective of this thesis is to design ceramide analogues as potential Des1 inhibitors by replacing the ceramide double bond with a structural rigid motif that can enhance ligand-protein interactions. The biological evaluation of these ceramide analogues, each incorporating different structural rigid motifs, aims at elucidating the molecular events involved in enzyme's inhibition. In addition, through enhancing our understanding of the structure of the enzyme, these studies seek to establish a framework for designing new Des1 inhibitors by defining guidelines based on structural features. Ultimately, the identification of a new and more potent ceramide analogues as a Des1 inhibitor is a desirable outcome.

The thesis has been divided into different chapters, each one with specific objectives:

Chapter III: Synthesis and biological evaluation as Des1 inhibitors of heterocycle containing ceramide analogues.

The aim of this chapter is to evaluate the effect on Des1 activity provoked by ceramide analogues incorporating 1,4-disubstituted triazole, 1,5-disubstituted triazole and 2,4-disubstituted furan moieties. For this purpose, the following aspects will be explored:

- Synthesis of ceramide analogues incorporating 1,4- or 1,5-disubstituted 1,2,3-triazoles and 2,4-disubstituted furan moieties.
- Synthesis of the *N*-hexanoyl, *N*-octanoyl, and *N*-decanoyl derivatives of the ceramides mentioned above to generate diversity and ensure good cell permeability.

- Evaluation of the synthetized analogues as Des1 inhibitors in intact cells and in cell lysates.

Chapter IV: Unveiling structural insights into Des1 using AlphaFold2: Towards the proposal of novel Des1 inhibitors

During the course of this thesis, AlphaFold2 (AF2) appeared at the 14th Critical Assessment of Techniques for Protein Structure Prediction (CASP). This software offered a highly confident 3D model for Des1 predicted from the amino-acid sequence of the enzyme.

Working with the AF2 predicted model of Des1, this chapter is focused on gaining structural insight of the enzyme and reveal the molecular events underlying enzyme inhibition in order to give a rationale for the design of new inhibitors. Working in collaboration with Professor Xavier Barril (ICREA Research Professor, University of Barcelona) the following specific objectives are addressed:

- Construction of a complete model of the enzyme incorporating the Fe_2O_2 species involved in enzyme's catalytic activity.
- Docking calculations of most relevant Des1 inhibitors (**GT11** and **XM462**) along with the natural substrate **dhCer**, for the identification of the ligand-protein key interactions necessary for enzyme inhibition.
- Docking calculations of previously synthetized heterocycle containing ceramide analogues described in Chapter III.
- Proposal of new Des1 inhibitor candidates sustained by docking calculations and structure-activity relationships.

Chapter V: Synthesis and biological evaluation as Des1 inhibitors of cyclopropenone containing ceramide analogues and derivatives.

The studies performed in the previous two chapters of this thesis led to the proposal of new Des1 inhibitors candidates. The aim of this chapter is to synthetize and evaluate these candidates as Des1 inhibitors. The specific objectives are the following:

- Synthesis of cyclopropenone ceramide analogues
- Derivatization of cyclopropenone ceramide analogue with Lawesson reagent or phosphorus pentasulfide to access cyclopropenethione ceramide analogue.
- Derivatization of cyclopropenone ceramide analogue through [3+2] cycloaddition with elemental sulphur to access 1,2-thiole-3-one ceramide analogue. Mechanistic study of the reaction.
- Evaluation of the cyclopropenone ceramide analogue and derivatives as Des1 inhibitors.

Chapter VI: Development of a Ru-catalysed RCM reaction on CPG-coupled DNA for the synthesis of DNA-encoded macrocyclic library.

The last chapter of the present PhD work describes the research carried out during a predoctoral stay at TU Dortmund under the supervision of Andreas Brunschweiger.

The objective of this chapter is to develop a Ru-catalysed RCM reaction on CPG-coupled DNA. The specific objectives are the following:

- Synthesis of a set of CPG-DNA diene conjugates.
- Evaluation of three different Ru-based catalysts (G-III, HG-II and DA) for the RCM.
- Screening of the best conditions for the RCM reaction on CPG-coupled DNA.
- Application of the best CPG-coupled DNA RCM conditions on a set of CPG-DNA diene conjugates. Identification, purification, and isolation of the cyclized products.

UNIVERSITAT ROVIRA I VIRGILI
TARGETING DES1: SYNTHESES OF CERAMIDE ANALOGUES WITH A RIGID SCAFFOLD, INHIBITORY ASSAYS, AND AF2-ASSISTED STRUCTURAL INSIGHTS REVEAL PR280 AS A POTENT INHIBITOR
Pablo Rivero Prieto

CHAPTER III

Synthesis and biological evaluation as Des1 inhibitors of heterocycle containing ceramide analogues

UNIVERSITAT ROVIRA I VIRGILI
TARGETING DES1: SYNTHESES OF CERAMIDE ANALOGUES WITH A RIGID SCAFFOLD, INHIBITORY ASSAYS, AND AF2-ASSISTED STRUCTURAL INSIGHTS REVEAL PR280 AS A POTENT INHIBITOR
Pablo Rivero Prieto

3.1 Introduction

The primary objective of this chapter is to synthetize a novel family of ceramide analogues as potential Des1 inhibitors. In the design and synthesis of the sphingolipid analogues, we focused on incorporating a rigid scaffold in place of the ceramide double bond, all while preserving the structural characteristics identified as essential for Des1 inhibition in previous SAR studies; that is, a (2*S*)-2-amino,3-alcohol moiety in *anti*-disposition, a free hydroxyl groups at C1 and a secondary amide functionality (Figure 3.1).[1]

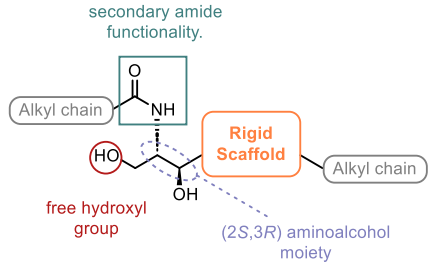

Figure 3.1. General structure of Ceramide analogues proposed as Des1 Inhibitors candidates.

Taking **GT11** as a reference,[2] the strategy chosen in the design of ceramide analogues involved the selection of a rigid scaffold capable of establishing additional interactions with the enzyme's binding site when compared to the cyclopropene ring present in **GT11**. The objective is to enhance ligand-protein interactions and, consequently, increase enzyme inhibition.

As previously mentioned, the primary challenge in designing new Des1 inhibitors is the absence of the crystalline structure of the enzyme, and

[1] a) Triola, G.; Fabriàs, G.; Casas, J.; Llebaria, A. *J. Org. Chem.* **2003**, *68*, 9924-9932. b) Bedia, C.; Triola, G.; Casas, J.; Llebaria, A.; Fabriàs, G. *Org. Biomol. Chem.* **2005**, *3*, 3707-3712. c) Camacho, L.; Simbari, F.; Garrido, M.; Abad, J. L.; Casas, J.; Delgado, A.; Fabriàs, G. *Bioorg. Med. Chem.* **2012**, *20*, 3173-3179. d) Casasampere, M.; Ordoñez, Y. F.; Pou, A.; Casas, J. *Chem. Phys. Lipids* **2016**, *197*, 33-44.

[2] a) Triola, G.; Fabrias, G.; Llebaria, A. Angew. Chem. **2001**, *113*, 2014–2016; b) Triola, G.; Fabrias, G.; Llebaria, A. *Angew. Chem. Int. Ed.* **2001**, *40*, 1960–1962.

consequently, the lack of precise structural information regarding the enzyme's active site. In 2017, a statistical analysis of the nature, geometry and frequency of atomic interactions between small molecule ligands and their receptors, as available in the PDB, was conducted.[3] Given the limited specific data for Des1 active site, this study offered useful information for the design of Des1 inhibitor candidates.

The research, conducted with 11.016 structures of small-molecule ligands bound to proteins meeting the investigators criteria, revealed that hydrophobic interactions were overwhelmingly the most prevalent interaction in protein-ligand complexes. Specifically, these interactions were predominantly observed between an aromatic ring of the ligand and an aliphatic moiety of the receptor, highlighting the prevalence of aromatic groups in small molecules inhibitors. Hydrogen bonds emerged as the second most frequent interaction type. However, the contribution of a hydrogen bond to binding can be either modest or even penalizing if the newly formed interaction does not offset the desolvation penalty associated.[4] In third place, π-stacking interactions were identified. This observation is not surprising, as is well-known that non-covalent interactions involving aromatic rings play a pivotal role in protein-ligand recognition and, consequently, into drug design.[5] An illustrative example, highlighting the importance and diversity of aromatic interactions, is found in the complex between the enzyme acetylcholinesterase (AChE) and the anti-Alzheimer drug **E2020** (Figure 3.2).[6] Thus, the experimental structure of the complex shows that **E2020** has a unique orientation along the active site in which multiple specific aromatic π-stacking interactions are responsible for the high affinity and selectivity of the drug towards the enzym.

---

[3] de Freitas, R. F.; Schapira, M. *Med. Chem. Commun.* **2017**, *8*, 1970-1981.

[4] Williams, D. H.; Westwell, M.S. *Chem. Soc. Rev.* **1998**, *27*, 57–64.

[5] Meyer, E. A.; Castellano, R. K.; Diederich, F. *Angew. Chem. Int. Ed.* **2003**, *42*, 1210 – 1250.

[6] a) Kryger, G.; Silman, I.; Sussman, J. L. *J. Physiol.* **1998**, *92*, 191 –194. b) Kryger, G.; Silman, I.; Sussman, J. L. *Structure* **1999**, *7*, 297 – 307.

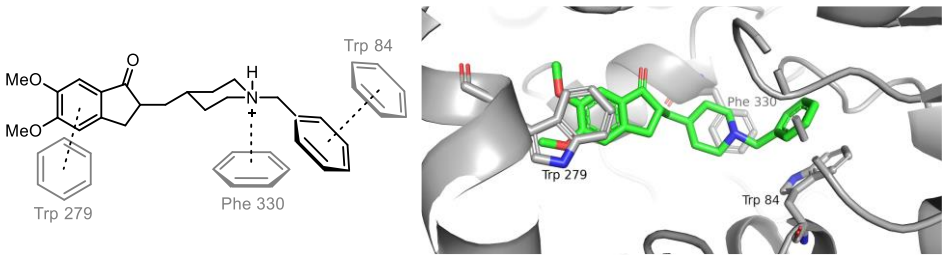

Figure 3.2 Binding mode of the anti-Alzheimer drug **E2020** within the active site of acetylcholinesterase from *Torpedo californica* (PDB code: 1EVE).[6]

This systematic analysis underscores not only the importance of well-known interactions, such as those of hydrophobic character, hydrogen bonds and π-stacking interactions, but also sheds light on interaction types that are occasionally overlooked in medicinal chemistry. One notable finding is the prevalence of weak C-H···O hydrogen bonds as the fourth most frequent interaction type found. The existence of these so-called weak hydrogen bonds is well documented.[7] They display variable a variable geometry,[8] have shown to be relevant in the protein-ligand complexes. Due to the smaller desolvatation penalty associated with their formation, they can sometimes compete favourably with the N-H···O and O-H···O hydrogen bonds.[9] Its importance in proteins and drug binding interactions has been demonstrated in the case of kinase inhibition, for which, a survey of biomolecular crystal structures provided compelling evidence for the existence of aromatic CH hydrogen bonds, especially for C-H groups adjacent to positively charged nitrogen atoms or different heteroatoms.[10]

[7] a) T. Steiner *New J. Chem.* **1998**, *22*, 1099–1103. b) S. Scheiner *Phys. Chem. Chem. Phys.* **2011**, *13*, 13860-13872.

[8] Panigrahi, S. K.; Desiraju, G. R. *Proteins* **2007**, *67*, 128–141.

[9] Panigrahi, S. K.; Desiraju, G. R. *Proteins* **2004**, *54*, 247–259.

[10] Pierce, A. C.; Sandretto, K. L.; Bemis, G. W. *Proteins* **2002**, *49*, 567–576.

In this context, we envisioned the synthesis of *N*-acyl sphingoid bases as potential Des1 inhibitors, incorporating 1,4- or 1,5-disubstituted 1,2,3-triazoles and 2,4-disubstituted furan moieties (Figure 3.3). The synthesis of complementary 1,4- and 1,5-regioisomeric disubstituted 1,2,3-triazoles will allow to evaluate the impact of different geometries in the final analogue. This proposal is justified by the previously reported significance of geometry in Des1 inhibition.[11] Additionally, short *N*-hexanoyl (**a**), octanoyl (**b**) and decanoyl (**c**) derivatives were proposed to generate diversity and ensure good cell permeability. The presence of these specific chain lengths have proved to be beneficial for the activity of **GT11** derivatives, whereas **GT11** analogues with shorter and longer alkyl chains in the amide moiety resulted inactive in Des1 inhibition.[1a]

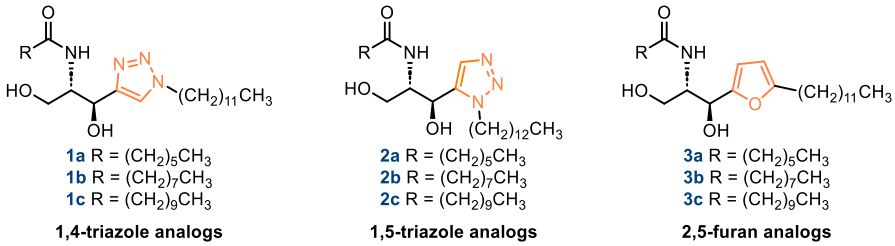

Figure 3.3. Heterocycle-containing ceramide analogues proposed as Des1 inhibitors candidates.

These inhibitors candidates incorporate a heterocycle as a rigid spacer between the head group and the lipophilic tale. The heterocyclic moiety could stablish π-stacking or H-bond interactions with the enzyme-binding site. As previously stated, these interactions show high prevalence in ligand-protein complexes and have not been explored yet for the inhibition of Des1. Previously reported ceramide analogue Des1 inhibitors rely mainly on the incorporation of hydrophobic groups in the sphingolipid structure (see introduction 1.3.2). Therefore, the proposed analogues could not only provide

[11] Pou, A.; Abad, J. L.; Ordóñez, Y. F.; Garrido, M.; Casas, J.; Fabriàs, G.; Delgado, A. *Chem. Commun.* **2017**, *53*, 4394-4397.

an enhance inhibition of the enzyme but also give some information about the nature of the enzyme active site, as this kind of structures have never been evaluated in the structure-activity relationship studies previously performed with Des1.[1]

3.1.1 Significance of 1,4 and 1,5-disubtituted 1,2,3-triazoles as pharmacophoric groups

The 1,2,3-triazole ring has emerged as an important motif in drug discovery due to the diverse and potent pharmacological activities that triazole derivatives present.[12] The triazole ring is present as a core structural component in an array of drug categories, such as antimicrobial, anti-inflammatory, analgesic, antiepileptic, antiviral, antineoplastic, antihypertensive, antimalarial, local anaesthetic, antianxiety, antidepressant, antihistaminic, antioxidant, antitubercular, anti-Parkinson's, antidiabetic, antiobesity and immunomodulatory agents, among others. The number of 1,2,3-triazole-containing drugs approved for clinical use is still limited (some examples shown in Figure 3.4). However, taking into account the synthetic contributions of Folkin and Meldal[13] and the advantageous properties of this heterocycle as a pharmacophoric group, one can expect the number to grow in next years.

[12] Kharb, R.; Sharma, P. C.; Yar, M. S. J. *Enzyme Inhib. Med. Chem.* **2011**, *26*, 1-21.

[13] See section: 3.2.3 Azide-alkyne 1,3-dipolar cycloadditions

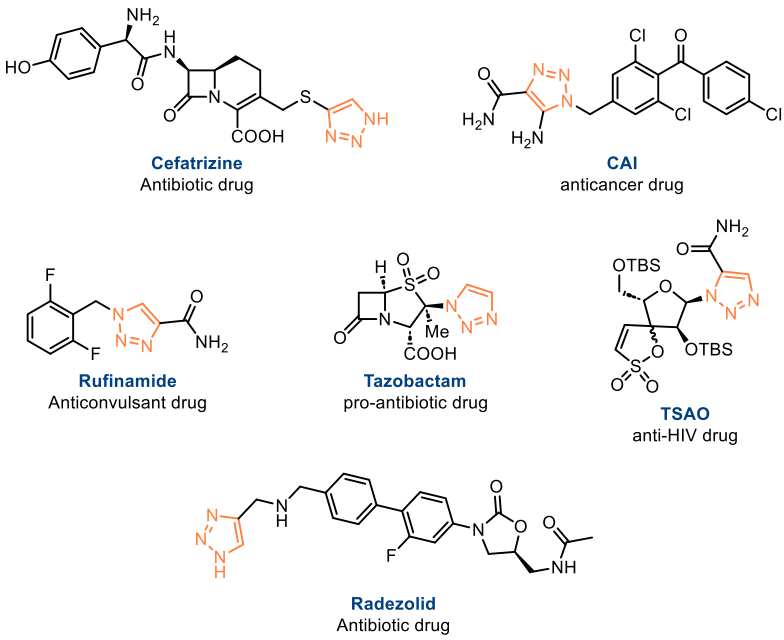

Figure 3.4. Some examples of pharmaceuticals approved for clinical use containing 1,2,3-triazole moieties.

The triazole motif can be readily synthesized through 'click' chemistry via copper- or ruthenium-catalysed azide-alkyne cycloaddition reactions.[13] [13] The advantages provided by click chemistry favours the use of 1,2,3-triazole moiety as 'linker' in medicinal chemistry, to build various structural hybrids like nucleoside, pyrimidine, naphthoquinone, betulinic acid, calanolide, and usnic acid enamine coupled analogues (Figure 3.5).[14] These 1,2,3-triazole-containing hybrids have demonstrated an enriched pharmacological activity profile in relation to that of the parent compound, showing the importance of the triazole ring.[15] The heterocycle, far from being an innocent linker, stablishes interaction with the enzyme in several examples. Moreover, as a structural rigid motif, it directs the spatial arrangement of the two fused units

[14] Rammohan, A.; Venkatesh, B. C.; Basha, N. M.; Zyryanov, G. V.; Nageswararao, M. *Chem. Biol. Drug Des.* **2023**, *101*, 1181-1203.

[15] Bozorov, K.; Zhao, J.; Aisa, H. A. *Bioorg. Med. Chem.* **2019**, *27*, 3511–3531.

in the enzyme-binding site. These distinctive properties of triazoles in hybrid compounds underscore their importance in the context of drug design.

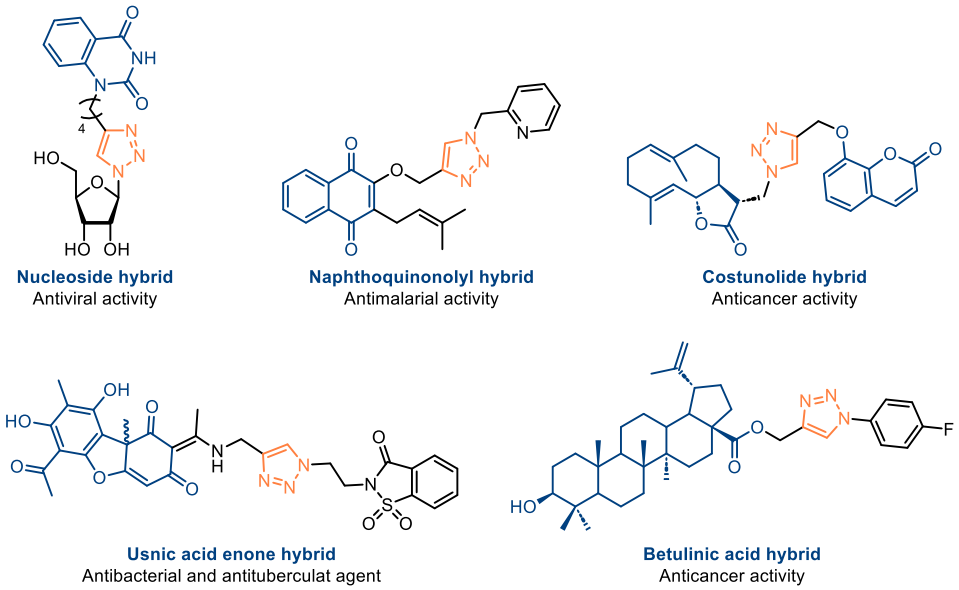

Figure 3.5. Examples of some natural pharmacophore-1,2,3-triazole hybrids with reported biological activity.

This heterocycle is relevant for drug discovery not just because its reliability as linking unit but also because of its favourable physicochemical properties.[16] It displays a strong dipole moment: the experimentally measured value for a tautomeric mixture of 1*H* and 2*H*-1,2,3-triazoles is 1.85 D at 25 ˚C (Figure 3.6, a), showing great agreement with theoretical values.[17] Abboud *et al.* provided theoretical dipole moment values calculated at the B3LYP/6-31G* level of 4.18 D and 5.06 D for 1,4 and 1,5-disubstituted 1,2,3-triazoles, respectively (Figure 3.6, b).[18] This strong dipole moment is expected to

[16] Kolb, H. C.; Sharpless, K. B. *Drug Discovery Today* **2003**, *8*, 1128-1137.

[17] Massarotti, A.; Aprile, S.; Mercalli, V.; Del Grosso, E.; Grosa, G.; Sorba, G.; Tron, G. C. *ChemMedChem* **2014**, *9*, 2497-2508.

[18] Abboud, J.L.; Foces-Foces, C.; Notario, R.; Trifonov, R.; Volovodenko, A.; Ostrovskii, V.; Alkorta, I.; Elguero, J. *Eur. J. Org. Chem.* **2001**, 3013-3024.

enhance the strength of both hydrogen bonds and π-stacking interactions stablished by the heterocycle.

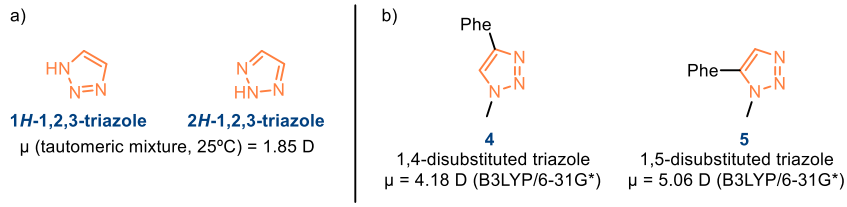

Figure 3.6. a) 1*H* and 2*H*-1,2,3-triazoles. b) 1,4 and 1,5-disubstituted 1,2,3-triazoles with reported theorical dipole moments values by Abboud *et al*.[18]

The aromatic character of 1,2,3-triazoles is well-stablished.[19] Thus, triazole moiety can participate in π-stacking interactions with aromatic amino acids of the enzyme active site. Multiple examples of these interactions can be found in the Protein Data Bank. For instance, in the enzyme *Acetylcholinesterase*, the 1,4-triazole present in enzyme's inhibitor compound **6**, engages in a face-face π-stacking interaction with phenylalanine residue Phe338 of the active site(Figure 3.7, a).[20] In the case of *carbonic anhydrase II* a 1,5-triazole ring, part of a complex with *p*-(5-ferrocenyl-1*H*-1,2,3-triazol-1-yl)benzenesulfonamide, **7**, takes part of an edge-face π-stacking interaction with Phe130 (Figure 3.7, b).[21]

[19] Kotelevskii, S. I.; Prezhdo, O. V. *Tetrahedron*, **2001**, *57*, 5715-5729.
[20] Bourne, Y.; Radic, Z.; Taylor, P.; Marchot, P. *J. Am. Chem. Soc.* **2010**, *132*, 18292–18300.
[21] Salmon, A. J.; Williams, M. L.; Hofmann, A.; Poulsen, S. A. *Chem. Commun.* **2012**, *48*, 2328–2330.

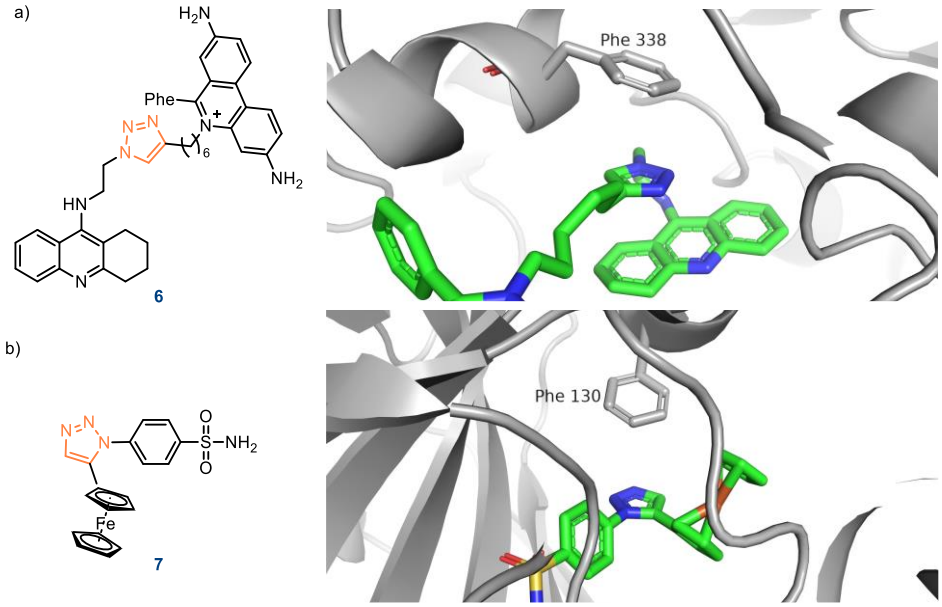

Figure 3.7. π-stacking interactions stablished between a 1,2,3-triazole ring and an amino-acid of the enzyme's active site: a) 1,4-triazole-Phe 338 face-face π-stacking interaction (PDB ID: 2XUF). b) 1,5-triazole-Phe130 edge-face π-stacking interaction (PDB ID: 3P3H).

1,2,3-triazoles play a versatile role in H-bond interactions within biological systems. They can serve as H-bond acceptor, owing to the presence of lone pairs on nitrogen atoms N2 and N3. Additionally, the "acidic" C-H bond within the triazole ring can also function as a weak H-bond donor (Figure 3.8).

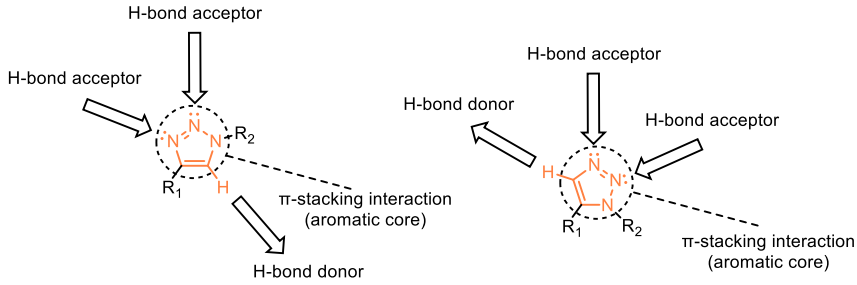

Figure 3.8. Summary of 1,2,3-triazole potential binding interactions.

Within the X-ray crystal structures of protein-ligand complexes accessible in the Protein Data Bank, there are also examples of triazole groups in ligands engaging in the aforementioned H-bond interactions. As an illustration, in the complex of compound **8** with *Enterobacter cloacae 908R beta-lactamase*, the triazole ring acts as an H-bond acceptor via its N2 atom, interacting with the amido functionality of Gln120 (Figure 3.9, a).[22] An example of a 1,4-disubstituted triazole ring acting as a weak H-bond donor can be find in the complex formed by *N*-glycoside **9** and *glycogen phosphorylase b* (Figure 3.9, b), in which one of the carbonylic oxygen of the protein backbone interacts with the C-H of the triazole moiety.[23]

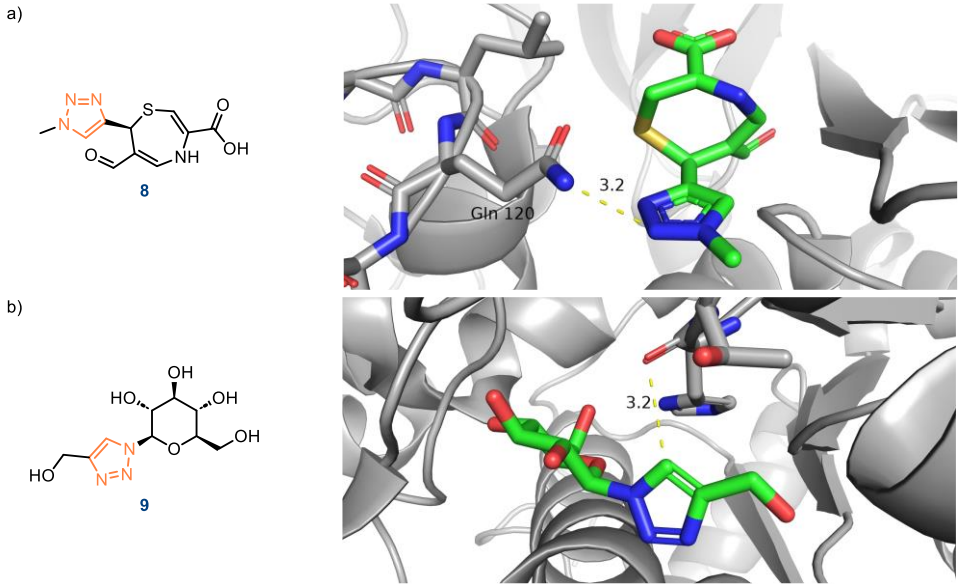

Figure 3.9. Exemples of H-bond interactions stablished between a 1,2,3-triazole ring and an amino-acid residue of the enzyme's active site: a) 1,4-disubstituted triazole as H-bond acceptor through N2 atom (PDB ID: 1Y54). b) 1,4-disubstituted triazole as a weak H-bond donor (PDB ID: 3G2I).

[22] Michaux, C.; Charlier, P.; Frère, J. M.; Wouters, J. *J. Am. Chem. Soc.* **2005**, *127*, 3262–3263.

[23] Chrysina, E. D.; Bokor, É.; Alexacou, K. M.; Charavgi, M. D.; Oikonomakos, G. N.; Zographos, S. E.; Leonidas, D. D.; Oikonomakos, N. G.; Somsák, L. *Tetrahedron: Asymmetry* **2009**, *20*, 733-740.

The structural features of 1,2,3-triazoles enable them to mimic different functional groups. For that reason, this motif has been widely used as bioisoster of other functionalities for the synthesis of new active molecules. In this sense, amide group replacement is the predominant approach reported in the literature. Furthermore, heterocyclic replacement is also usual (in particular five-member nitrogen-containing cycles), while esters and carboxylic acids replacements are less common.[24] Moreover, 1,2,3-triazoles, being flat bivalent elements, mimic the rigid conformational constrain exerted by double bonds while avoiding typical olefin drawbacks, such as isomerization or *in vivo* degradation. A good example of this bioisosterism in drug design is found in combretastatin A-4 (CA-4), an anti-mitotic agent acting against tubulin. CA-4 is a *cis*-configured stilbene, which is readily converted to the thermodynamically more stable, but less potent *trans*-isomer. Substitution of the *cis* double bond by a 1,2,3-triazole moiety provided a more potent analogue.[25]

The aforementioned pharmacophoric properties of 1,4- and 1,5-disubstituted 1,2,3-triazoles strongly encourages the synthesis of ceramide analogues incorporating these heterocycles. The presence of 1,2,3-triazole group is expected to increase the binding of these substrates with Des1 by the formation of π-stacking interactions and/or additional dipole-dipole interactions.

The synthesis of the two triazole regiosiomers would allow the evaluation of the geometry effects on inhibition. On one hand, 1,5-disubstituted-1,2,3-triazole would mimic the geometry of a *cis*-double bond, as the cyclopropene ring does in the case of **GT11** but offering extra interaction possibilities with the enzyme. Furthermore, it is believed that Des1 inhibition by **GT11** can be

[24] Bonandi, E.; Christodoulou, M. S.; Fumagalli, G.; Perdicchia, D.; Rastelli, G.; Passarella, D. *Drug Discov. Today*, **2017**, *10*, 1572-15821.

[25] Madadi, N. R.; Penthala, N. R.; Howk, K.; Ketkar, A.; Eoff, R. L.; Borrelli, M. J.; Crooks, P. A. *Eur. J. Med. Chem.* **2015**, *103*, 123-132.

an irreversible process by reaction of the cyclopropene ring with a cysteine residue of the desaturase active centre. Unlike the cyclopropene, the triazole moiety is unreactive towards cysteine residues. Thus, results of biological assays from these triazole derivatives could also bring light to the inhibition mechanism of this enzyme. Similar interactions but with a different geometry can be stablish by 1,4-disubstituted-1,2,3-triazoles. This would allow elucidating the importance of polar interactions and geometry in ceramide analogues as Des1 inhibitors.

3.1.2 Furan as pharmacophoric group

The furan ring is considered a relevant moiety in drug discovery, with applications in a wide range of treatments in the field of medicinal chemistry.[26] Thus, this heterocyclic structure can be found in several commercially available drugs (Figure 3.10) with antimicrobial (antibacterial, antifungal, and antiviral) and, central nervous system activities (antidepressant, anxiolytic, anticonvulsant, antiparkinsonian, in addition to their effect on Alzheimer's disease), as well as muscle relaxant, anti-glaucoma, cardiovascular, anti-ulcer, anti-inflammatory, analgesic, antioxidant, and anticancer properties.

[26] Saeid, H.; Al-sayed, H.; Bader, M. *Alq. J. Med. App. Sci.* **2023**, *1*, 44-58.

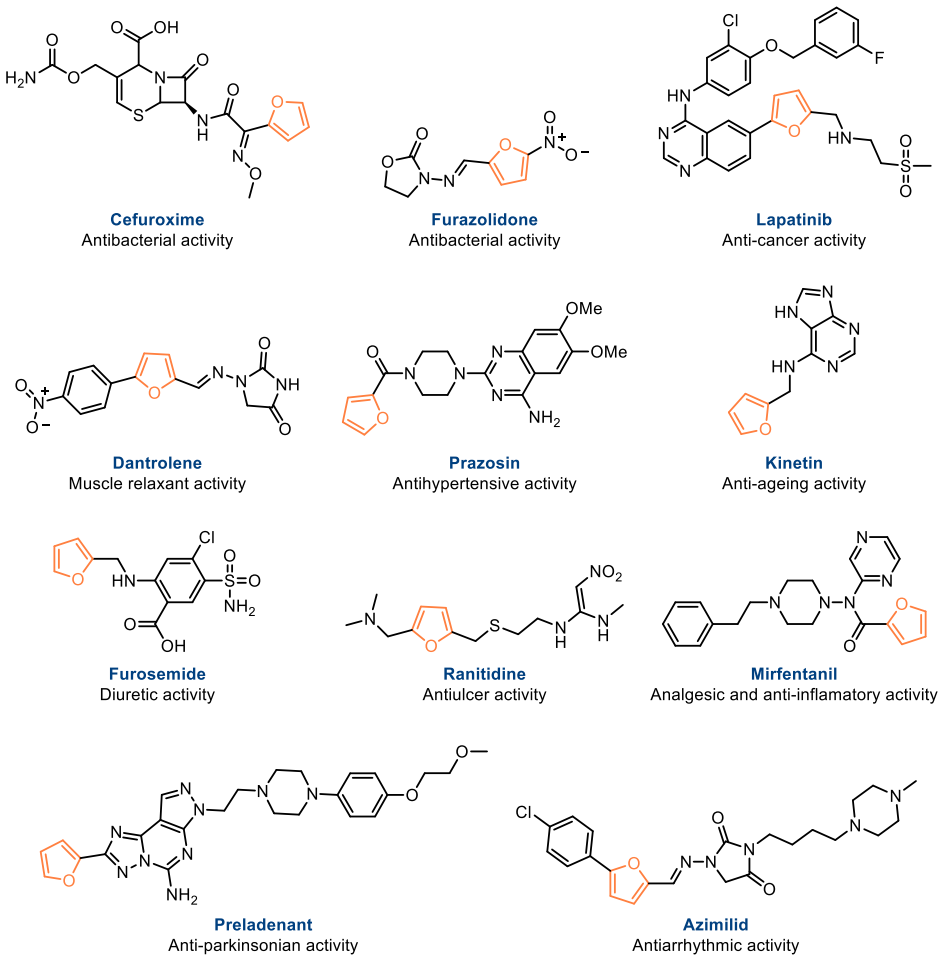

Figure 3.10. Some examples of clinical approved drugs containing a furan ring.

The aromatic nature of furan ring is well-stablished.[16] Although its aromaticity can be considered modest, the capacity of this heterocycle to form favourable π-stacking interactions has been documented,[27] different examples can be found in the Protein Data Bank. For instance, the furan ring of the antibiotic Cefuroxime interacts with phenyalanine Phe225 in the *penicillin-binding protein D2* (PBPD2) from *Listeria monocytogenes* by an edge-face

[27] Huber, R. G.; Margreiter, M. A.; Fuchs, J. E.; von Grafenstein, S.; Tautermann, C. S.; Liedl, K. R.; Fox, T. J. *Chem. Inf. Model.* **2014**, *54*, 1371-1379.

π-interaction (Figure 3.11, a).[28] In the complex between the diuretic Furosemide and *rAceMIF* tautomerase, anotherr edge-face π-stacking interaction was observed, involving in this case phenylalanine Phe108 (Figure 3.11, b).[29]

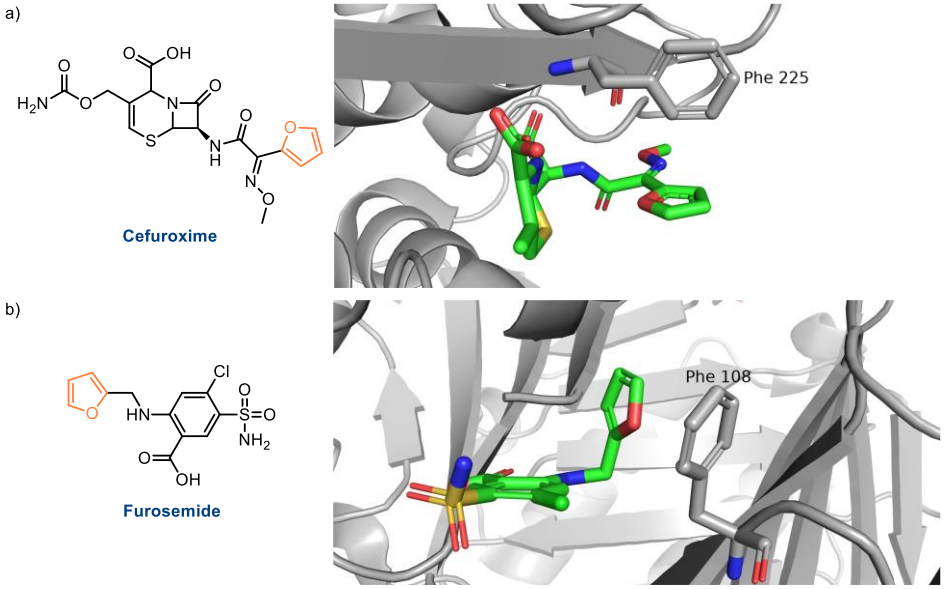

Figure 3.11 Examples of edge-face π-stacking interactions stablished between furan ring and amino acid residues of enzyme's active site. a) PBPD2 complex with Cefuroxime (PDB ID: 5ZQE). b) rAceMIF tautomerase complex with Furosemide (PDB ID: 3RF4).

Examples of furan ring stablishing face-face π-stacking interactions are also found in the PDB (Figure 3.12). In the complex of the antibiotic Furazolidone with the antibody *SPE7*, the furan ring interacts with a tryptophan residue, Trp93, of the enzym.[30] In the same way, the complex between *Bet* v1, major birch pollen allergen, and the plant hormone kinetin

[28] Jeong, J. H.; Cha, H. J.; Kim, Y. G. *Antimicrob. Agents Chemother.* **2018**, *62*, e00796-18.
[29] Cho, Y.; Vermeire, J. J.; Merkel, J. S.; Leng, L.; Du, X.; Bucala, R.; Cappello, M. *Chem. Biol.* ***2011***, *18*, 1089-1101.
[30] James, L. C.; Roversi, P.; Tawfik, D. S. *Science*, **2003**, *299*, 1362-1367.

shows a face-face π-stacking interaction between the furan ring and phenylalanine residue Phe22.[31]

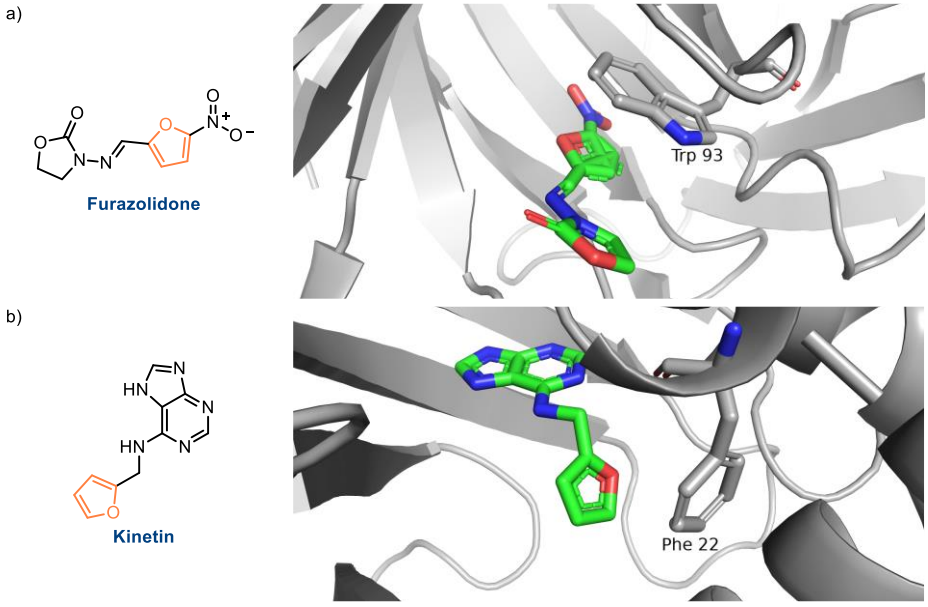

Figure 3.12 Examples of face-face π-stacking interactions stablished between furan ring and an amino-acid of enzyme's active site. a) SPE7 complex with Furazolidone (PDB ID: 1OAY). b) Bet v1 complex with Kinetin (PDB ID: 4A86).

Furan ring can also act as an H-bond acceptor due to the lone pair of the oxygen atom. Furthermore, a hydrogen bond donor compound may interact with the π system of this heterocycle.[32]

[31] Kofler, S.; Asam, C.; Eckhard, U.; Wallner, M.; Ferreira, F.; Brandstetter, H. *J. Mol. Biol.* **2012**, *422*, 109–123.

[32] a) Samanta, U.; Chakrabarti, P.; Chandrasekhar, J. *J. Phys. Chem. A* **1998**, *102*, 8964-8969. b) Jiang, X.; Tsona, N. T.; Tang, S.; Du, L. *Spectrochim. Acta A Mol. Biomol. Spectrosc.* **2018**, *191*, 155-164. c) Huang, D. M.; Wang, Y. B.; Visco, L. M.; Tao, F. M. *J. Phys. Chem. A* **2004**, *108*, 11375–11380.

In the complex formed between *adenosine A2A receptor* and preladenant conjugate **PSB-2113**[33] (Figure 3.13) the oxygen atom of the furan ring is interacting as H-bond acceptor with an asparganine residue (Asn253) of the protein active site.

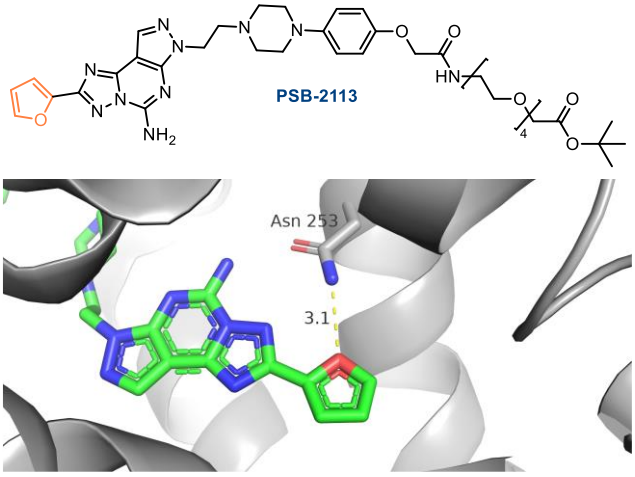

Figure 3.13 H-bond interaction between the furan ring of **PSB-2113** and Asn253 residue in *adenosine A2A receptor*. (PDB ID: 7PX4).

The aforementioned pharmacophoric properties of the 1,4- or 1,5-disubstituted 1,2,3-triazoles and 2,4-disubstituted furan moieties, as well as their prevalence in pharmacological active drugs, strongly encourages the synthesis of ceramide analogues incorporating these heterocycles.

[33] Claff, T.; Klapschinski, T. A.; Subhramanyam, U. K. T.; Vaassen, V. J.; Schlegel, J. G.; Vielmuth, C.; Voss, J. H.; Labahn, J.; Müller, C. E. *Angew. Chem.Int. Ed.* **2022**, *61*, e202115545.

3.2 Retrosynthetic analysis and synthetic background

3.2.1 Retrosynthetic analysis of heterocycle containing ceramide analogues

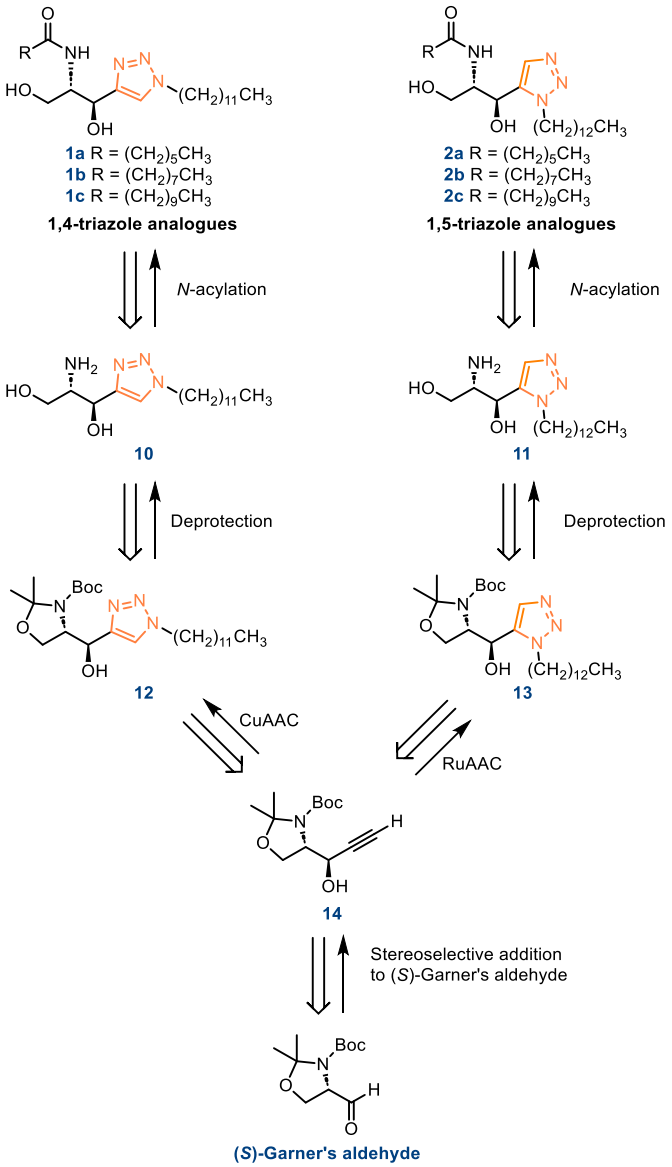

Scheme 3.1. Retrosynthetic analysis of targeted triazole ceramide analogues (**1a-c**, **2a-c**).

Targeted ceramide analogues **1a-c** and **2a-c** would be obtained through *N*-acylation of aminodiol **10** and **11** respectively (Scheme 3.1), generated by deprotection of *tert*-butyloxycarbonyl (Boc) and isopropylidene ketal protecting groups of triazole containing compounds **12** and **13**. Synthesis of triazole moieties was envisioned through a common propargylic alcohol intermediate, **14**. The synthesis of the 1,4-disubtituted-1,2,3,-triazole regioisomer in **12** should be possible through a Cu-catalyzed azide-alkyne 1,3-cycloaddition of **14** and dodecyl azide. Contrary, the 1,5-disubstituted-1,2,3,-triazole regioisomer in **13** should be generated by a less conventional azide-alkyne cycloaddition with tridecyl azide catalysed by Ruthenium or Nickel. Propargylic alcohol **14** with the desired *anti*-stereoconfiguration would be obtained by the stereoselective ethylination of (*S*)-Garner's aldehyde, the chiral building block of the proposed synthetic strategy.

In designing our synthetic approach for triazole ceramide analogues, **1a-c** and **2a-c**, careful consideration of the azide length was taken. Thus, a distinct azide was used for each cycloaddition reaction. The tridecyl azide, employed in the synthesis of **13**, introduces an additional methylene group compared to the dodecyl azide used in the synthesis of **12**. This deliberate modification aims to compensate for differences in substitution between the 1,4-disubstituted triazole and the 1,5-disubstituted regioisomer. This adjustment ensures that the sphingoid base maintains a consistent length across all triazole ceramide analogues. By avoiding the production of analogues with varying sphingoid lengths, we can assess the impact of ring geometry on Des1 inhibition without introducing additional variables into the comparison between the 1,4-disubstituted triazole analogues and the 1,5-disubstituted triazole analogues.

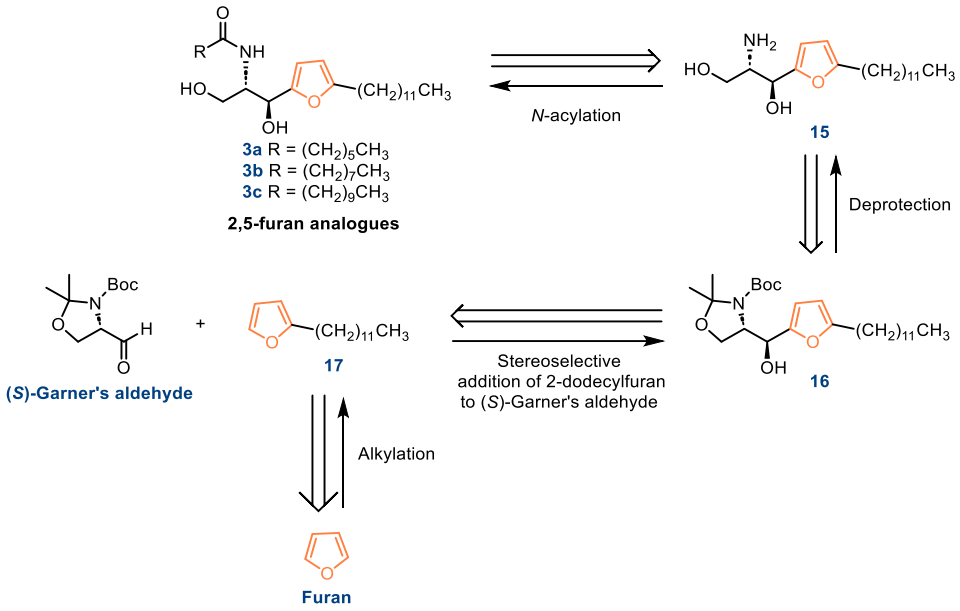

Scheme 3.2. Retrosynthetic analysis of targeted furan ceramide analogues (**3a-c**).

Furan ceramide analogues (**3a-c**) would be obtained from *N*-acylation of aminodiol **15** (Scheme 3.2), generated by deprotection of both protecting groups present in compound **16**, namely, *tert*-butyloxycarbonyl (Boc) and isopropylidene ketal. Introduction of the furan moiety present in compound **16** would be performed through the diastereoselective addition of 2-dodecylfuran, **17**, to (*S*)-Garner's aldehyde. 2-dodecylfuran is accessible through a furan ring alkylation in position 2.

3.2.2 Addition of organometallic reagents to Garner's aldehyde

Philip Garner was the first to report the synthesis of 1,1-dimethylethyl 4-formyl-2,2-dimethyloxazolidine-3-carboxylate, a compound that has since become more widely recognized as Garner's aldehyde.[34] This configurationally stable aldehyde has demonstrated its versatility as a chiral building block in the synthesis of numerous natural products and their synthetic intermediates.[35] It represents a key reagent for the current study, as a diastereoselective nucleophilic addition to Garner's aldehyde enables direct access to 2-amino-1,3-dihydroxypropyl substructures with the configuration present in sphingolipids and, therefore, in our target ceramide analogues (Scheme 3.3).

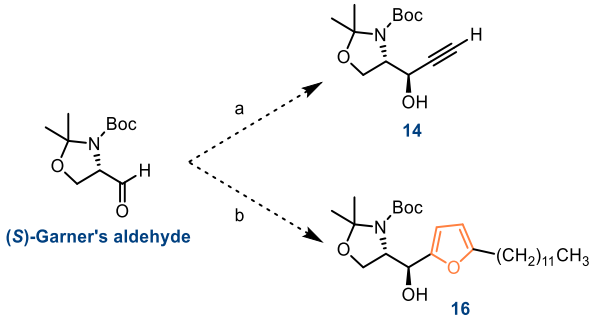

Scheme 3.3. Envisioned stereoselective nucleophilic additions on (*S*)-Garner's aldehyde for the synthesis of the triazole (via a) and furan (via b) ceramide analogues.

Through the addition of a nucleophile to Garner's aldehyde a new stereocenter is formed. Controlling the stereofacial selectivity during the nucleophilic attack, the *anti*-isomer or *syn*-isomer can be obtained as the major product, showing the versatility of the aldehyde as chiral building block (Scheme 3.4). The *anti*-selectivity can be rationalized with the Felkin-Anh non-

[34] a) Garner, P. *Tetrahedron Lett.* **1984**, *25*, 5855–5858. b) Garner, P.; Park, J. M. *Org. Synth.* **1990**, *70*, 18-28.

[35] Passiniemi, M.; Koskinen, A. M. P. *Beilstein J. Org. Chem.* **2013**, *9*, 2641–2659.

chelation transition state model,[36] as the nucleophilic attack would take place from the sterically least hindered side (*Re*-side attack) of the starting carbonyl compound. On the other hand, the *syn*-selectivity is explained with the Cram's chelation model,[37] observed when a chelating metal coordinates the carbonyl group of the aldehyde and that of the carbamate,[38] thus forcing the molecule to a configuration in which the most favourable face to the nucleophilic attack (*Si*-side attack) leads now to the *syn* final configuration.

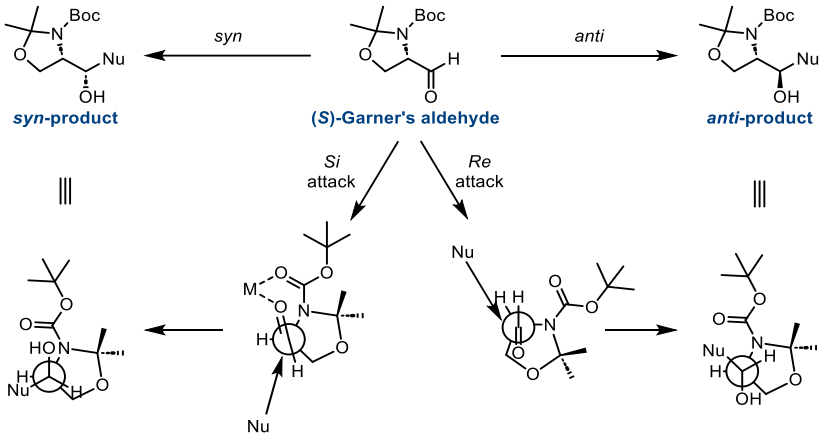

Scheme 3.4. Explanation of the *anti*- and *syn*-selectivity in the nucleophilic addition reaction to (*S*)-Garner's aldehyde.

Various factors influence the diastereoselectivity of a nucleophilic attack on Garner's aldehyde. Herold demonstrated that in the nucleophilic addition of lithium acetylide derivatives, the presence of aggregation-breaking additives such as HMPA or DMPU significantly increased the *anti*-selectivity, with diastereomeric ratios exceeding 20:1 (*anti*/*syn*).[39] HMPA's ability to

[36] Cherest, M.; Felkin, H.; Prudent, N. *Tetrahedron Lett.* **1968**, *18*, 2199-2204.

[37] a) Cram, D. J.; Abd Elhafez, F. A. *J. Am. Chem. Soc.* **1952**, *74*, 5828-5835. b) Cram, D. J.; Wilson, D. R. *J. Am. Chem. Soc.* **1963**, *85*, 1245-1249.

[38] Gruza, H.; Kiciak, K.; Krasiński, A.; Jurczak, J. *Tetrahedron: Asymmetry* **1997**, *8*, 2627–2631.

[39] Herold, P. *Helv. Chim. Acta* **1988**, *71*, 354–362.

coordinate the Li-cation disrupts lithium clusters, enhancing the nucleophilicity of the lithiated reagent and favouring the kinetic *anti*-adduct.

Conversely, in the presence of chelating metals such as Zn (II), Mg (II), or Sn (IV), the selectivity shifts towards the *syn*-product (1:20, *anti*/*syn* ratio),[40] as the reaction undergoes Cram's chelation control. These results emphasize the crucial role of additives in nucleophilic additions to Garner's aldehyde.

The choice of solvent is also relevant. THF exhibits quite strong coordination to Lewis acids, leading to increased electron density at the metal atom. This, in turn, reduces the metal atom's ability to coordinate with other Lewis bases, such the carbonyl group, and therefore disfavouring chelation control during the nucleophilic addition. This effect is widely observed in the addition of Grignard reagents.[41, 42] Thus, the addition of PhMgBr occurs with an inversion of selectivity when the solvent is changed, shifting form a 5:1 (*anti*/*syn*) ratio in THF to a 2:3 ratio in Et_2O. This can be attributed to Et_2O being a less coordinative solvent. Similar findings were reported by Coleman and Carpenter in vinyl lithium additions to Garner's aldehyde.[43] They observed a 5:1 (*anti*/*syn*) selectivity when the reaction was carried out in THF, with a decrease in *anti*-selectivity to 3:1 in Et_2O and 2:1 in toluene.

Temperature has been demonstrated to be a critical factor in these additions. Generally, most examples of nucleophilic additions to Garner's aldehyde found in the literature are conducted at low temperatures, typically ranging between 0 and -78 °C. A noteworthy case that illustrates the significant influence of temperature on the stereoselectivity of the addition was reported by Lam, when studying the addition of lithiated alkynyl species.[44] A complete inversion of selectivity was observed when the

[40] Gruza, H.; Kiciak, K.; Krasiński, A.; Jurczak, J. *Tetrahedron: Asymmetry* **1997**, *8*, 2627–2631.
[41] Williams, L.; Zhang, Z.; Shao, F.; Carroll, P. J.; Joullié, M. M. *Tetrahedron* **1995**, *52*, 11673–11694.
[42] Koskinen, A. M. P.; Hassila, H.; Myllymäki, V. T.; Rissanen, K. *Tetrahedron Lett.* **1995**, *36*, 5619–5622.
[43] Coleman, R. S.; Carpenter, A. J. *Tetrahedron Lett.* **1992**, *33*, 1697-1700.
[44] Wong, L.; Tan, S. S. L.; Lam, Y.; Melendez, A. J. *J. Med. Chem.* **2009**, *52*, 3618–3626.

temperature was lowered form -15 ˚C (exclusive formation of *syn*-product) to -40 ˚C (exclusive formation of *anti*-product).

The effect of temperature could be rationalized by the existence of two distinct transition states. At lower temperatures, operating under kinetic control, the Felkin–Anh product is predominant. In contrast, at higher temperatures, the nucleophilic addition follows a thermodynamically more stable transition state, probably resembling the chelation control.

Finally, certain trends can be noted regarding the nature of the nucleophilic reagent. More reactive nucleophiles tend to give the kinetic *anti*-products. When using these nucleophiles, the addition reaction occurs before the metal has chance to coordinate with any carbonyl group, causing the Felkin-Anh control.[42]

In conclusion, through the careful selection of the nucleophilic reagent, chelating or aggregates breaking additives, solvent, and the reaction temperature, asymmetric induction can be controlled in a nucleophilic attack to Garner's aldehyde. Moreover, it is worth noting that Garner[45] and numerous researchers have shown that there is practically no epimerization of the α-carbon center of the aldehyde during the addition reaction, making asymmetric addition a feasible and reliable method.

3.2.3 Azide-alkyne 1,3-dipolar cycloadditions

For the construction of the heterocyclic moiety present in the triazole containing ceramide analogues (**1a-c**, **2a-c**), an azide-alkyne 1,3-dipolar cycloaddition (AAC) reaction was envisioned. The exstensively studied AAC catalysed by copper (CuAAC) would allow access the 1,4-disubstituted triazole. However, obtaining the 1,5-disubstituted isomer requires a less conventional azyde-alkyne cycloaddition (Scheme 3.5).

[45] Garner, P.; Park, J. M. *J. Org. Chem.* **1990**, *55*, 3772–3787.

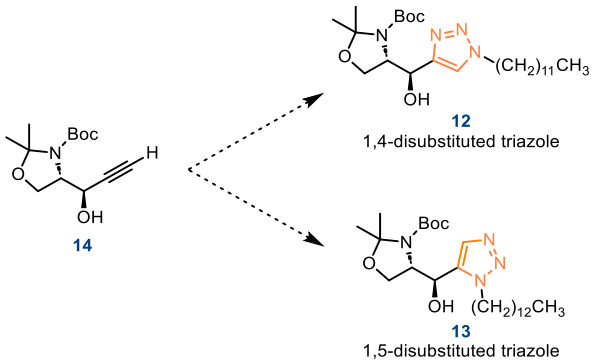

Scheme 3.5. Classical and less conventional azide-alkyne cycloadditions for the synthesis of triazole regioisomers **12** and **13**.

The 1,3-Dipolar cycloadditions of alkynes with azides are commonly known as the Huisgen cycloaddition, attributed to Huisgen and his research team who extensively explored the reaction integrating it into the framework of 1,3-dipolar cycloadditions.[46] However, the first example of this transformation was reported by Arthur Michael in 1893, describing the reaction of phenyl azide with dimethyl acetylenedicarboxylate.[46,47]

Due to its high activation energy (ca. 24-26 kcal/mol), azide-alkyne cycloadditions are impractically slow even at elevated temperatures and produce mixtures of regioisomers (Scheme 3.6).[48]

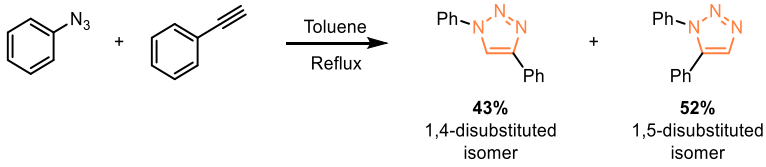

Scheme 3.6. Thermal azide-alkyne cycloaddition of azidobenzene with ethynylbenzene gives mixture of 1,4- and 1,5-disubstituted 1,2,3-triazoles.

[46] Breugst, M.; Reissig, H. U. *Angew. Chem. Int. Ed.* **2020**, *59*, 12293 – 12307.
[47] Michael, A. *J. Prakt. Chem.* **1893**, *48*, 94–95.
[48] Johansson, J. R.; Beke-Somfai, T.; Said Stålsmeden, A.; Kann, N. *Chem. Rev.* **2016**, *116*, 14726−14768.

In 2002, both Meldal and co-workers[49] and Fokin, Sharpless, and co-workers[50] independently reported that Cu(I) can catalyse the 1,3-cycloaddition of alkynes to organic azides, selectively yielding 1,4-disubstituted 1,2,3-triazoles under mild reaction conditions. Meldal and colleagues applied this reaction in the solid-phase synthesis of triazole-based peptidomimetics, using copper iodide as the catalyst.[49] Fokin, Sharpless, and co-workers developed a procedure for this reaction in solution, generating the catalyst *in situ* by reducing Cu(II) salts with sodium ascorbate.[50]

In 2013 Fokin demonstrated that two chemically equivalent copper atoms collaborate in the regioselective formation of 1,4-disubstituted 1,2,3-triazoles (Scheme 3.7).[51] After second π-bound copper atom is recruited, the catalytically active complex **II** is generated. The complex also incorporates a σ-bounded copper. The reversible coordination of the organic azide to the π-bound copper complex forms complex **III**. Following this step, a nucleophilic attack at N-3 of the azide by the β-carbon of the acetylide results in the formation of the first covalent C–N bond and produces intermediate **IV**. Due to the σ-bounded copper, the nucleophilic attack can only take place from the internal carbon, which defines the high regioselectivity of the reaction.

The formal oxidation state of copper increases upon the formation of the first C-N bond. The degenerate, proximal copper center in **IV** facilitate this oxidation event, with the second copper atom acting as a stabilizing donor ligand to the otherwise highly energetic and unstable mononuclear metallacycle intermediate.[51] Then, the second covalent C-N bond is formed, resulting in formation of copper triazolide **V** that leads to the formation of 1,4-disubstituted triazole.

---

[49] Tornoe, C. W.; Christensen, C.; Meldal, M. *J. Org. Chem.* **2002**, *67*, 3057–3064.

[50] Rostovtsev, V. V.; Green, L. G.; Fokin, V. V.; Sharpless, K. B. *Angew. Chem. Int. Ed.* **2002**, *41*, 2596–2599.

[51] Worrell, B. T.; Malik, J. A.; Fokin, V. V. *Science*, **2013**, *340*, 457-460.

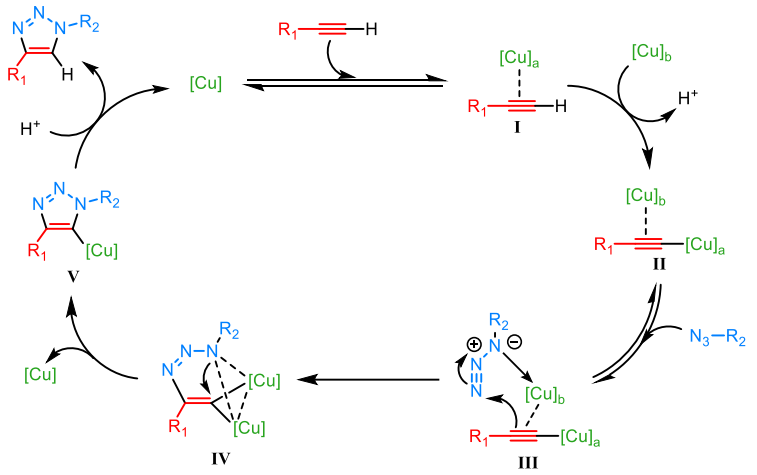

Scheme 3.7. Proposed catalytic cycle for the CuAAC reaction.

The success of this reaction is attributed to its mild reaction conditions, high yields, and exclusive formation of one regioisomer. Additionally, the reaction exhibits remarkable tolerance to nearly every functional group, including unprotected alcohols, carboxylic acids, and amines. It displays minimal sensitivity to steric factors, allowing even tertiary azides to undergo coupling in high yield. Moreover, the reaction can be performed in a wide range of solvents, including water, and boasts a highly favourable atom economy.[50] It has to be taken into account that only terminal alkynes can undergo CuAAC, as the formation of σ-bound copper acetylide is needed for the catalytic cycle.

The robustness of the reaction extends to the catalyst, different sources of Cu(I) have been used, most of them furnishing the corresponding triazole product with high yields. The most important factor for the success of the reaction is maintaining the Cu(I) specie during the process, avoiding its disappearance by disproportionation or oxidation to Cu(II). In this context, the use of Cu(II) salts with the addition of a reducing agent in a large excess is a wildly used strategy. In traditional solution chemistry the preferred method is the use of copper sulfate pentahydrate as Cu(II) source and sodium

ascorbate as reducing agent.[52] In certain applications, where the use of reducing agents can be problematic, as biological systems, copper–metal comproportionation is another used strategy for *in situ* Cu(I) generation.[53]

Oxidation of copper metal provides another method for generating the Cu(I) catalyst. Adding an excess of copper turnings to a mixture of the azide and alkyne in water/ alcohol mixtures affords the corresponding triazole in good yield.[54] However, drawbacks of this protocol include prolonged reaction times and a high copper loading requirement. In this context, nanosized Cu serves as an alternative with comparable efficiency to other methods,[55] although its solvation needs a slightly acidic environment, potentially limiting the substrate scope or requiring additional protection/deprotection steps in synthesis. Further, the use of Cu nanoclusters or Cu nanoparticles increases the cost of the synthesis.

Employing Cu(I) salts, such as CuI or CuBr, for azide-alkyne coupling has shown to be highly sensitive to reaction conditions.[56] It has been observed that the use of nitrogen-containing bases, such as *N*,*N*-Diisopropylethylamine (DIPEA) or 2,6-lutidine, give particularly high yields, perhaps by stabilizing the Cu(I) oxidation state by coordination, preventing Cu(I) disproportionation or oxidation. Indeed, a diverse array of triazole products has been synthesized using Cu(I) salts with good yields in the presence of excess base.[57]

---

[52] Meldal, M.; Tornøe, C. W. *Chem. Rev.* **2008**, *108*, 2952–3015.

[53] Deiters, A.; Cropp, T. A.; Mukherji, M.; Chin, J. W.; Anderson, J. C.; Schultz, P. G. *J. Am. Chem. Soc.* **2003**, *125*, 11782– 11783; b) Lee, L. V.; Mitchell, M. L.; Huang, S. J.; Fokin, V. V.; Sharpless, K. B.; Wong, C. H. *J. Am. Chem. Soc.* **2003**, *125*, 9588–9589.

[54] Himo, F.; Lovell, T.; Hilgraf, R.; Rostovtsev, V. V.; Noodleman, L.; Sharpless, K. B.; Fokin, V. V. *J. Am. Chem. Soc.* **2005**, *127*, 210–216.

[55] Orgueira, H. A.; Fokas, D.; Isome, Y.; Chan, P. C. M.; Baldino, C. M. *Tetrahedron Lett.* **2005**, *46*, 2911-2914.

[56] Fazio, F.; Bryan, M. C.; Blixt, O.; Paulson, J. C.; Wong, C. H. *J. Am. Chem. Soc.* **2002**, *124*, 14397–14402.

[57] Bock, V. D.; Hiemstra, H.; Van Maarseveen, J. H. *Eur. J. Org. Chem.* **2006**, 51-68.

While thermal azide-alkyne cycloaddition afforded mixtures of 1,4- and 1,5-disubstituted 1,2,3-triazoles, with the development of CuAAC the 1,4-isomer could be selectively synthetized. Therefore, a robust method for the 1,5-disubstituted triazoles was lacking at the time.

Between the 60s and 80s the synthesis of 4-metalated 1,5-disubstituted triazoles was reported by using selected metal (Sn, Ge, Si, and Na) acetylides. Also, Akimova *et al.* studied in detail the reactions of lithium and magnesium acetylides in the 1960s.[48] This last procedure was improved by Fokin and Sharpless, achieving better yields, and a broader scope that even included 1,4,5-trisubstituted 1,2,3- triazoles.[58] In this reaction, it is proposed that the lithium or magnesium acetylide undergoes a nucleophilic attack on the azide, leading to a subsequent ring closure and the formation of a metallotriazole. This metallotriazole can then be quenched or trapped with an electrophile (Scheme 3.8).[58] However, the use of this procedure requires stochiometric amounts of metal. Moreover, metal acetylides are incompatible with some functional groups.

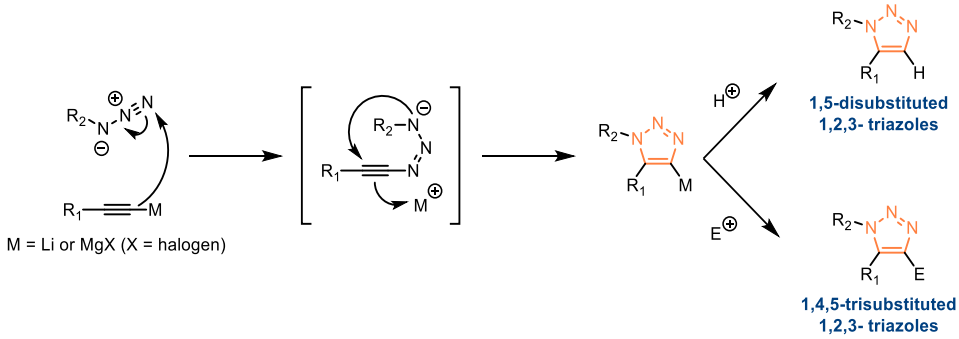

Scheme 3.8. Proposed mechanism for triazole formation using Li and Mg acetylides.

[58] Krasiński, A.; Fokin, V. V.; Sharpless, K. B. *Org. Lett.* **2004**, *6*, 1237–1240.

Ru(II) is known to catalyse different reactions involving alkynes, so in 2005 Fokin, Jia, and co-workers considered ruthenium as the logical choice in the search of a new catalyst for azide-alkyne cycloaddition.[59] They performed a catalyst screening for the reaction between benzyl azide and phenylacetylene (1:1.2 eq., respectively). The reaction was conducted in THF at reflux temperature for 4h in the presence of 2 % (mol/mol) of the ruthenium complex. Yields were calculated based on the integration of triazole and the unreacted azide (Table 3.1).[60]

$Ru(OAc)_2(PPh_3)_2$, $RuCl_2(PPh_3)_2$, $RuHCl(CO)(PPh_3)_2$, and $RuH_2(CO)(PPh_3)_2$ complexes afforded the 1,4-disubstituted 1,2,3-triazole **18b** (Table 3.1, entries 1-4). However, the $Cp^*RuCl(PPh_3)_2$ complex yielded a mixture of 1,5- and 1,4-disubstituted triazoles in an approximately 10:1 ratio (Table 3.1, entry 5). Then, by a simple switch to the most sterically hindered pentamethyl cyclopentadienyl (Cp*) analogue, $Cp^*RuCl(PPh_3)_2$, a complete selectivity for the 1,5-disubstituted triazole **18a** was achieved (Table 3.1, entry 6). Several other Ru(II) catalysts containing the [Cp*RuCl] unit were also useful in effecting this transformation, i.e., Cp*RuCl(COD), Cp*RuCl(NBD), and $[Cp^*RuCl_2]_2$ (Table 3.1, entries 7-9).[59,60] The unique catalytic properties of these complexes can be ascribed to the presence of the electron-rich Cp* ligand, which stabilizes higher formal oxidation states of the metal center.[60]

[59] Zhang, L.; Chen, X. G.; Xue, P.; Sun, H. H. Y.; Williams, I. D.; Sharpless, K. B.; Fokin, V. V.; Jia, G. C. *J. Am. Chem. Soc.* **2005**, *127*, 15998–15999.

[60] Boren, B. C.; Narayan, S.; Rasmussen, L. K.; Zhang, L.; Zhao, H.; Lin, Z.; Jia, G.; Fokin, V. V. *J. Am. Chem. Soc.* **2008**, *130*, 8923–8930.

Table 3.1 Regiochemical outcome of azide-alkyne cycloaddition with different Ru catalysts.

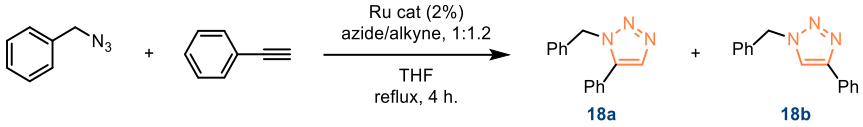

Entry	Ru catalyst	18a	18b
1	$RuCl_2(PPh_3)_3$	-	<5%
2	$Ru(OAc)_2(PPh_3)_2$	-	46%
3	$RuHCl(CO)(PPh_3)_3$	-	<5%
4	$RuH_2(CO)(PPh_3)_3$	-	56%
5	$CpRuCl(PPh_3)_2$	13%	1%
6	$Cp^*RuCl(PPh_3)_2$	100%	-
7	Cp*RuCl(COD)	100%	-
8	Cp*RuCl(NBD)	93%	-
9	$[Cp^*RuCl]_4$	100%	-

The authors focused on $Cp^*RuCl(PPh_3)_2$ and Cp*RuCl(COD) (Figure 3.14) catalysts due to their synthetic availability and stability. Increasing the temperature up to 110 °C provided a faster reaction for $Cp^*RuCl(PPh_3)_2$, but ambient temperature could be applied by running the reaction for a longer time at higher catalyst loading. Catalyst complex Cp*RuCl(COD) is more reactive than $Cp^*RuCl(PPh_3)_2$, because of the higher lability of cyclooctadiene ligand in comparison with triphenylphosphines. Reaction with this more reactive catalyst gave high yields at room temperature even after 30 minutes, being a particularly advantageous catalyst for reactions involving internal alkynes.

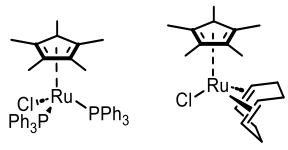

Figure 3.14. Structure of $Cp^*RuCl(PPh_3)_2$ and Cp*RuCl(COD) catalysts.

The [Cp*RuCl]-catalyzed cycloadditions proceed well in polar and nonpolar solvents such as tetrahydrofuran, dioxane, toluene, benzene, dimethylformamide, and 1,2-dichloroethane. Performing the reaction in protic solvents (MeOH, *i*-PrOH) resulted in reduced yields and the formation of byproducts.

The reaction is significantly affected by the steric demands on the azide. Thus, reactions with secondary azides are slower than those involving primary substrates and show slightly lower yields. Tertiary azides, with few exceptions, are generally reluctant to participate in catalysis. On the other hand, the catalysis is not very sensitive to the substituents on the alkyne. In fact, halide, alcohol, ether, acetal, nitrile, ester, amine, sulfonamide, and pyridine functionalities are compatible with the reaction conditions.

One advantage of RuAAC compared to CuAAC is that the former allows the cycloaddition reaction of internal alkynes, while the latter reaction involves the formation of a copper acetylide and thus requires a terminal alkyne. This provides access to 1,4,5-trisubstituted 1,2,3-triazoles.

The participation of both terminal and internal alkynes in RuAAC suggests that ruthenium acetylides are not involved in the catalytic cycle. The authors propose that the neutral [Cp*RuCl] is the catalytically active species, involved in a four-step catalytic cycle (Scheme 3.9).[60] The displacement of the spectator ligands produces the activated complex **I**, which is converted via an irreversible oxidative coupling to the ruthenacycle **II**. This step controls the regioselectivity of the overall process; the new C-N bond is formed between the more nucleophilic and less sterically demanding carbon of the alkyne and the terminal nitrogen of the azide. In the last step, the metallacycle intermediate undergoes reductive elimination, furnishing the 1,5-disubstituted 1,2,3-triazole and regenerating the catalyst.

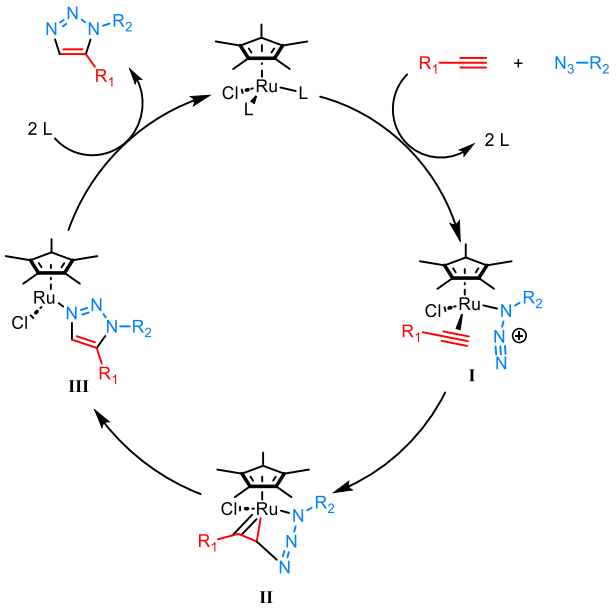

Scheme 3.9. Proposed catalytic cycle of the RuAAC reaction.

This proposed reaction mechanism was validated by DFT calculations using the B3LYP hybrid functional.[60, 61] The lowest energy pathway has a 13 kcal/mol barrier, showing that Ru is an efficient catalyst, allowing a much lower barrier than the same path without a catalyst (25-26 kcal/mol for methyl azide and propyne)[62].

In the case of internal alkynes, regioselectivity of the cycloaddition is influenced by several factors. In alkynes containing a hydrogen bond donor group in the propargylic position, the new bond is always formed between the β-carbon of the alkyne and the terminal nitrogen of the azide, exhibiting virtually exclusive regioselectivity.[60] This directing effect can be attributed to the formation of a strong H-bond of the propargylic group with the chloride ligand on the ruthenium. In the absence of such directing groups,

[61] Zhou, Y. B.; Ke, Z. F.; Zhao, C. Y. *Acta Chim. Sin.* **2006**, *64*, 2071−2078.

[62] Himo, F.; Lovell, T.; Hilgraf, R.; Rostovtsev, V. V.; Noodleman, L.; Sharpless, K. B.; Fokin, V. V. *J. Am. Chem. Soc.* **2005**, *127*, 210-216.

regioselectivity seems to be governed primarily by the electronic properties of the alkyne. As previously commented, the first N-C bond is formed between the more nucleophilic carbon of the alkyne and the electrophilic N-1 of the azide. In other words, the carbon with more negative density of the alkyne becomes C-4 in the final triazole.

In 2017, an alternative to the RuAAC for the synthesis 1,5-disubstituted triazoles was reported using Ni as catalyst.[63] After extensive screening, Cp_2Ni precatalyst and Xantphos ligand emerged as the best catalyst option for this reaction. In addition, the presence of a mild base showed beneficial for the reaction, Cs_2CO_3 being identified as the optimal choice (Scheme 3.10).

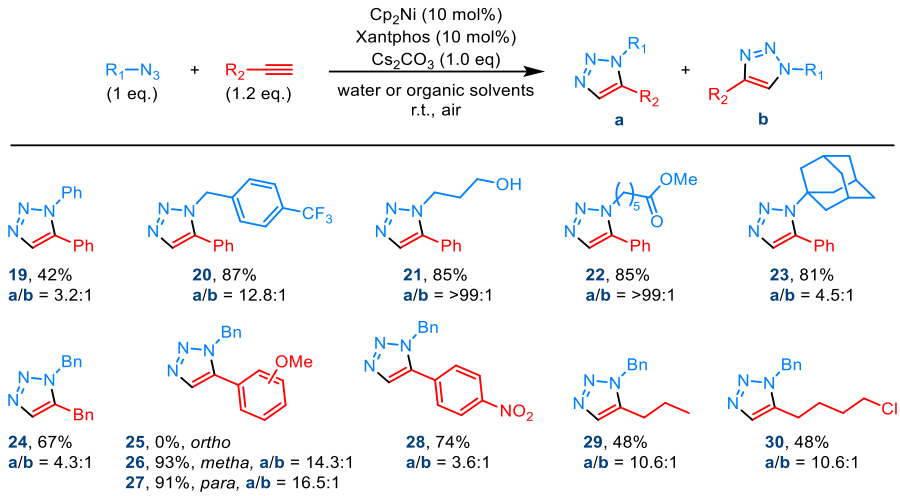

Scheme 3.10. General conditions and scope for NiAAC.

The methodology demonstrates a broad substrate scope, good functional group tolerance, high yields, and mild to high regioselectivities ranging from 11.4:1 to >99:1, favouring the 1,5-disubstituted triazole (Scheme 3.10, product a). However, the regioselectivity significantly decreased with steric

[63] Kim, W. G.; Kang, M. E.; Lee, J. B.; Jeon, M. H.; Lee, S.; Lee, J.; Choi, B.; Cal, P. M. S. D.; Kang, S.; Kee, J-M.; Bernades, G. J. L.; Rohde, J-U.; Choe, W.; Hong, S. Y. *J. Am. Chem. Soc.* **2017**, *139*, 12121–12124.

congestion on the substrates, with a low 3.2:1 ratio for phenyl azide, in the formation of **19**, or a 4.5:1 ratio for 1-azidoadamantane **23** as examples.

The reaction proceeded well in organic solvents such as toluene, DMF or dichloromethane, but with particular significance in water. Indeed, NiAAC is highly compatible with water as the sole solvent and can be carried out under air at room temperature. This offers a good alternative to RuAAC reactions using [Cp*RuCl] complexes, which are typically sensitive to water and air and often require elevated temperatures.[64] These conditions limit RuAAC application in biochemical contexts. The NiAAC utility in this field is highlighted by its ability to functionalize carbohydrates and amino acids in water and air atmosphere.

CuAAC and RuAAC significantly contributed to the modern synthetic toolbox, enabling the selective synthesis of 1,4 and 1,5-disubstituted 1,2,3-triazoles, respectively. Both reactions use mild conditions and are compatible with a wide range of functional groups, allowing the synthesis of a diverse array of 1,2,3-triazoles through an operationally simple transformation. NiAAC, although with lower regioselectivities, complements the previous strategies and offers an alternative to obtain the less explored 1,5-disubstituted triazole regioisomers.

[64] a) Oakdale, J. S.; Fokin, V. V.; Umezaki, S.; Fukuyama, T. *Org. Synth* **2013**, *90*, 96-104. b) Johansson, J. R.; Lincoln, P.; Nordén, B..; Kann, N. *J. Org. Chem.* **2011**, *76*, 2355-2359.

3.3 Synthesis of 1,4- and 1,5-disubstituted 1,2,3-triazole ceramide analogues

3.3.1 Synthesis of common intermediate 14

The synthesis of triazole ceramide analogues (**1a-c**, **2a-c**) presented in this chapter began with the preparation of propargylic alcohol **14**. This alkyne represents a common intermediate in the synthesis of all 1,2,3-triazole isomers targeted. The strategy followed for its synthesis consisted in the stereoselective addition of the commercially available ethinyltrimethylsilane to (*S*)-Garner's aldehyde, followed by the hydrolysis of the TMS group in alkyne **31** (Scheme 3.11).

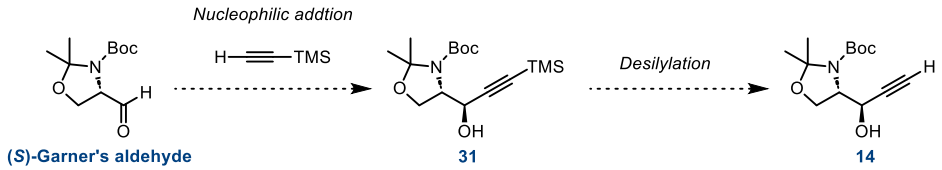

Scheme 3.11. Strategy for the synthesis of propargylic alcohol **14**.

The synthesis of compound **31** was described by Herlod.[39] In the reported procedure the organolithium reagent is generated by treating ethinyltrimethylsilane with butyl lithium for 1 hour at -78 °C. Then, (*S*)-Garner's aldehyde is added, and the nucleophilic addition of the generated organolithium compound is maintained over 2 hours at -78 °C in the presence of HMPA, to favour the kinetic *anti*-product. Applying the described conditions but elongating the addition time from 2 to 6 hours the desired propargylic alcohol **31** was obtain in a 60 % yield with the desired *anti*-configuration (Table 3.2, entry 1), the *syn*-isomer being not detected by ^{1}H NMR analysis. This represents a lower yield in comparison with the result described by Herold, in which product **31** was obtained in an 85% yield.

Nevertheless, we observed a low conversion of the starting (*S*)-Garner's aldehyde, recovering a great amount in the reaction crude. In an attempt to improve the reaction yield, we increased the nucleophilic addition time up to 18 hours (Table 3.2, entry 2) but no significant change in the reaction outcome was observed. By raising the temperature of the addition step to -55 ˚C and maintaining the reaction mixture at that temperature for 18 hours, product **31** was obtained in an 80 % yield (Table 3.2, entry 3). Under these conditions, we managed to increase the reaction yield without compromising the diasteroselectivity of the reaction, as the *syn*-isomer was not detected.

It is worth mentioning that a secondary product was detected during the reaction, which was identified as the desilylated compound **14**. This fact is not surprising considering the lability of the TMS group.

Table 3.2. Conditions assayed for the addition of ethynyltrimethylsilane to (*S*)-Garner's aldehyde.

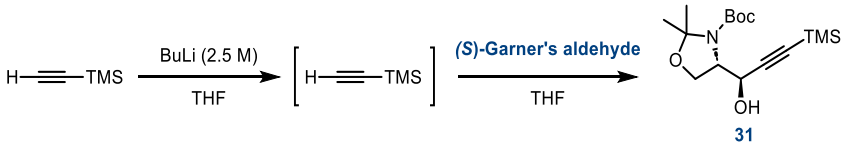

31

Entry	Lithiation step	Nucleophilic adition	Yield (31)
1	1 h, -78 ˚C	6 h, -78 ˚C	60 %
2	1 h, -78 ˚C	18 h, -78 ˚C	58%
3	1 h, -78 ˚C	18 h, -55 ˚C	80 %

In the following step, the desilylation of the terminal alkyne was achieved in 85 % yield, using TBAF as a fluoride source (Scheme 3.12).[65]

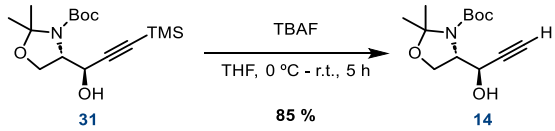

Scheme 3.12. Desilylation of terminal alkyne **30**.

Thus, propargylic alcohol **14** was successfully synthesized through a 2-step process with an overall 68 % yield. However, the two-reaction process is time consuming, involving long reaction times and requiring two chromatographic purifications. Moreover, with the observation of the desilylation taking place during the course of the nucleophilic addition, we considered that the yield could be improved. For this reason, the synthesis of propargylic alcohol **14** was conducted via a *one-pot* ethynylation and catalytic desylilation (Scheme 3.13).[66]

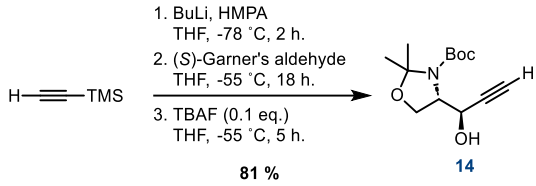

Scheme 3.13. *One-pot* ethynylation and catalytic desylilation of (*S*)-Garner's aldehyde.

In this procedure, the same conditions previously used for the organolithium generation and nucleophilic addition were maintained. Once the nucleophilic addition to the aldehyde was completed, the generated alkoxy intermediated was desilylated with the addition of a catalytic amount of TBAF (0.10 eq.) to the reaction mixture, furnishing compound **14** with an

[65] D'Aniello, F.; Mann, A.; Schoenfelder, A.; Taddei, M. *Tetrahedron*, **1997**, *53*, 1447-1456.

[66] Wong, F. F.; Chuang, S. H.; Yang, S. C.; Lin, Y. H.; Tseng, W. C.; Lin, S. K.; Huang, J. J. *Tetrahedron*, **2010**, *66*, 4068-4072.

81 % overall yield. This methodology represents a more efficient synthesis of propargylic alcohol **14**, which can be obtained in a *one-pot* transformation, using only catalytic amounts of TBAF, and requiring only a chromatographic purification. Furthermore, a notable enhancement in yield was observed compared to the 2-step process, with an increase from 68% to 81%.

The catalytic desilylation methodology proceeded exclusively under *one-pot* conditions, without the isolation of the nucleophilic addition product. The authors proposed (Scheme 3.14)[66] that after the nucleophilic addition of trimethylsilylacetylide to the aldehyde, intermediate **32** is formed. Subsequent desilylation by fluoride would generate dianion **33** and trimethylsilyl fluoride (TMSF). The alkoxy moiety in intermediate **33** can then displace the fluoride in the previously generated TMSF, yielding intermediate **34** and regenerating the fluoride anion. This anion is capable of desilylate another molecule of **32**, perpetuating in this way the cycle. Upon acidic work-up, the removal of TMS group in **34** would yield the desired propargylic alcohol **14**.

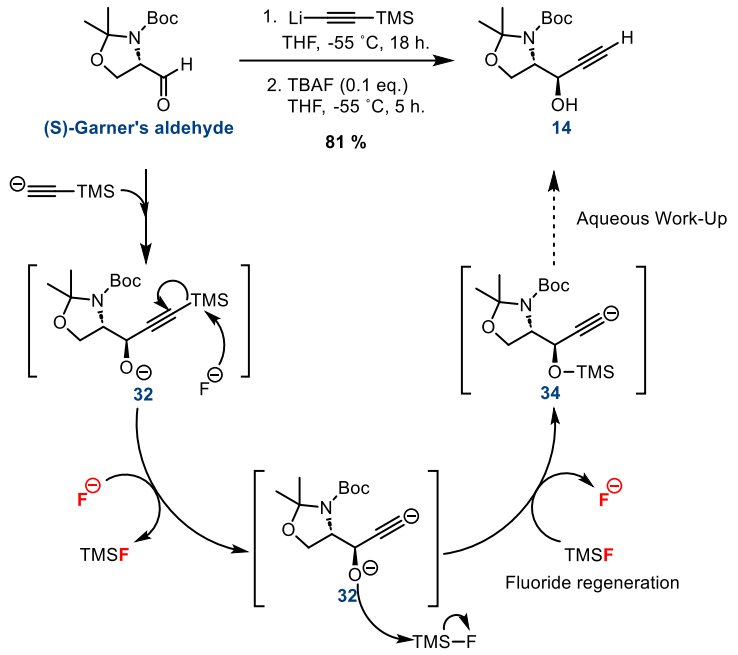

Scheme 3.14. Proposed mechanism for the *one-pot* ethynylation and catalytic desylilation of (*S*)-Garner's aldehyde.

3.3.2 Synthesis of 1,4- and 1,5-disubstituted 1,2,3-triazole moieties via azide-alkyne cycloaddition. Synthesis of products 12 and 13.

With propargilic alcohol **14** in hands, we proceeded with the synthesis of the triazole moieties. Previously, the organic azides for the cycloaddition reaction needed to be synthetized.[67]

Azides are synthetically versatile compounds with high chemical reactivity. The azido group can act as an electrophile, nucleophile, radical acceptor, and as a 1,3-dipole. Some of the physicochemical properties of the organic azides can be explained by considering the polar mesomeric structures (Scheme 3.15), which justify their diverse reactivity.[68] The structure **c** can explain the easy decomposition of an azide into the corresponding nitrene and nitrogen gas. Structure **d** determines the reactivity as a 1,3-dipole.

[67] Huanga, D.; Yan, G. *Adv. Synth. Catal.* **2017**, *359*, 1600-1619.
[68] Bräse, S.; Gil, C.; Knepper, K.; Zimmermann, V. *Angew. Chem. Int. Ed.* **2005**, *44*, 5188- 5240.

Furthermore, this structure, **d**, accounts for the regioselectivity of their reactions with electrophiles and nucleophiles, as an azide receives the attack on N-3 by a nucleophile, whereas electrophiles are attacked by N-1 of the azide.

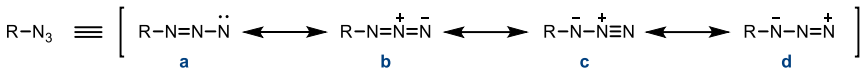

Scheme 3.15. Polar mesomeric structures of an organic azide.

Aliphatic azides are readily accessible by nucleophilic substitution (S_N2 type) with the highly nucleophilic azide ion. Sodium azide is the most common azide ion source used, with halides usually being the leaving group of choice. Using these reagents, excellent results are obtained with DMF as solvent under thermal conditions.[68]

Azidododecane, **37**, and azidotridecane, **38**, were synthetized as described from the corresponding bromides in 96 % and 92 % yield respectively (Scheme 3.16).[69]

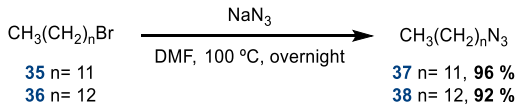

Scheme 3.16. Synthesis of azidododecane, **37**, and azidotridecane, **38**.

For the construction of the 1,4-disubstituted 1,2,3-triazole, propargylic alcohol **14** was reacted with alkyl azide **37** (Scheme 3.17) using $CuSO_4{\cdot}5H_2O$ as Cu(I) source, in the presence of an excess of sodium ascorbate to ensure the prevalence of the Cu(I) during the reaction. After a 48-hour reaction in a H_2O/CH_2Cl_2 mixture, product **12** incorporating the triazole motif was obtained with almost quantitative yield. 2

[69] Hu, J.; Zhu, T.; He, C.; Zhang, Y.; Zhang, Q.; Zou, G. *J. Mater. Chem. C*, **2017**, *5*, 5135- 5142.

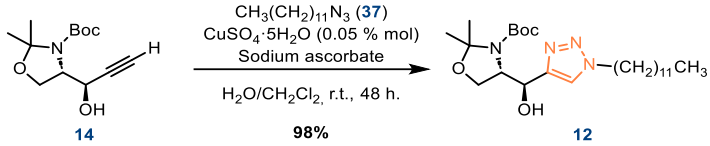

Scheme 3.17. Synthesis of 1,4-triazole derivative **12** via a CuAAC.

For the synthesis of 1,5-disubstituted 1,2,3-triazole moiety, the NiAAC and RuAAC reactions on propargylic alcohol **14** were assayed, evaluating Cp_2Ni/Xantphos, $Cp^*RhCl(PPh_3)_2$, and $Cp^*RuCl(COD)$ as catalytic systems under different conditions (Table 3.3).

Table 3.3. Conditions assayed for the regioselective 1,3-dipolar cycloaddition between alkyne **14** and azide **38**.

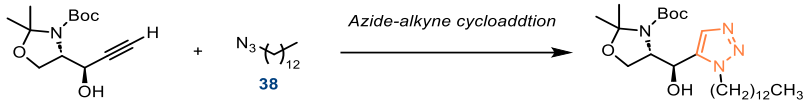

Entry	Catalyst	mol %	Conditions	Reaction time	Yield
1	Cp_2Ni/Xantphos	10/10	Cs_2CO_3 (1 eq.) H_2O, air, r.t.	3 days	n.r.[a]
2	Cp_2Ni/Xantphos	10/10	Cs_2CO_3 (1 eq.) CH_2Cl_2	3 days	n.r.[a]
3	$Cp^*RuCl(PPh_3)_2$,	2	THF, reflux	2 days	n.r.[a]
4	$Cp^*RuCl(PPh_3)_2$	2	1,4-dioxane, 60 °C	overnight	n.r.[a]
5	$Cp^*RuCl(PPh_3)_2$	2	toluene, r.t.	overnight	n.r.[a]
6	$Cp^*RuCl(PPh_3)_2$	2	toluene, 40 °C	overnight	27%
7	$Cp^*RuCl(PPh_3)_2$	2	toluene, 60 °C	5 h.	67%
8	$Cp^*RuCl(PPh_3)_2$	4	toluene, 60 °C	5 h.	63%
9	$Cp^*RuCl(COD)_2$	2	toluene, r.t.	overnight	60%
10	$Cp^*RuCl(COD)_2$	3	toluene, r.t.	overnight	58%
11	$Cp^*RuCl(COD)_2$	4	toluene, r.t.	overnight	69%
12	$Cp^*RuCl(COD)_2$	5	toluene, r.t.	overnight	72%

[a] n.r. = no reaction

When evaluating the Cp_2Ni/Xantphos catalytic system in H_2O as solvent under the described conditions (Table 3.3, entry 1) we did not observe any reaction evolution after three days. The alkyne, **14**, and the azide, **38**, were not efficiently dissolved during the reaction, as a suspension was observed. Although reactions in these conditions are reported to work as aqueous suspensions,[63] we decided to conduct the reaction in dichloromethane to confirm that the lack of reactivity was not due to the poor solubility of the reactants (Table 3.3, entry 2). A homogeneous solution was achieved in CH_2Cl_2, however, the reaction did not evolve either after 3 days, and only the starting material was recovered.

In view of these results, Cp*RuCl$(PPh_3)_2$, and Cp*RuCl(COD), were evaluated as catalysts. No reaction was observed by using Cp*RuCl$(PPh_3)_2$, in refluxed THF (Table 3.3, entry 3), 1,4-dioxane at 60 °C (Table 3.3, entry 4) or toluene at room temperature (Table 3.3, entry 5). Only the reaction in toluene at 40 °C provided the desired product in a 27 % (Table 3.3, entry 6). The result was improved by increasing the temperature at 60 °C while maintaining the 2 % catalyst loading. Under these conditions, triazole **13** was obtained in a 67 % yield (Table 3.3, entry 7). Doubling the catalyst loading did not increase the yield (Table 3.3, entry 8), although the consumption of starting alkyne **14** was observed after 5 h by TLC analysis.

All the reactions in presence of Cp*RuCl(COD) as a catalysts were performed at room temperature, as heating often results in rapid deactivation of the catalyst and low yields of the cycloaddition product.[60] Catalyst loading from 2 to 5 % were evaluated (Table 3.3, entries 9-12), verifying that reaction with 5% Cp*RuCl(COD) in toluene offered the best result (Table 3.3, entry 12), yielding triazole derivative **13** with a 72% yield.

Thus, both the Cp*RuCl$(PPh_3)_2$ and Cp*RuCl(COD) catalysts offered comparable results. Cp*RuCl$(PPh_3)_2$ provides a faster reaction, but heating at 60 °C was needed. A slightly higher yield was obtained with Cp*RuCl(COD), conducting the reaction at room temperature. The formation of the 1,4-

regioisomer was not observed in any of the experiment using [Cp*RuCl] complexes.

In the ^{1}H NMR analysis of triazole **12**, two series of signals were observed, which appeared as broad signals in the case of triazole **13**. This can be attributed to the coexistence of two rotamers caused by the presence of the carbamate functionality. The low barrier for rotation of C(carbonyl)-N bond in a carbamate allows the coexistence of 2 rotamers that interconvert to each other with different rates depending on the product.[70] This fact was confirmed by recording the ^{1}H NMR spectrum of triazole derivative **13** at different temperatures (Figure 3.15). When lowering the temperature to -50 °C, the existence of two different species becomes evident, because of the duplicity of signals corresponding to the H-2, H-3 and H-5 protons. Conversely, when increasing the temperature, the rate of interconversion between both rotamers is higher and allows observing a unique signal in each case; which is an average of the individual rotamers.

[70] Deetz, M. J.; Forbes, C. C.; Jonas, M.; Malerich, J. P.; Smith, B. D.; Wiest, O. *J. Org. Chem.* **2002**, *67*, 3949-3952.

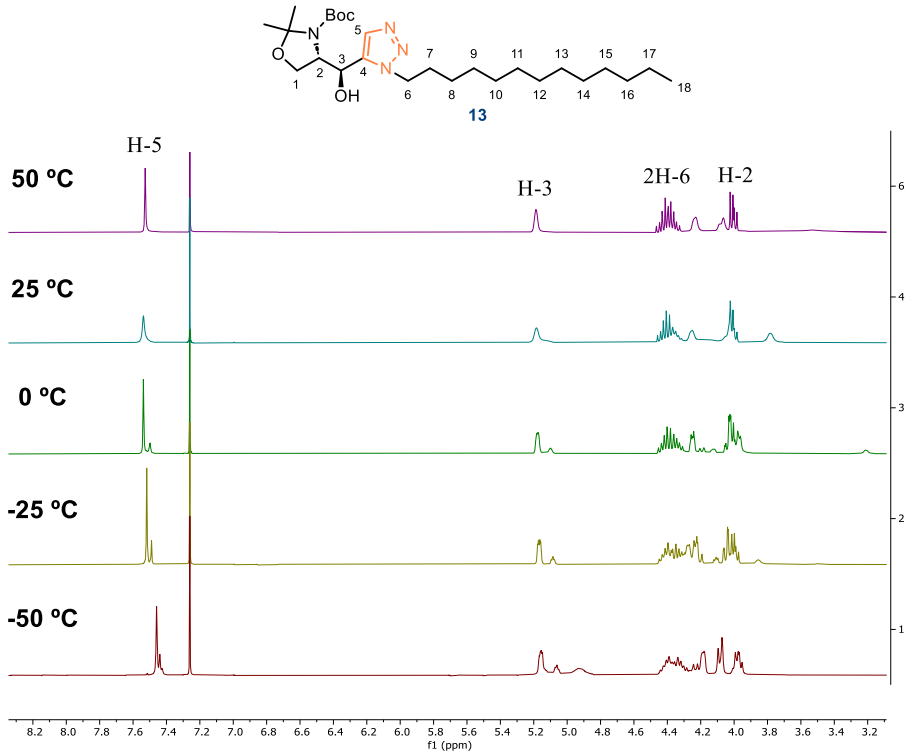

Figure 3.15. ^{1}H NMR spectra (400 MHz, $CDCl_3$) of compound **13** recorded at different temperatures ranging from -50 °C to 50 °C.

Both CuAAC and RuAAC have proven useful for selectively synthesizing the 1,4- and 1,5-disubstituted 1,2,3-triazole moieties. Once the triazole moiety is formed, a reliable analytical method to confirm the obtaining of the desired regioisomer is needed, as the 1,4- and 1,5-isomers are difficult to differentiate using simple ^{1}H NMR. In the initial reports by Fokin, Sharpless, Jia and coworkers the structural assignment was verified by X-ray crystallography or by 1D or 2D NMR techniques based on the nuclear Overhauser effect (NOE).[50,54] Alfonso and co-workers[71] used a gradient-enhanced indirect detection pulse sequence,[72] which makes use of the ^{1}H nucleus to obtain information about ^{15}N NMR shifts to differentiate between

[71] Corredor, M.; Bujons, J.; Messeguer, A.; Alfonso, I. *Org. Biomol. Chem.* **2013**, *11*, 7318–7325.
[72] Marquez, B. L.; Gerwick, W. H.; Williamson, R. T. *Magn. Reson. Chem.* **2001**, *39*, 499–530.

1,4- and 1,5-disubstituted 1,2,3-triazole isomers. Cerely *et al.* developed a simpler method by using ^{13}C NMR.[73] After analysing a collection of different substituted triazole isomers, focusing on the signal displayed by the unsubstituted carbon of the triazole ring, they observed a general trend. The C-5 carbon of the 1,4-disubstituted triazole displays a signal around 120 ± 3 ppm, while the corresponding C-4 carbon of the 1,5-disubstituted isomer appears around 133 ± 3 ppm (Figure 3.16).

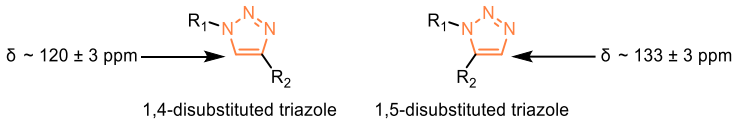

Figure 3.16. ^{13}C NMR as a tool for distinguishing between 1,4- and 1,5-disubstituted 1,2,3-triazole isomers.

Effectively, ^{13}C NMR proved useful for the confirmation of the structure of triazole regioisomers **12** and **13**, as both show the expected signal for the C-5 carbon at 123.9 ppm and 131.6 ppm respectively (Figure 3.17), thereby confirming the obtaining of the desired regioisomer in each case.

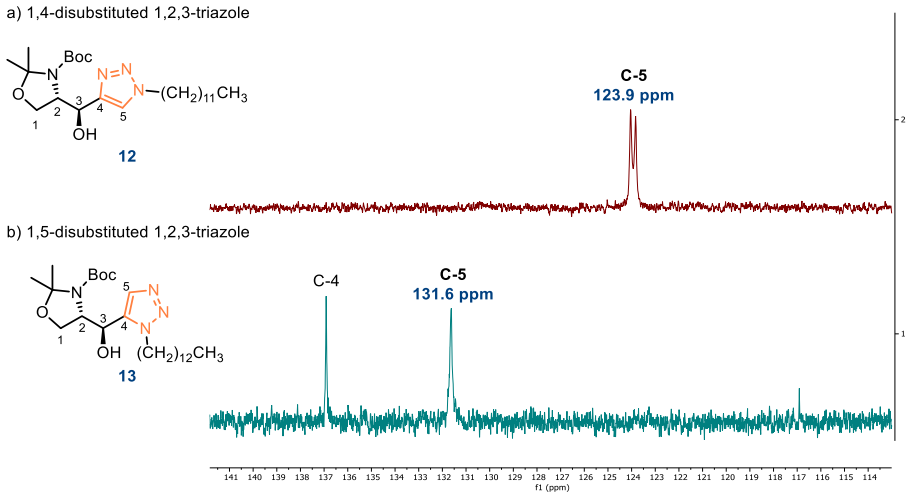

Figure 3.17. Amplified ^{13}C NMR spectrum of compound **12** and **13.**

[73] Creary, X.; Anderson, A.; Brophy, C.; Crowell, F.; Funk, Z. *J. Org. Chem.* **2012**, *77*, 8756–8761.

3.3.3 Deprotection and *N*-acylation steps. Accessing triazole ceramide analogues 1a-c and 2a-c.

After construction of the 1,4-disubstituted triazole moiety the simultaneous deprotection of both protecting groups present in compound **12** was performed using a TFA/H_2O mixture. The formation of aminodiol **10** resulted in 54 % yield. Final *N*-acylation of **10** with hexanoic, octanoic and decanoic acid using EDC and HOBt as coupling reagents furnished 1,4-disubstituted triazole ceramide analogues **1a-c** (Scheme 3.18).

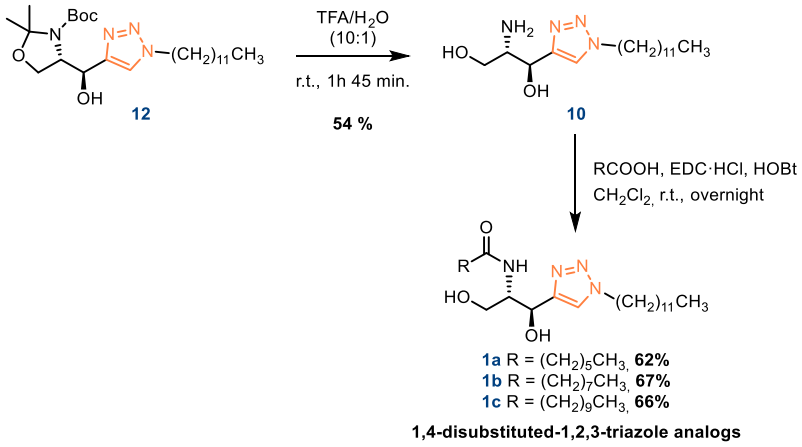

Scheme 3.18. Deprotection of **12** and *N*-acylation for the synthesis of triazole ceramide analogues **1a-c**.

Following the same strategy, hydrolysis of compound **13** and *N*-acylation furnished 1,5-disubstituted triazole ceramide analogues **2a-c** (Scheme 3.19).

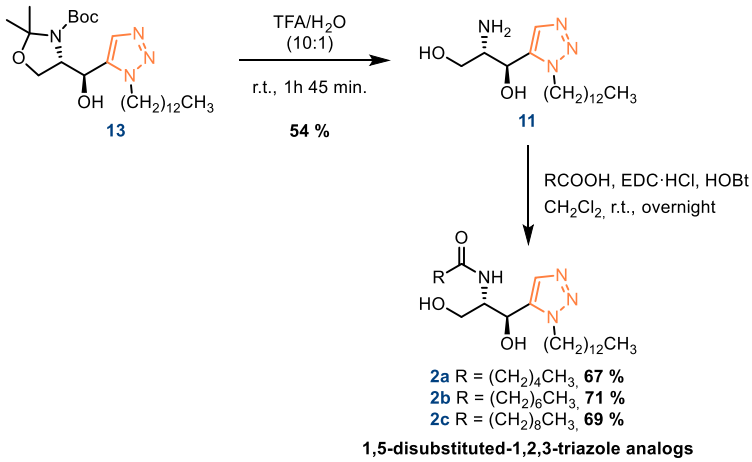

Scheme 3.19. Deprotection of **13** and *N*-acylation for the synthesis of triazole ceramide analogues **2a-c**.

X-ray diffraction analysis of crystallized ceramide analogue **2c** confirmed the desired *anti*-configuration of the 2-amido-3-hydroxy moiety (Figure 3.18).

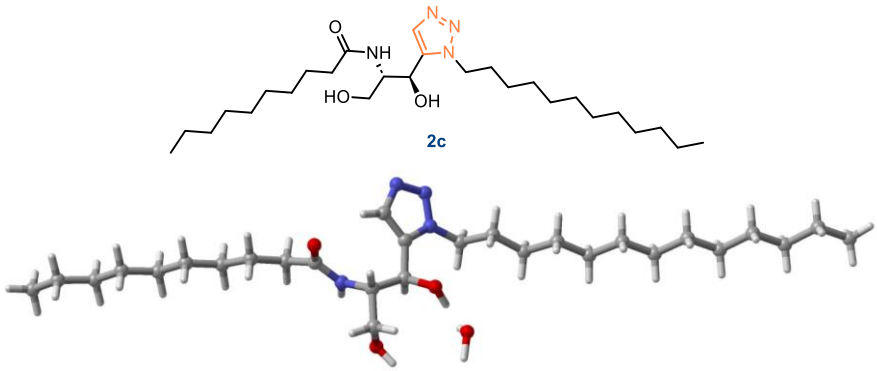

Figure 3.18. X-ray structure of 1,5-disubstituted triazole ceramide analogue **2c** (CCDC 2252494).

As a result, 6 ceramide analogues containing 1,4-, 1,5-disubstituted triazoles as the central core, **1a-c** and **2a-c**, have been successfully synthesized through a 4-step synthesis. Total yields of the synthesis range from 27 to 30 %.

3.4 Synthesis of 2,5-disubstituted furan ceramide analogues

3.4.1 Nucleophilic addition of 2-dodecylfuran to (*S*)-Garner's aldehyde

The synthesis of furan ceramide analogues started with a furan alkylation to obtain 2-dodecylfuran, **17**, which would then be added to (*S*)-Garner's aldehyde.

Alkyl furan compounds are readily accessible by direct lithiation of the furan ring, followed by subsequent reaction with an alkyl halide or aldehydes.[74] Regioselectivity in the lithiation is governed by two factors. Lithiating agents with little or no Lewis-acid character led to thermodynamic products derived from deprotonation of the most acidic hidrogen atom and concomitant lithiation at this position. In contrast, lithiating agents with Lewis-acid character, such as *n*-butyllithium, produce kinetic products derived from deprotonation at the position closest to the most effective Lewis base ligand, usually an heteroatom (if any in the molecule).[75] In the case of furan ring, the lithiation at position 2 is favoured by both factors mentioned before, so no problems of regioselectivity should be observed.

For the synthesis of 2-dodecylfuran, **17**, 2-furyllithium **39** was first generated by treating furan with BuLi solution. Then, the nucleophilic SN2-type reaction with 1-bromododecane, **35**, was performed. Different conditions for the reaction were assayed (Table 3.4).[76] When using equimolar quantities of the reagents (Table 3.4., entry 1) product **17** was obtained in a 58 % yield; the formation of the dialkylated product being observed. This issue was resolved by using an excess of furan and butyl lithium to generate an excess of the lithiated specie in the reaction mixture (Table 3.4., entry 2). Alkylated product was obtained in an improved yield (75 %) under these conditions. A

---

[74] Bock, I.; Bornoveki, H.; Ranft, A.; Theis, H. *Tetrahedron* **1990**, *46*, 1199-1210.

[75] Gschwend, H. W.; Rodriguez, H. R. *Org. React.* **1979**, *26*, 1-111.

[76] a) Eschen-Lippold, L.; Draeger, T.; Teichert, A.; Wessjohann, L.; Westermann, B.; Rosahl, S.; Arnold, N. *J. Agric. Food Chem.* **2009**, *57*, 9607-9612. b) Dondoni, A.; Junquera, F.; Merchán, F. L.; Merino, P.; Scherrmann, M. C.; Tejero, T. *J. Org. Chem.* **1997**, *62*, 5484-5496.

further increase in the yield (91 %) was achieved by maintaining the lithiation step at 0 ˚C instead of room temperature (Table 3.4., entry 3). In the end, the best results were obtained by extending the duration of the SN2 process, all other conditions remaining unchanged (Table 3.4., entry 4). In this way, 2-dodecyl furan, **17**, was obtained in almost quantitative yield.

Table 3.4. Conditions assayed for the furan alkylation with bromododecane, **34**.

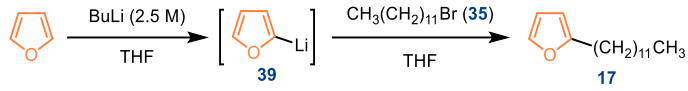

Entry	Bromide/furan/BuLi (molar ratio)	Lithiation step	SN2 step	yield
1[a]	1:1:1	1 h, 0 ˚C	5 h, r.t	58 %
2[a]	1:1.5:1.4	1 h, 0 ˚C + 1 h, r.t	5 h, r.t	75%
3[b]	1:1.5:1.4	2 h, 0 ˚C	5 h, r.t	91 %
4[b]	1:1.5:1.4	2 h, 0 ˚C	Overnight, r.t	99 %

[a]Furan concentration 0.74 M. [b]Furan concentration 0.3 M.

With 2-dodecylfuran in hands we performed its addition to (*S*)-Garner's aldehyde (Scheme 3.20). For the initial lithiation step, the conditions that provided best results in the previous furan alkylation (Table 3. 4, entry 4) were used. Afterwards, the diastereoselective addition of the obtained lithiated derivative to (*S*)-Garner's aldehyde was performed at -55 ˚C in the presence of HMPA for an overnight reaction. Alcohol derivative **16** was thus obtained as a 7:1 *anti/syn* ratio mixture in a good 83 % yield. Both diastereomers could not be separated by flash column chromatography so the synthesis was continued with the diastereomeric mixture.

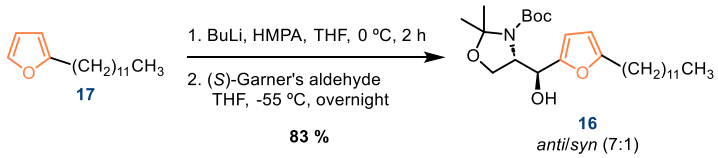

Scheme 3.20. Diasteroselective addition of 2-dodecylfuran, **17**, to (*S*)-Garner's aldehyde.

The determination of the *syn*/*anti* ratio was accomplished by integrating the signals corresponding to H-5 in the ^{1}H NMR spectrum (Figure 3.19). With the knowledge that nucleophilic additions to (S)-Garner's aldehyde under these conditions predominantly yield the *anti*-diastereomer, product **16** was identified as the major product of the reaction. This identification was substantiated by assessing the addition reaction at various temperatures, revealing the anticipated trend. Elevating the temperature resulted in a reduction in *anti*-selectivity, transitioning from 7.1:1 at -55 ˚C to 2.8:1 at -40 ˚C and 1.3:1 at -20 ˚C.

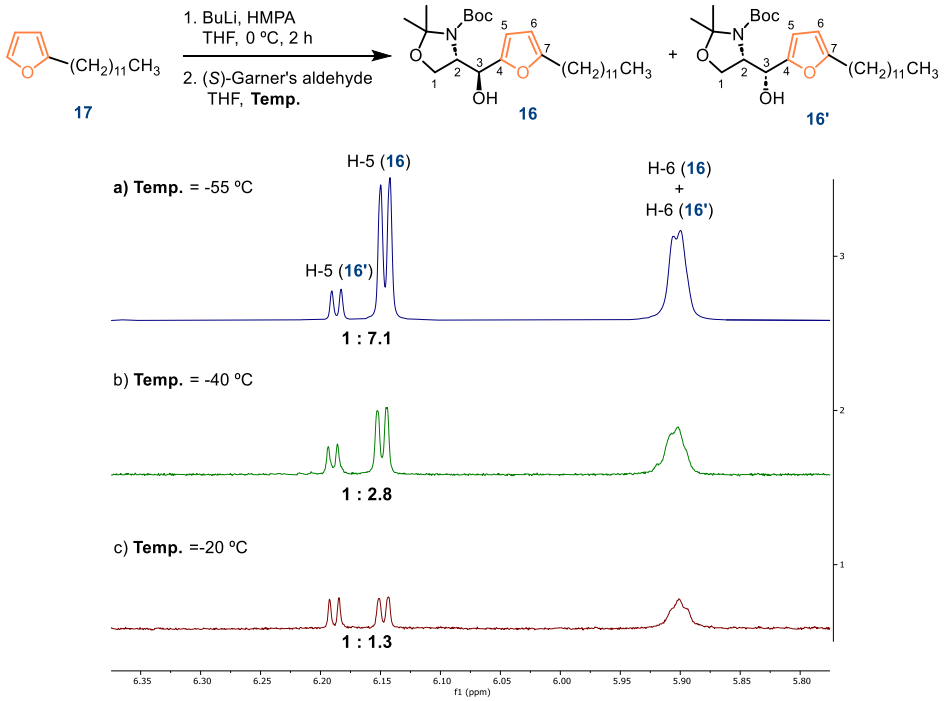

Figure 3.19. ^{1}H NMR spectra amplification to analyse the outcome of the 2-dodecylfuran addition to (*S*)-Garner's aldehyde conducted at different temperatures: a) -55 ˚C. b) -40 ˚C c) -20 ˚C.

3.4.2 Deprotection and *N*-acylation steps. Accessing furan ceramide analogues 3a-c.

After the synthesis of compound **16** incorporating the furan moiety, the deprotection of *tert*-butyloxycarbonyl and isopropylidene acetal groups was conducted. This deprotection step was not obvious, and different conditions were assayed (Table 3.5).

Table 3.5. Conditions assayed for the deprotection of **16**.

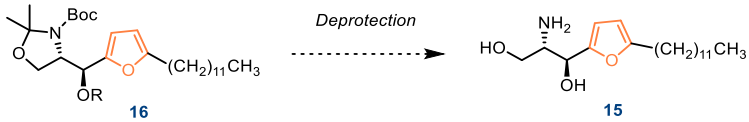

16 15

Entry	R	Conditions	Reaction outcome
1	H (**16**)	TFA/H_2O, r.t. 30 min.	Decomposition
2	H (**16**)	acetyl chloride/MeOH, r.t., 1 h.	C-3 methoxylation
3	H (**16**)	acetyl chloride/MeOH, 0 ˚C, 1 h.	C-3 methoxylation
4	H (**16**)	HCl (2M in Et_2O), r.t., 30 min	Decomposition
5	H (**16**)	HCl (2M in Et_2O), 0 ˚C, 1h15min	Decomposition
6	Ac (**16b**)	acetyl chloride/MeOH, r.t., 30 min	C-3 methoxylation
7	TBDPS (**16c**)	acetyl chloride/MeOH, r.t., 2 h.	C-3 methoxylation
8	TBDPS (**16c**)	TFA/H_2O, 0 ˚C, 20 min.	Decomposition
9	H (**16**)	1. TMSOTf, Et_3N/CH_2Cl_2, 0 ˚C, 30 min 2. TBAF (1 M in THF)/THF, r.t., overnight	Aminodiol **15** (90 % yield)

Treatment of **16** with TFA/H_2O led to product decomposition (Table 3.5., entry 1). Furan opening or Piancatelli rearrangement of the furfurylcarbinol moiety seemed probable decomposition pathways in the aqueous medium used in the reaction. To exclude water, hydrochloric acid was generated *in situ* using acetyl chloride and anhydrous MeOH (Table 3.5., entry 2). These

conditions were effectively used in the synthesis of a sphingosine analogue **41** by Antonio Delgado and coworkers (Scheme 3.21, a).[77] The acetyl chloride/MeOH combination resulted effective in deprotecting of both protecting groups in our compound **16**. However, these conditions also provoked the methoxylation of C-3 (Scheme 3.21, b). In the methoxylation reaction stereochemistry was not retained, a diasteromeric mixture in 2:1 molar relation was obtained. The reaction at lower temperature led to the same result (Table 3.5., entry 3).

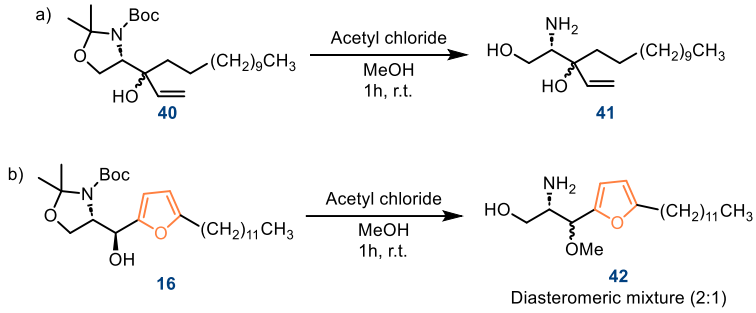

Scheme 3.21. Simoultaneous deprotections of *tert*-butyloxycarbonyl and isopropylidene acetal groups using acetyl chloride/MeOH applied to a vinyl sphingolipid derivative (a) and a furan sphingolipid derivative (b).

To exclude not only water but also methanol from the reaction media, commercial hydrochloride in Et_2O solution was used (Table 3.5., entry 4) but also caused product decomposition even working at low temperature (Table 3.5., entry 5). The reaction with acetyl chloride/MeOH previous protection of OH-3 in the starting material as acetyl ester (Table 3.5., entry 6) or *tert*-butyldiphenylsilyl ether (Table 3.5., entry 7) was not effective either, obtaining the 3-methoxyl derivative in both cases). Reaction of the *tert*-butyldiphenylsilyl ether derivative **16c** with TFA at low temperature also resulted in product decomposition (Table 3.5., entry 8). Thus, OH-3 protection

[77] Pons, G.; Riba, D.; Casasampere, M.; Izquierdo, E.; Abad, J. L.; Fabriàs, G.; Rodríguez-Ortega, P. G.; López-González, J. J.; Montejo, M..; Casas, J.; Delgado, A. *J. Org. Chem.* **2020**, *85*, 419–429.

revealed as an ineffective strategy to avoid decomposition or C-3 methoxylation.

In view of these results, we hypothesized the formation of carbocation **43** when compound **16** was treated with a Brønsted acid (Scheme 3.22). This carbocation would be stabilized by the presence of the furan ring. It could evolve towards the formation of **42** in the presence of methanol or towards decomposition when a nucleophile is absent in the reaction media. Although this behaviour might seem predictable, the effectiveness of the reaction on the substrate described by Delgado (Scheme 3.22) did not foreshadow the obtained results. In his case, the plausible carbocation intermediate would also be stabilized, as it is an allylic cation.

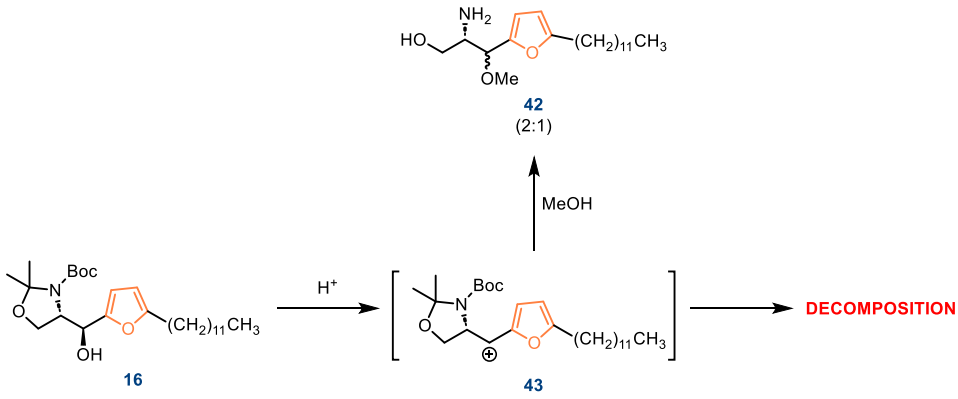

Scheme 3.22. Plausible mechanism for the reaction outcome when treating **18** with a Brønsted acid.

In base of these results, Lewis acids were considered as an alternative for the deprotection of **16** (Table 3.5., entry 9). Eventually, treatment of **16** with TMSOTf/Et_3N furnished silylated compound **44** (Scheme 3.23). Desilylation could be performed without purification of intermediate **44**, and aminodiol **15** was obtained in this way with an excellent 90 % yield for the two steps. Although separation of both diastereomers was still difficult after

deprotection, an enriched fraction of the *anti*-diastereomer with a *anti*/*syn* ratio of 18:1 could be isolated.

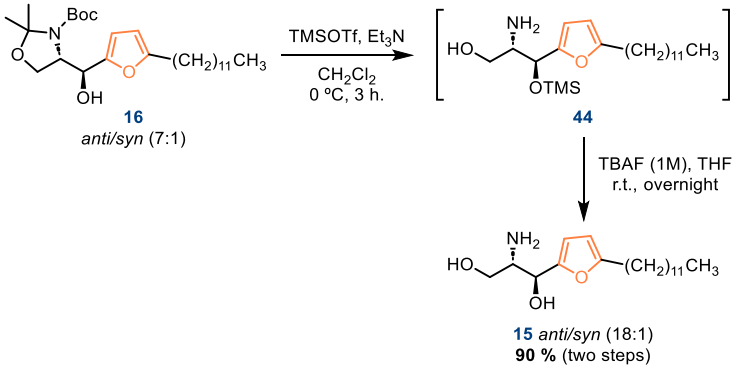

Scheme 3.23. Deprotection of compound **16**.

Final *N*-acylation of aminodiol **15** afforded furan derivatives **3a-c** in yields ranging from 61% to 77% as diastereoisomeric pure compounds (Scheme 3.24).

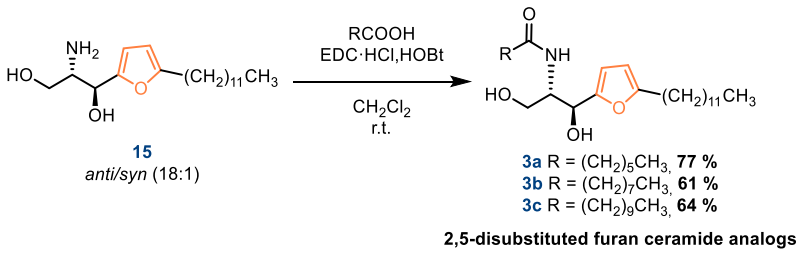

Scheme 3.24. *N*-acylation of aminodiol **15** to furnish furan ceramide analogues **3a-c**.

In summary, 3 ceramide analogues containing a 2,5-disubstituted furan ring as central core, **3a-c**, have been successfully synthesized through a 5-step synthesis with total yields ranging from 47 to 57 %.

3.5 Evaluation of heterocycle containing ceramide analogues (1a-c, 2a-c and 3a-c) as dihydroceramide desaturase 1 inhibitors.

3.5.1 Evaluation of Des1 activity with DHCerC6NBD.

6-[*N*-(7-nitro-2,1,3-benzoxadiazol-4-yl)amino]hexanoylsphinganine (**dhCerC6NBD**) and 6-[*N*-(7-nitro-2,1,3-benzoxadiazol-4-yl)amino]hexanoylsphingosine (**CerC6NBD**) serve as fluorescent analogues of dihydroceramide and ceramide, respectively (Figure 3.20). These fluorescent sphingolipids have been utilized to investigate sphingolipid metabolism and intracellular transport.[78]

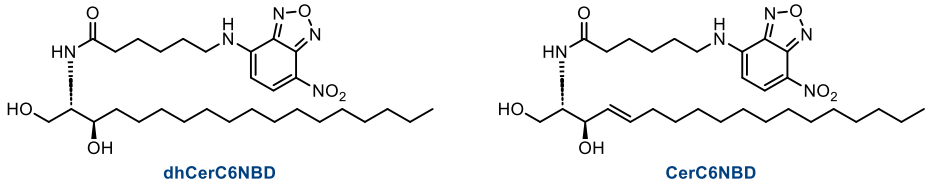

Figure 3.20. Fluorescent analogues of dihydroceramide (**dhCerC6NBD)** and ceramide (**CerC6NBD)**.

In a study aimed at characterizing the intracellular transport and metabolism of dihydroceramide, it was observed that **dhCerC6NBD** is desaturated to its ceramide analogue, **CerC6NBD**, in several cell lines.[79] Following this discovery, Prof. Gemma Fabriàs and coworkers developed a method using this fluorescent sphingolipid to measure dihydroceramide desaturase activity *in vitro* for inhibition studies.[80]

---

[78] a) Lipsky, N. G.; Pagano, R. E. *Science*, **1985**, *228*, 745–747. b) Pagano, R. E. *Methods Cell Biol.* **1989**, *29*, 75–85. c) Lipsky, N. G.; Pagano, R. E. *Proc. Natl. Acad. Sci. U. S. A.* **1983**, *80*, 2608–2612. d) Lipsky, N. G.; Pagano, R. E. *J. Cell Biol.* **1985**, *100*, 27–34.

[79] Kok, J. W.; Nikolova-Karakashian, M.; Klappe, K.; Alexander, C.; Merrill, Jr., A. H. *J. Biol. Chem.* **1997**, *272*, 21128–21136.

[80] Muñoz-Olaya, J. M.; Matabosch, X.; Bedia, C.; Egido-Gabás, M.; Casas, J.; Llebaria, A.; Delgado, A.; Fabriàs, G. *ChemMedChem* **2008**, *3*, 946-953.

The authors determined kinetic parameters of the enzymatic reaction by incubating different concentrations (ranging from 1 and 40 μM) of the substrate, **dhCerC6NBD**, for one hour in rat liver microsomes. Lipids were then analysed by HPLC with a fluorimetric detector (HPLC-FD), revealing that **DhCerC6NBD** was desaturated to **CerC6NBD** with a K_m of 7.7 μM and a V_{max} of 19.3 pmol $h^{-1}mg^{-1}$.

The authors also investigated the desaturation of **dhCerC6NBD** in Jurkat human leukaemia cells by incubating the substrate and conducting further HPLC-FD analysis of both media and cells. The analysis showed the presence of both **dhCerC6NBD** and **CerC6NBD**, as well as the 1-phoshate, 1-glucosyl and 1-phosphocholine derivatives of **DhCerC6NBD** (Figure 3.21). The identity of all these metabolites was confirmed by LC-MS.

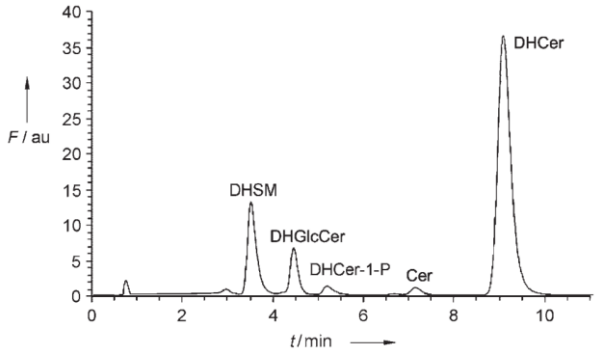

Figure 3.21. HPLC-FD profile of fluorescent sphingolipids produced from dHCerC6NBD in Jurkat A3 cells.[80]

Following these experiments, **DhCerC6NBD** demonstrated itself as a good substrate to measure dihydroceramide desaturase activity *in vitro*. The authors applied this technique in the evaluation of **XM462** and **GT11** as Des1 inhibitors,[80] finding good agreement with previous values calculated using different techniques.

3.5.2 Effect of heterocycle containing ceramide analogues (1a-c, 2a-c and 3a-c) on Des1 activity

In the context of a collaboration with Prof. Gemma Fabriàs and Dr. Josefina Casas (RUBAM, Department of Biological Chemistry, Institute for Advanced Chemistry of Catalonia, IQAC), the effect of synthetized analogues on Des1 activity was evaluated. Two different assays were conducted using **dhCerC6NBD** as fluorescent substrate for Des1 activity evaluation. Des1 activity in presence of the inhibitors candidates was evaluated both in intact cells and in cell lysates, allowing a comparison of the effect of the inhibitors candidates in cells and in a cell-free environment.

To determine the enzyme activity in intact cells, T98 cancer cells were incubated 24 h with the candidate inhibitors **1a-c**, **2a-c** and **3a-c**. Then, the fluorescent substrate (**dhCerC6NBD**) was added to the medium, and cells were incubated for 4 h at 37 ˚C and 5 % CO_2, the optimal conditions for the enzymatic reaction to take place. Both the extracellular and intracellular media were analysed by HPLC coupled to a fluorescent detector to evaluate the extent of the enzymatic reaction. The same assay was applied to cell lysates. T98 cell lysates were prepared using the standard methodologies (see experimental section) and then incubated with both the substrate (**dhCerC6NBD**) and test compounds for 4 h. Again, the outcome of the enzymatic reaction was analysed by HPLC-FD. The results of these experiments are shown in Figure 3.22.

Triazole derivatives (**1a-c**, **2a-c**) caused statistically significant Des1 inhibition in intact T98 cells ranging from 10% to 50% at a concentration of 10 μM, being the 1,4-disubstituted triazole *N*-decanoyl chain ceramide analogue **2c** the compound that reached the maximum inhibition. For the furan series, only the *N*-hexanoyl chain ceramide **3a** showed a significant 40% inhibitory activity in intact cells (Figure 3.22).

Additionally, Des1 inhibition experiments using **1a-c**, **2a-c** and **3a-c** in T98 cell lysates resulted negative (Figure 3.22), indicating that none of these derivatives inhibits Des1 in T98 cell lysates, a cell-free environment.

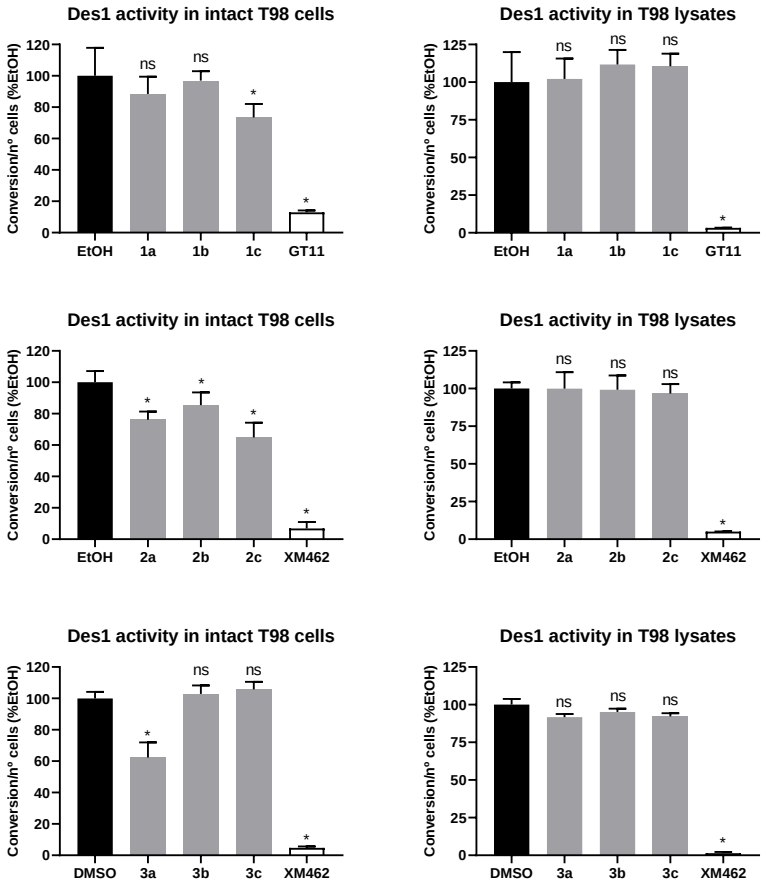

Figure 3.22. Effect of compounds **1a-c**, **2a-c**, **3a-c** on the activity of Des1. T98G cell lysates or T98G cells were incubated with EtOH/DMSO (control), compounds **1a-c**, **2a-c**, **3a-c** (10 μM) or **GT11**/**XM462** (10 μM) (positive control). The Des1 substrate (dhCerC6NBD, 10 μM) was then added and cells were collected 4 h later. Medium and cell samples were analyzed by HPLC coupled to a fluorescence detector. Values are the mean of 2 independent experiments with triplicates. Asterisks indicate statistical significant over DMSO or EtOH controls at $P<0.05$ (unpaired, two-tailed, *t*—test).

With these results, we conclude that the ceramide analogues **1a-c**, **2a-c** and **3a-c**, do not directly affect the enzyme active site. The moderate inhibition observed in intact cells can be considered indirect, as in a cell-free environment the ceramide analogues did not impact Des1 activity. The analogues might affect Des1 activity in intact cells by disrupting the previous electron transport chain or through the down-regulation of Des1 gene expression.

Due to the lack of structural information of the enzyme, it is difficult to explain the absence of direct inhibitory activity of the synthetized ceramide analogues. Nevertheless, the obtained results show that introduction of 5-member heterocycles such as triazole and furan into the ceramide structure proved detrimental for Des1 inhibition.

UNIVERSITAT ROVIRA I VIRGILI
TARGETING DES1: SYNTHESES OF CERAMIDE ANALOGUES WITH A RIGID SCAFFOLD, INHIBITORY ASSAYS, AND AF2-ASSISTED STRUCTURAL INSIGHTS REVEAL PR280 AS A POTENT INHIBITOR
Pablo Rivero Prieto

CHAPTER IV

Unveiling structural insights into Des1 using AlphaFold2: Towards the proposal of novel Des1 inhibitors

UNIVERSITAT ROVIRA I VIRGILI
TARGETING DES1: SYNTHESES OF CERAMIDE ANALOGUES WITH A RIGID SCAFFOLD, INHIBITORY ASSAYS, AND AF2-ASSISTED STRUCTURAL INSIGHTS REVEAL PR280 AS A POTENT INHIBITOR
Pablo Rivero Prieto

4.1 Introduction

4.1.1 AlphaFold2's breakthrough

Proteins are the molecular motors of all biological systems. Gaining insights into proteins and unravelling their functional roles is essential for comprehending biological processes and advancing in drug design.

Rational drug discovery employs engineered small molecules to selectively interact with proteins and modulate their function.[1] A protein's biological mechanism is determined by its three-dimensional (3D) native structure, which in turn is encoded in its 1D string of amino acid monomers.[2] Consequently, knowing the 3D structure of a protein enhances the understanding of its function and mode of action, facilitating the targeted design of small molecules. Moreover, having this information of the targeted protein enables the application of computational methods like pocket detection,[3] molecular docking,[4] virtual screening,[5] and free energy calculations.[6] These computational approaches streamline the drug design process, making it both time-efficient and cost-effective.

---

[1] Kuntz, I. D. *Science*, **1992**, *257*, 1078-1082.

[2] Dill, K. A.; MacCallum, J. L. *Science*, **2012**, *338*, 1042-1046.

[3] a) Le Guilloux, V.; Schmidtke, P.; Tuffery, P. *BMC Bioinformatics* **2009**, *10*, 168-178. b) Zhao, R.; Cang, Z.; Tong, Y.; Wei, G. W. *Bioinformatics* **2018**, *34*, i830−i837.

[4] a) Ruiz-Carmona, S.; Álvarez-García, D.; Foloppe, N.; Garmendia-Doval, A. B.; Juhos, S.; Schmidtke, P.; Barril, X.; Hubbard, R. E.; Morley, S. D. *PLoS Comput. Biol.* **2014**, *10*, e1003571. b) Eberhardt, J.; Santos-Martins, D.; Tillack, A. F.; Forli, S. *J. Chem. Inf. Model.* **2021**, *61*, 3891−3898.

[5] a) Jones, G.; Willett, P.; Glen, R. C.; Leach, A. R.; Taylor, R. *J. Mol. Biol.* **1997**, *267*, 727−748. b) Friesner, R. A.; Banks, J. L.; Murphy, R. B.; Halgren, T. A.; Klicic, J. J.; Mainz, D. T.; Repasky, M. P.; Knoll, E. H.; Shelley, M.; Perry, J. K.; Shaw, D. E.; Francis, P.; Shenkin, P. S. *J. Med. Chem.* **2004**, *47*, 1739−1749. c) Jain, A. N. *J. Med. Chem.* **2003**, *46*, 499−511. d) Rarey, M.; Kramer, B.; Lengauer, T.; Klebe, G. *J. Mol. Biol.* **1996**, *261*, 470−489.

[6] a) Rizzi, A.; Jensen, T.; Slochower, D. R.; Aldeghi, M.; Gapsys, V.; Ntekoumes, D.; Bosisio, S.; Papadourakis, M.; Henriksen, N. M.; de Groot, B. L.; Cournia, Z.; Dickson, A.; Michel, J.; Gilson, M. K.; Shirts, M. R.; Mobley, D. L.; Chodera, J. D. *J. Comput. Aided Mol. Des.* **2020**, *34*, 601–633. b) Cournia, Z.; Allen, B.; Sherman, W. *J. Chem. Inf. Model.* **2017**, *57*, 2911−2937. c) Raniolo, S.; Limongelli, V. *Nat. Protoc.* **2020**, *15*, 2837−2866.

However, determining the 3D structure of a protein at atomic resolution is a great challenge. Although multiple technologies have been used to solve protein structures, including nuclear magnetic resonance (NMR),[7] X-ray crystallography,[8] and cryo-electron microscopy (cryo-EM),[9] only about 200,000 protein structures have been determined, covering less than 0.1% of the protein universe.[10] For the human proteome, less than 10% of the proteins have at least some experimentally obtained coordinates and around 17% of the residues in the human proteome can be mapped to an experimental structure.[11] This means that for the large majority of proteins no experimental structures have been reported to date.

Homology modelling offers a computational alternative to the difficult task of experimental protein structure determination.[12] Also known as comparative modelling or template-based modelling, it is based on the hypothesis that proteins' 3D structures are more conserved than their amino acid sequences. Therefore, similar amino acid sequences should have similar 3D structures.[13] This method shows high accuracy for proteins that have homologs with experimentally determined 3D structures, but this fact also constitutes its limitation. Template-based modelling strongly depends on the template structures, a template with a sequence similarity greater than 25 % being needed to build a confident 3D protein structure.[12]

In this context, the so-called *de novo* modelling has emerged; which aims to model the structures of proteins that lack experimental characterization, based only on their amino acid sequences. Anfinsen and Scheraga formulated the hypothesis behind this field: a protein's native structure stands for a free

---

[7] Wüthrich, K. *J. Biol. Chem.* **1990**, *265*, 22059–22062.

[8] Shi, Y. *Cell* **2014**, *159*, 995–1014.

[9] Earl, L. A., Falconieri, V. & Milne, J. L. Subramaniam, S. *Curr. Opin. Struct. Biol.* **2017**, *46*, 71–78.

[10] Yang, Z.; Zeng, X.; Zhao, Y. Chen, R. *Sig. Transduct. Target Ther.* **2023**, *8*, 115.

[11] David, A.; Islam, S.; Tankhilevich, E.; Sternberg, M. J. *J. Mol. Biol.* **2022**, *434*, 167336.

[12] Muhammed, M. T.; Aki-Yalcin, E. *Chem. Biol. Drug Des.* **2019,** *93*, 12–20.

[13] a) Al-Lazikani, B. Jung, J.; Xiang, Z.; Honig, B. *Curr. Opin. Chem. Biol.* **2001**, *5*, 51–56. b) Xiang, Z.. *Curr. Protein Pept. Sci.* **2006**, *7*, 217–227.

energy minimum determined by its amino acid sequence, or in other words, the 3D structure of a protein is only determined by its amino acid sequence.[14] Unlike the homology modelling, the *de novo* modelling does not depend on the known protein structures.

In the realm of protein structure prediction, CASP (Critical Assessment of Structure Prediction) is a seminal event. This community-wide experiment takes place biennially to establish the current state of the art in protein structure prediction.[15] Participants submit computational models that attempt to predict the folding of an amino acid sequence of a set of proteins for which the experimental structures are not yet public; submissions are then compared with the experimental results by independent assessors. CASP is double-blinded, ensuring that participants lack access to experimental structures, and assessors remain unaware of the contributors' identities.[16] Due to its objectivity and fairness, CASP enjoys a very high reputation in structural biology and computational biology communities.[17]

The DeeMind team won the CASP13 challenge with AlphaFold (AF) in 2019,[18] an artificial intelligence system employing a deep learning algorithm to tackle the problem of protein folding. Two years later, AlphaFold (AF2), a different and improved version of AF, won CASP14 achieving outstanding results.[19]

CASP employs the Global-Distance-Test-Score (GDTS) as the primary metric to measure the overall accuracy of protein predictions, indicating the proximity of Cα atoms in the predicted model to those in the corresponding experimental structure. GDTS values range from 0% to 100%, with 100%

---

[14] a) Earl, L. A.; Falconieri, V.; Milne, J. L.; Subramaniam, S. *Curr. Opin. Struct. Biol.* **2017**, *46*, 71–78. b) Anfinsen, C. B. *Science* **1973**, *181*, 223-230. c) Anfinsen, C.; Scheraga, H. *Adv. Protein Chem.* **1975**, *29*, 205–300.

[15] https://predictioncenter.org/

[16] Kryshtafovych, A.; Schwede, T.; Topf, M.; Fidelis, K.; Moult, J. *Proteins* **2019**, *87*, 1011-1020.

[17] Marcu, Ş. B.; Tăbîrcă, S.; Tangney, M. *Front. Artif. Intell. Appl.* **2022**, *5*, 875587.

[18] Kryshtafovych, A.; Schwede, T.; Topf, M.; Fidelis, K.; Moult, J. *Proteins* **2019**, *87*, 1011–1020.

[19] Kryshtafovych, A.; Schwede, T.; Topf, M.; Fidelis, K.; Moult, J. *Proteins* **2021**, *89*, 1607–1617.

representing the most accurate structure prediction. For most targets, AF2 achieved a GDTS value of 90% or higher, which is comparable to experimental accuracy.[20] The performance of DeepMind's system in CASP14 surpassed that of all other participants, obtaining results with unprecedented accuracy.[19] AF2 predicted structures exhibited a median backbone accuracy of 0.96 Å r.m.s.d.$_{95}$ (Cα root-mean-square deviation at 95% residue coverage), while the next best performing method had a median backbone accuracy of 2.8 Å r.m.s.d.$_{95}$.[21] Moreover, AF2's all-atom accuracy stood at 1.5 Å r.m.s.d.$_{95}$, compared to the 3.5 Å r.m.s.d.$_{95}$ of the best alternative method, showing AF2's capability to produce highly accurate predictions for side chains as well.[21]

For the above reasons, AF2 is the first computational method that can regularly predict protein structures with very high atomic accuracy even in cases in which no similar structure are known.[21] Furthermore, AF2 has shown a better performance than template-based methods even when a strong template is available.[20]

For the critical use and understanding of the predicted structures, AF2 introduces per-residue confidence metric, the predicted Local Distance Difference Test (pLDDT) (Figure 4.1).[22] On a scale from 0 to 100, the pLDDT estimates how well the prediction would agree with an experimental structure based on the local distance difference test Cα (lDDT-Cα).[23] A pLDDT above 90 indicates a very high-confidence prediction, between 90 and 70 signifies intermediate confidence, between 70 and 50 indicates low

[20] Schauperl, M.; Denny, R. A. *J. Chem. Inf. Model.* **2022**, *62*, 3142−3156.

[21] Jumper, J.; Evans, R.; Pritzel, A.; Green, T.; Figurnov, M.; Ronneberger, O.; Tunyasuvunakool, K.; Bates, R.; Žídek, A.; Potapenko, A.; Bridgland, A.; Meyer, C.; Kohl, S. A. A.; Ballard, A. J.; Cowie, A.; Romera-Paredes, B.; Nikolov, S.; Jain, R.; Adler, J.; Back, T.; Petersen, S.; Reiman, D.; Clancy, E.; Zielinski, M.; Steinegger, M.; Pacholska, M.; Berghammer, T.; Bodenstein, S.; Silver, D.; Vinyals, O.; Senior, A. W.; Kavukcuoglu, K.; Kohli, P.; Hassabis, D. *Nature* **2021**, *596*, 583–589.

[22] DeepMind; EMBL-EBI. AlphaFold Protein Structure Database. https://alphafold.ebi.ac.uk/ (accessed December 14, 2023).

[23] Mariani, V.; Biasini, M.; Barbato, A.; Schwede, T. *Bioinformatics* **2013**, *29*, 2722–2728.

confidence, and any residue with a pLDDT below 50 should be disregarded.[21,22]

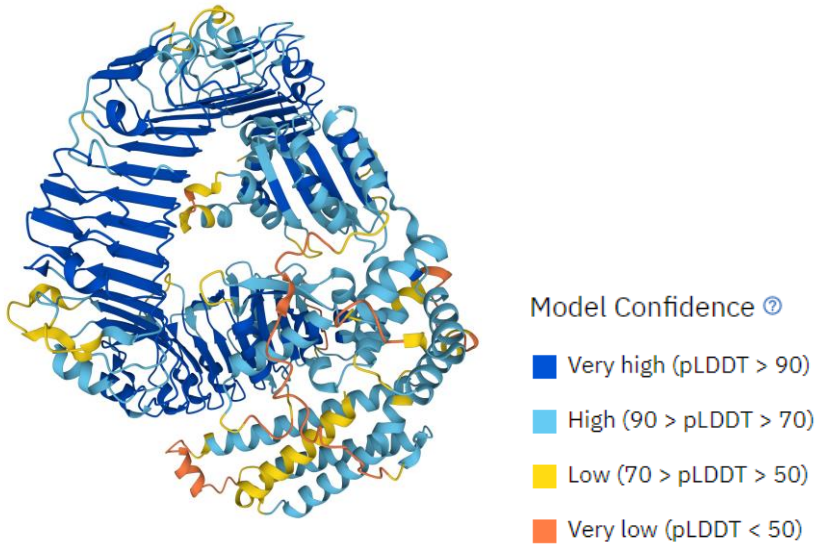

Figure 4.1. Predicted structure of Disease resistance protein (RPM1) by AF2 (AF-Q8W3K0-F1) with the colour code representation of pLDDT.

In collaboration with the European Molecular Biology Laboratory of the European Bioinformatics Institute (EMBL-EBI), the DeepMind team released, in August 2021, an open database of AF2 predicted protein structures for the entire human proteome.[21,22]

It is important to highlight to which extent AF2 predictions increased the previous structural coverage of human proteome. Prior to AF2, high-quality structural data covered 31% of the residues in the human proteome. This consisted of 17% of residues with high-quality experimentally determined structures and an additional 14% of residues accessible through template-based homology modelling with good accuracy. AF2 predicted models made a significant contribution to the human proteome that lacked structure coverage, adding an extra 19% of residues predicted with high confidence

structures (pLDDT > 90), a percentage that can be expanded to 30 % if residues with good confidence (pLDDT > 70) are also considered.[24]

If the comparison is expanded at the protein level, it should be taken into account that before AF2, 5,027 proteins lacked any structural information. When considering only very-high-confidence AF2 predictions (pLDDT > 90), this number is reduced to 1,499. Additionally, if all the predictions with lower confidence levels are included, the quantity of proteins without available structural information significantly diminishes to 29.[24] Importantly, relevant enzymes in the biomedical context are found among these proteins with no previously known three-dimensional structure that now have a high-accuracy model available thanks to AF2. Examples include alkylglycerol monooxygenase, AGMO, (Figure 4.2a) an enzyme involved in lipid metabolism linked to numerous diseases such as cancer and diabetes;[25] phosphatidylethanolamine *N*-methyltransferase, PEMT, (Figure 4.2b) another lipid metabolism enzyme among the first genes associated with non-alcoholic fatty liver disease;[26] and dihydroceramide desaturase 1, Des1, the subject of the present thesis.

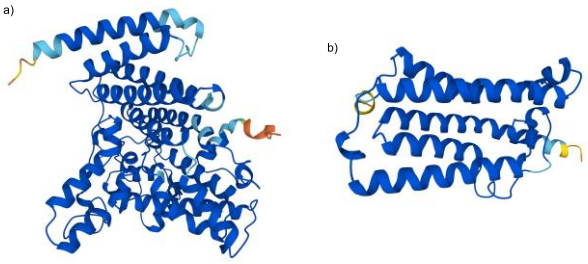

Figure 4.2. High confidence AF2 structure prediction of: a) Alkylglycerol monooxygenase, AGMO (AF-H7C0E0-F1). b) Phosphatidylethanolamine *N*-methyltransferase, PEMT (AF-Q71UY0-F1).

[24] Porta-Pardo, E.; Ruiz-Serra, V.; Valentini, S.; Valencia, A. *PLoS Comput. Biol.* **2022**, *18*, e1009818.

[25] Sailer, S.; Keller, M. A.; Werner, E. R.; Watschinger, K. *Life* **2021**, *11*, 88.

[26] Song, J.; Da Costa, K.A.; Fischer, L.M.; Kohlmeier, M.; Kwock, L.; Wang, S.; Zeisel, S.H. *FASEB J.* **2005**, *19*, 1266-1271.

For the above reasons, AF2 represents a ground-breaking event in structural biology, revolutionizing the field of protein structure predictions. However, it is crucial to understand its limitations to appropriately utilize the predicted 3D models and generate reliable information. AF2 generates a unique 3D structure of a protein based on its amino acid sequence, these predicted structures are highly representative of the solution conformation of proteins,[27] but nature is far more complicated than that.

Proteins exist in multiple conformations, all relevant for its functional role. In some cases, a single representative structure might not be sufficient to describe a protein. An illustrative example of this limitation is evident in the human tyrosine-protein kinase ABL1, known to have both an active (open) and inactive (closed) conformation.[28] While both conformations have been experimentally characterized and deposited in the Protein Data Bank (PDB), AF2 only predict a structure resembling the active (open) form.

Proteins *in vivo* can undergo multiple posttranslational modifications (PTMs) to regulate diverse cellular processes. PTMs can provoke changes in the protein structure such as domain movement, loop conformational change, protein dimerization and others. As PTMs are not included in the input sequence of AF2, structural changes due to PTMs can not be predicted.[20]

Predicting multidomain structures has proven challenging. Although AF2 also won this category in CASP14,[19] predictions for multidomain proteins were less accurate compared to the single domain level, capturing the domain−domain orientation accurately being the most significant challenge.[29] In addition, the PDB itself is biased towards single-domain structures, so suitable examples to learn from are much more limited. Proteins can also form

---

[27] Zweckstetter, M. *Protein Sci.* **2021**, *30*, 2333−2337.

[28] a) Nagar, B.; Bornmann, W. G.; Pellicena, P.; Schindler, T.; Veach, D. R.; Miller, W. T.; Clarkson, B.; Kuriyan, J. *Cancer Res.* **2002**, *62*, 4236−4243. b) Cowan-Jacob, S. W.; Fendrich, G.; Floersheimer, A.; Furet, P.; Liebetanz, J.; Rummel, G.; Rheinberger, P.; Centeleghe, M.; Fabbro, D.; Manley, P. W. *Acta Crystallogr. D* **2007**, *63*, 80−93.

[29] Pereira, J.; Simpkin, A. J.; Hartmann, M. D.; Rigden, D. J.; Keegan, R. M.; Lupas, A. N. *Proteins* **2021**, *89*, 1687-1699.

complex structures with other proteins, prosthetic groups, cofactors, DNA and RNA, inducing structural changes. AF2 only predicts single amino acid chains, preventing the study of such multidomain interactions.

Similarly, AF2 is limited in predicting protein-ligand complexes, as predictions are purely based on the proteins' amino acid sequence. The complexity of protein-ligand binding further complicates predictions. Firstly, a protein exists in multiple conformations, and the ligand selectively binds to one of these conformations. Secondly, the induced-fit model explains how the substrate provokes a change in conformation to the active site of the enzyme to achieve a perfect fit. These considerations regarding ligand-protein interactions explain observed differences in experimentally determined *apo* and *holo* structures for some proteins, differences not captured by AF2, which only offers a model.

Nevertheless, obtaining the accurately predicted structure of an apo-protein marks a significant breakthrough for drug design, as in combination with other computational methods promotes structure-based drug discovery. As discussed in the following section, impressive success stories already published demonstrate the potent tool that AF2 represents for drug discovery. It is also important to stress that, to address the previously mentioned limitations of AF2, the research community has work hard. Several groups have successfully overcome some of the limitations by combining AF2 with other computational tools or tried to improve the AF2 algorithm itself.[30]

[30] a) Del Alamo, D.; Sala, D.; Mchaourab, H. S.; Meiler, J. *eLife* **2022**, *11*, e75751. b) Stein, R. A.; Mchaourab, H. S. *PLoS Comput. Biol.* **2022**, *18*, e1010483. c) Ghani, U.; Desta, I.; Jindal, A.; Khan, O.; Jones, G.; Kotelnikov, S.; Padhorny, D.; Vajda, S.; Kozakov, D. *bioRxiv* **2022**, DOI: 10.1101/2021.09.07.459290. d) Bryant, P.; Pozzati, G.; Elofsson, A. *Nat. Commun.* **2022**, *13*, 1265. e) Evans, R.; O'Neill, M.; Pritzel, A.; Antropova, N.; Senior, A.; Green, T.; Žídek, A.; Bates, R.; Blackwell, S.; Yim, J.; Ronneberger, O.; Bodenstein, S.; Zielinski, M.; Bridgland, A.; Potapenko, A.; Cowie, A.; Tunyasuvunakool, K.; Jain, R.; Clancy, E.; Kohli, P.; Jumper, J.; Hassabis, D. *bioRxiv* **2022**, DOI: 10.1101/2021.10.04.463034. f) Reynisdottir, T.; Anderson, K. J.; Boukas, L.; Bjornsson, H. T. *PLoS Genet.* **2022**, *18*, e1010278. g) McBride, J. M.; Polev, K.; Abdirasulov, A.; Reinharz, V.; Grzybowski, B. A.; Tlusty, T. *bioRxiv* **2023**, DOI: 10.1101/2022.04.14.488301. h) Zhang, Y.; Vass, M.; Shi, D.;

4.1.2 AlphaFold2 in drug discovery

Drug discovery is one of the major application areas that require protein structure information. Understanding the nature and topography of a target is critical in drug discovery, as chemical and shape complementarity between protein and ligand are key for drug affinity.

The structures predicted by AF2 can significantly contribute to structure-based drug discovery, being especially relevant for protein targets with limited or no previous structural information. Access to the three-dimensional structure of the target allows for the identification of pockets and functional relevant regions on the protein, as well as *in silico* exploration of the target using different techniques. Despite its recent development, the research community has demonstrated that AF2 is a valuable tool for drug discovery.[31] Some noteworthy examples are briefly discussed in this section.

Ren *et al.* presented the first demonstration of applying AlphaFold2 to the hit identification process in drug discovery.[32] Authors applied an AF2 structure to their endo-to-end AI-powered drug discovery engines. The biocomputational platform PandaOmics provided the protein of interest for the treatment of hepatocellular carcinoma (HCC). In this way, CDK20 was selected as the target, a protein with limited reported inhibitors and no available 3D-structural information. The CDK20 structure predicted by

---

Abualrous, E.; Chambers, J. M.; Chopra, N., Higgs, C.; Kasavajhala, K.; Li, H.; Nandekar, P.; Sato, H.; Miller, E. B.; Repasky, M. P.; Jerome, S. V. *J. Chem. Inf. Model.* **2023**, *63*, 1656–1667. i) Hekkelman, M. L.; de Vries, I.; Joosten, R. P.; Perrakis, A. *Nat. Methods* **2023**, *20*, 205-213.

[31] a) Liu, F.; Jiang, X.; Yang, J.; Tao, J.; Zhang, M. *Bioinform.* **2022**, *23*, bbac365. b) Park, H. M.; Park, Y.; Vankerschaver, J.; Van Messem, A.; De Neve, W.; Shim, H. *Pharm.* **2022**, *15*, 310. c) Hong, L. L.; Liu, Y. N.; Kong, J. Q. *Int. J. Biol. Macromol.* **2024**, *254*, 127721. d) Medvedev, K. E.; Schaeffer, R. D.; Chen, K. S.; Grishin, N. V *Sci. Rep.* **2023**, *13*, 11988. e) Baselious, F.; Robaa, D.; Sippl, W. *Comput. Biol. Med.* **2023**, *167*, 107700.

[32] Ren, F.; Ding, X.; Zheng, M.; Korzinkin, M.; Cai, X.; Zhu, W.; Mantsyzov, A.; Aliper, A.; Aladinskiy, V.; Cao, Z.; Kong, S.; Long, X.; Liu, B. H. M.; Liu, Y.; Naumov, V.; Shneyderman, A.; Ozerov, I. V.; Wang, J.; Pun, F. W.; Polykovskiy, D. A.; Sun, C.; Levitt, M.; Aspuru-Guzik, A.; Zhavoronkov, A. *Chem. Sci.* **2023**, *14*, 1443–1452.

AlphaFold2 has an overall high confidence level, although with the exception of the C-terminal end (Figure 4.3, a, orange region). For this reason, the authors decided to exclude this low-confidence region from the predicted structure. Subsequently, the structure was submitted as an input for molecule generation using Chemistry42.[33]

In total, Chemistry42 designed 8,918 ligand compounds able to bind properly with CDK20. After molecular docking and clustering, 54 molecules with diverse hinge core structures were prioritized, and 7 compounds were selected for synthesis. A small molecule hit, named ISM042-2-001, was identified (Figure 4.3, b) which, after being tested in biological assays, showed an equilibrium dissociation constant value (Kd) of 9.2 ± 0.5 μM. It is noteworthy that only 30 days elapsed between target identification and the obtaining of this biological result.

Based on the binding mode of the hit molecule observed in the molecular docking of the compound, the authors conducted a second round of compound generation, trying to maximize the previously observed favourable interactions. Thus, 6 out of 16 generated molecules were synthesized and biologically tested. A second hit, called ISM042-2-049, was identified (Figure 4.3, c). It showed a 24-fold improvement in binding affinity, with measured Kd value of 360.0 ± 14.1 nM.

[33] Ivanenkov, Y. A.; Polykovskiy, D.; Bezrukov, D.; Zagribelnyy, B.; Aladinskiy, V.; Kamya, P.; Aliper, A.; Ren, F.; Zhavoronkov, A. *J. Chem. Inf. Model.* **2023**, *63*, 695–701.

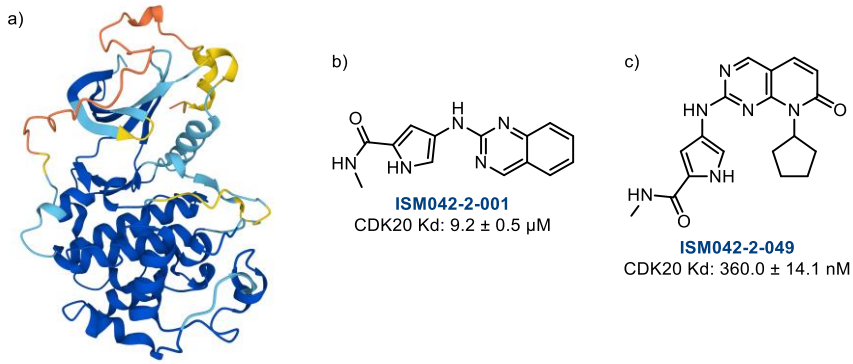

Figure 4.3. a) AF2 predicted structure of CDK20 (AF-Q8IZL9-F1). b) First hit molecule identified. c) Second hit molecule identified after optimization of favourable interactions observed in docking.

The same strategy was applied to salt-inducible kinase 2 (SIK2),[34] a potential target for anti-inflammation and anti-cancer therapy. The AF2 structure of SIK2 presents loops predicted with very low confidence (Figure 4.4, a); however, the authors did not specify how they considered these areas.

In this case, the molecular docking of four previously reported SIK2 inhibitors with the AF2 predicted structure of SIK2 allowed the identification of H-bond interactions essential for inhibition. The study also provided a deeper comprehension of the different regions within the enzyme's active site and its nature. This information guided the generation of compounds via Chemistry42 platform using the structure of SIK2 provided by AF2, leading to the identification of a first hit, compound **SIK2-7g** (Figure 4.4, b, IC_{50} = 23 nM). Further optimization based on the docking studies of **SIK2-7g** furnished SIK2 inhibitor **SIK2-8f** (Figure 4.4, c), with significantly enhanced potency (IC_{50} = 0.6 nM) and selectivity against SIK2 compared with the reported inhibitors.

[34] Zhu, W.; Liu, X.; Li, Q.; Gao, F.; Liu, T.; Chen, X.; Zhang, M.; Aliper, A.; Ren, F.; Ding, X.; Zhavoronkov, A. *Bioorg. Med. Chem.* **2023**, *91*, 117414.

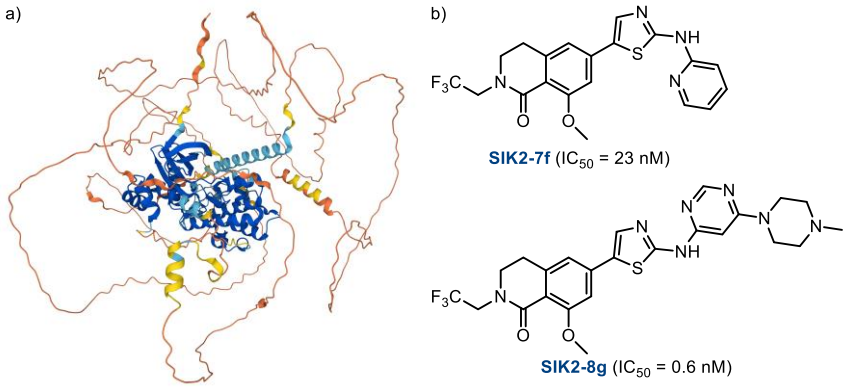

Figure 4.4. a) AF2 predicted structure of SIK2 (AF-Q9H0K1-F1). b) Novel SIK2 inhibitors revealed through AI-powered drug discovery engines.

The discovery of new active molecules against biologically relevant targets remains limited. However, researchers are leveraging AlphaFold2 predictions to conduct computational studies that illuminate crucial targets, serving as a foundation for future drug development.

Weng *et al*. employed AF2 to predict the 3D structure of WSB1 (SOCS-box-containing WD-40 protein), a new potential anticancer target lacking 3D structural information.[35] The AF2 predicted structure (Figure 4.5, a) was used to perform molecular docking, including AutoDock-GPU and Glide, to screen for WSB1 inhibitors. **G490-0341** (Figure 4.5, b) exhibited the most favourable binding mode and stability, indicating its potential as a starting point for further investigation. This study provides some valuable insights into the structure of WSB1 and the binding behaviour of its inhibitors, facilitating the future development of new compounds able to inhibit WSB1.

[35] Weng, Y.; Pan, C.; Shen, Z.; Chen, S.; Xu, L.; Dong, X.; Chen, J. *Evid.-Based Complement. Alternat. Med.* **2022**, 4629392.

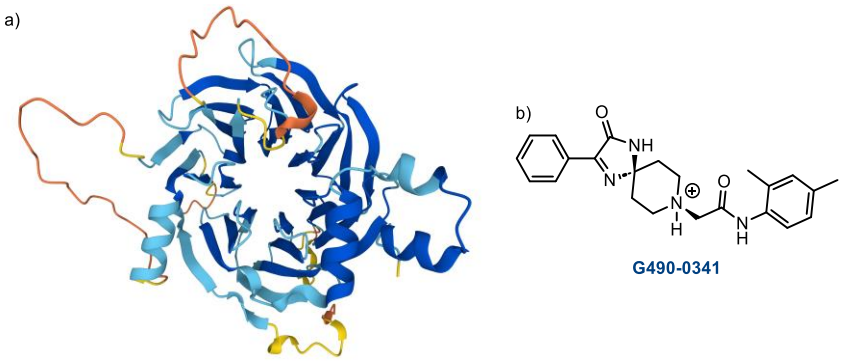

Figure 4.5. a) AF2 predicted structure of WSB1 (AF-A0A024Qz51-F1). b) Structure of **G490-0341**.

Similarly, Liang *et al.*[36] identified **JMJD897–99** as a novel oncogene correlated with immunosuppression and DNA repair through bioinformatics analysis. Subsequently, they used AF2 to predict the 3D structure of JMJD8 and conducted virtual screening to identify two promising JMJD8 inhibitor candidates, although they were not biologically evaluated.

Yang *et al.*[37] obtained the spike protein structures of 10 main globally endemic SARS-CoV-2 strains using AlphaFold2 with high accuracy. In contrast to previous classifications based on different SARS-CoV-2 strains, the authors classify them by structural similarity. This approach may reflect the current characteristics of the epidemic more accurately than those based on protein sequence alone may. Furthermore, by virtual screening the ZINC database[38] against a high-accuracy predicted structure of Delta spike protein, five compounds exhibited high binding affinity, which might contribute towards the development of clinical anti-SARS-CoV-2 medicines.

---

[36] Liang, X.; Zhang, H.; Wang, Z.; Zhang, X.; Dai, Z.; Zhang, J.; Luo, P.; Zhang, L.; Hu, J.; Liu, Z.; Bi, C.; Cheng, Q. *Front. Immunol.* **2022**, *13*, 875786.

[37] Yang, Q.; Jian, X.; Syed, A. A. S.; Fahira, A.; Zheng, C.; Zhu, Z.; Wang, K.; Zhang, J.; Wen, Y.; Li, Z.; Pan, D.; Lu, T.; Wang, Z.; Shi, Y. *Research* **2022**, 9781758.

[38] Irwin, J. J.; Shoichet, B. K. J. *Chem. Inf. Model.* **2005**, *45*, 177-182.

4.2 Results and discussion

4.2.1 Construction of a Des1 complete 3D model

As previously commented, there are no *apo* or *holo* X-ray crystal structures of human dihydroceramide desaturase 1 (Des1). Template-based modelling is also impractical due to the absence of close homologues in the PDB. However, the advent of AlphaFold2 in the course of this thesis provided, to our delight, a highly confident model for Des1, with an average predicted Local Distance Difference Test (pLDDT) of 96.31 (Figure 4.6).[39] Regions of lower confidence (70 > pLDDT > 50) involve only seven residues, corresponding to the C-terminal and the N-terminal loop. We assume that these small and peripheral regions are not relevant for the enzyme activity.

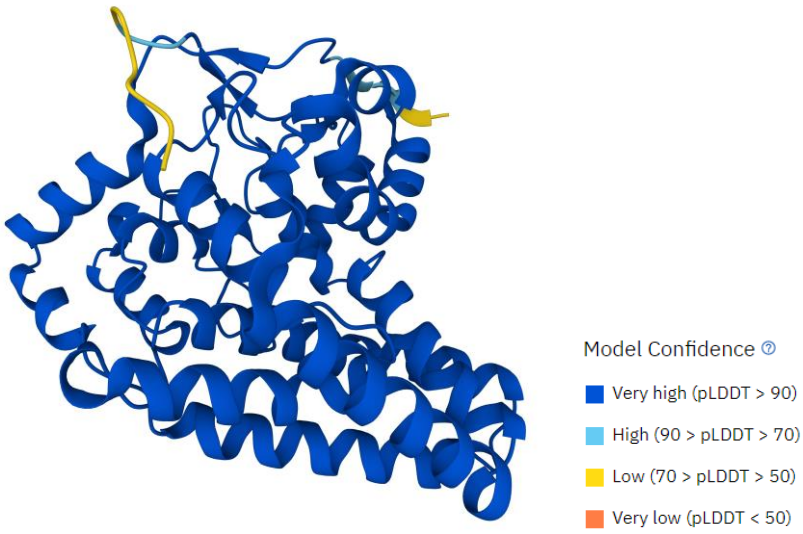

Figure 4.6. 3D structure of Des1 predicted by AF2.

[39] AlphaFold by EMBL-EBI. AlphaFold: O15121. https://alphafold.ebi.ac.uk/entry/O15121 (accessed December 1, 2023).

An initial observation of the model, with polar amino acids coloured in red and non-polar amino acids in grey, reveals a discernible distribution pattern Figure 4.7). The polar amino acids predominantly cluster in one region, indicative of Des1's transmembrane nature, situated in the endoplasmic reticulum and mitochondrial bilipidic membranes.[40] Non-polar amino acids are inferred to be inserted into the membrane, while polar amino acids are concentrated in the hydrophilic region outside the membrane.

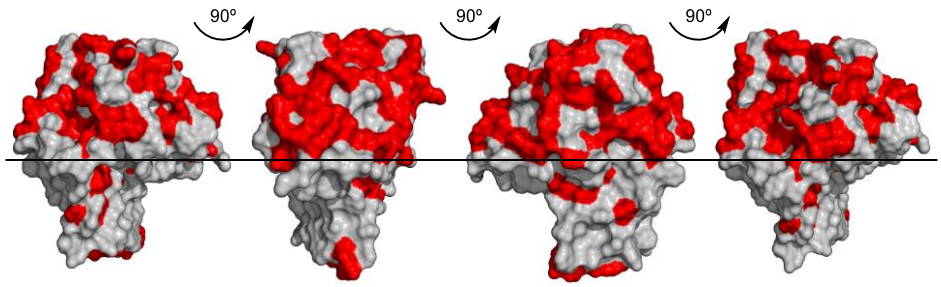

Figure 4.7. Surface representation of Des1 model predicted by AF2. Polar amino acids are coloured in red and non-polar amino acids in grey.

Furthermore, a well-defined deep pocked is evident (Figure 4.8, a). When only the interior surface of the pocket is represented, its shape and nature is revealed (Figure 4.8, b-d). As one can see in the different perspectives offered in Figure 4.8, the pocket has a flat and wide shape. The pocket, primarily composed of non-polar amino acids, features a high concentration of polar amino acids at its end.

[40] UniProt. UniProtKB Entry: O15121. https://www.uniprot.org/uniprotkb/O15121/entry (accessed December 1, 2023).

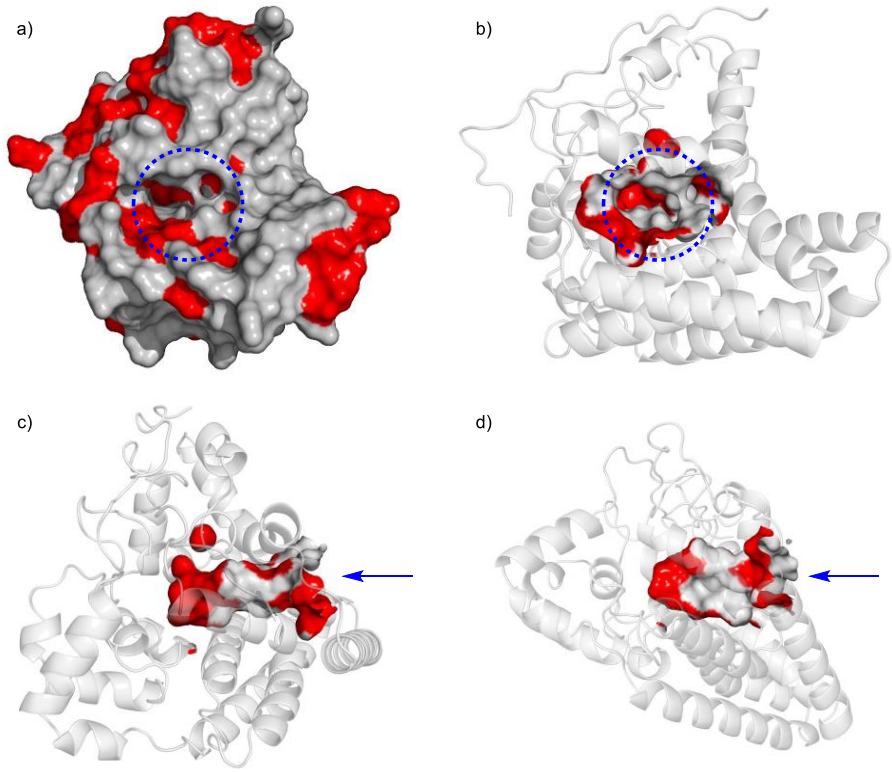

Figure 4.8. Surface representation of Des1 model predicted by AF2 with polar amino acids colored in red and non-polar amino acids in grey. In blue is signalled the aperture of a well-defined pocket. a) Front view of the pocket identified in Des1. b) Front view of the pocket identified in Des1, only representing the interior surface. c) Lateral view of the pocket identified in Des1, only representing the interior surface. d) Bottom view of the pocket identified in Des1, only representing the interior surface.

As previously mentioned, AF2 predictions are solely based on the amino acid sequence and lack information about prosthetic groups. Des1 contains a non-heme oxo-diiron specie with a Fe_2O_2 molecule in the active binding site, crucial to catalyze the desaturation of the natural substrate.[41] Therefore, to obtain a complete model of the enzyme, the oxo-bridged diiron specie had to be introduced in the 3D structure.

[41] Savile, C. K., Fabriàs, G.; Buist, P. H. *J. Am. Chem. Soc.* **2001**, *123*, 4382-4385.

In the context of a collaboration with Professor Xavier Barril (ICREA Research Professor, University of Barcelona) the Fe_2O_2 was positioned in the region of high concentration of polar amino acids at the end of the pocket. In this region, nine histidine and one glutamic acid residues were identified (Figure 4.9, a). These residues are described to participate in the coordination of oxo-bridged diiron species,[42] which strongly supports the insertion of the Fe_2O_2 in this position. The Fe_2O_2 group (Figure 4.9, b) was located with one iron atom coordinated by five histidine residues (His89, His93, His128, His132, and His262), and the second one to four histidine residues (His131, His233, His263, and His259) and a glutamic acid residue (Glu232).

To the best of our knowledge, this represents the first reported complete 3D model of the Fe_2O_2-Des1 system (Figure 4.10).

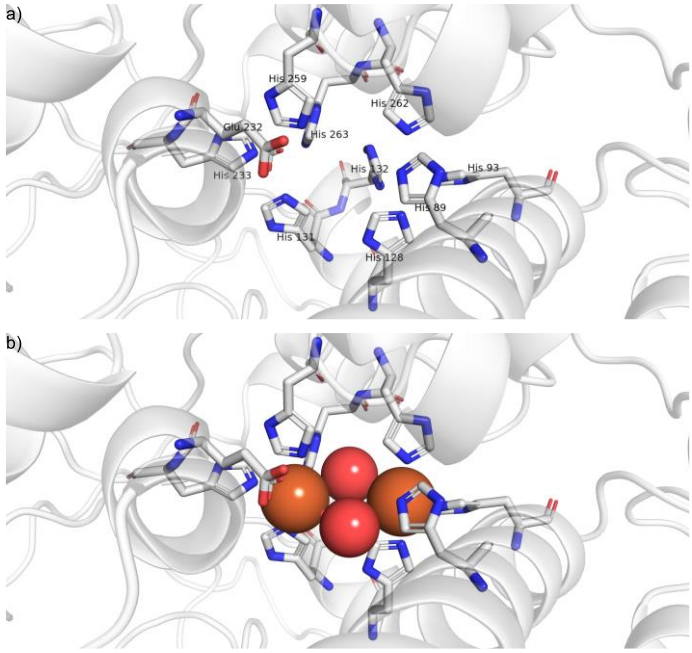

Figure 4.9. a) High concentration of polar amino acids at the end of Des1 binding site: His89, His93, His128, His131, His132, His233, His259, His262, His263 and Glu232. b) Positioning of the Fe_2O_2 specie coordinated by 9 histidine and 1 glutamate residues of Des1.

[42] Nogueira, M. L. C.; Pastore, A. J.; Davidson, V. L. *Arch. Biochem. Biophys.* **2021**, *705*, 108917.

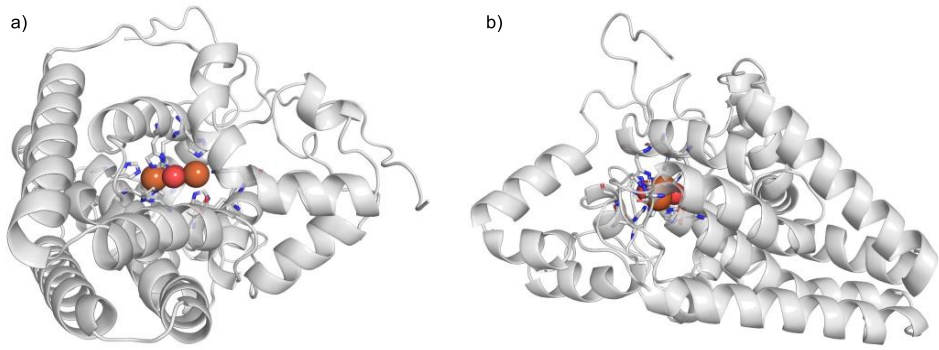

Figure 4.10. Front (a) and lateral (b) view of Fe_2O_2-Des1 system 3D model.

4.2.2 Molecular docking studies with Des1-Fe_2O_2 3D model.

With the constructed 3D complete model of dihydroceramide desaturase 1 (Des1-Fe_2O_2 complex) at our disposal, we conducted docking studies to gain a deeper understanding of the molecular events involved in the enzyme inhibition. Docking calculations were performed as part of the collaboration with Xavier Barril (ICREA Research Professor, University of Barcelona).

In this investigation, molecular docking calculations and subsequent interpretation will be employed to address concerns related to Des1 inhibition mechanism, following the strategy outlined in Scheme 4.1. Through docking calculations of reference inhibitors **GT11** and **XM462**, we aim to gain insights into the molecular events underlying enzyme inhibition, identifying key ligand-enzyme interactions. This study also sights to elucidate the absence of inhibitory activity *in vitro* observed in the triazole and furan ceramide analogs (**1a-c**, **2a-c**, **3a-c**) discussed in the preceding chapter of this thesis. Interpretation of the obtained results could serve as guidance for the design and proposal of future Des1 inhibitors.

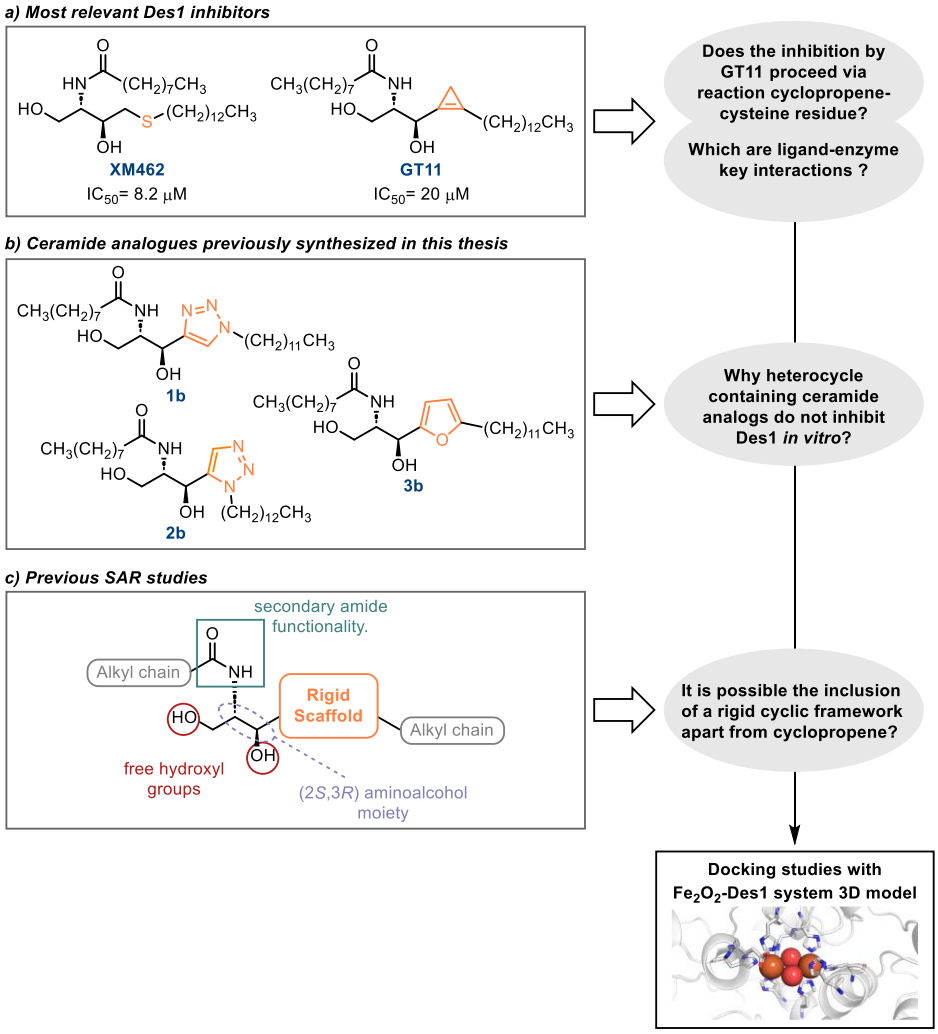

Scheme 4.1. Aims and strategy of molecular docking studies with Fe_2O_2-Des1 system 3D model.

To initiate the study, the Des1-Fe_2O_2 complex was prepared for docking in MOE software using the Protein Preparation protocol.[43] Docking calculations were performed with the reference Des1 inhibitors **GT11** and **XM462**, as well as the natural substrate **dhCer** to have information about key

[43] Molecular Operating Environment (MOE), 2019.01; Chemical Computing Group ULC, 1010 Sherbooke St. West, Suite #910, Montreal, QC, Canada, H3A 2R7, 2021

ligand-enzyme interactions governing Des1 inhibition. In each case an exhaustive docking was performed (50 independent genetic algorithm optimizations) and top 10 docking poses were visualized. The best scoring pose forming favorable interactions with the enzyme was selected as the candidate-binding pose.

The best binding mode for **dhCer** (Figure 4.11, a) revealed a folded conformation of both alkyl chains, positioning C4 in close proximity to one Fe atom of the Fe_2O_2 specie. This is in good agreement with the knowledge that C4-H bond cleavage is the first event taking place in the double bond formation in **dhCer**.[19] In this binding position an H-bond interaction between Tyr170 and OH-1 was also stablished.

Analysing the docking poses of **GT11** and **XM462** we assumed that the binding model would be similar to that observed in **dhCer**, as the active compounds are structural analogs of the natural substrate. Following this approach and knowing that the C4-C5 bond dehydrogenation is catalysed by the diiron-dioxo complex, the binding mode of **GT11** with the cyclopropene ring near one iron metal centre was selected (Figure 4.11, b). The proposed binding mode for **GT11** also exhibited a folded conformation of the hydrophobic chains. Two H-bond interactions were identified, with OH-3 hydrogen bonding to an oxygen at the dioxo-diiron complex, while OH-1 formed a hydrogen bond with Tyr170.

For compound **XM462**, a folded conformation of the alkyl and acyl chains was also observed (Figure 4.11, c). The best docking pose exhibited the same H-bond interaction between the oxygen atom at the complex and OH-3, as observed in **GT11**. In this case, the sulfur atom is in close proximity to the same iron metal center. Additionally, the OH-1 group participated in a hydrogen bond with the Tyr120 phenolic group (Figure 4.11, c). The different orientation of OH-1 in **GT11** and **XM462** could be forced by the size of sulphur atom in the latter.

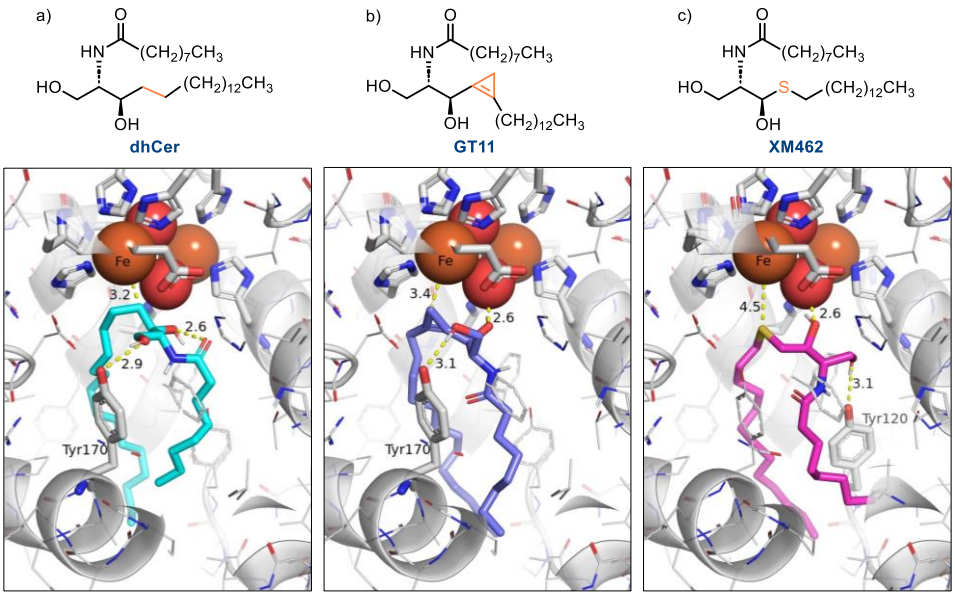

Figure 4.11. Binding mode of dihydroceramide (a), **GT11** (b) and **XM462** (c). Aminoacid residues involved in ligand-enzyme interactions are marked and indicated in sticks; those not involved in specific interactions are represented with lines. The length of interactions in Å is specified.

Observed interactions for the natural substrate and known inhibitors of Des1 with Des1-Fe_2O_2 complex are summarized in Table 4.1.

Table 4.1. Summary of enzyme-ligand interactions identified in the docking of Dihydroceramide, **GT11** and **XM462.**

Compound[a]	Tyr170	Tyr120	Oxygen (Fe_2O_2)	Fe_2O_2 cluster proximity
DhCer	OH-1 H-bond	-	-	CH-4
GT11	OH-1 H-bond	-	OH-3 H-bond	Cyclic methylene
XM462	-	OH-1 H-bond	OH-3 H-bond	S atom

a. A folded conformation of alkylic chains was observed in all cases.

Based on this study, the main requisites for Des1 inhibitory activity in a ceramide-like ligand include:

a) A folded conformation of the ligand hydrophobic chains in the Des1 active site.
b) Close proximity of positions 4 or 5 of ceramide to the Fe_2O_2 cluster.
c) An OH-3 hydrogen bond with one of the oxygen atoms of the dioxo-diiron specie.
d) Involvement of the primary hydroxyl group in a hydrogen bond interaction with a residue of the enzyme.

It is worth mentioning that there are no cysteine residues in the Des1 active center. This piece of evidence opens the door to exploring an inhibition mechanism for **GT11** that differs from the previously proposed, which involves a reaction of the cyclopropene moiety with a cysteine residue of the enzyme's active site.[44] The present study points out an alternative inhibition mechanism consisting of specific and strong non-covalent interactions of the ligand with polar residues and the prosthetic group located at the end of the long deep channel constituted by the active site.

Additionally, the amido group of **GT11**, in its most probable binding position, is distant from residues for potential polar interactions, challenging the hypothesis of its involvement in an H-bond interaction. This hypothesis arises from the structure-activity relationship studies conducted on GT11,[45] where methylation of the secondary amide led to a loss of inhibitory activity. This effect could be attributed, therefore, to steric influences rather than a loss of hydrogen-bond donor capacity.

[44] Triola, G.; Fabriàs, G.; Llebaria, A. *Angew. Chem. Int. Ed.* **2001**, *40*, 1960-1962.
[45] Bedia, C.; Triola, G.; Casas, J.; Llebaria, A.; Fabriàs, G. *Org. Biomol. Chem.* **2005**, *3*, 3707-3712.

Following the identification of interactions stablished between the enzyme and reference inhibitors, molecular docking was performed with synthesized compounds **1b**, **2b**, and **3b**. As ceramide analogues **1a-c**, **2a-c**, **3a-c** showed no inhibition in cell lysates regardless the length of the *N*-acyl chain, for comparative purposes the docking study focused on ceramide analogues **b**, containing the same acyl chain as **GT11** and **XM462**.

Regarding compound **1b**, with a 1,4-disubstituted triazole core, as docking study evidenced, the bulky size of the ring moiety affects the folding of the structure and, as a result, the arrangement of the hydroxyl groups. This provoked the loss of all the previously identified favourable H-bond interactions (Figure 4.12, a).

In contrast, the 1,5-disubstituted triazole ring of compound **2b**, behaving like a *cis*-olefino mimetic surrogate, approached the iron metal center more effectively, allowing the structure to fold more adequately (Figure 4.12, b). In this case, the hydrogen bond between the OH-3 and the dioxo-diiron oxygen was formed. However, the key H-bond interaction involving OH-1 group was not observed, possibly due to the ring's size or even its nature.

For compound **3b**, with a 2,4-disubstituted furan core, similar in size to the triazole group, both OH-1 and OH-3 were unable to participate in favourable interactions due to the different arrangement of the heterocycle compared to the cyclopropane moiety in **GT11** (Figure 4.12, c).

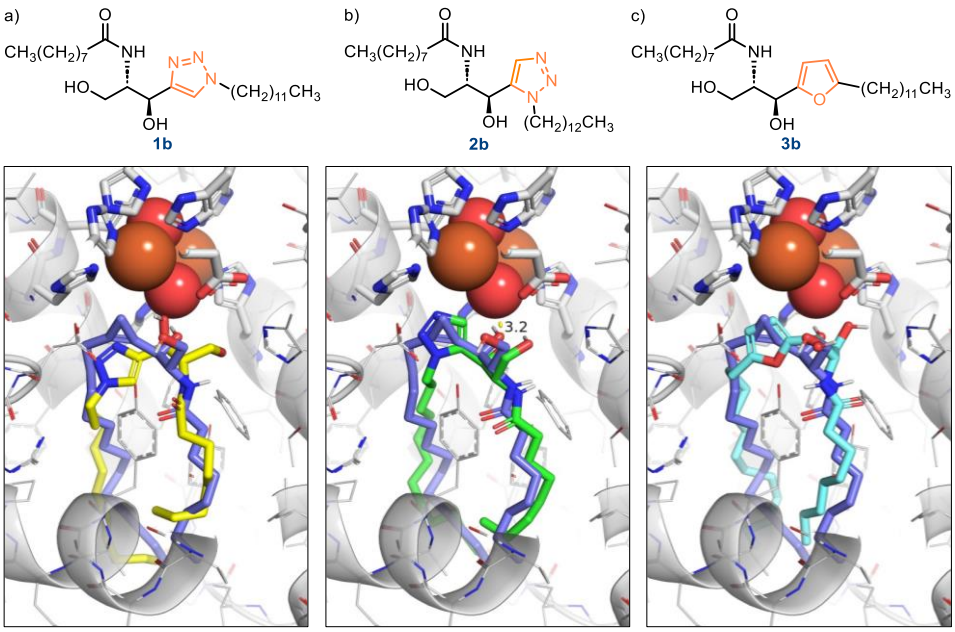

Figure 4.12. Binding mode of **1b** (a, yellow), **2b** (b, green) and **3c** (c, cyan) overlapped with that of **GT11** (blue). Interaction between OH-3 and the dioxo-diiron oxygen is indicated in the binding mode of product **2b** (b).

With these results, it appears that the ligand-enzyme interactions observed in **GT11** and **XM462** are crucial for the inhibition of the enzyme. It seems that both H-bonds are necessary, as if the ligand only establishes one of them, as in the case of ceramide analog **2b**, it still is not able to inhibit the protein. This study indicates that five-membered ring scaffolds are not good surrogates for the cyclopropene moiety in **GT11**, with the bulkiness of the ring likely causing a distortion of the optimal position of the ligand in the active site of the enzyme. Furthermore, no additional π-stacking or hydrogen bonding interactions involving the heterocycle are observed. This evidence could explain the lack of direct Des1 inhibitory activity displayed by the heterocycle-containing ceramide analogs **1a-c**, **2a-c**, **3a-c**.

Thus, the results obtained in the docking studies with the constructed model of Des1 align with those of inhibitory assays, for both reference inhibitors and the synthesised compounds, and may provide the basis for the proposal of new Des1 inhibitors.

4.2.3. Proposal of a new Des1 inhibitors candidate

In view of these results, we decided to evaluate the binding mode of a ceramide analog containing a smaller rigid scaffold. We focused our attention on the cyclopropenone ring as a rigid scaffold (Figure 4.13), as it is expected to retain the folded conformation of the alkyl chains observed in the docking of active Des1 inhibitors. Moreover, we hypothesize that the oxo moiety could interact with the iron center in the prosthetic group.

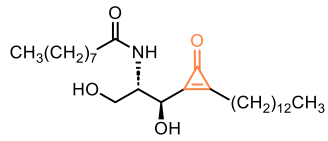

45

Figure 4.13. Proposed cyclopropenone ceramide analog, **45**.

As depicted in Figure 4.14 ceramide analogs **45** present a docking pose in which the cyclopropenone moiety is proximal to one iron center of the complex, possibly due to an oxo coordination to the iron atom. This promotes a proper arrangement in the active site in which the alkyl chains present a folded conformation, and the hydroxyl groups are involved in favourable H-bond interactions. In this case, the OH-1 group formed a H-bond with Glu232 residue, and the OH-1 group with the dioxo-diiron oxygen atom.

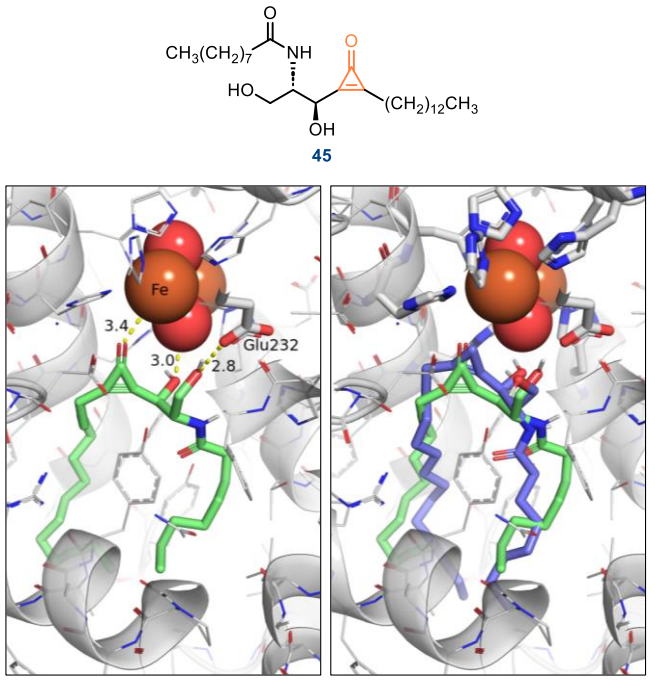

Figure 4.14. Binding mode of **45** (left) and binding modes of **45** (green) overlapped with that of **GT11** (blue). Aminoacid residues involved in ligand-enzyme interactions are marked and indicated in sticks; those not involved in specific interactions are represented with lines. The length of interactions in Å is specified.

The three crucial interactions previously observed for the reference inhibitors were also identified for compounds **45**. Thus, ceramide analogs containing a cyclopropenone as structural rigid motif can be considered as a promising Des1 inhibitor candidate. Its exploration is detailed in Chapter V of this thesis.

CHAPTER V

Synthesis and biological evaluation as Des1 inhibitors of cyclopropenone containing ceramide analogues and derivatives

UNIVERSITAT ROVIRA I VIRGILI
TARGETING DES1: SYNTHESES OF CERAMIDE ANALOGUES WITH A RIGID SCAFFOLD, INHIBITORY ASSAYS, AND AF2-ASSISTED STRUCTURAL INSIGHTS REVEAL PR280 AS A POTENT INHIBITOR
Pablo Rivero Prieto

5.1 Introduction

Taking into account that ceramide analogues incorporating five-membered ring scaffolds showed ineffective inhibiting Des1 in cell lysates (Chapter III), we hypothesized in the last chapter that a smaller rigid scaffold would be a better candidate for Des1 inhibition. This hypothesis was supported by docking calculations (Chapter IV), which showed that geometry conferred by the 3-membered cycle enabled the analogues containing a cyclopropenone to establish favourable polar interactions with the enzyme. Thus, the synthesis and biological evaluation of ceramide analogues incorporating a cyclopropenone moiety, **45a-c**, will be addressed in this chapter (Figure 5.1).

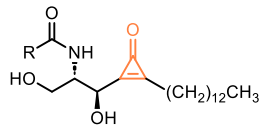

45a R = $(CH_2)_5CH_3$
45b R = $(CH_2)_7CH_3$
45c R = $(CH_2)_9CH_3$

Cyclopropenone ceramide analogues

Figure 5.1. Proposed cyclopropenone ceramide analogues, **45a-c**.

Synthetized for the first time by Berslow,[1] cyclopropenones are chemical entities with unique properties. Their three-membered ring exhibits aromatic character,[2] large dipole moment (μ = 4–5 D), high basicity, and significant angle strain.[3] Protonation of the carbonyl oxygen yield a 2p aromatic hydroxycyclopropenyl cation (Scheme 5.1).[2,3] Moreover, cyclopropenones can undergo nucleophilic attack at either the carbonyl carbon or at the olefinic carbons (1,2- or 1,4-nucleophilic addition respectively) (Scheme 5.1).

---

[1] Breslow, R.; Haynie, R.; Mirra, J. *J. Am. Chem. Soc.* **1959**, *81*, 247–248.

[2] a) Staley, S. W.; Norden, T. D.; Taylor, W. H.; Harmony, M. D. *J. Am. Chem. Soc.* **1987**, *109*, 7641-7641.b) Wang, H. J.; Schleyer, P. V. R.; Wu, J. I.; Wang, Y. *Int. J. Quantum Chem.* **2011**, *111*, 1031–1038.

[3] Potts, K. T.; Baum, J. S. *Chem. Rev.* **1974**, *74*, 189–213.

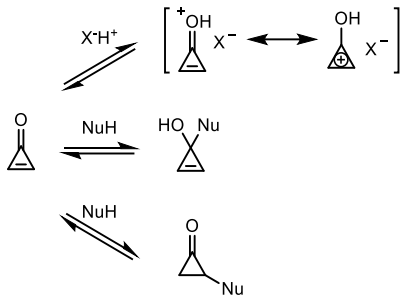

Scheme 5.1. Electrophilic and basic character of cyclopropenones.

Cyclopropenone have garnered attention in the biological community for their applications in the chemical ligation of biomolecules. Demonstrating utility in this context due to their electrophilic properties and stability in cellular media. Several examples of their successful use in this context have been reported in recent years.[4] However, examples of cyclopropenones as ligands against a biologically relevant target are limited, some of them being natural products.

Natural products containing the cyclopropenone moiety are quite rare, and only a few compounds have been isolated (Figure 5.2), some of them showing interesting biological activities. In 1981, Schuster and co-workers isolated three cyclopropenone-containing natural products (**46**-**48**) from the plant *Telekia speciosa*.[5] Compound **49** was isolated in 2010 by Zhang and Jim from the aerial parts of the flowering plant *Inula lineariifolia*.[6] Penitricin was isolated from *Penicillium aculeatum*[7] and is the only naturally occurring

[4] a) Shih, H. W.; Prescher, J. A. *J. Am. Chem. Soc.* **2015**, *137*, 10036−10039. b) Row, R. D.; Prescher, J. A. *Org. Lett*. **2018**, *20*, 5614−5617. c) Row, R. D.; Shih, H. W.; Alexander, A. T.; Mehl, R. A., Prescher, J. A. *J. Am. Chem. Soc.* **2017**, *139*, 7370−7375. d) Istrate, A.; Geeson, M. B.; Navo, C. D.; Sousa, B. B.; Marques, M. C.; Taylor, R. J.; Journeaux, T.; Oehler S. R.; Mortensen, M. R.; Deery, M. J.; Bond, A. D.; Corzana, F.; Jiménez-Osés, G. Bernades, G. J. L. *J. Am. Chem. Soc.* **2022**, *144*, 10396−10406. e) Lv, S.; Xu, F.; Fan, Y.; Ding, K.; Li, Z. *J. Med. Chem.* **2023**, *66*, 2851−2864.

[5] Bohlmann, F.; Jakupovic, J.; Muller, L.; Schuster, A. *Angew. Chem.* **1981**, *93*, 280-281.

[6] Nie, L. Y.; Qin, J. J.; Huang, Y.; Yan, L.; Liu, Y. B.; Pan, Y. X.; Jin, H. Z.; Zhang, W. D. *J. Nat. Prod*. **2010**, *73*, 1117-1120.

[7] Okuda, T.; Yokose, K.; Furumai, T.; Maruyama, H.B. J. *Antibiot.* **1984**, *37*, 718-722.

cyclopropenone compound which shows biological activity as an antibiotic.[8] Synthesis and evaluation of Penitricin derivatives showed that the presence of both, α-hydroxymethyl and cyclopropenone structural functionalities are essential for eliciting antibacterial activity.[9]

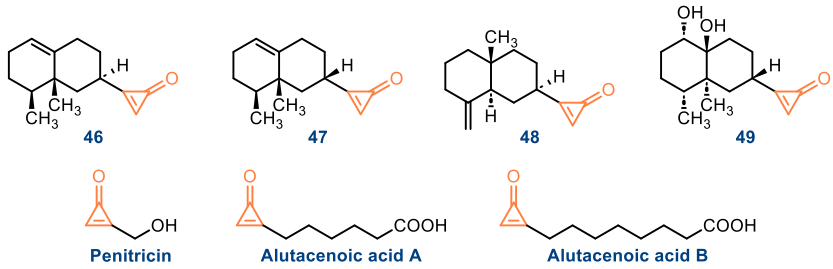

Figure 5.2. Cyclopropenone-containing natural products.

Alutacenoic acids A and B were isolated from *Penicillium aculeatum*; these fungal metabolites do not present antibacterial activity but are specific inhibitors of factor XIIIa, showing irreversible inhibition of the enzyme.[10] Factor XIIIa, a plasma transglutaminase, is pivotal in the blood coagulation cascade. Inhibitors of factor XIIIa may have therapeutic potential for thrombosis, atherosclerosis, and coronary heart disease.[11] Docking studies of these compounds showed that the carbonyl oxygen of the cyclopropenone moiety forms an H-bond with the indole NH group of Trp279 and the terminal olefinic carbon is in close proximity to the sulphur atom of Cys314.[12] Thus, a nucleophilic attack of Cys314 thiol, forming an enzyme-ligand adduct, provides a feasible explanation for the irreversible inhibition of the enzyme.

---

[8] Okuda, T.; Shimma, N.; Furumai, T. *J. Antibiot.* **1984**, *37*, 723-727.

[9] Tokuyama, H.; Isaka, M.; Nakamura, E.; Ando, R.; Morinaka, Y. *J. Antibiot.* **1992**, *45*, 1148-1154.

[10] Kogen, H.; Kiho, T.; Tago, K.; Miyamoto, S.; Fujioka, T.; Otsuka, N. Suzuki-Konagi, K.; Ogita, T. *J. Am. Chem. Soc.* **2000**, *122*, 1842-1843.

[11] a) Kloczko, J.; Wojtukiewicz, M.; Bielawiec, M.; Zarzycka, B.; Kinalska, I. *Acta Haematol.* **1986**, *76*, 81-85. b) Francis, C. W.; Connaghan, D. G.; Scott, W. L.; Marder, V. J. *Circulation* **1987**, *75*, 1170-1177. c) Kloczko, J.; Wojtukiewicz, M.; Bielawiec, M.; Zuch, A. *Thromb. Res.* **1988**, *51*, 575-581.

[12] Iwata, Y.; Tago, K.; Kiho, T.; Kogen, H.; Fujioka, T.; Otsuka, N.; Suzuki-Konogai, K.; Ogita, T.; Miyamoto, S. *J. Mol. Graphics Mod.* **2000**, *18*, 591-599.

More recently, cyclopropenone containing compounds have attracted considerable interest for their biological applications as proteinase inhibitors. Thinking of the electrophilic properties of cyclopropenones, R. Ando *et al.* designed a new class of cysteine proteinase peptidyl inhibitors including this moiety (Figure 5.3, a).[13] This class of enzymes contain a cysteine in the active site that could be engaged in a nucleophilic attack with the cyclopropenone functionality. Inhibitors showed strong inhibitory activities only to cysteine proteinases such as m-calpain, cathepsin B, and cathepsin L and not to serine and asparatic proteinases. However, studies on inhibitory mechanism revealed that these cyclopropenone-containing compounds are competitive and reversible inhibitors. Thus, the proposed inhibition via reaction of the inhibitor with the cysteine residue of the enzyme could not be confirmed. Possibly, these inhibitors behave as classical competitive inhibitors by occupying the enzyme active site without undergoing any covalent modification. Inhibitors may also become protonated in the enzyme active site leading to the formation of the aromatic hydroxycyclopropenyl cation. This process is reversible and aligns with the observed reversible nature of the inhibition. The authors did not conduct studies addressing these possibilities.

M. Cohen. *et al.* studied the inhibition of the prototype cysteine protease papin by the peptidyl cyclopropenone **50** (Figure 5.3, b),[14] finding that it showed up as an irreversible inhibitor of this enzyme. Compound **50** was also tested as inhibitor of cathepsin B, showing a reversible inhibition, as previously observed by R. Ando *et al*.[13] Thus, the same compound exhibits two very different inhibitory mechanisms towards two different enzymes belonging to the same family of proteases. Titration experiments with 5,5'-dithiobis-(2-nitrobenzoic acid), DTNB, indicated that the inhibitor alkylates the free thiol of papain, being the obtained adduct stable even under

[13] Ando, R.; Sakaki, T.; Morinaka, Y.; Takahashi, C.; Tamao, Y.; Yoshii, N.; Katayama, S.; Saito, K.; Tokuyama, H.; Isaka, M.; Nakamura, E. *Bioorg. Med. Chem.* **1999**, *7*, 571-579.

[14] Cohen, M.; Bretler, U.; Albeck, A. *Protein Sci.* **2013**, *22*, 788-799.

denaturation conditions. For this reason, nucleophilic attack of the catalytic thiol at the inhibitors cyclopropenone carbonyl to yield a thiohemiacetal seems not probable. Such complex would undergo hydrolysis under the denaturation conditions, which would be manifested in a titratable thiol. A reasonable mechanism then is the addition of the nucleophilic catalytic thiol across the cyclopropenone C=C double bond.

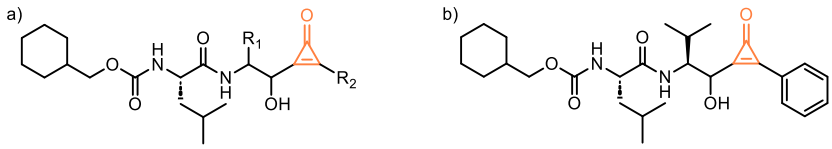

Figure 5.3. a) General structure of reversible inhibitors of m-calpain, cathepsin B, and cathepsin L. b) Structure of 51, an irreversible inhibitor of papin.

Another interesting study regarding cyclopropenones as biological active compounds was carried out by J. Quintana and co-workers.[15] Cyclopropene fatty acids, such as compounds **52** (Figure 5.4.), are known to inhibit different carboxylic acyl-CoA desaturases.[16] However, cylopropenone (**53**) and carboxycyclopropene derivatives (**54**) are inactive as desaturase inhibitors.[15] The inhibition mechanism of desaturases by cyclopropene fatty acids was unclear, but according to some authors, this inhibition is irreversible and occurs by reaction of the cyclopropene ring with a cysteine residue of the desaturase active centre.[17] To prove this hypothesis authors incubated cyclopropenes **51** and **52**, cyclopropenone **53** and 3-carboxycyclopropene **54** (Figure 5.4) with 1-propanethiol at 25 °C in $CDCl_3$ as an aprotic solvent, since

[15] Quintana, J.; Barrot, M.; Fabriàs, G.; Camps, F. *Tetrahedron* **1998**, *54*, 10187-10198.

[16] a) Johnson, A. R.; Pearson, J. A.; Shenstone, F. S.; Fogerty, A. C. *Nature* **1967**, *214*, 1244-1245. b) Johnson, A. R.; Fogerty, A. C.; Pearson, J. A.; Shenstone, F. S.; Bersten, A. M. *Lipids* **1968**, *4*, 265-269. c) Fogerty, A. C.; Johnson, A. R.; Pearson, J. A. *Lipids* **1972**, *7*, 335-338. d) Clark, J. R.; Kircher, H. W. *Lipids* **1972**, *7*, 769-772.

[17] a) Raju, P. K.; Reiser, R. *J. Biol. Chem.* **1967**, *242*, 379-384. b) Allen, E.; Johnson, A. R.; Fogerty, A. C.; Pearson, J. A.; Shenstone, F. S. *Lipids* **1967**, *2*, 419-423.

the desaturase active site is hydrophobic. The thiol reacted only with cyclopropenes **51** and **52**, to form the corresponding alkylthiocyclopropanes, and not with cyclopropenone **53** or 3-carboxycyclopropene **53**. These results support that inhibition of desaturases by cyclopropene fatty acids is caused by reaction with a cysteine residue of the enzyme active site and helps to understand the lack of biological activity of cyclopropenones due to their inert character towards thiols.

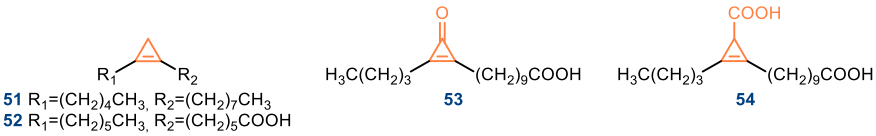

Figure 5.4. Cyclopropenes, cyclopropenone and 3-carboxycyclopropene evaluated by J. Quintana and co-workers towards the nucleophilic attack of 1-propanethiol.

The previous study suggests that, unlike cyclopropenes, cyclopropenones are not good candidates as desaturase inhibitors. Indeed, in the publication presenting the cyclopropene-containing Des1 inhibitor, **GT11**,[18] authors comment that these precedents served as inspiration for the design of this inhibitor. When **GT11** revealed as a potent Des1 inhibitor, authors hypothesized that Des1 was inhibited by the reaction of the cyclopropene ring with a cysteine residue of the active site, although this fact was not confirmed. Nevertheless, as a result of our study based on AlphaFold2, we have been able to verify the absence of any cysteine residue in the active site of Des1. This fact could, in principle, rule out the proposed inhibitory mechanism for **GT11**.

In this context, the proposal of ceramide analogues incorporating a cyclopropenone ring, **45a-c**, was not conceived to inhibit Des1 via reaction with a cysteine residue of the enzyme, which seems unlikely after the studies

[18] a) Triola, G.; Fabriàs, G.; Llebaria, A. *Angew. Chem.* **2001**, *113*, 2014–2016; b) Triola, G.; Fabriàs, G.; Llebaria, A. *Angew. Chem. Int. Ed.* **2001**, *40*, 1960–1962.

performed by Quintana.[15] On the contrary, the design of these compounds as inhibitors of Des1 is based on the belief that 3-membered cycles will allow a proper folding of the substrate in enzyme active site. Indeed, in the docking of this compound with the constructed model of Des1 (chapter IV), we observed that the rigid cyclopropenone ring forces a conformational arrangement of the alkyl chains that favours the establishment of two H-bond interactions between the ligand and the enzyme. Moreover, an interaction of the carbonyl and the oxodiiron species seems probable in the ligand binding mode.

5.2 Retrosynthetic analysis

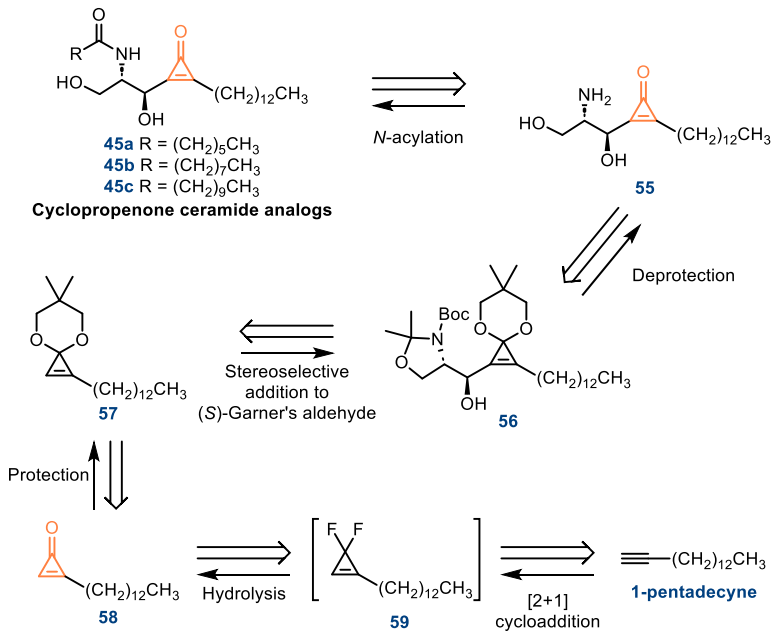

Scheme 5.2. Retrosynthetic analysis of cyclopropenone ceramide analogues **45a-b**.

Ceramide analogues **45** would be obtained by *N*-acylation of aminodiol **55** obtained after the hydrolysis of the three protecting groups in **56.** The aforementioned product, **56**, would be synthesized through a stereoselective addition of the lithium salt of compound **57** to (*S*)-Garner's aldehyde.

Cyclopropenone acetal **57** would be obtained, in turn, from the reaction of neopentylglycol with the corresponding cyclopropenone **58**, accessible via the hydrolysis of difluorinated intermediate **59** that could be accesible via a [2+1] cycloaddition reaction on 1-pentadecyne.

5.3 Synthesis of cyclopropenone ceramide analogues 45a-c.

5.3.1 Synthesis of monosubstituted cyclopropenone 58.

Synthetic procedures to obtain cyclopropenones can be mainly divided into four groups. Three of them involve the hydrolysis of *gem*-disubstituted cyclopropenes derivatives, where the substituents are either halogen or alkoxy groups. The fourth methodology can be considered a modified Favorskii reaction, involving ring closure of α,α'-dihalo ketones.

The fist synthesis of diphenylcyclopropenone, carried out by Berslow, employed the cyclopropene acetal route (Scheme 5.3).[1] In this procedure, the addition of phenylchlorocarbene generated from **60** to acetal **61** formed the cyclopropane acetal moiety in **62**. Additional base treatment forced a β-elimination process to afford the cyclopropene acetal **63**, that after hydrolysis furnished diphenylcyclopropenone **64**. This procedure has been applied in the synthesis of various arylphenylcyclopropenones using the appropriate arylidene chloride.[19]

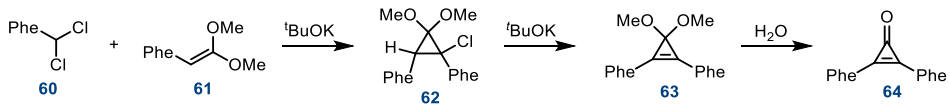

Scheme 5.3. Cyclopropene acetal route for the synthesis of cyclopropenones.

[19] Bird, C. W.; Harmer, A. F. *J. Chem. Soc. C.* **1969**, 959-960.

A simpler method involves the addition of a dihalocarbene to acetylenes (Scheme 5.4). The generated 3,3-dihalocyclopropenes are usually not isolated, as direct hydrolysis furnishes the desired cyclopropenones. Vol'pin utilized this methodology for the synthesis of diphenylcyclopropenone **64**,[20] and several examples of the application of this procedure can be found in the literature, using various dihalocarbene sources.[21]

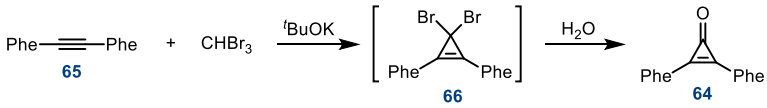

Scheme 5.4. Dihalocarbene-insertion route for the synthesis of cyclopropenones.

The trichlorocyclopropenylium ion has also been employed for the synthesis of cyclopropenones (Scheme 5.5).[22] Thus, reaction of trichloropropenium tetrachloroaluminate, **67**, with aryl groups via the Friedel-Crafts pathway provides access to *gem*-dichlorodiarylcyclopropenes, **68**, or aryltrichlorocyclopropenes **70**. The former can be readily hydrolysed into the corresponding cyclopropenone **69**. The electronic substitution of the aromatic group determines whether a mono- or disubstituted cyclopropenone is obtained. With strongly activating substituents, the reaction continues until the replacement of all the three halogens and yields the triarylcyclopropenylium ion salt.[22c] Aryltrichlorocyclopropenes, **70**, can subsequently react with a second aryl group (Ar') to furnish diarylcyclopropenones, **72**.[22d]

---

[20] Vol'pin, M.E.; Koreshkov, Y.D.; Kursanov, D. N. *Russ. Chem. Bull.* **1959**, *8*, 535–536.

[21] a) Breslow, R.; Altman, L. J. *J. Am. Chem. Soc.* **1966**, *88*, 504–509. b) Breslow, R.; Peterson, R. J. *Am. Chem. Soc.* **1960**, *82*, 4426–4427. c) Farnum, D. G.; Chickos, J.; Thurston, P. E. *J. Am. Chem. Soc.* **1966**, *88*, 3075–3081. d) Breslow, R.; Altman, L. J.; Krebs, A.; Mohacsi, E.; Murata, I.; Peterson, R. A.; Posner, J. *J. Am. Chem. Soc.* **1965**, *87*, 1326–1331. e) Ciabattoni, J.; Nathan III, E. C. *J. Am. Chem. Soc.* **1969**, *91*, 4766–4771.

[22] a) Tobey, S. W.; West, R. *J. Am. Chem. Soc.* **1964**, *86*, 4215–4216. b) Zecher, D. C.; West, R. *J. Am. Chem. Soc.* **1967**, *89*, 153–155. c) West, R.; Zecher, D. C.; Goyert, W. *J. Am. Chem. Soc.* **1970**, *92*, 149–154. d) West, R.; Zecher, D. C.; Tobey, S. W. *J. Am. Chem. Soc.* **1970**, *92*, 168–172.

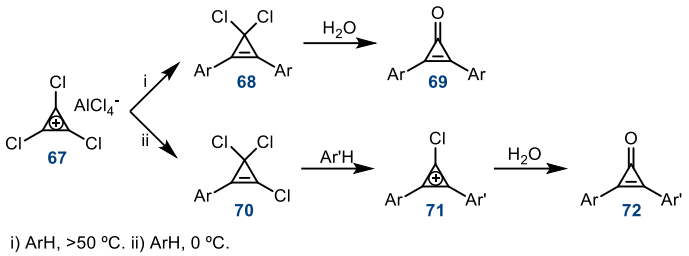

Scheme 5.5. Trichlorocyclopropenylium ion route for the synthesis of cyclopropenones.

Finally, cyclopropenones can be synthesized through the modified Favorskii reaction (Scheme 5.6).[23, 21d, 21e] Treatment of α,α'-dihalo ketones with a base leads to the elimination of the corresponding hydrogen halide, generating intermediate **74** (Scheme 5.6, a). After a second elimination, cyclopropenone **75** is obtained. This methodology can also be applied to acetals instead of ketones (Scheme 5.6, b).[24]

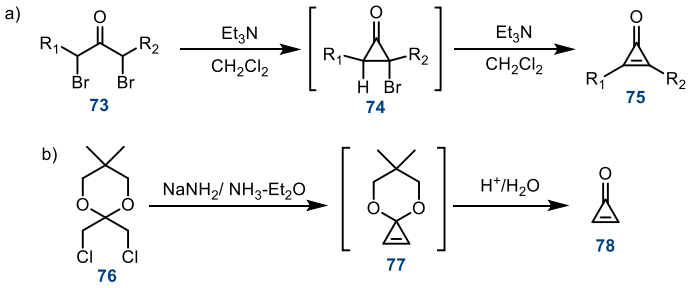

Scheme 5.6. Modified Favorskii reaction for the synthesis of cyclopropenones. a) α,α'-dihalo ketones as starting materials. b) α,α'-dihalo acetals as starting materials.

[23] a) Breslow, R.; Eicher, T.; Krebs, A.; Peterson, R. A.; Posner, J. *J. Am. Chem. Soc.* **1965**, *87*, 1320–1325. b) Breslow, R.; Posner, J.; Krebs, A. *J. Am. Chem. Soc.* **1963**, *85*, 234. c) Ciabattoni, J.; Nathan III, E. C. *J. Am. Chem. Soc.* **1968**, *90*, 4495–4496. d) McCorkindale, N. J.; Raphael, R. A.; Scott, W. T.; Zwanenburg, B. *Chem. Commun. (London)*, **1966**, 133-134.

[24] Nakamura, M.; Isobe, H.; Nakamura, E. *Chem. Rev.* **2003**, *103*, 1295–1326.

For the synthesis of the terminal cyclopropenone **58**, the dihalocarbene-insertion strategy was selected as the more convenient approach (Scheme 5.7), given that a terminal alkyne with the exact chain length required for the synthesis of ceramide analogues is commercially available. Furthermore, this procedure had already been used successfully with other substrates in our laboratory. Now, concretely, we envisioned a difluorocyclopropenation of 1-pentadecyne to generate *gem*-difluorocyclopropene **59** that would furnish, by subsequent hydrolysis, the desired cyclopropenone **58** (Scheme 5.7).

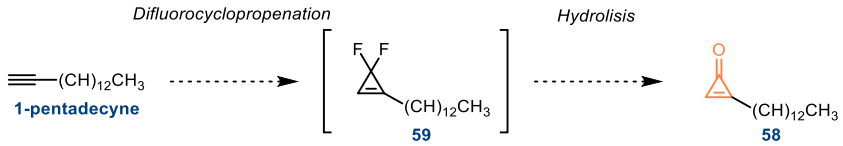

Scheme 5.7. Strategy for the synthesis of cyclopropenone **58**.

Ruppert-Prakash reagent (trifluoromethyltrimethylsilaneTMSCF$_3$),[25] was selected as the difluorocarbene source for the difluorocyclopropenation reaction. This reagent has been also widely used as a nucleophilic trifluoromethylating agent.[26] To activate TMSCF$_3$ as a difluorocarbene source, treatment with NaI or tetrabutylammonium difluorotriphenylsilicate is necessary.[27] The treatment with NaI releases the trifluoromethyl group, which, due to its instability, undergoes decomposition to yield difluorocarbene and a fluoride anion (Scheme 5.8).

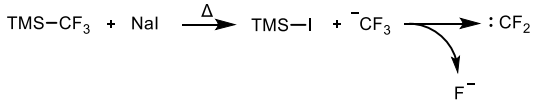

Scheme 5.8. Generation of difluorocarbene from TMSCF$_3$.

[25] Wang, F.; Luo, T.; Hu, J.; Wang, Y.; Krishnan, H. S.; Jog, P. V.; Ganesh, S. K.; Prakash, G. K. S.; Olah, G. A. *Angew. Chem.* **2011**, *123*, 7291–7295.

[26] Rubiales, G.; Alonso, C.; De Marigorta, E. M.; Palacios, F. *Arkivoc* **2014**, 362–405.

[27] Wang, J.; Luis, J.; Pozo, C.; Sorochinsky, A. E.; Fustero, S.; Soloshonok, V. A.; Liu, H. *Chem. Rev.* **2014**, *114*, 2432–2506.

Reported conditions for the difluorocyclopropenation reaction using Ruppert-Prakash reagent were applied to 1-pentadecyne (Scheme 5.9),[28] furnishing intermediate **59** with full conversion of the starting material. Treatment of intermediate **59** with a silica suspension in hexane/AcOH mixture generated cyclopropenone **58** in a 96% yield for both steps. It is worth mentioning that this reaction could be scaled up to 7.62 mmol of 1-pentadecyne, furnishing 1.730 g of cyclopropenone **58**.

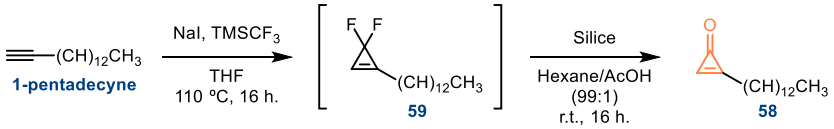

Scheme 5.9. Synthesis of cyclopropenone **58**.

The obtaining of the *gem*-difluorocyclopropene intermediate **59** was confirmed by ^{19}F NMR analysis of the crude reaction mixture (Figure 5.5.), obtaining a unique signal as multiplet at -104.2 ppm. The consumption of 1-pentadecyne was followed by TLC and ^{1}H NMR analysis of the crude. Compound **59** could not be isolated and fully characterised due to its rapid hydrolysis towards cyclopropenone **58**.

[28] Wang, F.; Luo, T.; Hu, J.; Wang, Y.; Krishnan, H. S.; Jog, P. V.; Ganesh, S. K.; Prakash, G. K. S.; Olah, G. A. *Angew. Chem. Int. Ed. Engl.* **2011**, *50*, 7153–7157.

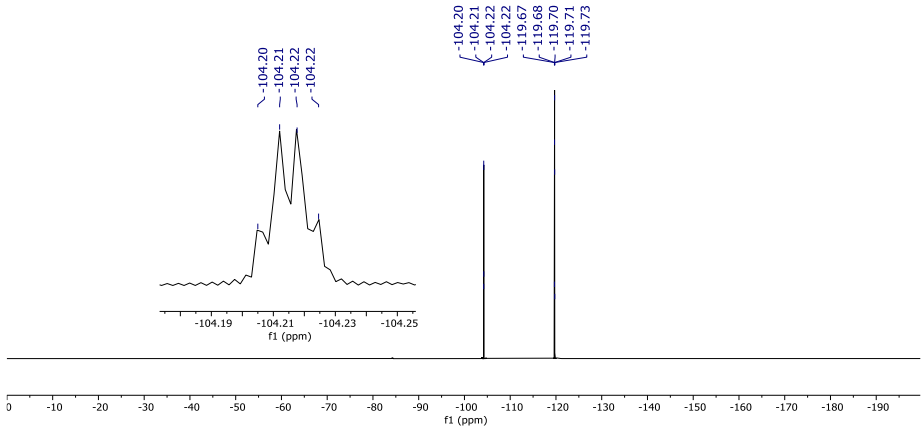

Figure 5.5. Amplification of ^{19}F NMR spectra of **59**. The signal present at -119.70 ppm corresponds to the internal reference: 1,4-difluorobenzene.

The cyclopropenone formation from a *gem*-difluorocyclopropene can be rationalized by the initial release of a fluoride ion, resulting in the formation of the aromatic fluorocyclopropenyl cation. This cation can react with water, leading to the cyclopropenone derivative after HF elimination (Scheme 5.10).[29]

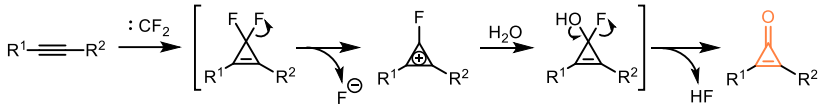

Scheme 5.10. Proposed mechanism for the obtaining of cyclopropenones from alkynes via 3,3-*gem*-difluoropropenes

5.3.2 Stereoselective addition of tridecylcyclopropenone acetal, 57, to (*S*)-Garner's aldehyde.

To incorporate the cyclopropenone moiety and accessing the sphingolipid structure, a stereoselective addition to (*S*)-Garner's aldehyde was envisioned. As commented in chapter III of this thesis, this addition generates, by an

[29] Cheng, Z. L.; Chen, Q. Y. *Chin. J. Chem.* **2006**, *24*, 1219-1224.

appropriate selection of reaction conditions, the desired 2-amino-1,3-dihydroxypropyl substructures with *anti*-configuration.

Direct addition of cyclopropenone to the (*S*)-Garner's aldehyde is not feasible, as treatment with strong bases in an attempt to generate the metalated species resulted in decomposition. As reported by Nakamura *et al.*,[30] cyclopropenone acetal functional groups are useful compounds for the synthesis of functionalized cyclopropenones. They demonstrated that cyclopropenone acetals can be deprotonated and metalated at the vinylic position, being able to react with a variety of electrophiles, including carbonyl compounds.[31] Following the nucleophilic attack, the cyclopropenone acetal can be hydrolysed to the corresponding cyclopropenone under various aqueous acidic conditions, allowing for the synthesis of a variety of functionalized cyclopropenones.

In this context, before carrying out the addition to (*S*)-Garner's aldehyde, cyclopropenone **58** was transformed into its corresponding acetal (Scheme 5.11). Due to its aromaticity, cyclopropenones are stable compounds; hence, the acetalization requires rather harsh reaction conditions. Thus, cyclopropenone **58** was treated with triethyloxonium fluoroborate to generate the cyclopropenium ion.[32] Then, treatment with neopentyl glycol under basic conditions furnished acetal **57** with an 89% yield.

With cyclopropenone acetal **57** in hands, the diastereoselective addition to (*S*)-Garner's aldehyde was undertaken (Scheme 5.11). For the generation of the lithiated derivative, compound **57** was treated with BuLi at -55 ˚C for 30 min. It was noted that prolonging the time of the lithiation step led to a reduction in the overall reaction yield, probably due to cyclopropenone acetal

[30] a) Isaka, M.; Matsuzawa, S.; Yamago, S.; Ejiri, S.; Miyachi, Y.; Nakamura, E. *J. Org. Chem.* **1989**, *54*, 4727-4729. b) Isaka, M.; Ando, R.; Morinaka, Y.; Nakamura, E. *Tetrahedron Lett.* **1991**, *32*, 1339-1342.

[31] Isaka, M.; Ejiri, S.; Nakamura, E. *Tetrahedron* **1992**, *48*, 2045- 2057.

[32] a) Yoshida, H.; Kinoshita, H.; Kato, T.; Kanehira, N.; Ogata, T.; Matsumoto, K. *Synthesis* **1987**, 393-394. b) Breslow, R. *Pure Appl. Chem.* **1971**, *28*, 111-130.

decomposition under the lithiation conditions. After treatment with BuLi, the addition step to (*S*)-Garner's aldehyde was performed at the same temperature for an overnight reaction. In this way, product **56** was obtained in 76% yield as a unique diastereomer.

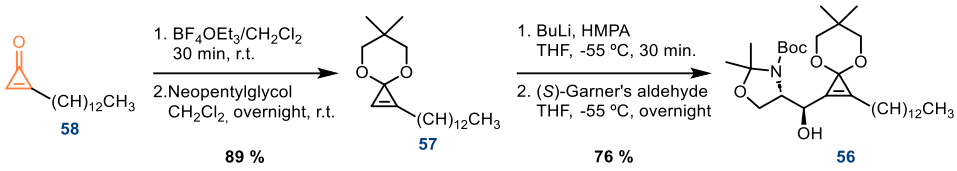

Scheme 5.11. Synthesis of cyclopropenone acetal **57** and diastereoselective addition to (*S*)-Garner's aldehyde to access compound **56**.

As previously observed during the synthesis of triazole ceramide analogues (chapter III), broad signals were observed in the ^{1}H NMR spectrum of product **57**, probably due to the coexistence of two rotamers. This was confirmed by recording the ^{1}H NMR spectrum at different temperatures. As it can be seen in Figure 5.6, at low temperatures two series of signals can be differentiated, that converge to form a unique set of signals at higher temperatures.

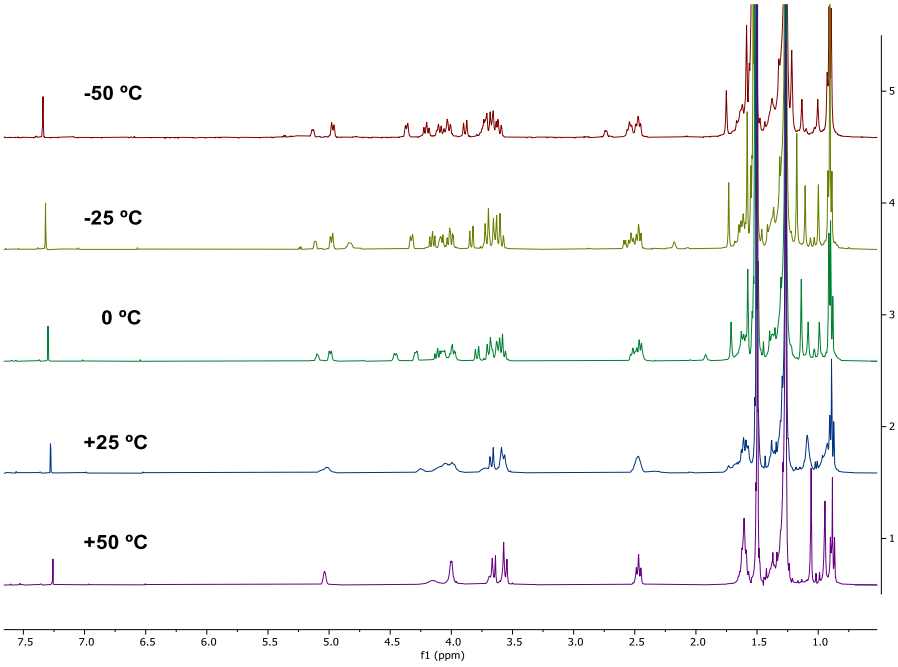

Figure 5.6. ^{1}H NMR spectra of compound **56** recorded at different temperatures.

5.3.3 Deprotection and *N*-acylation steps. Accessing cyclopropenone ceramide analogues 45.

After successfully obtaining product **56** via stereoselective addition to (*S*)-Garner's aldehyde, deprotection step to reveal aminodiol and cyclopropenone functionalities was assayed. The three protecting groups present in product **57**, namely *tert*-butyloxycarbonyl, isopropylidene acetal and 2,2-dimetil-1,3-dioxane, are labile under acidic conditions. Thus, a simultaneous cleavage was attempted by treating compound **56** with TFA in water (Scheme 5.12). All protecting groups were successfully hydrolysed, but analysis of the ^{1}H NMR spectrum of the purified product revealed that the signal corresponding to H-2 proton, geminal to the amine, located at 4.18 ppm instead of the expected chemical shift of 3.0 ppm. This higher chemical shift suggests that after hydrolysis, the amine was protonated and the corresponding trifluoroacetate salt was obtained even after treatment of the reaction crude with $NaHCO_3$.

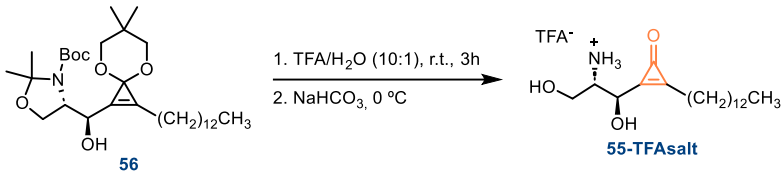

Scheme 5.12. Deprotection of compound **56** with TFA.

Different procedures were assayed to neutralize the amonium salt obtained (**55-TFAsalt)**: treatment with aqueous NaOH; Amberlite IRA-402 in CH_2Cl_2/MeOH mixture; MeOH/CH_2Cl_2/NH_4OH mixture; and Et_3N/CH_2Cl_2. All these methodologies proved ineffective.

To explore if the difficulties of neutralizing the obtained salt were caused by the trifluoroacetate anion, the deprotection of compound **56** was performed with HCl (Scheme 5.13). The ^1H NMR spectrum of the crude indicated the successful cleavage of all protecting groups, but the product was again obtained in form of a salt, as H-2 signal appeared at 3.6 ppm. In this case, presumably, the chloride salt, **55-Clsalt,** was obtained. Fortunately, **55-Clsalt** could be neutralized by treatment with a MeOH/CH_2Cl_2/NH_4OH (9:1:0.1) mixture, and the desired aminodiol **55** was obtained with a 62 % yield.

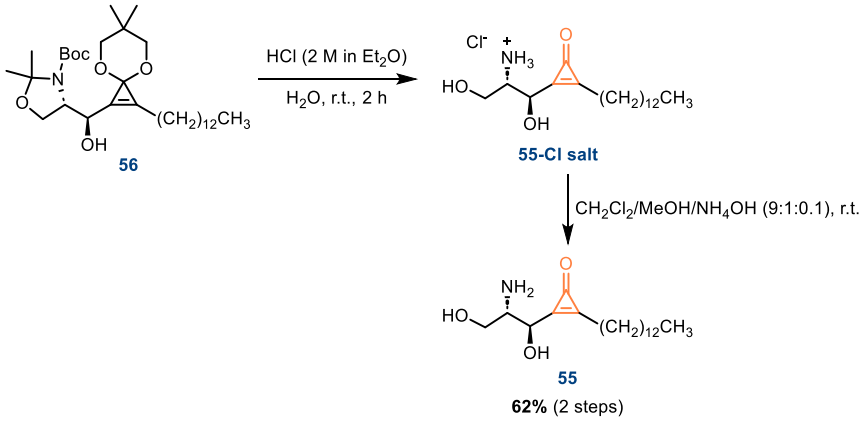

Scheme 5.13. Deprotection of compound **56** with HCl to access aminodiol **55**.

^{1}H NMR analysis proved to be a useful technique for the detection of the protonated amine in **55.** If the ^{1}H NMR spectra of both obtained salts are compared (Figure 5.7, a and b), a clear difference in the chemical shift of the signal corresponding to H-2 proton can be observed, indicative of the different anion present in each case. Moreover, when compared to the neutral specie, an evident difference in chemical shifts is observed too (Figure 5.7, c). The downfield displacement of the signal indicates the protonation of the amine and the presence of a salt. The obtaining of the neutral aminodiol could be confirmed by ^{1}H NMR, as the H-2 signal of the aminodiol derivative appeared in the expected chemical shift (3 ppm).

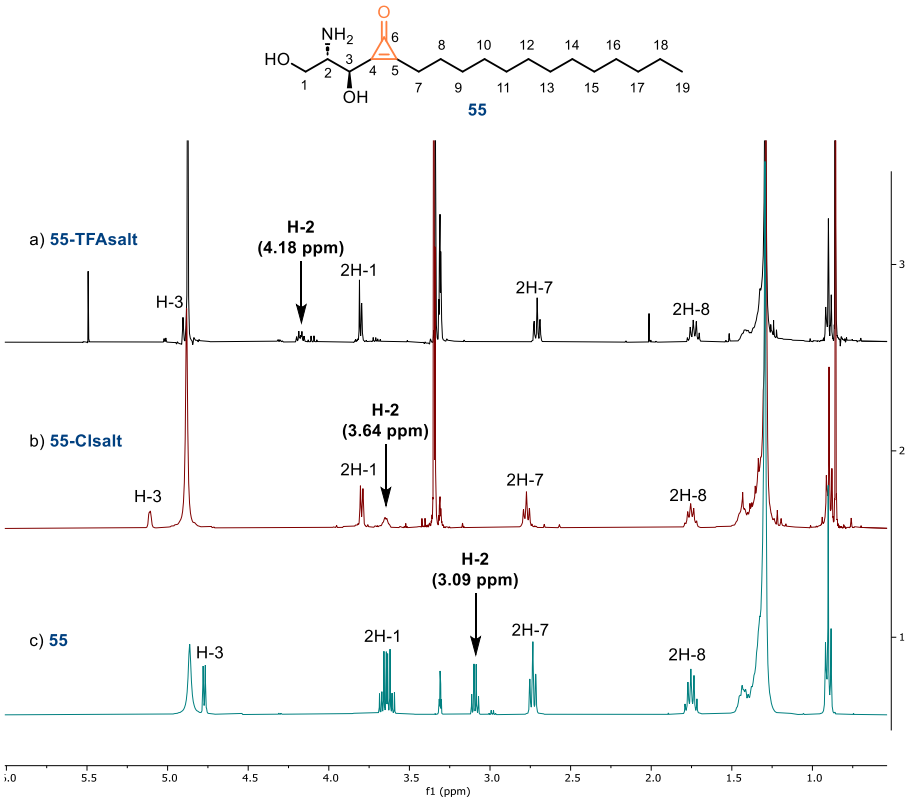

Figure 5.7. ^{1}H NMR spectra comparison between a) **55-TFAsalt**. b) **55-ClsaIt**. c) **55**.

Finally, *N*-acylation of aminodiol **55** (Scheme 5.14) with hexanoic, octanoic and decanoic acid using EDC and HOBt as coupling reagents

furnished target cyclopropenone ceramide analogues **45a-c** with yields ranging from 66% to 73%.

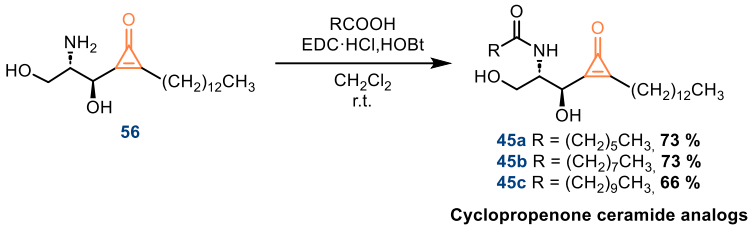

Scheme 5.14. *N*-acylation of aminodiol **55** to furnish cyclopropenone ceramide analogues **45a-c**.

X-ray diffraction analysis of crystallized ceramide analogue **45b** confirmed the desired *anti*-configuration of the 2-amido-3-hydroxy moiety (Figure 5.8).

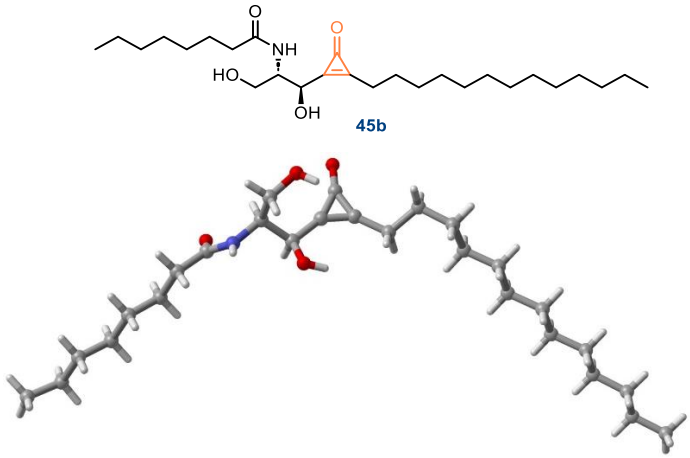

Figure 5.8. X-ray structure of cyclopropenone triazole ceramide analogue **45b** (CCDC 2252495).

As a conclusion, the three target ceramide analogues incorporating a cyclopropenone ring as central core, **45a-c**, have been successfully synthetized through a 6-step synthesis, with total yields ranging from 26 to 29 %.

5.4 Sulphur-containing cyclopropenone derivatives

The objective of this sections is to assess whether the inclusion of a sulphur atom can enhance enzyme inhibition through its interaction with the iron within the oxodiiron species. Precedents of sulphur-iron interactions between a ligand and a non-heme iron have been indeed described in the literature. Concretely, J. Boyd and co-workers presented two sesquiterpene-like inhibitors of a 9-*cis*-epoxycarotenoid dioxygenase with a thioether functionality in the structure.[33] Computational docking calculations supported an inhibition mechanism through coordination of the sulphur atom to the non-heme iron in the enzyme active site.

In this context, the synthesis of ceramide analogues incorporating cyclopropenethione, **79**, and 1,2-thiole-3-one, **80**, moieties was envisioned as potential candidates for Des1 inhibitors. Both ceramide analogues could be accessed through a unique synthetic step starting from cyclopropenone ceramide analogue **49b** (Scheme 5.15). On one hand, the use of Lawesson's reagent (LR) or phosphorus pentasulfide (P_4S_{10}) would furnish cyclopropenethione ceramide anlog **79**. On the other hand, [3+2] cycloaddition reaction of cyclopropenone **45b** with elemental sulphur would form the 1,2-thiole-3-one moiety.[34] In the cycloaddition reactions two different regioisomers, **80** and **80'**, are expected.

[33] a) Boyd, J.; Gai, Y.; Nelson, K. M.; Lukiwski, E.; Talbot, J.; Loewen, M. K.; Owen, S.; Zaharia, L. I.; Cutler, A. J.; Abrams, A. R.; Loewen, M. C. *Bioorg. Med. Chem.* **2009**, *17*, 2902-2912.

[34] Wu, J.; Gao, W. X.; Huang, X. B.; Zhou, Y. B.; Liu, M. C.; Wu, H. Y. *Org. Lett.* **2020**, *22*, 5555-5560.

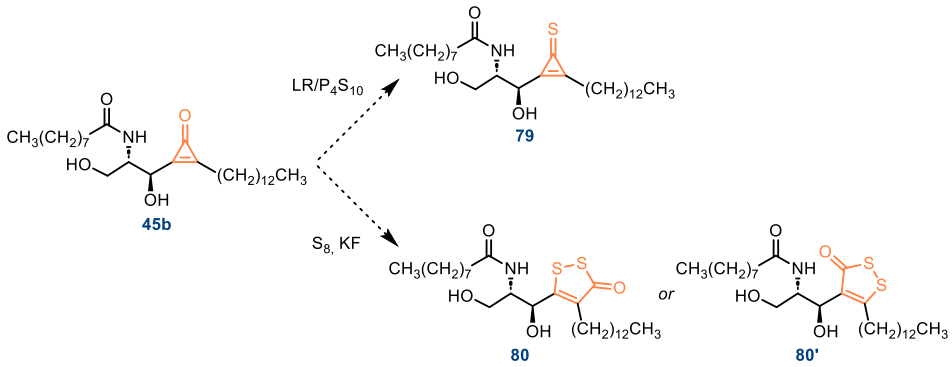

Scheme 5.15. Target sulphur-containing ceramide analogues, **79** and **80**, accessible through a single synthetic step from cycloporpenone ceramide analogue **45b**.

5.4.1 Docking calculations with cyclopropenethione and 1,2-thiole-3-one ceramide analogues.

Docking studies using the Fe_2O_2-Des1 system were conducted with cyclopropenethione ceramide analogue **79** and both regioisomers of 1,2-thiole-3-one ceramide analogues, **80** and **80'**. The same procedure as previously described was applied in these docking calculations.

In the case of compound **79** a similar binding mode to cyclopropenone ceramide analogue **45b** was obtained (Figure 5.9), as expected. In this case, the sulphur atom of the cyclopropenethione moiety was proximal to Fe atom, suggesting a plausible coordination interaction. Moreover, two H-bond interactions were stablished by the hydroxyl groups at C-1 and C-3 with Glu232 and the oxygen atom of the Fe_2O_2 specie, respectively.

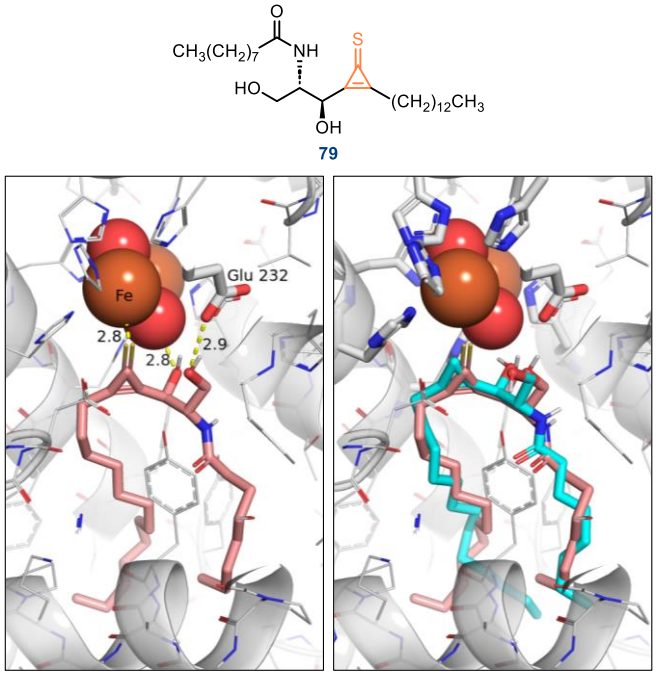

Figure 5.9. Binding mode of **79** (left) and binding modes of **79** (pink) overlapped with that of **GT11** (blue). Aminoacid residues involved in ligand-enzyme interactions are marked and indicated in sticks; those not involved in specific interactions are represented with lines. The length of interactions in Å is specified.

Cyclopropenethione ceramide analogue **79** stablished the key interactions previously observed for **GT11** and **XM462**, thus this ceramide analogues can be considered as a promising Des1 inhibitor candidate.

In the case 1,2-thiole-3-one ceramide analogue the binding mode resembled more to those observed for the furan and triazole ceramide analogues (Figure 5.10).

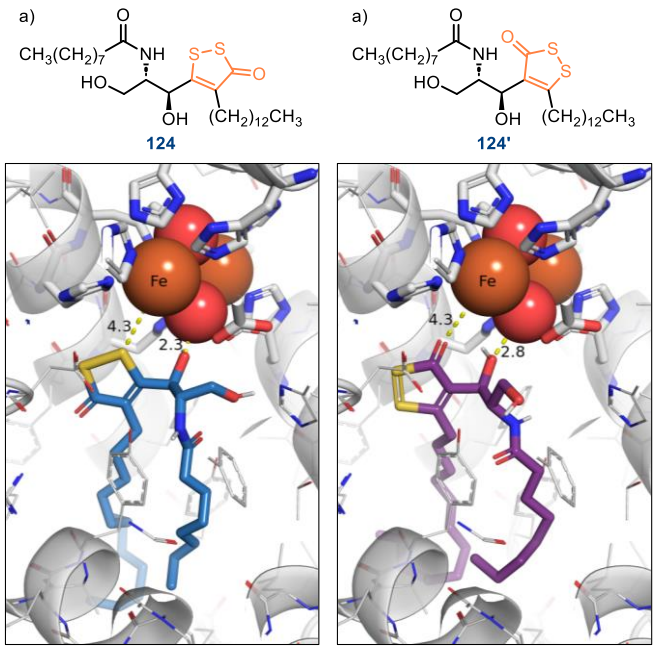

Figure 5.10. Best binding mode for 1,2-thiole-3-one ceramide analogues **80** and **80'**. Aminoacid residues involved in ligand-enzyme interactions are marked and indicated in sticks; those not involved in specific interactions are represented with lines. The length of interactions in Å is specified.

In the best binding pose for analogue **80** a sulphur atom of the cycle is in proximity to an iron metal center (Figure 5.10, a), suggesting a potential interaction. The hydroxyl group at position 3 stablishes a hydrogen bond with the oxygen of the Fe_2O_2 species. However, OH-1 does not participate in any favourable interaction with the enzyme. A comparable scenario was observed for regioisomer **80'** (Figure 5.10, b). In this case, the carbonyl group, instead of the sulphur atom, was oriented toward the iron center. In this disposition, the hydrogen bond interaction between OH-3 and the oxygen of the Fe_2O_2 species was also present. However, once more, OH-1 failed to stablish the key favourable interaction with the enzyme.

Taking into account the precedents established throughout this thesis, the results of the docking calculations do not portend good inhibitory activity.

Neither of the regiosiomers, **80** or **80'**, stablished the three interactions identified as crucial for Des1 inhibition (chapter IV). However, the biological evaluation of compounds **80** and **80'** as Des1 inhibitor would provide another opportunity to establish a correlation between docking studies and biological results, thus gaining a deeper understanding of the constructed Des1-Fe_2O_2 system.

5.4.2 Synthesis of cyclopropenethione ceramide analogue 79.

Phosphorus pentasulfide (P_4S_{10}) and Lawessons's reagent (LR) are the most widely used agents for transforming a carbonyl functional group into a thiocarbonyl (Figure 5.11).[35] Generally, it is claimed that LR has advantages over P_4S_{10} as it requires lower reaction times and less excess of reagent.

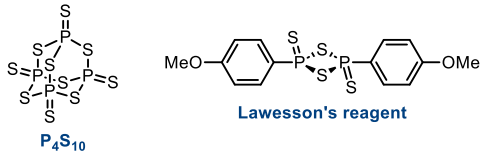

Figure 5.11. P_4S_{10} and Lawesson's reagent structure.

Mechanistic studies of the reactions using both reagents[36] suggest that the process involves a dissociation equilibrium (Scheme 5.16, a), which yields **81** and **82** respectively. These dissociation products can react with carbonyl functional groups to form four-membered ring intermediates, **83**, which evolve to the corresponding thioketone **85** (Scheme 5.16, b). The reaction ends with specie **84**, as P-O bond is more stable than the P-S bond. This is one of the important driving forces of the reaction using these reagents.[37]

---

[35] Ozturk, T.; Ertas, E.; Mert, O. *Chem. Rev.* **2007**, *107*, 5210–5278.

[36] a) Lecher, H. Z.; Greenwood, R. A.; Whitehouse, K. C.; Chau, T. H. *J. Am. Chem. Soc.* **1956**, *78*, 5018-5022. b) Perregaard, J.; Scheibye, S.; Meyer, H. J.; Thomsen, I.; Lawesson, S.-O. *Bull. Soc. Chim. Belg.* **1977**, *86*, 679.

[37] Jesberger, M.; Davis, T. P.; Barner, L. *Synthesis* **2003**, 1929-1958.

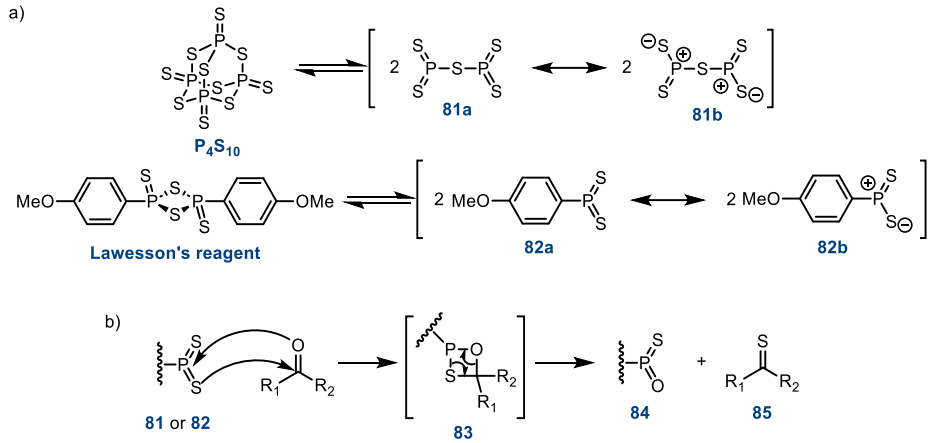

Scheme 5.16. a) Dissociation mechanism of P_4S_{10} and LR. b) Thionation mechanism using P_4S_{10} and Lawessons's reagent.

LR has been reported to convert almost all kinds of oxo groups to thiols, but examples of its applications to obtain cyclopropenthiones are scarce.[4e,38] Figure 5.12 shows all cyclopropenethiones, that to our knowledge, have been synthesized by the direct transformation of a cyclopropenone. The examples are limited, predominantly dealing with cyclopropenethiones substituted with aromatic groups. However, some examples including ether, hydroxyl, amide and ester functionalities can be found. In all instances, authors treated the corresponding cyclopropenone substrate with LR in CH_2Cl_2 under inert atmosphere at room temperature; with reaction times ranging from 30 min to 2 h.[4e,38] With these precedents, LR was chosen as thionation agent.

[38] a) Nogueira, J. M.; Bylsma, M.; Bright, D. K.; Bennett, C. S. *Angew. Chem. Int. Ed.* **2016**, *55*, 10088-10092. b) Romeo, J. R.; McDermott, L., Bennett, C. S. *Org. Lett.* **2020**, *22*, 3649–3654. c) Mlostoń, G.; Wręczycki, J.; Robak, A.; Urbaniak, K.; Bieliński, D. M.; Palusiak, M.; Sutuła, S.; Woźniak, K.; Heimgartner, H. *J. Fluor. Chem.* **2023**, *270*, 110170. d) Zhao, W. T.; Shi, M. *Tetrahedron Lett.* **2015**, *56*, 5086-5089. e) Klimova, E. I.; Vázquez López, E. A.; Alamo, M. F.; Ortiz-Frade, L. A.; Hernández-Sánchez, G.; Sotelo Domínguez, V. H.; García, M. M. *J. Heterocycl. Chem.* **2012**, *49*, 1156-1162. f) Row, R. D.; Prescher, J. A. *Org. Lett.* **2018**, *20*, 5614–5617. g) García, J. J. S.; Castella-Lasaga, J. A.; Flores-Alamo; M., Stivalet, J. M. M.; Klimova, E. I. *Polyhedron*, **2019**, *171*, 353-364. h) Klimova, E. I.; Rubio, C. G.; García-Valdés, J.; Nuñez-Cruz, E.; Martínez-Klimova, E.; Beletskaya, I. P.; Flores-Álamo, M.; García, J. J. S. *J. Organomet. Chem.* **2020**, *922*, 121363.

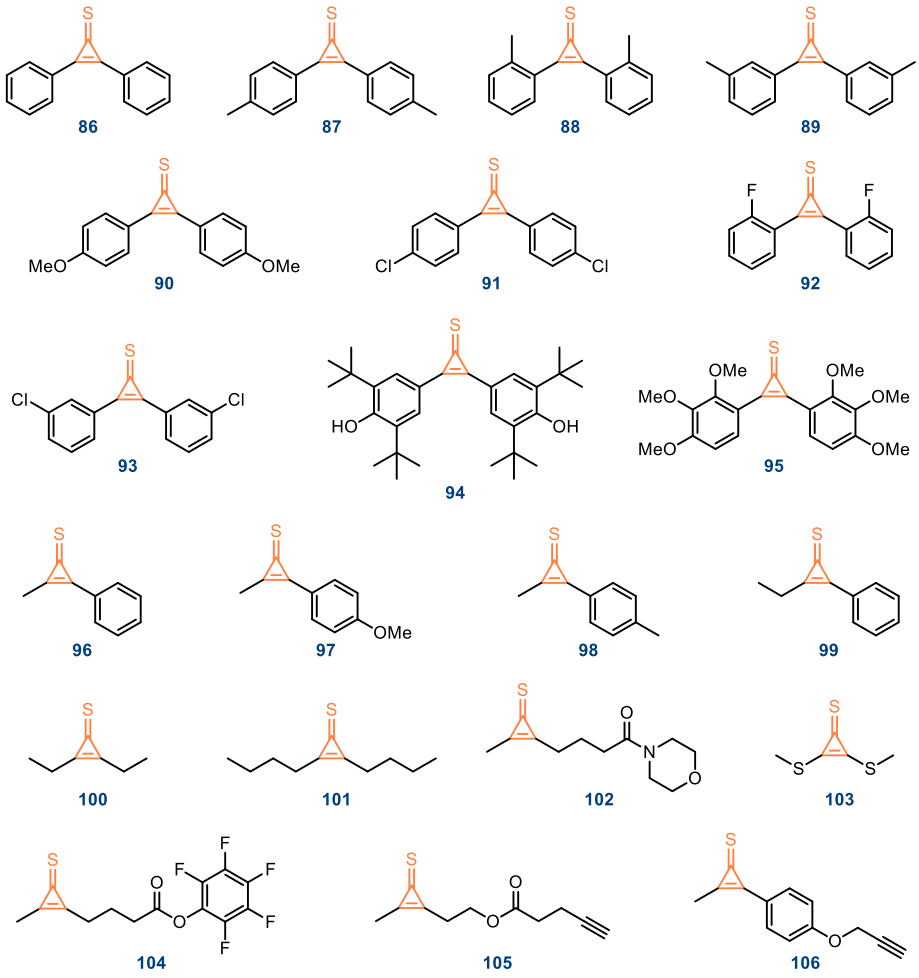

Figure 5.12. Cyclopropenethiones described in the bibliography that are synthesized by direct transformation of a cyclopropenone derivative using Lawessons's reagent.

The reported conditions were applied to ceramide analogue **45b** (Scheme 5.17), but after 1 hour of reaction, a complex mixture of decomposition products was obtained. The same outcome took place when lowering the temperature to 0 ˚C.

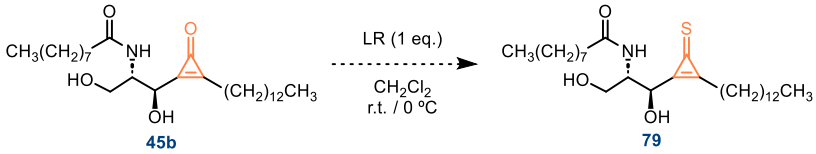

Scheme 5.17. Evaluation of Lawesson's reagent on ceramide analogue **79**.

After this first assay, LR was evaluated at a different point of the synthetic route. With this aim, protected compound **56** was treated with a $CH_2Cl_2/CDCl_3$ (1:1) mixture at room temperature to selectively cleave 2,2-dimetil-1,3-dioxane protecting group (Scheme 5.18). Under these conditions compound **107** containing the cyclopropenone moiety was obtained in almost quantitatively yield. Previous conditions for the transformation of cyclopropenone to cyclopropenethione resulted successful when applied to compound **107** (Scheme 5.18). However, high presence of decomposition products was observed in the crude of reaction, and compound **108** was obtained with a rather low 36% yield.

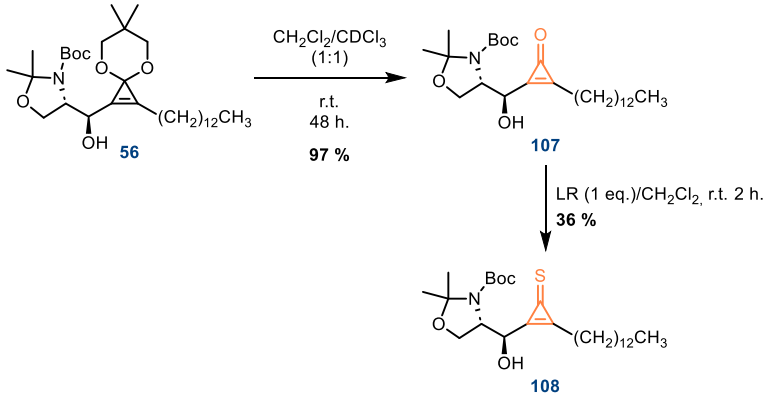

Scheme 5.18. Synthesis of cyclopropenethione containing compound **108**.

Once constructed the cyclopropenethione moiety, the deprotection of *tert*-butyloxycarbonyl and isopropylidene acetal was investigated. Different conditions were explored; including the use of Brønsted acids (Table 5.1, entries 1-7), the slow generation of anhydrous hydrochloric acid by dropwise addition of acetyl chloride in MeOH (Table 5.1, entries 8 and 9), and Lewis

acids (Table 5.1, entry 10). Reaction conditions were evaluated at room temperature and at 0 ˚C. Additionally, the stepwise deprotection of both protecting groups was also assayed by using the acid resin Amberlyst-15 (Table 5.1, entry 11) to selectively cleave isopropylidene acetal; or using oxalyl chloride (Table 5.1, entry 12), reported as a mild deprotection procedure for *N-tert*-butyloxycarbonyl group.[39]

Table 5.1. Conditions assayed for the deprotection of compound **101**.

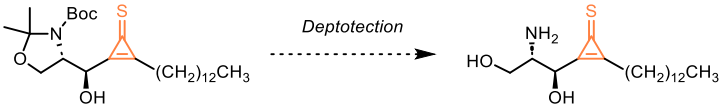

108 109

Entry	Conditions	Reaction outcome
1	TFA/H_2O (10:1), r.t.	Decomposition
2	TFA/H_2O (10:1), 0 ˚C	Decomposition
3	HCl (1M in Et_2O), r.t.	Decomposition
4	HCl (1M in Et_2O), 0 ˚C	Decomposition
5	HCl (1M in Et_2O)/H_2O, r.t ˚C	Decomposition
6	HCl (1M in Et_2O)/H_2O, 0 ˚C	Decomposition
7	HCl (1M in Et_2O)/MeOH, r.t. ˚C	Decomposition
8	acetyl chloride/MeOH, 0 ˚C	Decomposition
9	acetyl chloride/MeOH, r.t.	Decomposition
10	TMSOTf, Et_3N/CH_2Cl_2, 0 ˚C	Decomposition
11	Amberlyst-15/CH_2Cl_2, r.t.	Decomposition
12	oxalyl chloride/MeOH, r.t.	Decomposition

Irrespective of the conditions tested, compound **108** consistently decomposed within 30 or 45 minutes. The decomposition pathway could not be elucidated, as no intermediate or decomposition product was isolated either during the reaction or in the subsequent work-up.

[39] George, N.; Ofori, S.; Parkin, S.; Awuah, S. G. *RSC Adv.* **2020**, *10*, 24017-24026.

In view of the unsuccessful attempts in the deprotection of *tert*-butyloxycarbonyl and isopropylidene acetal groups and the low yield obtained in the construction of the cyclopropenethione moiety, the exploration of the synthesis of ceramide analogue containing cyclopropenethione moiety, **79**, was concluded.

5.4.3 Synthesis of 1,2-thiole-3-one ceramide analogue. Elucidating the mechanism behind the selective [3+2] cycloaddition reaction of cyclopropenone derivatives and elemental sulphur.

- Elucidating the mechanism behind the selective [3+2] cycloaddition reaction of cyclopropenone derivatives and elemental sulphur.

Cyclopropenones have been extensively utilized as substrates in transition-metal-catalysed ring-opening reactions, exploiting the inherent release of ring strain. This approach provides a powerful tool for the construction of both carbocycles and heterocycles. In this context, J. Wu *et al.* reported the synthesis of five-membered 1,2-thiole-3-ones from cyclopropenone derivatives via [3+2] cycloaddition by using elemental sulphur.[40] The protocol exhibits mild reaction conditions, high efficiency, excellent atom economy, gram-scale capacity, relatively wide scope and exceptional regioselectivity (Figure 5.13), as evidenced by X-ray crystallography of selected obtained products.

The reaction proceeds more efficiently with the addition of inorganic fluorides, such as KF, NaF or CsF. The process is conducted under ambient air conditions, and a reduced yield is observed when replacing it with a nitrogen N_2 atmosphere. Likewise, the addition of oxidants (BQ, *m*-CPBA, and ^{t}BuOO^{t}Bu) or TEMPO under N_2 atmosphere accelerates the formation of the product, yielding similar results to those obtained under air atmosphere.

[40] Wu, J.; Gao, W. X.; Huang, X. B.; Zhou, Y. B.; Liu, M. C.; Wu, H. Y. *Org. Lett.* **2020**, *22*, 5555-5560.

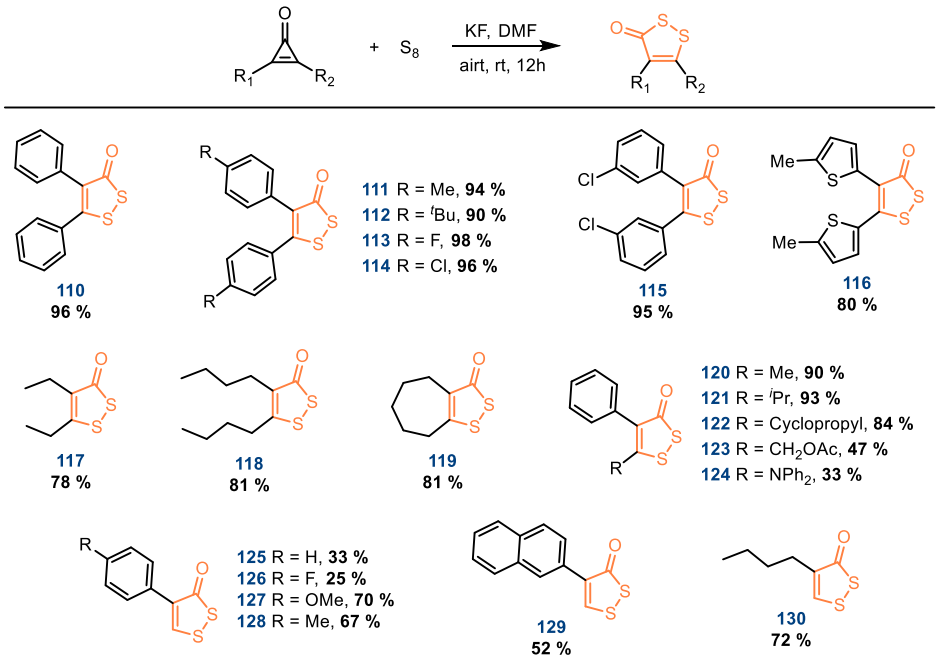

Figure 5.13 Scope and conditions for the [3+2] cycloaddition of cyclopropenone derivatives with elemental sulfur described by J. Wu *et al*.

According to Wu's proposed mechanism (Scheme 5.19, a),[40] S_8 would initiate the reaction by attacking the C-1 atom of the cyclopropenone carbonyl group (Scheme 5.19 a, intermediate **I**), leading to the subsequent liberation of S_6 to form **II**. Intermediate **II** would then undergo a ring opening/cyclization sequence, ultimately yielding the heterocyclic compound through intermediate **III**. Additionally, a distinct rearrangement from intermediate **II** has also been proposed by Klimova[41] involving intermediate **IV** (Scheme 5.19, b). An alternative mechanism proposed by Klimova involves the initial nucleophilic attack of a sulphur molecule on the C-2 atom of the three-membered ring, to afford intermediate **V**, followed by a subsequent ring opening leading intermediate **VI** and ring closure process (Scheme 5.19, c).

[41] Sánchez García, J. J.; Joo-Cisneros, R. S.; García-Bassoco, D.; Flores-Alamo, M.; Méndez Stivalet, J. M.; García-Valdés, J.; Klimova, E.K. *J. Organomet. Chem.* **2021**, *944*, 121809-1211819.

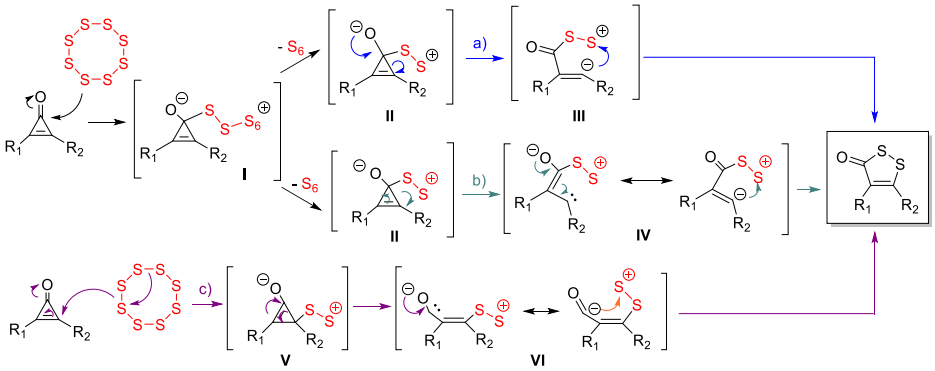

Scheme 5.19. Mechanisms proposed by Wu (a) and Kimova. (b, c) for the [3+2] cycloaddition of cyclopropenone derivatives with elemental sulphur.

Not all the described mechanisms readily explain the observed high regioselectivity of the process. Besides, the literature proposed mechanisms do not consider the potential role of fluoride salts in activating elemental sulphur, consistently suggesting that the reaction proceeds solely from S_8.

In collaboration with with Quantum Chemistry Group (Universitat Rovira i Virgili) of Prof. J. Carbó and Dr. M. Besora, the different mechanistic pathways for the [3+2] cycloaddition of cyclopropenone with S_8 as the sulphur source were computationally explored. G. D. Núñez carried out all calculations using the Density Functional Theory (DFT) method with the ωB97XD functional[42] and the 6-31g(d,p)[43] basis set for all the atoms. The solvent effects were considered employing an implicit solvation model, SMD,[44] for *N*,*N*-dimethylformamide. All energies presented correspond to Gibbs free-energies in solution at 298,15 K and 1 M, and they are reported in kcal.mol-1.

As previously stated, [3+2] cycloaddition of cyclopropenone with elemental sulphur was conducted in the presence of KF. Hence, it is very likely that the activation of elemental sulphur with fluoride anion takes place.

---

[42] Chai, J. D.; Head-Gordon, M. *Phys. Chem. Chem. Phys*. **2008**, *10*, 6615-6620

[43] a) Gordon, M. S. *Chem. Phys. Lett.* **1980**, *76*, 163-168. b) Binning, R. C.; Curtiss, L. A. *J. Comput. Chem.* **1990**, *11*, 1206-1216. c) McLean, A. D.; Chandler, G. S. *J. Chem. Phys.* **1980**, *72*, 5639-5648.

[44] Marenich, A. V.; Cramer, C. J.; Truhlar, D. G. *J. Phys. Chem. B* **2009**, *113*, 6378-6396.

Different computational studies have explored the S_8 ring opening process by nucleophiles such as cyanide, or phosphines.[45] Moreover, it has been recently reported that tetrabutylammonium exhibits high efficiency as a source of the fluoride anion for the nucleophilic activation of elemental sulphur.[46]

Calculations in this regard support the activation of S_8 by a fluoride anion, leading to the formation of more stable fluorooctasulfide through a low kinetic barrier (Scheme 5.20).

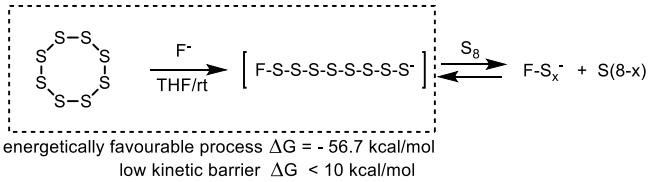

Scheme 5.20. Ring cleavage of S_8 and formation of fluoropolysulfide anions.

According to this results the reaction mechanism has been explored considering fluorooctasulfide anion as sulphur source. Unsymmetrical cyclopropenone 2-phenylcycloprop-2-en-1-one, **131**, was chosen as a substrate for its simplicity and for being a cyclopropenone whose regioselectivity in the reaction has been experimentally determined. Through the text the following notation will be used: **X-^{n}IntY$_p$** or **X-^{n}TSY$_p$**, where X will be F_8 for the singlet fluorooctasulfide anion $^1FS_8^-$; n will be 1 for the singlet free energy surface; Int or TS for intermediate and transition state respectively; Y will be the numbering of each intermediate and transition state along each mechanism and p will note if the path leads to the observed product with an O, or to the non-observed with an N.

[45] Sharma, J.; Champagne, P. A. *J. Comput. Chem.* **2022**, *43*, 2131-2138.

[46] Mlostoń, G.; Wręczycki, J.; Robak, A.; Urbaniak, K.; Bieliński, D.M.; Palusiak, M.; Sutuła, S.; Woźniak, K.; Heimgartner, H. *J. Fluor. Chem.* **2023**, *270*, 110170-110177.

The mechanistic study from fluorooctasulfide anion provides a good explanation for the obtaining of the observed regiosomer **O** (Figure 5.14). The reaction would proceed via conjugated addition of the sulfide anion to the less hindered double bond carbon of the cyclopropenone moiety to give intermediate **F8-^{1}Int1**o, located at 17.6 kcal.mol^{-1} above reactants. This intermediate would be achieved through transition state **F8-^{1}TS1**o located at 19.6 kcal.mol^{-1} above reactants. The alternative approach of the reactant to the more hindered double bond carbon would lead transition state F8-^{1}**TS1**$_N$ (+25.6 kcal.mol^{-1}), resulting in a less energetically favourable outcome by a difference of 6 kcal/mol.

The enolate intermediate **F8-^{1}Int1**o, stabilized through resonance by the aromatic ring, could afford the low energy ketenethialdehyde intermediate **F8-^{1}Int2**o at -19.8 kcal.mol^{-1} via ring opening with concomitant formation of a carbon-sulfur double bond and expulsion of a fluoroheptasulfide ion. **F8-^{1}Int2**o, in turn, would suffer an intramolecular nucleophilic addition, explainable from its dipolar resonant form, to afford thiet-2-one intermediate **F8-^{1}Int3**o (-20.4 kcal.mol^{-1}).

Wentrup has described the transformation of ketenes with a thiocarbonyl group in alfa position towards the corresponding thiet-2-ones.[47] The latter is highly susceptible to nucleophilic attack at the carbonyl group with ensuing ring opening. Indeed, **F8-^{1}Int3**o would led to **F8-^{1}Int4**o (-25.4 kcal.mol^{-1}) via nucleophilic acyl substitution by the sulfur anion previously expelled. Sulfide **F8-^{1}Int4**o would afford the experimentally obtained regiosiomer **O** via nucleophilic ring closing and fluorohexasulfide displacement.

The overall barrier of the process is 19.6 kcal.mol^{-1}, value that fits well with a reaction taking place at room temperature within 12 hours.

[47] J. R. Ammann, R. Flammang, M. W. Wong, C. Wentrup *J. Org. Chem.* **2000**, *65*, 2706-2710.

The mechanism proposed as a result of this computational study (Figure 5.14) would introduce novelty compared to those previously presented in the literature. While it postulates a conjugate addition as an initial step, like one of the mechanisms proposed by Kimova (Scheme 19, c), the resulting outcome would be totally different, implying the transit of the process through **Int3**. This mechanism would provide an explanation for the regioselectivity observed.

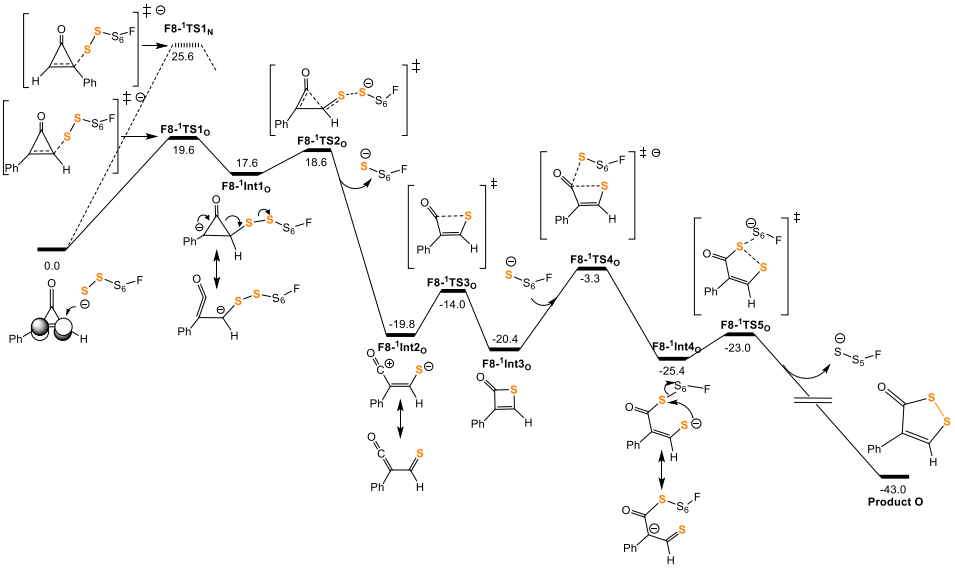

Figure 5.14. Postulated reaction mechanism for the [3+2] cycloaddition of 2-phenylcycloprop-2-en-1-one from fluorooctasulfide anion FS_8^-. Dashed lines correspond to the reaction pathways leading to the experimentally non-observed regioisomer, solid ones to the observed regioisomer. Energies correspond to relative free energies in solution and in kcal.mol^{-1}.

The computational study of the reaction promoted by fluoride-activated sulfur was extended to other differently substituted cyclopropenones. The results obtained are consistent with experimental findings,34 as the reaction pathway leading to the observed regioisomer traverses a transition state of lower energy, with differences with the alternative transition state from 2.4 to 6.0 kcal.mol^{-1} (Table 5.2).

Table 5.2. Summary of computational results for the reaction promoted by fluoride-activated sulphur.

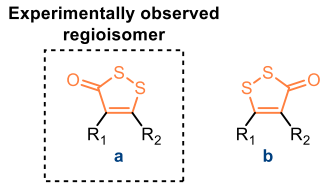

Entry	R_1	R_2	$\Delta G^{\ddagger}$ TS1 (a)	$\Delta G^{\ddagger}$ TS1 (b)	$\Delta(\Delta G^{\ddagger})$
1	Ph	H	19.6	25.6	+ 6.0
2	Ph	Me	23.9	26.6	+ 2.7
3	Me	H	23.6	26.0	+ 2.4
4	Et	H	23.3	25.9	+ 2.6

Relative free-energies and barriers in kcal/mol (25 °C, 1 atm)

The differences observed when R_1 is a phenyl group (Table 5.2, entries 1 and 2) could be explained by a greater stabilization by the aromatic ring of the enolate intermediate formed. The smaller energy difference between the two possible approximations of the sulphur nucleophile observed when R_2 is a methyl group regarding to the hydrogen substituent (2.7 *vs* 6.0 kcal/mol, Table 5.2, entry 2 *vs* 1) would be due to the higher steric hindrance caused by the methyl group at the entrance of the nucleophile.

The results obtained with non-symmetric cyclopropenones substituted with alkyl groups (Table 5.2, entries 3 and 4) would preferably be due to steric impediments that would condition the regioselective approach of the nucleophile.

- Synthesis of 1,2-thiole-3-one ceramide analogue

As previously commented, ceramide analogues incorporating five-member heterocycles were ineffective inhibiting Des1 in lysates. However, the easy access to a new ceramide analogue incorporating a 1,2-thiole-3-one moiety, prompted us to conduct its synthesis, as only required one additional synthetic transformation. Furthermore, performing the biological assessment of this analogue would enable the evaluation of a scaffold containing two

sulphur atoms. As previously commented, these sulphur atoms have the potential to coordinate the non-heme iron within the active site of Des1.

Thus, the conditions reported by J. Wu *et al.* were applied to ceramide analogue **45b** (Scheme 5.21), yielding a unique regioisomer, **80**, in 50 %. The excellent regioselectivity of the process is in line with the few reported cases of this reaction applied on asymmetrically substituted cyclopropenones, where only one regioisomer is obtained.

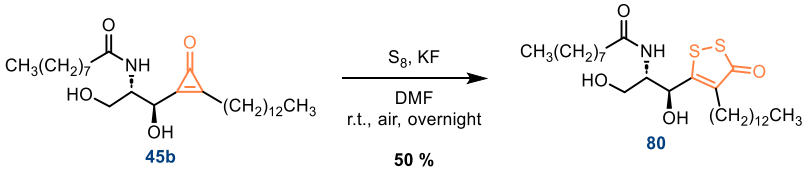

Scheme 5.21. Synthesis of 1,2-thiole-3-one ceramide analogue **80**.

The formation of the 1,2-thiole-3-one scaffold was confirmed by HRMS (see experimental section), but the identification of the obtained regioisomer presented a great challenge. The product could not be crystallized, making X-ray crystallographic analysis unfeasible. Heteronuclear Multiple Bond Correlation experiments (HMBC) showed a strong coupling between 2H-7 protons and the carbonyl carbon (Figure 5.15), while coupling between of H-3 and the carbonyl carbon was not observed. This piece of evidence suggests that regioisomer **80** was the product obtained in the cycloaddition reaction. Moreover, a comparison of predictive calculations of the ^{13}C NMR shifts for C-4 and C-5 in compounds **80** and **80'** showed a closer agreement of the former with the experimentally registered ^{13}C NMR spectrum. Although with this limited information is not possible to make a definitive assignment, regioisomer **80** seems the most probable option.

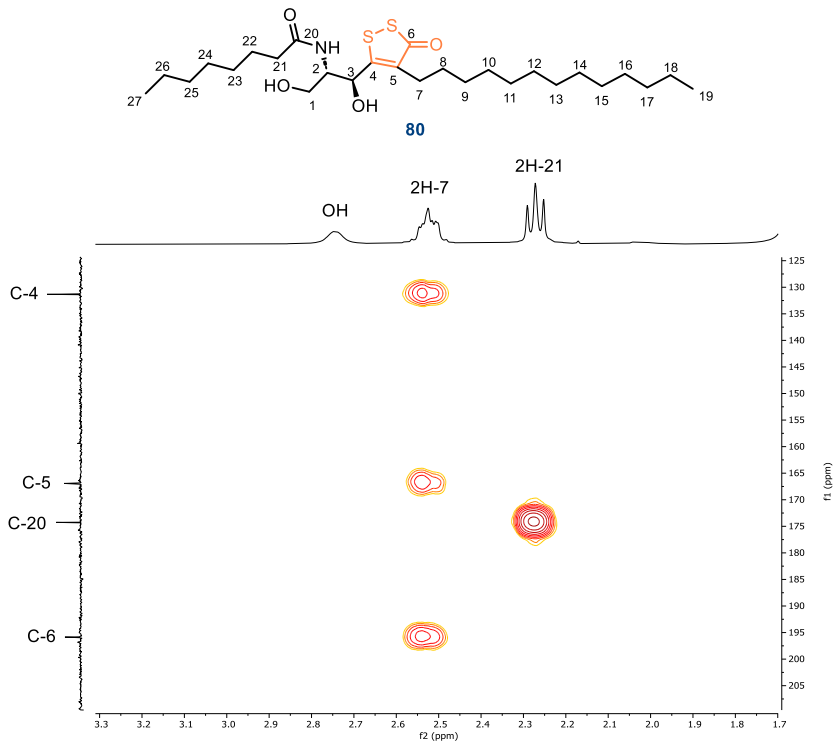

Figure 5.15. HMBC spectra of compound **80**.

5.5 Evaluation of cyclopropenone ceramide analogue, 45b, and 1,2-thiole-3-one ceramide analogue, 124, as Des1 inhibitors.

As ceramide analogueues **1a-c**, **2a-c** and **3a-c** had shown similar inhibition results in cell lysates regardless the length of the *N*-acyl chain, only the *N*-octanoyl chain analogue **45b** (also present in **GT11**) was evaluated as Des1 inhibitor. Moreover, 1,2-thiole-3-one ceramide **80** analogue bearing the same *N*-acyl chain was evaluated. The same procedure used for the evaluation of heterocycle containing ceramide analogues, **1a-c**, **2a-c** and **3a-c** was applied (see chapter III, section 3.5).

Des1 inhibition activity of the analogue was tested *in vitro* with intact T98 tumor cells using **XM462** as positive control of inhibition in the presence of fluorescent **dhCerC6NBD** (N-[6-[(7-nitro2-1,3-benzoxadiazol-4-yl)amino]hexanoyl]- D *-erythro*-sphinganine) as substrate (Figure 5.16).

Ceramide analogue **45b** displayed an 86 % of inhibition (at 10 μM) in intact T98-cells, a similar value to that of **XM462** (85 % at 10 μM). More importantly, this compound showed a remarkable 92% of inhibition in T98 cell lysates, surpassing the value obtained for **XM462** (78%), which suggests a direct inhibition effect against Des1.

On the other hand, ceramide analogue **80** showed a moderate 27 % inhibition in intact cells but did not inhibit Des1 activity in cell lysates (Figure 5.16). These results suggests that this analogue might affect in some extent the enzyme's electron transport chain or the redox status of the cell. Nevertheless, this compound does not act as a direct Des1 inhibitor, as seems to be evident by the results obtained for the evaluation of Des1 activity in cell lysates.

The Des1 inhibition induced by **45b** is dose-dependent (Figure 5.17) with an IC_{50} value of 0.7 μM (10 μM d**hCerC6NBD** substrate).

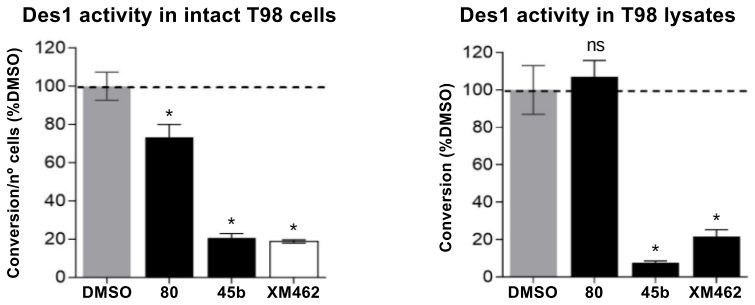

Figure 5.16. Effect of **45b** and **80** on Des1 activity. T98G cell lysates or T98G cells were incubated with DMSO (control), compunds **45b**, **80** (10 μM) or **XM462** (10 μM) (positive control). Then, the Des1 substrate (dhCerC6NBD, 10 μM) was added and cells were collected 4 h later. Medium and cell samples were analyzed by HPLC coupled to a fluorescence detector. Values are the mean of 2 independent experiments with triplicates. Asterisks indicate statistical significance over vehicle (EtOH) at $P<0.0001$ (unpaired, two-tailed t test).

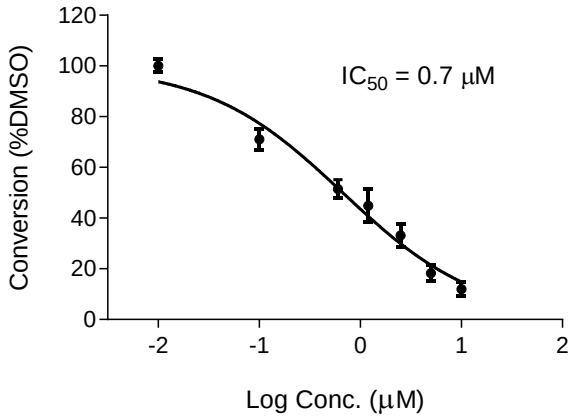

Figure 5.17. Concentration-dependence of dihydroceramide desaturase inhibition by **45b** in T98 lysates. Enzyme activity was determined as indicated in the experimental section using a substrate concentration of 10 μM and different concentrations of **45b** (0.1, 0.6, 1.2, 2.5, 5, and 10 μM). Data correspond to the mean ±SD of 2 independent experiments with three replicates. The calculated IC_{50} value is 0.7 μM.

Cyclopropenone ceramide analogue **45b** exhibited a strong Des1 activity inhibition in intact T98-cells and in T98 cell lysates. These results would imply that the inhibition is caused by a direct interaction of the inhibitor with the enzyme, and that the effect is not caused by affecting the electron transport chain or modifying the redox status of the cell, as these effects are supressed when the activity is evaluated in cell lysates.

Indeed, compound **45b** exhibited more potent Des1 inhibition *in vitro* than the reference inhibitors. Analogue **45b** inhibits Des1 with an IC_{50} of 0.7 μM (evaluated in T98 cell lysates); lower than IC_{50} values of 20 μM for **GT11** and 8.2 μM for **XM462** when these inhibitors were evaluated in rat liver microsomes.

Cyclopropenone ceramide analogue **45b** will be denoted as **PR280** to facilitate its identification as a novel Des1 inhibitor.

5.6 PR280 stability against thiols

Although dihydroceramide desaturase 1 does not contain cysteine residues in the active site, as confirmed by the 3D-structure predicted by AF2, three cysteine residues: Cys 79, Cys 100, and Cys 154 (Figure 5.18, in red) can be observed outside the active site of the enzyme, two of them in a peripheral area of Des1 (Cys100 and Cys 154).

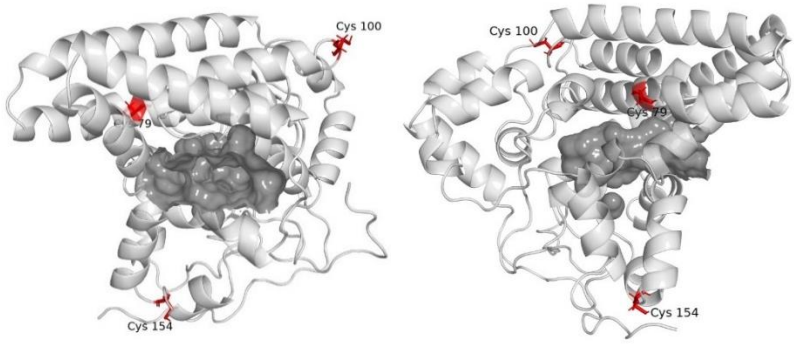

Figure 5.18. Front and lateral view of Des1-Fe_2O_2 3D-structure with cysteine residues coloured in red and interior surface of the active site coloured in grey.

To confirm that none of the three distant cysteine residues could be involved in a hypothetical allosteric inhibition of Des1 by reaction of the cyclopropenone moiety of **PR280**, we conducted a chemical assay following the methodology outlined by J. Quintana *et al*.[15] Thus **PR280** (1 eq.) was incubated with ethanethiol (3 eq.) in $CDCl_3$ at 27 °C, and *p*-difluorobenzene (1 eq.) was added as reference. The evolution of the mixture was monitored by ^1H NMR, verifying that ceramide analogue **PR280** remained unchanged after 14 days (Figure 5.19).

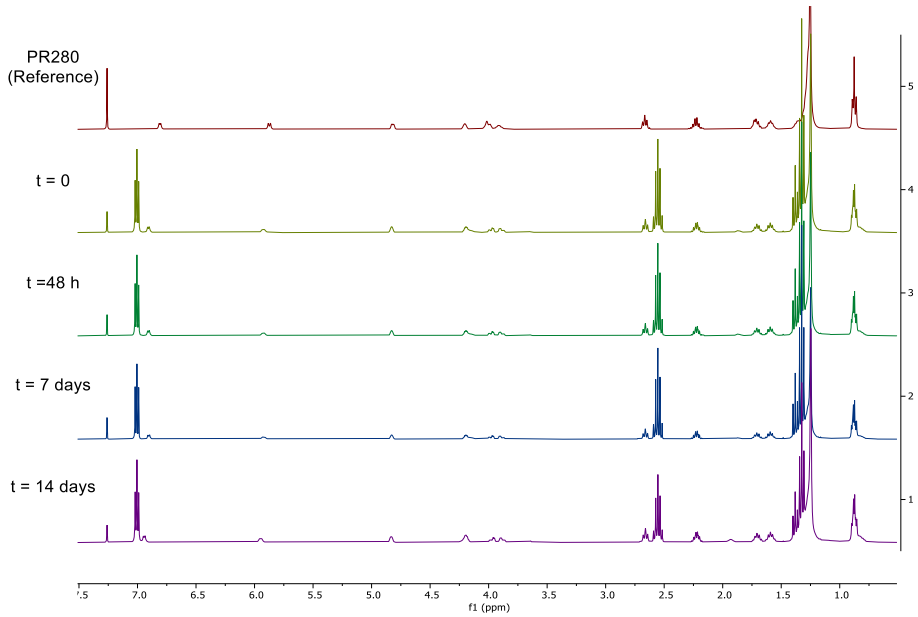

Figure 5.19. Significant ^{1}H NMR spectra of the **PR280** incubation with ethanethiol during time.

This assay provides chemical evidence for the inertness of cyclopropenone ceramide analogue in the presence of thiols. This suggest that a nucleophilic attack of a cysteine residue is not involved in the inhibitory mechanism of **PR280.**

5.7 Proposal of a second generation PR280 ceramide analogueues via i*n silico* optimization using Fe_2O_2-Des1 system 3D model.

After the identification of cyclopropenone ceramide analogue **PR280** as a potent Des1 inhibitor, *in silico* structure-based optimization was undertaken to design a library of second-generation **PR280** derivatives and identify a more potent inhibitor against the target. Thus, a virtual screening strategy involving docking calculations with the constructed Fe_2O_2-Des1 system was devised.

The structure of ceramide analogue **PR280** can be divided into four distinct regions (Figure 5.20): the polar head (blue), encompassing the two hydroxyls and the amide functionalities; the cyclopropenone rigid scaffold (orange); the alkyl chain linked to the cyclopropenone (grey); and the alkyl chain linked to the polar head through the amide bond (green). The cyclopropenone rigid scaffold was identified as essential in the analogue's structure, proving effective in inhibiting Des1 likely by imposing a proper arrangement of the entire structure in the enzyme's active site, as observed in docking calculations. The secondary amide functionality and the hydroxyl groups were previously identified as essential for enzyme inhibition in structure-activity relationship studies reported in the bibliography.

In this context, our strategy for the virtual screening was generating a library of **PR280** analogues modifying the amide substitution (green). While introducing variability in both alkyl chains is possible, modifying the amide substitution is more convenient from a synthetic perspective, as *N*-acylation is the last step of the **PR280** synthetic route. This strategy aims to find an amide substitution that can enhance the interactions of the ceramide analogue with the enzyme while preserving the structural elements that have been previously identified as crucial for the enzyme's inhibition. This project was performed in collaboration with prof. Xavier Barril (ICREA Research Professor, University of Barcelona).

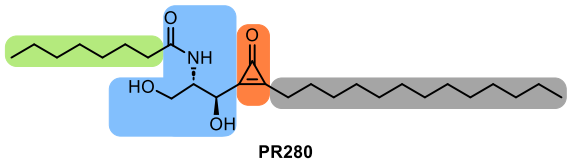

Figure 5.20. Structure of ceramide analogue **PR280** divided in 4 different regions based on their chemical nature.

Initially, a library containing commercial carboxylic acids was generated. In order to match Lipinski's rule of five,[48] the molecular weight of the carboxylic acids was truncated to below 180 Da. Considering that the Des1 active site is predominantly constituted by non-polar amino acids, we prioritized structures capable of undergoing non-polar interactions. Furthermore, we emphasized structures containing quaternary carbons. Quaternary carbon, a prevalent feature in natural product structures, has been associated with more effective and selective binding to target proteins. Molecules with quaternary carbons exhibit increased aqueous solubility, metabolic stability, and target selectivity. Additionally, quaternary carbons confer a 3D shape to the structure, which is advantageous for targets with large binding sites, such as Des1 (Figure 5.21).[49]

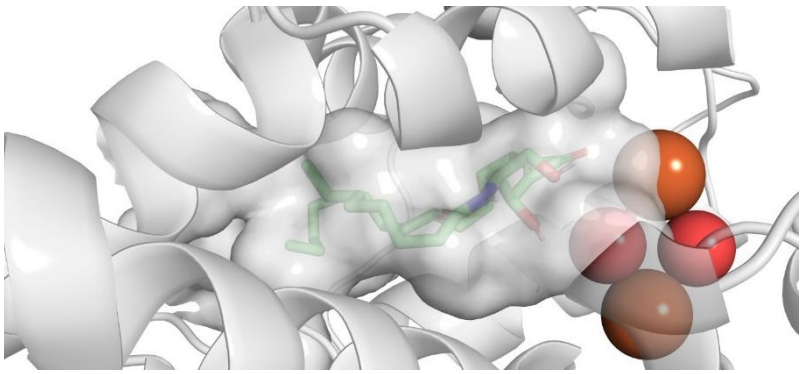

Figure 5.21. Lateral view of the interior surface of the active site with the best docking pose obtained for cyclopropenone ceramide analogue **PR280**.

Applying the aforementioned criteria, a library containing 2027 commercially available carboxylic acids was obtained. The corresponding virtual library, consisting of 2027 ceramide analogues (see annex), was

[48] Lipinski, C. A.; Lombardo, F.; Dominy, B. W.; Feeney, P. J. *Adv. Drug Delivery Rev.* **1997**, *23*, 3–25.

[49] a) Lovering, F.; Bikker, J.; Humblet, C. *J. Med. Chem.* **2009**, *52*, 6752–6756. b) Talele, T. T. *J. Med. Chem.* **2020**, *63*, 13291−13315. c) Wei, W.; Cherukupalli, S.; Jing, L.; Liu, X.; Zhan, P. *Drug Discov. Today* **2020**, *25*, 1839−1845. d) Hiesinger, K.; Darín, D.; Proschak, E.; Krasavin, M. *J. Med. Chem.* **2021**, *64*, 150−183.

generated by the virtual reaction of aminodiol **56** with the previously generated carboxylic acids library using MOE (Scheme 5.22).[50]

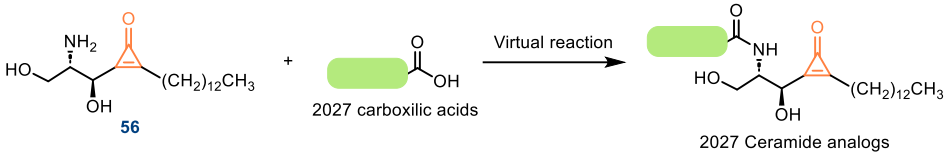

Scheme 5.22. Generation of the virtual library of cyclopropenone containing ceramide analogues.

A tethered docking was performed with the constructed library. In the docking, ligand poses were restricted and forced to overlay the substructure corresponding to the rigid scaffold and polar head of the reference docking pose obtained for the reference ligand **PR280** (Figure 5.22). In the tethering, we assumed that the binding mode of the analogue does not change with the different substitutions of the amide, and a binding position with the cyclopropene moiety close to the Fe_2O_2 specie would take place. With this strategy, the generation of docking poses that do not match the expected binding pose previously observed for **PR280** were avoided, saving computational effort and enabling the evaluation of the large virtual library containing 2027 cyclopropenone ceramide analogues.

[50] Molecular Operating Environment (MOE), 2019.01; Chemical Computing Group ULC, 1010 Sherbooke St. West, Suite #910, Montreal, QC, Canada, H3A 2R7, 2021.

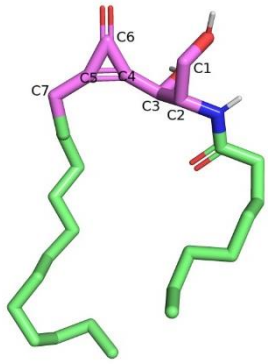

Figure 5.22. Best scored docking pose of the reference inhibitor **PR280**. The tethered substructure is coloured in pink.

Following docking calculations, the ceramide analogues in the virtual library were scored and ranked (see annex). The top 45 ceramide analogues were visualized and rationally analyzed (see experimental part), finally selecting 10 compounds as the most promising Des1 inhibitor candidates (Table 5.3).

Ceramide analogues were selected trying to achieve a chemically diverse collection, and three main groups could be identified. Ceramide analogues of each group were selected trying to promote a different class of protein-ligand interactions, furthermore, any extra polar interactions stablished was considered as positive. Although all the carboxylic acids to synthetize the ceramide analogues present in the library were commercially available, the prize and ease of shipment were also considered in the selection of the best ceramide analogues as Des1 inhibitors candidates.

Table 5.3. Ceramide analogues selected after the virtual screening of cyclopropenone containing ceramide analogues virtual library.

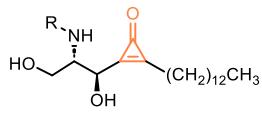

PR280-X

Entry	R	Rank	Score	Observed interactions
Aromatic groups				
1	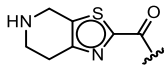 PR280-1	3	-22.612	- Parallel displaced π-stacking (Tyr170) - H-bond: NH-carbonyl backbone
2	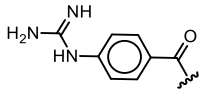 PR280-2	4	-22.548	- Parallel displaced π-stacking (Tyr170) - H-bond: NH-carbonyl backbone
3	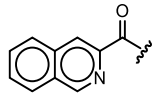 PR280-3	7	-21.199	- Parallel displaced π-stacking (Tyr170)
4	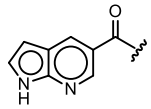 PR280-4	26	-19.697	- Parallel displaced π-stacking (Tyr170) - H-bond: NH-carbonyl backbone
Including polar groups				
5	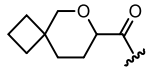 PR280-5	9	-20.887	- H-bond: OH-O (Tyr 120)
6	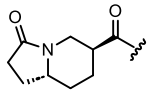 PR280-6	21	-19.856	
7	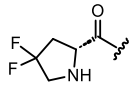 PR280-7	27	-19.687	- Weak H-bond: NH-π (Tyr170) - *gem*-difluoro group in a non-polar environment.
Apolar gropus				
8	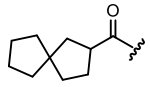 PR280-8	8	-20.955	- Aliphatic compound in a in a non-polar environment.
9	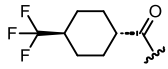 PR280-9	13	-20.383	- Aliphatic groups in a in a non-polar environment.
10	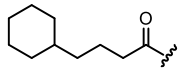 PR280-10	31	-19.512	- Aliphatic compound in a in a non-polar environment.

Four compounds containing aromatic substitution in the primary amide were selected (Table 5.3, entries 1-4) as they can undergo hydrophobic interactions with the hydrophobic active site of Des1. Compound **PR280-1**, containing a thiazole ring, would stablish an H-bond interaction with a carbonyl group of the protein backbone. This H-bond interaction was also observed in the guanidine group of compound **PR280-2** and the pyrrole ring of compound **PR280-4**. It was observed that bicyclic structures occupied the wide active site of the enzyme to a greater extent.

Three compounds including polar groups in the amide substitution were selected (Table 5.3, entries 5-7). These compounds were observed to better fit the 3D structure of the active site thanks to the presence of quaternary centres in the structure. Moreover, compound **PR280-5** was involved as acceptor in an H-bond interaction with Tyr 120, and a weak H-bond was stablished between **PR280-7** and Tyr170. The evaluation of this compounds as Des1 inhibitors would allow to determine if saturated structures with 3D shape, provoked by the presence of quaternary centres, could be beneficial in comparison with the flat structures of aromatic compounds **PR280-(1-4).**

Finally, three compounds with non-polar substituents in the amide were selected (Table 5.3, entries 8-10). The docking of these compounds also showed that the presence of quaternary centres makes the analogues fit better within the contours of the active site. In this case, hydrophobic interactions in the active site would be enhanced. The selection of these compounds aims to increase the number of favourable hydrophobic interactions, which is less challenging than optimizing directionality-constrained hydrogen-bonds.[51]

[51] Hann, M. M. *Multifaceted Roles Crystallogr. Mod. Drug Discov.* **2015**, *2*, 183–196.

Considering that active Des1 inhibitor **PR280** was also included in the virtual screening and obtained an intermolecular score of -10.328 (ranked at position 652), analogues **PR280-(1-10)** stand out as promising Des1 inhibitors. Moreover, the synthesis and biological evaluation of these analogues will allow to elucidate which chemical scaffold (aromatic, polar or apolar) is better to enhance the inhibitory capacity of ceramide analogues based on cyclopropenone structures.

Chapter VI

Development of a Ru-catalysed RCM reaction on CPG-coupled DNA for the synthesis of DNA-encoded macrocyclic library

UNIVERSITAT ROVIRA I VIRGILI
TARGETING DES1: SYNTHESES OF CERAMIDE ANALOGUES WITH A RIGID SCAFFOLD, INHIBITORY ASSAYS, AND AF2-ASSISTED STRUCTURAL INSIGHTS REVEAL PR280 AS A POTENT INHIBITOR
Pablo Rivero Prieto

The work described in this chapter was carried as part of a research stay in the laboratory of Prof. Andreas Brunschweiger (Faculty of Chemistry and Chemical Biology, Technische Universität Dortmund, Germany).

In this chapter, the numbered products refer to DNA-conjugates, distinct from the products discussed in the rest of the thesis. Consequently, the product enumeration is restarted to facilitate readability.

6.1 Introduction

6.1.1 DNA-encoded chemical libraries

DNA-encoded chemical library (DECL) technology is used by the pharmaceutical industry as an efficient method to discover small molecules capable of modulating biologically relevant targets, as it allows the synthesis and screening of unprecedented chemical diversity and library sizes.[1] DECL technology is a recent addition to pharmaceutical industry's toolbox, as the concept was first discussed around 30 years ago.[2] Today, this technology is employed by numerous pharmaceutical companies and has garnered interest from an increasing number of academic laboratories. DECL has already demonstrated successful histories of hit identifications. Furthermore, some drug candidates derived from DECL hits have been tested in clinical trials for various diseases.[3]

---

[1] Satz, A. L.; Brunschweiger, A.; Flanagan, M. E.; Gloger, A.; Hansen, N. J. V.; Kuai, L.; Kunig, V. B. K.; Lu, X.; Madsen, D.; Marcaurelle, L. A.; Mulrooney, C.; O'Donovan, G.; Sakata, S.; Scheuermann, J. *Nat Rev Methods Primers* **2022**, *2*, 3.

[2] Brenner, S.; Lerner, R. A. *Proc. Natl. Acad. Sci. U.S.A.* **1992**, *89*, 5381-5383.

[3] a) Harris, P. A.; Berger, S. B.; Jeong, J. U.; Nagilla, R.; Bandyopadhyay, D.; Campobasso, N.; Capriotti, C. A.; Cox, J. A.; Dare, L.; Dong, X.; Eidam, P. M.; Finger, J. N.; Hoffman, S. J.; Kang, J.; Kasparcova, V.; King, B. W.; Lehr, R.; Lan, Y.; Leister, L. K.; Lich, J. D.; MacDonald, T. T.; Miller, N. A.; Ouellette, M. T.; Pao, C. S.; Rahman, A.; Reilly, M. A.; Rendina, A. R.; Rivera, E. J.; Schaeffer, M. C.; Sehon, C. A.; Singhaus, R. R.; Sun, H. H.; Swift, B. A.; Totoritis, R. D.; Vossenkämper, A.; Ward, P.; Wisnoski, D. D.; Zhang, D.; Marquis, R. W.; Gough, P. J.; Bertin, J. *J. Med. Chem.* **2017**, *60*, 1247-1261. b) Ding, Y.; Belyanskaya, S.; DeLorey, J. L.; Messer, J. A.; Franklin, G. J.; Centrella, P. A.; Morgan, B. A.; Clark, M. A.; Skinner, S. R.; Dodson, J. W.; Li, P.; Marino, J. P.; Israel, D. I. *Bioorg Med Chem* **2021**, *41*, 116216. c) Luther, J. M.; Ray, J.; Wei, D.; Koethe, J. R.; Hannah, L.; DeMatteo, A.; Manning, R.; Terker, A. S.;

A complete DECL is a complex mixture, in which each small molecule is present in low quantities and linked to a unique DNA strand (Figure 6.1), which enables the identification of the small molecule conjugate by DNA sequencing. DNA-encoded compounds consist of the genotype and the phenotype, which are covalently bound by a flexible linker moiety. The genotype carries the amplifiable DNA-barcode, usually formed by three codes and a terminal primer, this can be amplified by polymerase chain reaction (PCR) and read out. The phenotype consists of the small molecule, which binds to the target.

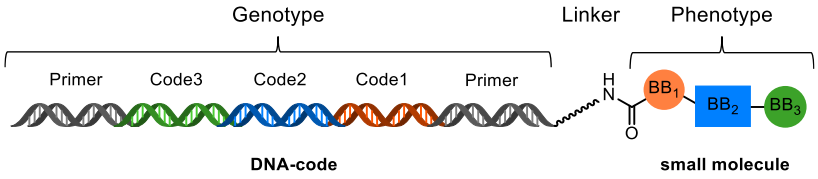

Figure 6.1. DNA-encoded small molecule (BB: Building block).

DNA encoding facilitates the construction and screening of large chemical libraries, as the conjugation of a unique DNA fragment to each compound of the library serves as an amplifiable ''bar code'' for the identification of individual library members even with low concentrations, as DNA can be amplified by polymerase chain reaction (PCR). However, DNA barcoding

Peng, D.; Nian, H.; Yu, C.; Mashayekhi, M.; Gamboa, J.; Brown, N. J. *Hypertension* **2021**, *78*, 1092-1102. d) Cuozzo, J. W.; Clark, M. A.; Keefe, A. D.; Kohlmann, A.; Mulvihill, M.; Ni, H.; Renzetti, L. M.; Resnicow, D. I.; Ruebsam, F.; Sigel, E. A.; Thomson, H. A.; Wang, C.; Xie, Z.; Zhang, Y. *J. Med. Chem.* **2020**, *63*, 7840-7856. e) Puglioli, S.; Schmidt, E.; Pellegrino, C.; Prati, L.; Oehler, S.; De Luca, R.; Galbiati, A.; Comacchio, C.; Nadal, L.; Scheuermann, J.; Manz, M. G.; Neri, D.; Cazzamalli, S.; Bassi, G.; Favalli, N. *Chem.* **2023**, *9*, 411-429. f) Harris, P. A.; Marinis, J. M.; Lich, J. D.; Berger, S. B.; Chirala, A.; Cox, J. A.; Eidam, P. M.; Finger, J. N.; Gough, P. J.; Jeong, J. U.; Kang, J.; Kasparcova, V.; Leister, L. K.; Mahajan, M. K.; Miller, G.; Nagilla, R.; Ouellette, M. T.; Reilly, M. A.; Rendina, A. R.; Rivera, E. J.; Sun, H. H.; Thorpe, J. H.; Totoritis, R. D.; Wang, W.; Wu, D.; Zhang, D.; Bertin, J.; Marquis, R. W. *ACS Med. Chem. Lett.* **2019**, *10*, 857-862. g) Hou, N.; Shuai, L.; Zhang, L.; Xie, X.; Tang, K.; Zhu, Y.; Yu, Y.; Zhang, W.; Tan, Q.; Zhong, G.; Wen, Z.; Wang, C.; He, X.; Huo, H.; Gao, H.; Xu, Y.; Xue, J.; Peng, C.; Zou, J.; Schindewolf, C.; Menachery, V.; Su, W.; Yuan, Y.; Shen, Z.; Zhang, R.; Yuan, S.; Yu, H.; Shi, P.-Y.; Bu, Z.; Huang, J.; Hu, Q. *ACS Cent. Sci.* **2023**, *9*, 217-227.

presents several other benefits. This identification method offers a limitless number of potential encoding sequences, the DNA strand is soluble in aqueous solutions, which facilitates DEL screening under physiological conditions. DNA-linked small molecules present predictable behaviours such as retention times and analytical signals, which facilitate its synthesis, purification, and analysis (this holds true regardless of the small molecule attached). Finally, the DNA barcode can be generated in a combinatorial manner, as it can be ligated using DNA ligases.

DECLs are generally produced using split-and-pool combinatorial chemistry strategy, a technique that allows for the low-cost synthesis of millions of small molecules.[4] DECL synthesis starts with the headpiece (Figure 6.2), which consists in a short single-stranded or double-stranded DNA oligonucleotide which contains a chemical linker moiety, usually a polyethylene glycol chain with a terminal amino group.[5]

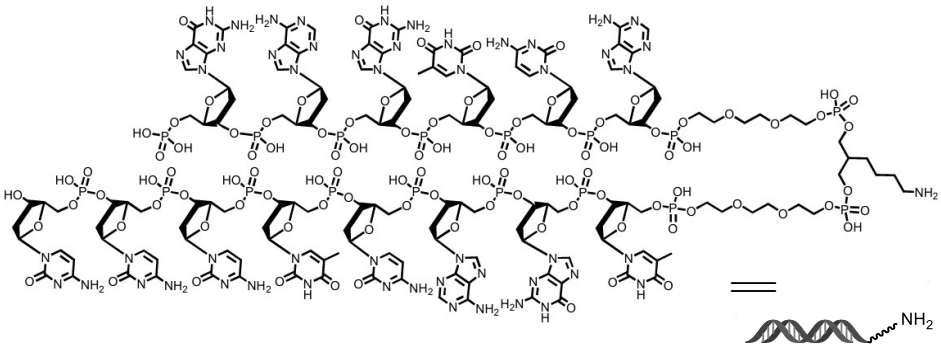

Figure 6.2 Example of a headpiece for DECL synthesis.

[4] Goodnow, R. A.; Dumelin, C. E; Keefe, A. D *Nat. Rev. Drug Discov.* **2017**, *16*, 131-147.

[5] Clark, M. A.; Acharya, R. A.; Arico-Muendel, C. C.; Belyanskaya, S. L.; Benjamin, D. R.; Carlson, N. R.; Centrella, P. A.; Chiu, C. H.; Creaser, S. P.; Cuozzo, J. W.; Davie, C. P.; Ding, Y.; Franklin, G. J.; Franzen, K. D.; Gefter, M. L.; Hale, S. P.; Hansen, N. J. V.; Israel, D. I.; Jiang, J.; Kavarana, M. J.; Kelley, M. S.; Kollmann, C. S.; Li, F.; Lind, K.; Mataruse, S.; Medeiros, P. F.; Messer, J. A.; Myers, P.; O'Keefe, H.; Oliff, M. C.; Rise, C. E.; Satz, A. L.; Skinner, S. R.; Svendsen, J. L.; Tang, L.; van Vloten, K.; Wagner, R. W.; Yao, G.; Zhao, B.; Morgan, B. A. *Nat. Chem. Biol.* **2009**, *5*, 647-654.

The combinatorial *split-and-pool* workflow proceeds through cycles that consist of a DNA barcode elongation step and a chemical synthesis step, building up the small molecule and the DNA barcode simultaneously in each cycle (Scheme 6.3). The process starts with the headpiece, which is split into as many reaction vessels as building blocks will be employed (*split*). Then, in each reaction vessel, a DNA barcode that encodes for the building block that is going to be introduced is ligated by the action of T4 ligase. After successful ligation, a purification step takes place. Finally, the chemical synthesis step takes place, and a building block is linked. The above cycle of encoding and synthesis is closed by pooling all encoded compounds into a single vessel (*pool*), constituting the first *split-and-pool* cycle. The mixture can now undergo the next cycle; at least three cycles are needed to generate a functional coding system.

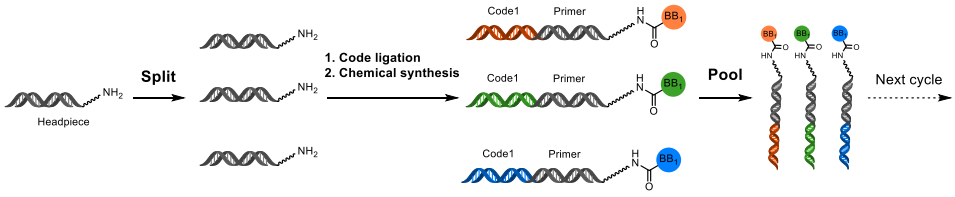

Scheme 6.1. Representation of the firs *spli-and-pool* cycle in a DECL synthesis.

A library design employing three combinatorial cycles, each with a split size of 100 building blocks (100 × 100 × 100), provides 10^6 compounds from just 300 building blocks (100 + 100 + 100) and 600 operations (300 chemical reactions + 300 DNA ligations). The combinatorial workflow leads to exponential library growth and allows the synthesis of ultra-large numbers of compound. With three or four combinatorial cycles, library sizes of 10^8–10^9 compounds can be reached.[6]

[6] Mannocci, L.; Zhang, Y.; Scheuermann, J.; Leimbacher, M.; De Bellis, G.; Rizzi, E.; Dumelin, C.; Melkko, S.; Neri, D. *Proc. Natl Acad. Sci. USA* **2008**, *105*, 17670-17675.

Split-and-pool combinatorial synthesis is the most used method for DECL synthesis.[7] However, other alternatives have been developed which introduce some variabilities to the former methodology, such as DNA-templated techniques,[8] DNA-encoded solid-phase chemistry,[9] DNA-encoded self-assembling library technology,[10] and DNA-encoded fragment screening.[11]

The final DECL is then screened on a biological target for hit finding. Usually, a protein is immobilized on a solid support and incubated with the DECL. Later on, the unbound library members are removed during the washing steps (Scheme 6.2). The molecules that bind the target are then eluted by heat denaturation of the protein, amplified by PCR and identified by sequencing of their DNA-barcodes. The identified compounds, *hits*, must be resynthesized without DNA-tag and validated through the corresponding assay. Unlike a biochemical assay, DECL selection requires the direct binding of the library molecule to the target protein, and thus, the presence of trace by-products or other impurities have a minimal impact on the screening.

---

[7] Furka, A.; Sebestyén, F.; Asgedom, M.; Dibó, G. *Int. J. Pept. Protein Res.* **1991**, *37*, 487-493.

[8] a) Blakskjaer, P.; Heitner, T.; Hansen, N. J. V. *Curr. Opin. Chem. Biol.* **2015**, *26*, 62-71. b) Usanov, D. L.; Chan, A. I.; Maianti, J. P.; Liu, D. R. *Nat. Chem.* **2018**, *10*, 704-714. c) O'Reilly, R. K.; Turberfield, A. J.; Wilks, T. R. *Acc. Chem. Res.* **2017**, *50*, 2496-2509.

[9] a) MacConnell, A. B.; McEnaney, P. J.; Cavett, V. J.; Paegel, B. M. *ACS Comb. Sci.* **2015**, *17*, 518-534. b) Paciaroni, N. G.; Ndungu, J. M.; Kodadek, T. *Chem. Commun.* **2020**, *56*, 4656-4659. c) Satz, A. L.; Kuai, L.; Peng, X. *Bioorg. Med. Chem. Lett.* **2021**, *39*, 127851.

[10] Scheuermann, J.; Neri, D. *Curr. Opin. Chem. Biol.* **2015**, *26*, 99-103.

[11] Reddavide, F. V.; Lin, W.; Lehnert, S.; Zhang, Y. *Angew. Chem.* **2015**, *127*, 8035-8039.

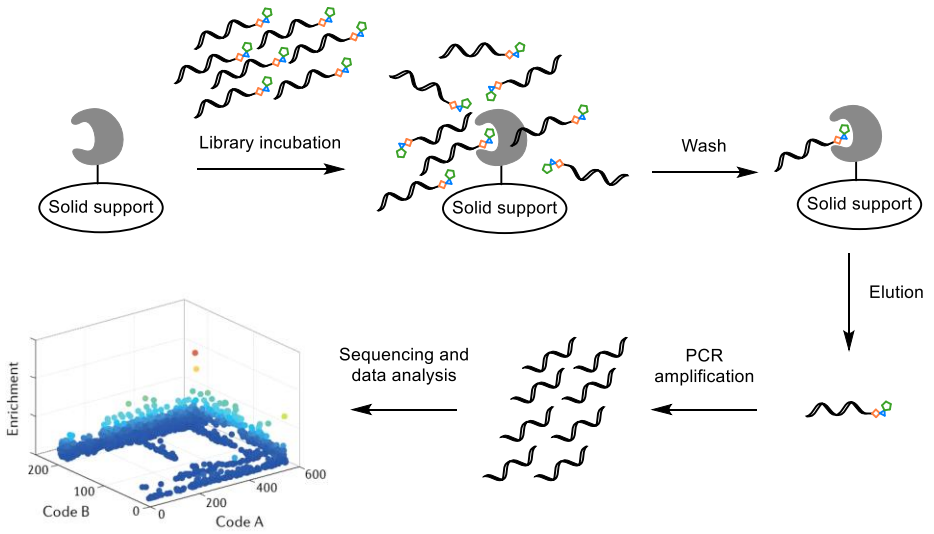

Scheme 6.2 Affinity-based DECL selections against an immobilized target protein.

DNA-encoded libraries have emerged as a promising method for hit finding in the pharmaceutical industry, offering several advantages over other screening approaches. DECL screening requires a small ampunt of protein, involves minimal assay development, and do not necessitate specialized instrumentation or robotics. These screenings explore structurally complex chemical space, providing a unique advantage in the search for novel hits. Additionally, prior structural knowledge of the target or its ligands is not necessary. In contrast to public-knowledge-based rational design, which relies on existing patent and literature databases, DECL opens the possibility to discover novel hit molecules that may elude rational or computational analysis.

These characteristics makes DECL an attractive first option for hit finding, providing a valuable alternative to traditional screening methods in drug discovery.

6.1.2 Coverage of chemical space in DECLs

The success of a DECL screening heavily relies on the structural diversity in the library and the chemical space covered. In this sense, the DNA barcode represents a great challenge for the development of new on-DNA synthetic methodologies, as the genetic information must be preserved during the reaction. On-DNA synthetic methodologies are needed for the construction of chemically diverse and rich DECL.

For a long time, DECLs have been produced using very large number of starting materials but with a limited set of synthetic transformations to concatenate three, four or even five building blocks. Carbonyl reactions such as amide bond formation, reductive amination, nucleophilic substitution of aromatic and aliphatic halides, and C-C sp2 cross-coupling reactions have been extensively used.[12] These reactions produced DECLs biased towards sp^2-rich compounds, moreover, concatenating three to four building blocks tend to furnish products with high molecular weight that are challenging to optimize towards drugs.

Currently, library design is focusing on generating structural diverse libraries that contain compounds matching Lipinski's rule of five, sometimes sacrificing the total number of library components and targeting family-focused libraries.[13]

In this context, DNA-compatible synthesis is the key to expanding the DECL chemical space, but some considerations have to take into account in the development of new on-DNA synthetic procedures. Generally, on-DNA reactions must be operated at high dilution (~1 mmol/L), with 10% water as the co-solvent, under mild conditions (pH 4-14, 25-90 °C), on small scales (~25 nmol), avoiding oxidants and many Lewis acids. The reactions must be highly chemoselective for modification of the conjugated small molecule rather than the DNA barcode. Ideally, these reactions should use off-the-shelf starting

[12] Götte, K.; Chines, S.; Brunschweiger, A. *Tetrahedron Lett.* **2020**, *61*, 151889.
[13] Martín, A.; Nicolaou, C. A.; Toledo, M. A. *Commun. Chem.* **2020**, *3*, 1-9.

materials, be robust over a broad substrate scope and give well-defined products with high conversions. It is worth mentioning that there is not a strict rule determining when a reaction is too damaging to the barcode to be useful. When designing a DECL, the DNA damage and the potential increase in chemical diversity must be considered.

In the last years, new strategies have been developed for encoded compound synthesis and have met with great success.[14] Recent advances in expanding DECL synthetic toolbox include DNA-compatible photo-promoted chemical transformation,[15] as they are typically performed under mild conditions; nanoheterogeneous reaction media, exemplified by micellar nanoreactors;[16] reactions on solid phase, either by alternative barcoding strategies or by immobilizing DNA on ion exchange resins.[17]

6.1.3 DECL synthesis on DNA coupled to controlled pore glass solid support

The imposition of working in aqueous cosolvents in solution phase on-DNA synthesis has excluded many reactions that involve water-sensitive reagents or intermediates. Alternatively, DNA-encoded compounds can be synthetized with the oligonucleotide covalently coupled to a controlled pore glass (CPG) solid phase (Scheme 6.3).

---

[14] Ma, P.; Zhang, S.; Huang, Q.; Gu, Y.; Zhou, Z.; Hou, W.; Yi, W.; Xu, H. *Acta Pharm. Sin. B.* **2024**, *14*, 492-516 (and the references therein).

[15] Matsuo, B.; Granados, A.; Levitre, G.; Molander, G. A. *Acc. Chem. Res.* **2023**, *56*, 385-401.

[16] Škopić, M. K.; Götte, K.; Gramse, C.; Dieter, M.; Pospich, S.; Raunser, S.; Weberskirch, R.; Brunschweiger, A. *J. Am. Chem. Soc.* **2019**, *141*, 10546-10555.

[17] a) Škopić, M. K.; Salamon, H.; Bugain, O.; Jung, K.; Gohla, A.; Doetsch, L. J.; dos Santos, D.; Bhat, A.; Wagner, B.; Brunschweiger, A. *Chem. Sci.* **2017**, *8*, 3356-3361. b) Flood, D. T.; Asai, S.; Zhang, X.; Wang, J.; Yoon, L.; Adams, Z. C.; Dillingham, B. C.; Sanchez, B. B.; Vantourout, J. C.; Flanagan, M. E.; Piotrowski, D. W.; Richardson, P.; Green, S. A.; Shenvi, R. A.; Chen, J. S.; Baran, P. S.; Dawson, P. E. *J. Am. Chem. Soc.* **2019**, *141*, 9998-10006.

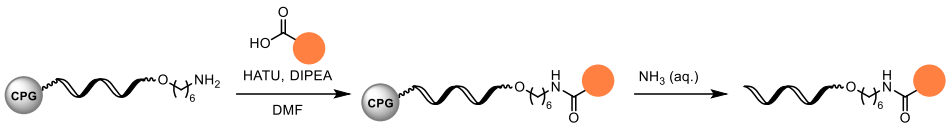

Scheme 6.3 Example of a chemical reaction on CPG-coupled DNA.

This strategy allows the use of common (dry) organic solvents in the synthesis of the small molecules, opening up the possibility of exploring a variety of new on-DNA organic transformations. It also offers handling and operational facilities as excess of reagents, metal ions or contaminants can be washed away by filtrations. Furthermore, the CPG-coupled DNA carries nucleobases protecting groups showing an enhanced chemical stability. However, a drawback of this strategy is the mandatory nucleobase deprotection and oligonucleotide cleavage from CPG steps. These steps are simultaneously performed by treatment with aqueous ammonia solution, which may hydrolyse esters and degrade base-sensitive molecules.

Liu's group, at Harvard University, showed that the CPG-coupled nucleobase-protected DNA sequences tolerated cleavage of Boc-protecting group from amino acid conjugates without damaging the nucleobases by short incubation with trifluoroacetic acid.[18] This finding significantly broadened the scope of amino acids as substrates for DECL synthesis.

The Brunschweiger's group at TU Dortmund University used the CPG-coupled DNA to expanded the scaffolds accessible in the synthesis of DECL, accessing products enriched in quaternary carbons. Reported methodologies include the synthesis of isoquinolines and pyrrolidines (Scheme 6.4, b and c);[19] isocyanide multicomponent reactions (Scheme 6.4, d), including the Ugi, Ugi-

[18] a) Tse, B. N.; Snyder, T. M.; Shen, Y.; Liu, D. R. *J. Am. Chem. Soc.* **2008**, *130*, 15611-15626. b) Yuen, L. H.; Dana, S.; Liu, Y.; Bloom, S. I.; Thorsell, A. G.; Neri, D.; Donato, A. J.; Kireev, D.; Schüler, H.; Franzini, R. M. *J. Am. Chem. Soc.* **2019**, *141*, 5169-5181.

[19] Potowski, M.; Kunig, V. B. K.; Losch, F.; Brunschweiger, A. *Med. Chem. Commun.* **2019**, *10*, 1082-1093.

azide, and Groebke-Blackburn-Bienaymé reactions;[20] furthermore, the aza-Diels-Alder reaction (Scheme 6.4, e) and the Povarov and Biginelli reactions were also effective (Scheme 6.4, f).[21]

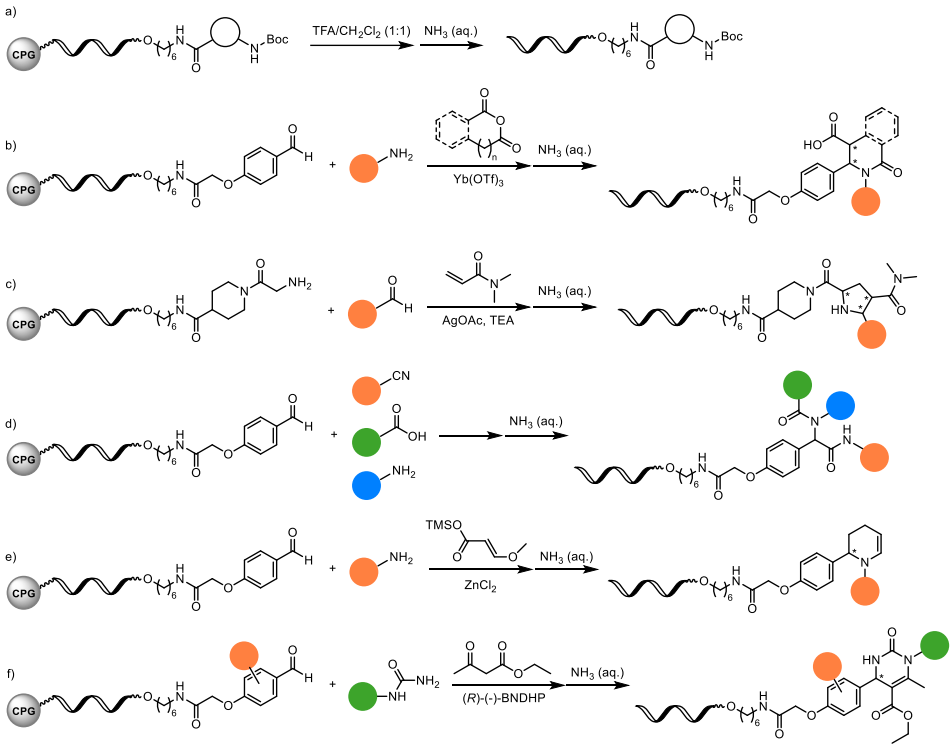

Scheme 6.4 Examples of synthetic methodologies on CPG-coupled DNA.

Brunschweiger's group conducted a study evaluating hexathymidine adapter (hexT) and three different decamer DNA oligonucleotides (TC_10mer, ATC_10mer, and ATGC_10mer) stability against different conditions.[21] Oligonucleotides were incubated with three aqueous acids, 33 metal salts and 20 organocatalysts dissolved in dry organic solvents. After standard DNA cleavage with aqueous ammonia and analysis, almost no DNA

[20] Kunig, V. B. K.; Ehrt, C.; Dömling, A.; Brunschweiger, A. *Org. Lett.* **2019**, *21*, 7238-7243.

[21] Potowski, M.; Losch, F.; Wünnemann, E.; Dahmen, J. K.; Chines, S.; Brunschweiger, A. *Chem. Sci.* **2019**, *10*, 10481-10492.

damage was observed for hexT and TC_10mer oligonucleotides. Only Ce(III), Pd(II), Rh(II) and Ru(II) salts caused a still tolerable degradation between 20 and 40%. This catalyst tolerance profile of solid phase-coupled DNA can serve as guidance for the development of new synthetic procedures on CPG-coupled DNA.

6.1.4 Towards a macrocyclic DNA-encoded chemical library

In 2001, the euchromatic portion of the human genome was sequenced.[22] This achievement has expanded the pool of potential drug targets, offering new avenues for drug development.[23]

It is considered that around 3,000 of the genes in the human genome are related to disease, out of these only 600-1,500 are considered druggable by "traditional" small molecule drugs,[24] i.e., drugs that comply with the Lipinski's rule of five (Ro5). However, there is an even larger number of novel targets that have been less explored, as these are *difficult-to-drug* using small molecules within Ro5. These *difficult-to-drug* targets have binding sites that are large, flat, groove-shaped, tunnel-shaped, flexible, or featureless.[25] For example, the human proteome is estimated to have 100,000-1,000,000 binary protein-protein interactions (PPIs),[26] which may constitute one of the most important sources of novel targets for drug discovery.[27] However, PPI sites

---

[22] International Human Genome Sequencing Consortium. *Nature* **2004**, *431*, 931–945.

[23] Blanco, M. J.; Gardinier, K. M. *ACS Med. Chem. Lett.* **2020**, *11*, 228-231.

[24] Hopkins, A. L.; Groom, C. R. *Nat. Rev. Drug Discovery* **2002**, *1*, 727-730.

[25] Doak, B. C.; Zheng, J.; Dobritzsch, D.; Kihlberg, J. *J. Med. Chem.* **2016**, *59*, 2312-2327.

[26] a) Venkatesan, K.; Rual, J. F.; Vazquez, A.; Stelzl, U.; Lemmens, I.; Hirozane-Kishikawa, T.; Hao, T.; Zenkner, M.; Xin, X.; Goh, K. I.; Yildirim, M. A.; Simonis, N.; Heinzmann, K.; Gebreab, F.; Sahalie, J. M.; Cevik, S.; Simon, C.; de Smet, A. S.; Dann, E.; Smolyar, A.; Vinayagam, A.; Yu, H.; Szeto, D.; Borick, H.; Dricot, A.; Klitgord, N.; Murray, R. R.; Lin, C.; Lalowski, M.; Timm, J.; Rau, K.; Boone, C.; Braun, P.; Cusick, M. E.; Roth, F. P.; Hill, D. E.; Tavernier, J.; Wanker, E. E.; Barabasi, A. L.; Vidal, M. *Nat. Methods* **2009**, *6*, 83-90. b) Zhang, Q. C.; Petrey, D.; Deng, L.; Qiang, L.; Shi, Y.; Thu, C. A.; Bisikirska, B.; Lefebvre, C.; Accili, D.; Hunter, T.; Maniatis, T.; Califano, A.; Honig, B. *Nature* **2012**, *490*, 556-560.

[27] Alzyoud, L.; Bryce, R. A.; Al Sorkhy, M.; Atatreh, N.; Ghattas, M. A. *Sci. Rep.* **2022**, *12*, 7975.

are large and undefined, thus small-molecule ligands need to be larger, outside Ro5 (e.g., MW > 500).[28] In this sense, outside Ro5 space offers significant possibilities for discovery.[29]

In this context, macrocycles have several features that make them suitable to tackle *difficult-to-drug* targets.[30] Because of their shape, size, and complexity, they can engage targets through numerous and spatially distributed binding interactions, thereby increasing both binding affinity and selectivity. Moreover, macrocycle flexibility facilitates interactions with dynamic protein targets, flat or groove-shaped sites. Furthermore, cyclization provides a degree of structural preorganization that may reduce the entropy cost of receptor binding compared to linear analogues.

In spite of their size (12 membered rings minimum)[31] macrocycles may have sufficient cell permeability and bioavailability to reach intracellular targets after oral administration.[32] Their conformation adaptabiity to the environment, *chameleonicity*, allow them to balance aqueous solubility and passive cell permeability.[33]

In total, 67 macrocycles have been approved as drugs by the U.S. Food and Drug Administration, representing only 4% of the drugs approved.[31] Most of them are natural products or derivatives thereof, dominating over *de novo*-designed compounds in a ratio greater than 4:1.

---

[28] Kuenemann, M. A.; Labbe, C. M.; Cerdan, A. H.; Sperandio, O. *Sci. Rep.* **2016**, *6*, 23815.

[29] Doak, B. C.; Over, B.; Giordanetto, F.; Kihlberg, J. *Chem. Biol.* **2014**, *21*, 1115–1142.

[30] a) Mallinson, J.; Collins, I. *Future Med. Chem.* **2012**, *4*, 1409-1438. b) DeLorbe, J. E.; Clements, J. H.; Whiddon, B. B.; Martin, S. F. *ACS Med. Chem. Lett.* **2010**, *1*, 448-452. c) Giordanetto, F.; Kihlberg, J. *J. Med. Chem.* **2014**, *57*, 278-295.

[31] García-Jiménez, D.; Poongavanam, V.; Kihlberg, J. *J. Med. Chem.* **2023**, *66*, 5377-5396.

[32] a) Giordanetto, F.; Kihlberg, J. *J. Med. Chem*. **2014**, *57*, 278-295. b) Bogdan, A. R.; Davies, N. L.; James, K. *Org. Biomol. Chem.* **2011**, *9*, 7727.

[33] Rzepiela, A. A.; Viarengo-Baker, L. A.; Tatarskii, V.; Kombarov, R.; Whitty, A. *J.Med.Chem.* **2022**, *65*, 10300-10317.

In this context, construction of a DNA-encoded macrocyclic library holds significant promise for drug discovery. This approach enables the synthesis and evaluation of a vast array of chemically diverse macrocycles, providing an opportunity to discover biologically active macrocycles that are not accessible through the modification of natural products. The "simplicity" of a DECLs screening would allow the evaluation of the macrocyclic library on several *difficult-to-drug* targets without the need for previous structural knowledge, greatly accelerating the process of hit finding in a class of understudied targets. Consequently, there is a desirable aim to develop on-DNA synthetic transformations leading to the efficient synthesis of macrocycles.

In this sense, expanding the Ring-closing metathesis (RCM) reaction [34] in the context of on-DNA synthetic transformations would allow the synthesis of DNA-encode macrocyclic libraries. RCM shows a broad and well-studied functional group tolerance, with commercially available Ru-based catalysts. It has been successfully applied in aqueous media[35] and has shown to be relevant for the pharmaceutical industry in the production of drug-like compounds.[36] Indeed, there are some examples of macrocyclic drugs approved by the FDA which have been prepared by RCM (Scheme 6.5).

[34] Nicolaou, K. C.; Bulger, P. G.; Sarlah, D. *Angew. Chem. Int. Ed.* **2005**, *44*, 4490-4527. (ande the references therein)

[35] a) Kirkland, T. A.; Lynn, D. M.; Grubbs, R. H. *J. Org. Chem.* **1998**, *63*, 9904-9909. b) Tomasek, J.; Schatz, J. *Green Chem.* **2013**, *15*, 2317.

[36] a) Hughes, D.; Wheeler, P.; Ene, D. *Org. Process Res. Dev.* **2017**, 21, 1938-1962. b) Higman, C. S.; Lummiss, J. A. M.; Fogg, D. E *Angew. Chem. Int. Ed.* **2016**, *55*, 3552-3565.

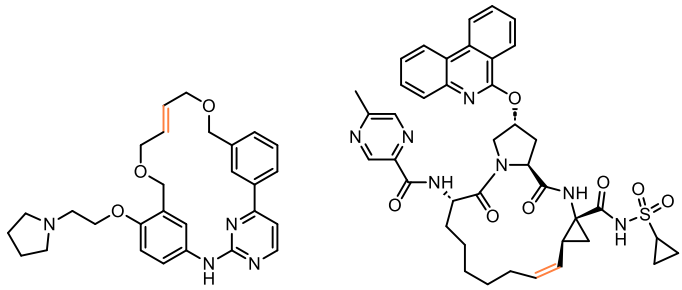

Scheme 6.5. Examples of macrocyclic drugs prepared by RCM.

6.1.5 Precedents of RCM on-DNA

X. Lu *et al.* reported the first RCM on-DNA in 2017 (Scheme 6.6, a)[37] in a H_2O/^{t}BuOH (3:2) cosolvent system. Under optimized conditions, 3rd generation Grubbs catalyst (**G-III**) yielded the best results after 1 h at room temperature, using $MgCl_2$ as additive to protect the DNA from Ru-induced decomposition. The substrate scope included small saturated heterocycles (5-, 6-, 7-, 8-membered ring) and three examples of large macrocycles (14- and 16-membered ring).

In 2020, O. B. C. Monty and coworkers reported the second example of RCM on-DNA (Scheme 6.6, b),[38] also employing an in-solution synthesis approach. Monty and coworkers developed a fully homogeneous catalyst-solvent system by adding methyl acetate to the solvent mixture. To prevent catalyst degradation under basic conditions and aid in masking coordinating functional groups NH_4Cl was added, together with $MgCl_2$, into the reaction mixture. Additionally, the use of the resistant catalyst **DA** (1,2-diphenylethane-1,2-diamine derivative of 3rd generation Grubbs catalyst)

[37] Lu, X.; Fan, L.; Phelps, C. B.; Davie, C. P.; Donahue, C. P. *Bioconjugate Chem.* **2017**, 28, 1625-1629.
[38] Monty, O. B. C.; Nyshadham, P.; Bohren, K. M.; Palaniappan, M.; Matzuk, M. M.; Young, D. W.; Simmons, N. *ACS Comb. Sci.* **2020**, *22*, 80-88.

(Scheme 6.6, b), minimized side reactions and maximized conversion. These improved conditions allowed the use of less amount of the Ru reagent.

Under the optimized conditions, the reaction exhibits high functional group tolerance, showcasing a broad substrate scope, and was applicable to a single-substrate DNA-encoded chemical library that includes sequencing analysis.

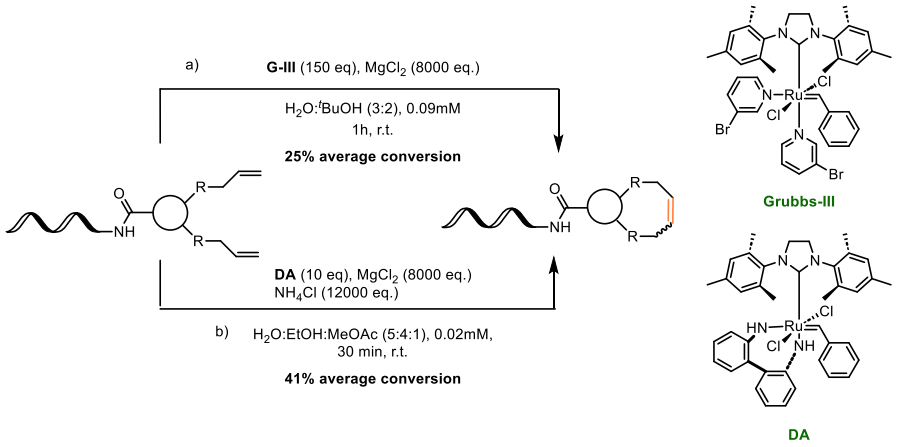

Scheme 6.3 Conditions for the on-DNA RCM reported by X. Lu *et al.* (a) and O. B. C. Monty *et al.* (b). Structure of **G-III** and **DA** catalysts.

Despite the improvements achieved by Monty and coworkers, both strategies encountered similar challenges, including difficulties in solubilizing the Ru-based catalyst, arduous catalyst and DNA extraction processes, and catalyst and DNA decomposition during the reaction, resulting in low to moderate conversion rates for the RCM reaction.

The development of the RCM reaction on controlled pore glass (CPG) coupled DNA synthesis would solve some of the problems identified in previously reported RCM on-DNA. This strategy would enable the use of dry organic solvents, allowing the solubilization of the Ru-based catalyst. Dry conditions could also enhance the reaction's conversion. Moreover, the use of solid-supported DNA would facilitate the removal of excess ruthenium catalyst at the end of the reaction through straightforward washing steps.

6.2 Results and discussion

6.2.1 Synthesis of CPG-DNA diene conjugates as substrate for Ru-catalysed RCM

The base-protected CPG-coupled TC_10mer was chosen as the CPG-coupled oligonucleotide for the development of the Ru-catalysed RCM reaction on solid-supported DNA. This oligonucleotide showed good chemical stability when incubated with Ru-based catalysts.[21]

The synthesis of a model substrate to explore the RCM (Scheme 6. 6) started with the CPG-DNA conjugate **1**, featuring a DMT-protected amino moiety linked to the oligonucleotide by a C6 alkyl chain (5'-amino-C6-TTC CTC TCC T-3'). The removal of the DMT protecting group was achieved by treating conjugate **1** with trichloroacetic acid (TCA) for 1 minute at room temperature. The unmasked amine moiety was then acylated with protected aminoacid **2** using HATU, as coupling reagent, in the presence of *N*,*N*-Diisopropylethylamine (DIPEA). Aminoacid **2** features two orthogonally protected amines, allowing the selective cleavage of each protecting group. Treatment of CPG-DNA conjugate **3** with piperidine selectively cleaved the fluorenylmethoxycarbonyl (Fmoc) protecting group. Acylation of the deprotected amine with hept-6-enoic acid yielded product **4**. Boc cleavage with TFA and subsequent acylation using hept-6-enoic acid delivered CPG-DNA conjugate **5** incorporating two terminal olefins.

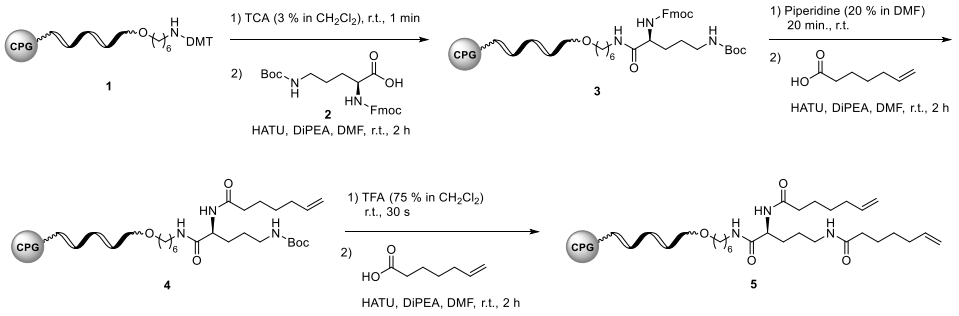

Scheme 6.6. Synthesis of CPG-DNA conjugate **5** incorporating two terminal olefines.

After each synthetic step, a fraction of the product (0.7-0.9 mg, ~20 mmol) was cleaved from the solid support by a short 30-minute treatment with AMA solution (30 % aqueous ammonia / 40 % aqueous methylamine,1:1 (vol/vol)). Each fraction was analysed by MALDI-TOF-MS to ensure the obtaining of the desired product and completion of the reaction, confirming that no starting material remained unreacted. If this was not the case, the synthetic procedure was repeated. Following this procedure, deprotection steps were repeated five times, while amide coupling was performed three times (see experimental section for a more detailed description).

Following the same synthetic strategy, a collection of CPG-DNA conjugates was synthetized (Figure 6.4).

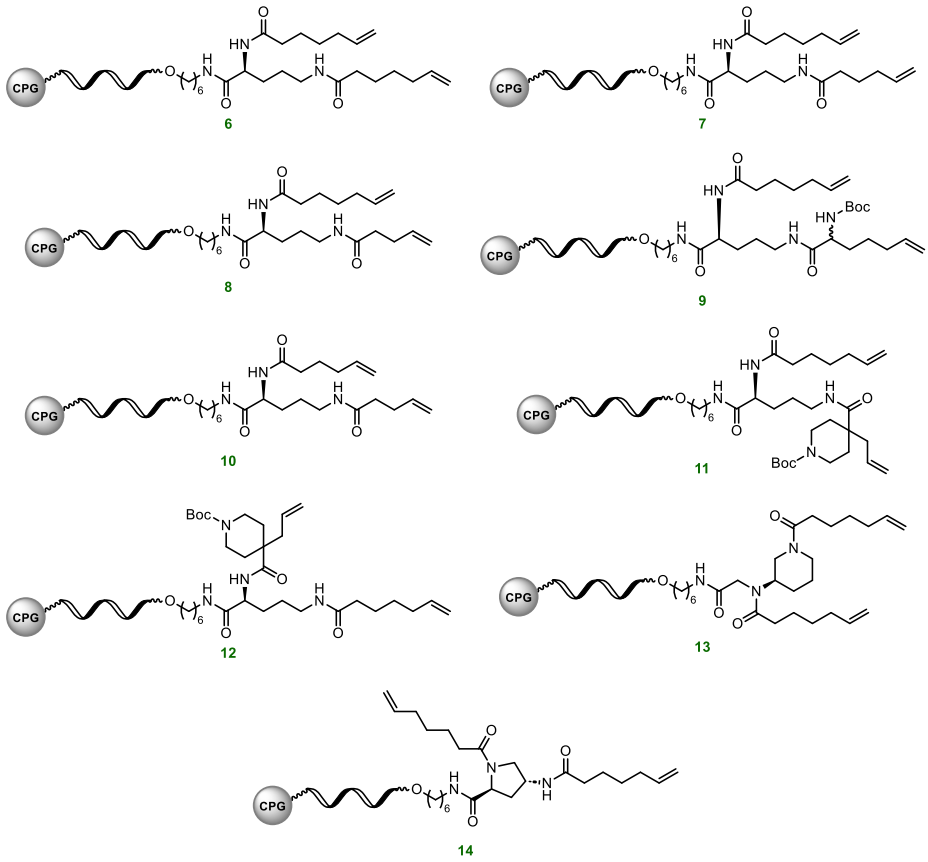

Figure 6.4. Synthetized CPG-DNA conjugates.

6.2.2 RCM on CPG-coupled DNA conjugates

The procedure designed for the RCM on CPG-coupled DNA involves:

- Performing the RCM reaction by mixing the reagents in an Eppendorf tube.
- Washing steps with organic solvents in a filter column to eliminate non-CPG-bounded subproducts.
- Incubation with Potassium tris(3,5-dimethyl-1-pyrazolyl)borate (KTP) solution in THF to coordinate ruthenium.
- Washing steps with organic solvents in a filter column to eliminate Ru-KTP complex.

Ruthenium can coordinate the phosphate backbone of the oligonucleotide; thus, an extra step in the work-up of the reaction was introduced to eliminate ruthenium form the CPG-DNA macrocyclic conjugates.

First, the setup of the reaction was addressed. To evaluate how detrimental the presence of oxygen is for the reaction, the RCM of CPG-DNA conjugate **5** was set up inside and outside a glove-bag. The reaction was performed with 10 equivalents of **G-III** catalyst in dry and degassed toluene for 2 h at room temperature (Scheme 6.7).

When setting up the reaction inside the glove-bag, two cycles of vacuum-argon were performed in the glove-bag before introducing all the reactants (degassed and dry toluene, **G-III** catalyst, and CPG-DNA conjugate **5**). The reaction was set up inside the glove-bag, sealed with parafilm, and the mixture of reactants was stirred for 2 h at room temperature outside the glove-bag. The same procedure was repeated but conducting the setting up of the reaction at open air.

A clear difference in the colour of each reaction mixture was observed at the end of the reactions (Figure 6.5). When the reaction was set up inside the glove-bag, the colour of the solution did not change after 2 h. However, when the reaction was set up at open air, the colour evolved from green to brown

after 2 h. This change in colour could be related to catalyst deactivation through ruthenium oxidation.

Analysis of both reaction contents confirmed the observations. In the MALDI-TOF-MS analysis of the reaction set up inside the glove-bag, the expected mass of the cyclized product **11** was found. On the other hand, the MALDI-TOF-MS analysis of the reaction that was set up at open air indicated that degradation of the starting material occurred during the reaction. With these results, it was concluded that RCM on CPG-coupled DNA needs to be set up inside the glove-bag.

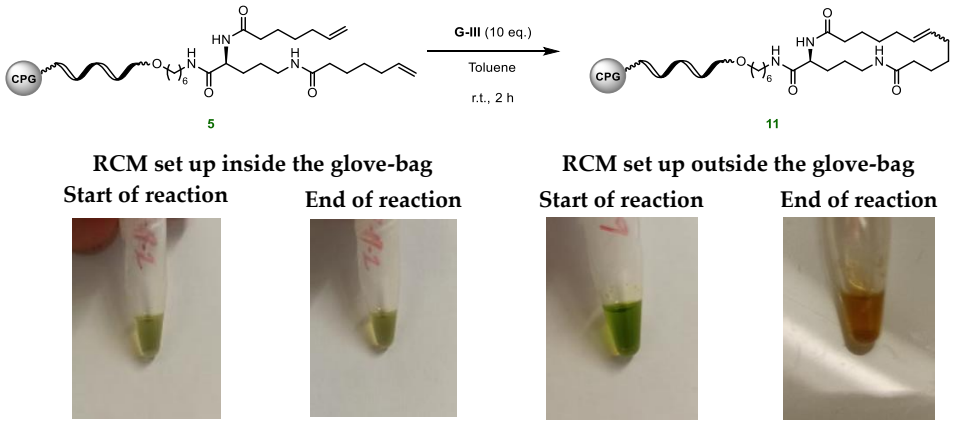

Scheme 6.5. Visual evaluation of RCM on CPG-DNA conjugate performed inside and outside a glove-bag.

Identification of CPG-DNA conjugate **11** proved that the designed strategy was successful for the synthesis of macrocycles. Consequently, the optimization of reaction conditions was addressed (Table 6.1). For the RCM, three different Ru-based catalysts were evaluated (Figure 6.6). For each catalyst, different reaction times, reaction temperatures, and catalyst loadings were tested. Each reaction was analysed by MALDI-TOF-MS to confirm the obtaining of the product and by analytical RP-HPLC to evaluate the formation of byproducts or products decomposition. The relative area of the product obtained in the analytical HPLC analysis was used to compare the outcome of the different reactions; it is important to note that this value does not represent reaction conversion.

Table 6.1. RCM on CPG-coupled DNA conditions screening.

Entry[a]	Catalyst	Solvent[b]	Reaction Time	T	Cat. Eq.[c]	Relative area (%)[d]
1	DA	Toluene	30 min	r.t	1	15,2
2	DA	Toluene	30 min	r.t	10	22,1
3	DA	Toluene	30 min	50 ˚C	1	21,2
4	DA	Toluene	30 min	50 ˚C	10	17,5
5	DA	Toluene	2 h	r.t	10	20,4
6	H-II	Toluene	30 min	r.t.	1	s. m .
7	H-II	Toluene	2h	r.t	1	21,7
8	H-II	Toluene	2h	r.t	10	17,7
9	H-II	Toluene	2h	50 ˚C	1	11,6
10	H-II	Toluene	2h	50 ˚C	10	12,3
11	G-III	Toluene	30 min	r.t.	1	s. m .
12	G-III	Toluene	2h	r.t	1	6,2
13	G-III	Toluene	2h	r.t	10	10,7
14	G-III	Toluene	2h	50 ˚C	1	5,4
15	G-III	Toluene	2h	50 ˚C	10	11,4

[a] All the experiments were carried out with 1 mg (20 nmols) of CPG-bound DNA conjugate and set up inside a glove-bag.
[b] Commercially available dry solvent was degassed by bubbling argon during 30 min.
[c] In order to control the catalyst equivalents in the reaction mixture the total volume of reaction was 50 µL in all the experiments. A 0.02 M stock solution of the catalyst in dry and degassed toluene was prepared and the needed volume added.
[d] The relative area of the product after analytical HPLC analysis was used to compare the outcome of the different reactions. Although it does not represent yield of reaction, this value allows to take into account impurities already present in the starting material, decomposition products and subproducts formation.

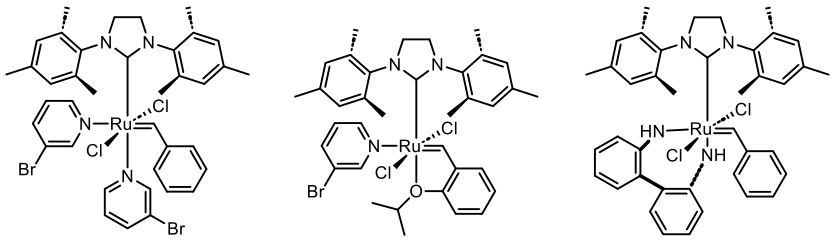

Figure 6.6. Structure of the Ru-based catalysts evaluated for the RCM on CPG-DNA conjugates. Abbreviations: 3rd generation Grubbs catalyst, **G-III**; 3rd generation Grubbs catalyst, **HG-II**; 1,2-diphenylethane-1,2-diamine derivative of 3rd generation Grubbs catalyst, **DA**.

A short reaction time, 30 min, was revealed as detrimental for the reactions catalysed with **G-III** and **HG-II** catalysts (Table 6.1, entries **6** and **11**). When working with these catalysts, the different reaction conditions were evaluated with a 2 h reaction time. In the case of the more active **DA** catalyst, shorter reaction times showed good results, and increasing the reaction time to 2 h (Table 6.1, entries **5**) did not improve reaction outcome. These results seem to indicate that DA catalyst is highly active at the initial moments of the reaction, and catalyst deactivation takes place early, thus increasing reaction time does not affect reaction outcome.

Some more general trends were observed: increasing the temperature from r.t. to 50 °C (Table 6.1, entries **3**, **4**, **9**, **10**, **14**, **15**) had a negative impact in the reaction, probably accelerating catalyst decomposition. In terms of catalyst loading, increasing from 1 eq. to 10 eq. increased the recovery of the cyclized product (Table 6.1, entries **2**, **4**, **5**, **8**, **10**, **13**, **15**).

Altogether, the best results were obtained when using 10 equivalents of **DA** catalyst in toluene for 30 minutes at room temperature (Table 6.1, entry 2).

The previous designed strategy for the RCM on CPG-coupled DNA-conjugates with the optimized reaction conditions was applied to the collection of CPG-DNA diene conjugates previously synthetized (Figure 6.7).

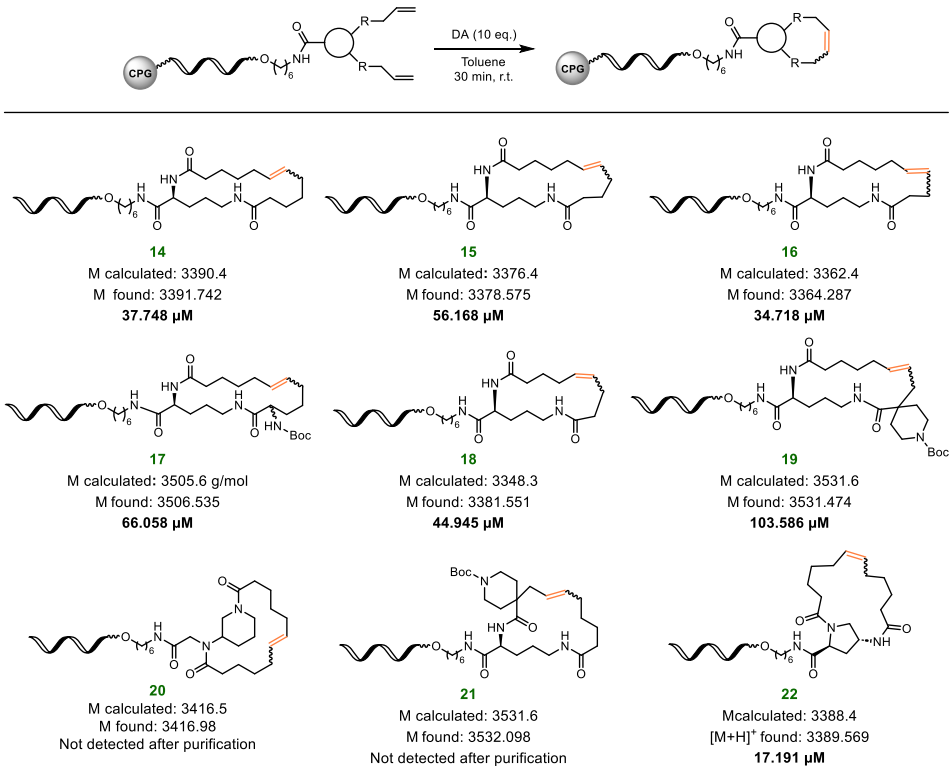

Figure 6.7. DNA macrocyclic conjugates synthetized by RCM on CPG-coupled DNA. The final concentration after purification is shown in bold.

The outcome of each reaction was analysed by MALDI-TOF-MS, confirming the successful synthesis of the desired macrocyclic DNA conjugate in all cases. Moreover, the reaction crude was analysed by analytical RP-HPLC. In the analysis only a few byproducts were detected, with the cyclized product being the predominant species observed in the chromatogram. Notably, the starting material was not detected in any of the analyses.

Nevertheless, chromatogram quality was suboptimal, with significant baseline drift observed in some cases. Additionally, the intensities of the MS spectra were lower than anticipated. This suggests that ruthenium may not be efficiently removed at the end of the RCM reaction, thereby affecting both analyses. This requires further investigation, and if confirmed, the efficiency of ruthenium removal at the end of the RCM reaction needs to be improved.

DNA macrocyclic conjugates were isolated by semi-preparative ion pair RP-HPLC. The concentration of the recovered samples was analysed by NanoDrop technique, with the resulting values depicted in blue in figure 6.7.

The NanoDrop technique is a widely used method for measuring the concentration of nucleic acids, including oligonucleotides, in a sample.[39] The NanoDrop utilizes UV-Vis spectrophotometry to quantify nucleic acid concentrations. By measuring the extent of UV-Vis absorption by nucleic acids, the concentration of nucleic acids in the sample can be determined. Among its advantages, NanoDrop technique requires only a small sample volume (1-2 μL) for the measurement.

The analysed samples were isolated with concentrations ranging from 17.2 to 103.6 μM. The obtaining of the pure DNA-conjugates with concentrations in the micromolar range validates this strategy as adequate for the synthesis of DECL.

However, compounds **20** and **21** could not be isolated, as they were not detected after semi-preparative ion pair RP-HPLC, probably due to its low concentration in the sample. Throughout the synthetic sequence of compounds **20**, **21**, and **22** (which was isolated with the lowest concentration) not all the reactions were driven to completion. Consequently, this led to a mixture different DNA-conjugates. Upon subjecting this mixture to RCM furnished the deisred product (identified by MS analysis of the reaction crude) was formed. However, its concentration was insufficient for purification and isolation.

These results demonstrated that RCM on CPG-coupled DNA is a feasible strategy for synthesizing a DNA-encoded macrocyclic library. Compounds **23**, **25** and **28** serve as examples of DNA-conjugates that could undergo an extra *split-and-pool* cycle in a hypothetic DECL synthesis, as these compounds contain a protected amine functionality that can be synthetically modified.

[39] Desjardins, P.; Conklin, D. *J. Vis. Exp.* **2010**, *22*, e2565.

However, to fully understand the reach and reliability of the transformations presented, further investigation is needed. It would be desirable to present a broad substrate scope including different functional groups.

Improving the quality of HPLC chromatograms is also desirable, possibly achieved by addressing the extraction of ruthenium in the reaction work-up. Additionally, a method to determine the conversion of the RCM reaction needs to be applied. Although the provided data suggest the feasibility of synthesizing a DNA-encoded library, calculating the average conversion of RCM on CPG-coupled DNA would provide context regarding the effectiveness of this strategy compared to previously reported procedures for RCM on-DNA.

CHAPTER VII

General Conclusions

UNIVERSITAT ROVIRA I VIRGILI
TARGETING DES1: SYNTHESES OF CERAMIDE ANALOGUES WITH A RIGID SCAFFOLD, INHIBITORY ASSAYS, AND AF2-ASSISTED STRUCTURAL INSIGHTS REVEAL PR280 AS A POTENT INHIBITOR
Pablo Rivero Prieto

7.1 General conclusions

A set of ceramide analogueues, incorporating a 1,4-disubstituted triazole, 1,5- disubstituted triazole, 2,5- disubstituted furan, cyclopropenone and 1,2-thiole-3-one ring system as rigid spacers between the polar headgroup and the alkyl tail of the sphingolipid structure, was successfully synthetized (Figure 7.1).

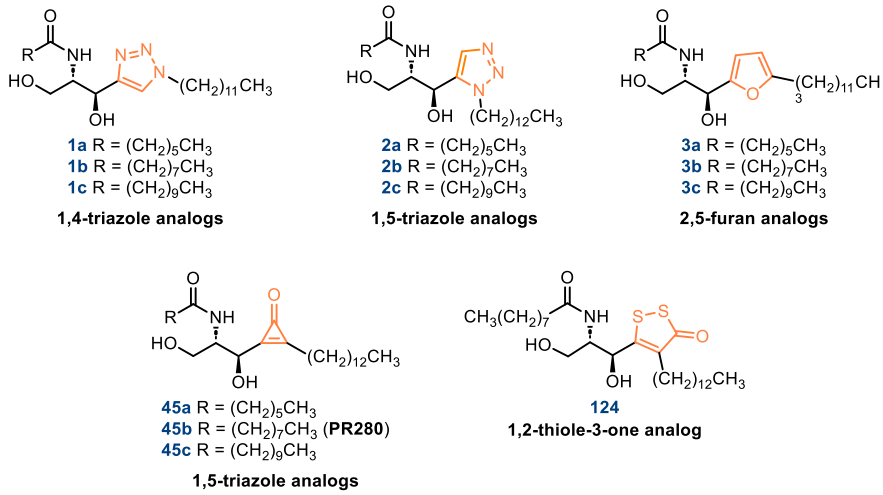

Figure 7.1. Synthetized ceramide analogues containing different rigid scaffolds.

- Ceramide analogueues containing 1,4- and 1,5-disubstituted 1,2,3-triazoles as the central core (**1a-c** and **2a-c**) were effectively obtained through 4-step syntheses with yields ranging from 27 to 30 %. The *one-pot* ethynylation of (*S*)-Garner's aldehyde with ethynyltrimethylsilane and subsequent catalytic desylilation provided a robust methodology for the generation of the corresponding propargylic alcohol as a unique diastereomer and in a good yield. The CuAAC and the RuAAC reactions proved to be appropriate methodologies for the synthesis of the 1,4- and 1,5-disubstituted triazole rings, respectively.
- Ceramide analogueues containing a 2,5-disubstituted furan ring as central core (**3a-c**) were successfully synthesized through a 5-step synthesis

with total yields ranging from 47 to 57 %. The stereoselective addition of 2-dodecylfuran to (*S*)-Garner's aldehyde allowed the effective incorporation of the furan ring in the sphingolipid-like structure. The deprotection of *tert*-butyloxycarbonyl and isopropylidene protecting groups presented a great challenge in the presence of the furan ring; in this regard, the use of TMSOTf proved to be a better alternative compared to commonly employed methodologies.

- Ceramide analogueues incorporating a cyclopropenone ring as central core (**45a-c**) were successfully synthetized through a 6-step synthesis with total yields ranging from 26 to 29 %. Difluorocyclopropenation with Ruppert-Prakash reagent and subsequent hydrolysis provided a good strategy for the gram-scale synthesis of tridecylcyclopropenone. The tridecylcyclopropenone acetal addition to (*S*)-Garner's aldehyde under kinetic control allowed the efficient synthesis of the sphingolipid structure incorporating the cyclopropenone moiety.
- Ceramide analogueue with 1,2-thiole-3-one moiety as central core (**124**) was successfully synthetized via [3+2] cycloaddition of cyclopropenone ceramide analogueue **49b** with elemental sulphur.

In the context of a collaboration with Prof. Gemma Fabriàs and Dr. Josefina Casas (RUBAM, Department of Biological Chemistry, IQAC), **the synthetized ceramide analogueues were evaluated as Des1 inhibitors in intact T98 cells and in T98 cell lysates**.

- Ceramide analogueues incorporating a five-member ring as rigid spacer, **1a-c**, **2a-c**, **3a-c** and **124**, showed moderate to low inhibition of Des1 activity when evaluated in intact cells, but no significant inhibition was observed in cell lysates. These results suggest that these ceramide analogues do not inhibit the enzyme's activity by a direct interaction. Based on these results, it was concluded that 5-member rings are not good surrogates of ceramide double bond in the design of ceramide analogues as Des1 inhibitors.

- In contrast, cyclopropenone ceramide analogue **PR280** exhibited a strong inhibition in both intact T98 cells and in T98 cell lysates, suggesting a direct interaction with the enzyme active site as the cause of inhibition. The Des1 inhibition induced by **PR280** is dose-dependent with an IC_{50} value of 0.7 μM; which is lower than the values showed for the reference inhibitors **GT11** (20 μM) and **XM462** (8.2 μM) evaluated in rat liver microsomes.

Working in collaboration with Xavier Barril (ICREA Research Professor, University of Barcelona) **the Des1 structure predicted by AlphaFold2 was used to construct a complete Fe_2O_2-Des1 system**, in which the Fe_2O_2 species that is involved in the catalytic activity of the enzyme was incorporated to the 3D structure. **To the best of our knowledge, this represents the first reported complete 3D model of Des1**.

- Docking calculations of Des1 inhibitors **GT11**, **XM462** and **PR280** with Fe_2O_2-Des1 system revealed four common molecular events:
    a) A folded conformation of the ligand hydrophobic chains in the Des1 active site.
    b) Close proximity of positions 4 or 5 of ceramide analogueues to the Fe_2O_2 cluster.
    c) An OH-3 hydrogen bond with one of the oxygen atoms of the dioxo-diiron specie.
    d) Involvement of the primary hydroxyl group in a hydrogen bond interaction with a residue of the enzyme.
- Conversely, in the docking calculations with ceramide analogueues containing 5-member rings it was observed that the bulkiness of the ring causes a distortion of the binding mode of the ligand in the active site. This provoked the loss of favourable ligand-enzyme interactions observed for **GT11**, **XM462** and **PR280**. In conclusion, the incorporation of the triazole, furan or 1,2-thiole-3-one moieties did not show any beneficial effect in the design of new Des1 inhibitors.
- A correlation between docking observations and biological results was maintained in all the cases evaluated in this thesis. Thus, it was concluded

that the interactions observed in the docking calculations of Des1 inhibitors **GT11**, **XM462** and **PR280** are necessary for the inhibition of the enzyme. When these interactions are not observed in the docking of ceramide analogues, the compound results inactive as Des1 inhibitor, as is the case of **1a-c**, **2a-c**, **3a-c** and **124**.

- The present study suggests an inhibition mechanism for ceramide analogues **GT11** and **PR280** involving specific and strong non-covalent interactions of the ligand with polar residues and the prosthetic group located at the active site. In this context, the absence of cysteine residues in the active site of Des1 structure predicted by AF2 rules out the previously proposed inhibition mechanism for **GT11**, which involve nucleophilic attack of a cysteine residue in the active site. Consequently, this proposed mechanism can also be dismissed for **PR280**. Furthermore, the chemical stability of PR280 towards thiols was demonstrated.

The project developed in the Brunschweiger group at Dortmund Technical University, as part of an international research stay, concerned **the development of solid-supported on-DNA RCM**.

- It was concluded that the strategy designed for the RCM on controlled pore glass (CPG) solid phase coupled DNA is a feasible approach for synthesizing a DNA-encoded macrocyclic library.
- This approach was succsesfully applied to a collection of 9 DNA-CPG diene conjugates, furnishing the desired cyclized products. Seven of the nine DNA-CPG cyclic conjugates could be purified and isolated, demonstrating the feasibility of the strategy in DNA-encoded chemical library (DECL) synthesis. However, further development of the methodology is desirable to understand its reach and reliability.

CHAPTER VIII

Experimental section

UNIVERSITAT ROVIRA I VIRGILI
TARGETING DES1: SYNTHESES OF CERAMIDE ANALOGUES WITH A RIGID SCAFFOLD, INHIBITORY ASSAYS, AND AF2-ASSISTED STRUCTURAL INSIGHTS REVEAL PR280 AS A POTENT INHIBITOR
Pablo Rivero Prieto

SECTION 1: Targeting Des1: Syntheses of ceramide analogues with a rigid scaffold, inhibitory assays, and AF2-Assisted structural insights reveal PR280 as a potent inhibitor

8.1 General considerations

Proton (1H NMR), carbon (13C NMR) and fluorine (19F NMR) nuclear magnetic resonance spectra were recorded on a Varian Mercury spectrometer or a Bruker Avance Ultrashield (400 MHz for 1H, 100.6 MHz for 13C and 376.5 MHz for 19F). Spectra were fully assigned using COSY, HSQC, HMBC and NOESY. All chemical shifts are quoted on the δ scale in ppm using the residual solvent as internal standard (1H NMR: CDCl3 = 7.26 and 13C NMR: CDCl3 = 77.00). The coupling constants (*J*) are described in Hz using the following abbreviations: s = singlet, d = doublet, t = triplet, q = quadruplet, p = quintuplet, m = multiplet, dd = doublet of doublets, dt = doublet of triplets, td = triplet of doublets, ap = apparent, br = broad.

Infrared (IR) spectra were recorded on a Jasco FT/IR-600 Plus ATR Specac Golden Gate spectrophotometer. Absorption maxima (νmax) are reported in wavenumbers (cm-1).

Optical rotations were measured on a Perkin Elmer 241 polarimeter with a path length of 1.0 dm and are reported with implied units of 10-1 deg cm2 g-1. Concentrations (c) are given in g/100 mL.

High resolution mass spectra (HRMS) were recorded on an Agilent 1100 Series LC/MSD mass spectrometer with electrospray ionization (ESI) by the Servei de Recursos Científics (URV). Nominal and exact m/z values are reported in Daltons.

Thin layer chromatography (TLC) was carried out using commercial aluminum backed sheets coated with 60F254 silica gel. Visualization of the silica plates was achieved using a UV lamp (max = 254 nm) and, *p*-anisaldehyde/EtOH/H_2SO_4 or $KMnO_4$/Na_2CO_3/H_2O as developer as indicated.

Flash column chromatography was carried out using silica gel 60 Å (230-400 mesh). Mobile phases are reported in relative composition (e.g. 1:1

EtOAc/hexane v/v). All solvents were used as supplied (Analytical, synthesis or HPLC grade), without prior purification.

All reagents were used as received from commercial suppliers. All reactions sensitive to air and/or moisture were carried out in anhydrous conditions: performing vacuum-argon cycles in the flasks to be used, previously dried with a heating gun under vacuum, as well as transferring the reagents and solvents with cannulas or syringes previously purged with argon. Drying of organic solvents was achieved by treatment with activated 3 Å molecular sieves.[1] Molecular sieves were previously activated by heating at 240 ˚C under vacuum for 24 h. The procedures described below are the ones that performed with the highest yield.

8.2 Synthetic procedures and compound characterization

Note: although the name of products follows the IUPAC criteria, for clarity and comparative purpose, the numbering of protons and carbons in the NMR data is consistent with that corresponding to the sphingolipid numbering, specified in the drawings of the corresponding structures.

(*S*)-*tert*-butyl 4-((*R*)-1-hydroxyprop-2-yn-1-yl)-2,2-dimethyloxazolidine-3-carboxylate (14)

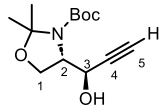

Ethynyltrimethylsilane, (0.25 mL, 1.77 mmol) was dissolved in dry THF (8.4 mL). The resulting solution was cooled down to -78 ºC and BuLi solution (2.5 M in hexanes, 0.7 mL, 1.75 mmol) was added dropwise. The resulting mixture was stirred for 1 h at -78 ºC. Then, HMPA (0.38 mL, 2.18 mmol) was added and the mixture was stirred for another additional hour. After this time, **(*S*)-Garner's aldehyde**, (252.1 mg, 1.10 mmol) dissolved in dry THF (1

[1] Bradley, D.; Williams, G.; Lawton, M. *J. Org. Chem.* **2010**, *75*, 8351-8354.

mL) was added. The mixture was warmed up to -55 ºC and stirred at this temperature overnight (18 h.). After this time, TBAF solution (1 M in THF, 0.12 mL, 0.12 mmol) was added and the resulting mixture was stirred for 5 additional hours at -55 ºC.

Afterwards, the reaction mixture was neutralized with NH_4Cl aqueous solution. After dilution with brine both phases were separated, and the aqueous phase was extracted with Et_2O. The combined organic extracts were dried over anhydrous $MgSO_4$ and concentrated under vacuum to give a yellowish oily residue. The residue was purified by flash column chromatography on silica gel (hexane/ethyl acetate, 8:2) and finally a yellow oil was obtained, which was identified as the desired terminal alkyne **14** (244.2 mg, 0.96 mmol, 87 % yield).

R_f = 0.33 (hexane/ethyl acetate, 8:2); α_D^{25} -54.7 (c 0.8, $CHCl_3$); **^{1}H NMR** (400 MHz, $CDCl_3$) δ in ppm: 5.05 (d, $J_{OH,3}$ = 8.1 Hz ,1H, OH), 4.51 (d, $J_{3,OH}$ = 8.1 Hz, 1H, H-3), 4.19-4.16 (m, 1H, H-2), 4.10 (t ap, *J*= 8.3 Hz, 1H, H-1), 3.91-3.88 (m, 1H, H-1'), 2.43 (s, 1H, H-5), 1.59 (s, 3H, isopropylidene), 1.50 (s, 3H, isopropylidene), 1.49 (s, 9H, *tert*-butyl); **^{13}C NMR** (100.6 MHz, $CDCl_3$) δ in ppm: 154.5 (Boc carbonyl), 95.2 (isopropylidene quaternary C), 82.1 (C-4), 81.7 (Boc quaternary C), 74.2 (C-5), 65.2 (C-1), 64.4 (C-3), 62.7 (C-2), 28.5 (Boc Me groups), 26.0 (isopropylidene Me groups), 25.4 (isopropylidene Me groups); **HRMS** (TOF ES+) for $[M+Na]^+$ $C_{13}H_{21}NNaO_4^+$ (m/z): calculated: 278.1363 found: 278.1367. **FT-IR (ATR)** ν in cm^{-1}: 3.438, 3.310, 3.256, 2.978, 2.930, 2.116, 1.684, 1.389, 1.365, 1.258, 1.170, 1.067, 1.046, 849, 770, 657, 554 cm^{-1}.

***Tert*-butyl (4*S*,1'*R*)-2,2-dimethyl-4-[1'-hydroxy-3'-(trimethylsilyl)-2'-propynyl]oxazolidine-3-carboxylate (31).**

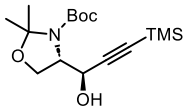

Ethynyltrimethylsilane, (0.25 mL, 1.77 mmol) was dissolved in dry THF (8.4 mL). The resulting solution was cooled down to -78 ºC and BuLi solution (2.5 M in hexanes, 0.7 mL, 1.75 mmol) was added dropwise. The resulting mixture was stirred for 1 h at -78 ºC. Then, HMPA (0.38 mL, 2.18 mmol) was added and the mixture was stirred for another additional hour. After this time, **(*S*)-Garner's aldehyde**, (250.1 mg, 1.09 mmol) dissolved in dry THF (1 mL) was added. The mixture was warmed up to -55 ºC and stirred at this temperature overnight (18 h.). Afterwards, the reaction mixture was neutralized with NH_4Cl aqueous solution. After dilution with brine both phases were separated, and the aqueous phase was extracted with Et_2O. The combined organic extracts were dried over anhydrous $MgSO_4$ and concentrated under vacuum to give a yellowish oily residue. The residue was purified by flash column chromatography on silica gel (hexane/ethyl acetate, from 9:1 to 8:2), to yield propargylic alcohol **31** (646 mg, 80 % yield, 98 % conversion) as a colourless oil.

R_f = 0.54 (hexane/ethyl acetate, 8:2); $\boldsymbol{\alpha_D^{25}}$ -29.7 (c 1.0, $CHCl_3$); **^{1}H NMR (400 MHz, $CDCl_3$)** δ in ppm 5.37 (d, $J_{OH,3}$ = 9.1 Hz, 1H, OH), 4.45 (d, $J_{3,OH}$ = 9.1 Hz, 1H, H-3), 4.17-4.11 (m, 1H, H-2), 4.11-4.06 (m, 1H, H-1), 3.87-3.81 (m, 1H, H-1'), 1.58 (s, 3H, isopropylidene), 1.51 (s, 3H, isopropylidene), 1.50 (s, 9H, Boc), 0.15 (s, 9H, $SiMe_3$). **^{13}C NMR (100 MHz, $CDCl_3$)** δ in ppm 154.5 (Boc carbonyl), 103.4 (C-4), 95.2 (isopropylidene quaternary C), 90.7 (C-5), 81.6 (Boc quaternary C), 65.3 (C-1), 64.6 (C-3), 63.0 (C-2), 28.5 (Boc Me groups), 25.9 (isopropylidene Me group), 25.8 (isopropylidene Me group), -0.06 ($SiMe_3$). **HRMS (ESI-TOF):** $[M+Na]^+$ *m*/*z* calculated for $C_{16}H_{29}NO_4SiNa$: 350.1764; found: 350.1767.

1-Azidododecane (37)[2]

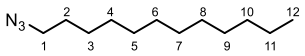

1-bromododecane (3.450 g, 13.84 mmol) and sodium azide (2.726 g, 41.94 mmol) were dissolved in dry DMF (42 mL). The resulting mixture was heated to 100 ºC and stirred at this temperature overnight.

After this time, the reaction mixture was cooled down to room temperature and diluted with Et_2O. Then, the organic solution was washed with brine to extract the DMF present in the reaction mixture. The organic phase was then dried over anhydrous $MgSO_4$ and concentrated under vacuum to give a yellowish oily residue. The residue was purified by flash column chromatography on silica gel (hexane) obtaining 1-azidotridecane, **37**, as a colourless liquid (2.0267g, 13.29 mmol, 96%).

R_f = 0.52 (100 % hexane); **^{1}H NMR (400 MHz, $CDCl_3$)** δ in ppm: 3.25 (t, $J_{1,2}$ = 7.0 Hz, 2H, H-1), 1.63-1.56 (m, 2H, H-2), 1.38-1.26 (m, 18H, from H-3 to H-11), 0.88 (t, $J_{12,11}$ = 6.8 Hz, 3H, H-12). **^{13}C NMR (100 MHz, $CDCl_3$)** δ in ppm: 51.6 (C-1), 32.1 (CH_2), 29.78 (2 CH_2), 29.77 (CH_2), 29.69 (CH_2), 29.6 (CH_2), 29.5 (CH_2), 29.3 (CH_2), 29.0 (C-2), 26.9 (C-3), 22.8 (C-11), 14.3 (C-12).

***tert*-butyl (*S*)-4-((*S*)-(1-dodecyl-1H-1,2,3-triazol-4-yl)(hydroxy)methyl)-2,2-dimethyloxazolidine-3-carboxylate (12)**

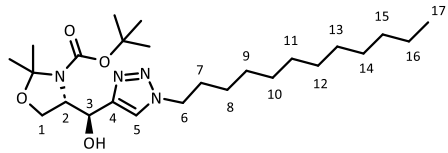

1-Azidododecane, **37**, (378.1 mg, 1.79 mmol) and terminal alkyne **14** (398.5 mg, 1.56 mmol) were dissolved in dry CH_2Cl_2 (8.5 mL) and stirred at room temperature. Then, a solution of $CuSO_4 \cdot 5H_2O$ (21.3 mg, 0.086 mmol) in

[2] Full characterization: Lindner, H.; Amberg, W. M.; Carreira, E. M. *J. Am. Chem. Soc.* **2023**, *145*, 22347-22353.

distilled H_2O (1.5 mL) followed by a solution of sodium ascorbate (31.6 mg, 0.16 mmol) in distilled H_2O (1.5 mL) were added dropwise. The resulting mixture was stirred at room temperature for 48 h.

After this time, the reaction mixture was diluted with brine, both phases were separated and the aqueous one was extracted with CH_2Cl_2. The combined organic extracts were dried over anhydrous $MgSO_4$, filtered, and concentrated under reduced pressure. The reaction crude was then purified by flash column chromatography on silica gel (hexane/ethyl acetate, from 3:1 to 3:2), to yield the desired product **12** (714.6 mg, 1.53 mmol, 98 %) as a colourless oil.

R_f = 0.33 (hexane/ethyl acetate, 6:4); α_D^{25} -27.6 (c 0.6, $CHCl_3$); Spectroscopic data of the mixture of both rotamers (a and b): **^{1}H NMR (400 MHz, CD_3OD)** δ in ppm: 7.87 (s, 1H, H-5a), 7.85 (s, 1H, H-5b), 5.10 (d, $J_{3a\text{-}2a}$ = 3.1 Hz, 1H, H-3a), 5.04 (d, $J_{3b\text{-}2b}$ = 4.3 Hz, 1H, H-3b), 4.40-4.35 (m, 4H, H-6), 4.26-4.23 (m, 2H, H-2), 4.12-4.04 (m, 2H, H-1), 3.99-3.89 (m, 2H, H-1'), 1.92-1.89 (m, 4H, H-7), 1.65 (s, 3H, H_a isopropylidene), 1.56 (s, 3H, H_b isopropylidene), 1.50 (s, 6H, isopropylidene), 1.43-1.34 (m, 18H, Boc), 1.34-1.26 (m, 36H, from H-8 to H-16), 0.90 (t, $J_{17\text{-}16}$ = 6.8 Hz, 6H, H-17). **^{13}C NMR (100 MHz, CD_3OD)** δ in ppm: 154.3 and 153.7 (Boc carbonyl), 150.8 and 150.5 (C-4), 124.0 and 123.8 (C-5), 95.8 and 95.4 (isopropylidene quaternary C), 81.7 and 81.3 (Boc quaternary C), 67.6 and 67.5 (C-3), 65.3 and 65.1 (C-1), 63.0 and 62.8 (C-2), 51.3 (C-6), 33.1 (CH_2), 31.4 (C-7) 30.77 (CH_2), 30.76 (CH_2), 30.67 (CH_2), 30.6 (CH_2), 30.5 (CH_2), 30.2 (CH_2), 28.6 (Boc Me groups), 27.5 (CH_2), 27.3 and 26.5 (isopropylidene Me group), 25.0 and 23.8 (isopropylidene Me group), 23.6 (CH_2), 14.5 (C-17); **HRMS** (TOF ES+) for $[M+Na]^+$ $C_{25}H_{46}N_4O_4Na^+$(m/z): calculated: 489.3417 found: 489.3416. **FT-IR (ATR)** ν in cm^{-1}: 3419, 3135, 2925, 2855, 1698, 1463, 1389, 1173, 1075, 853.

(1*S*,2*S*)-2-amino-1-(1-dodecyl-1H-1,2,3-triazol-4-yl)propane-1,3-diol (10)

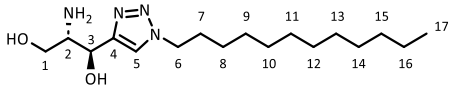

1,4-disubstituted triazole **12** (720.4 mg, 1.54 mmol) was dissolved in a H_2O/TFA (1:10, 15.4 mL) mixture and stirred at room temperature for 1h45min. After this time, the reaction mixture was slowly poured into a saturated aqueous $NaHCO_3$ (350 mL) solution at -10 ºC. Bubbling was observed due to neutralization of the excess of TFA.

The resulting suspension was extracted with AcOEt, the combined organic extracts were dried over anhydrous $MgSO_4$ and concentrated under vacuum to give a white oily residue. The residue was purified by flash column chromatography on silica gel (CH_2Cl_2/MeOH/Et_3N, 9:1:0.1) to yield the desired aminodiol **10** as a white solid (273.8 mg, 0.84 mmol, 54 % yield).

R_f = 0.12 (CH_2Cl_2/MeOH/Et_3N, 9:1:0.1); α_D^{25} +1.5 (c 1.0, MeOH); **^{1}H NMR (400 MHz, CD_3OD)** δ in ppm: 7.91 (s, 1H, H-5), 4.81 (d, $J_{3\text{-}2}$ = 6.2 Hz, 1H, H-3), 4.40 (t, $J_{6\text{-}7}$ = 7.1 Hz, 2H, H-6), 3.66 (dd, $J_{1\text{-}1'}$ = 10.9 Hz, $J_{1\text{-}2}$ = 4.3 Hz, 1H, H-1), 3.57 (dd, $J_{1'\text{-}1}$ = 10.9 Hz, $J_{1'\text{-}2}$ = 6.6 Hz, 1H, H-1'), 3.19-3.14 (m, 1H, H-2), 1.94-1.87 (m, 2H, H-7), 1.330-1.29 (m, 18H, from H-8 to H-16), 0.90 (t, $J_{17\text{-}16}$ = 6.8 Hz, 3H, H-17). **^{13}C NMR (100 MHz, CD_3OD)** δ in ppm: 150.2 (C-4), 124.1 (C-5), 69.1 (C-3), 63.8 (C-1), 58.1 (C-2), 51.4 (C-6), 33.1 (CH_2), 31.3 (C-7), 30.77 (CH_2), 30.76 (CH_2), 30.68 (CH_2), 30.6 (CH_2), 30.5 (CH_2), 30.1 (CH_2), 27.5 (CH_2), 23.8 (CH_2), 14.5 (C-17). **HRMS** (TOF ES+) for $[M+Na]^+$ $C_{17}H_{34}N_4O_2Na^+$ (m/z): calculated: 349.2579 found: 349.2577; **FT-IR (ATR)** ν in cm^{-1}: 3333, 3289, 3213, 3150, 2916, 2849, 1617, 1469, 1152, 1065, 827.

_N_-((1_S_,2_S_)-1-(1-dodecyl-1H-1,2,3-triazol-4-yl)-1,3-dihydroxypropan-2-yl)hexanamide (1a)

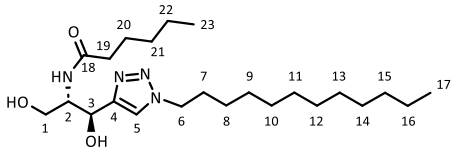

Hexanoic acid (17.3 μL, 0.14 mmol), EDC (26.5 mg, 0.14 mmol) and HOBt (18.9 mg, 0.14) were dissolved in dry CH_2Cl_2 (6.9 mL) and stirred at room temperature for 30 min. The resulting mixture was added over a solution of aminodiol **10** (30.0 mg, 0.092 mmol) in dry CH_2Cl_2 (7.5 mL) and stirred at r.t. overnight. After this time water was added, both phases were separated, and the aqueous phase was extracted with CH_2Cl_2. The combined organic extracts were dried over anhydrous $MgSO_4$ and concentrated under vacuum to give a yellow oily residue which was purified by flash column chromatography on silica gel (CH_2Cl_2/MeOH, 96:4). Finally, ceramide analogue **1a** was obtained as a colourless oil (24.2 mg, 0.056 mmol, 62% yield).

R_f = 0.18 (CH_2Cl_2/MeOH, 96:4); α_D^{25} -33.8 (c 0.4, $CHCl_3$); **^{1}H NMR (400 MHz, $CDCl_3$)** δ in ppm: 7.60 (s, 1H, H-5), 6.55 (d, $J_{NH\text{-}2}$ = 6.5 Hz, 1H, NH), 5.65 (bs, 1H, OH-3), 5.09 (d, $J_{3\text{-}2}$ = 2.0 Hz, 1H, H-3), 4.90 (bs, 1H, OH-1), 4.35-4.27 (m, 3H, H-2, H-6), 4.17 (dd, $J_{1\text{-}1'}$ = 12.0 Hz, $J_{1\text{-}2}$ = 1.6 Hz, 1H, H-1), 3.79 (dd, $J_{1'\text{-}1}$ = 12.0 Hz, $J_{1'\text{-}2}$ = 4.8 Hz, 1H, H-1'), 2.19-2.05 (m, 2H, H-19), 1.91-1.84 (m, 2H, H-7), 1.55-1.44 (m, 2H, H-20), 1.31-1.15 (m, 22H, from H-8 to H-16, H-21 and H-22), 0.87 (t, $J_{CH3\text{-}CH2}$ = 6.5 Hz, 3H, CH_3), 0.85 (t, $J_{CH3\text{-}CH2}$ = 7.3 Hz, 3H, CH_3); **^{13}C NMR (400 MHz, $CDCl_3$)** δ in ppm: 175.8 (C-18), 149.3 (C-4), 122.7 (C-5), 71.6 (C-3), 62.3 (C-1), 56.4 (C-2), 50.7 (C-6), 36.4 (C-19), 32.0 (CH_2), 31.3 (CH_2), 30.3 (C-7), 29.73 (2 CH_2), 29.66 (CH_2), 29.53 (CH_2), 29.46 (CH_2), 29.1 (CH_2), 26.6 (CH_2), 25.5 (C-20), 22.8 (CH_2), 22.4 (CH_2), 14.3 (CH_3), 14.0 (CH_3). **HRMS** (TOF ES+) for $[M+Na]^+$ $C_{23}H_{44}N_4O_3Na^+$ (m/z): calculated: 447.3311 found: 447.3309; **FT-IR (ATR)** ν in cm^{-1}: 3388, 3236, 3064, 2922, 2852, 1734, 1645, 1559, 1211, 1062, 774.

***N*-((1*S*,2*S*)-1-(1-dodecyl-1H-1,2,3-triazol-4-yl)-1,3-dihydroxypropan-2-yl)octanamide (1b)**

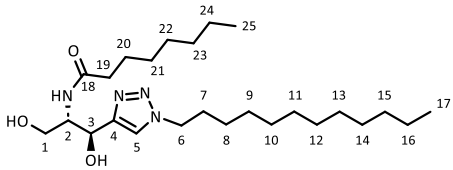

Octanoic acid (21.9 μL, 0.14 mmol), EDC (26.5 mg, 0.14 mmol) and HOBt (18.9 mg, 0.14 mmol) were dissolved in dry CH_2Cl_2 (6.9 mL) and stirred at room temperature for 30 min. The resulting mixture was added over a solution of aminodiol **10** (30.0 mg, 0.092 mmol) in dry CH_2Cl_2 (7.5 mL) and stirred at r.t. overnight. After this time water was added, both phases were separated and the aqueous phase was extracted with CH_2Cl_2. The combined organic extracts were dried over anhydrous $MgSO_4$ and concentrated under vacuum to give a yellow oily residue which was purified by flash column chromatography on silica gel (CH_2Cl_2/MeOH, 96:4). Finally, ceramide analogue **1b** was obtained as a colourless oil (28.0 mg, 0.062 mmol, 67% yield).

R_f = 0.19 (CH_2Cl_2/MeOH, 96:4); α_D^{25} -4.6 (c 0.41, $CHCl_3$); **^{1}H NMR (400 MHz, $CDCl_3$)** δ in ppm: 7.59 (s, 1H, H-5), 6.53 (d, $J_{NH\text{-}2}$ = 6.4 Hz, 1H, NH), 5.63 (bs, 1H, OH-3), 5.08 (d, $J_{3\text{-}2}$ = 1.8 Hz, 1H, H-3), 4.35-4.27 (m, 3H, H-2, H-6), 4.17 (dd, $J_{1\text{-}1'}$ = 12.1 Hz, $J_{1\text{-}2}$ = 1.7 Hz, 1H, H-1), 3.79 (dd, $J_{1'\text{-}1}$ = 12.1 Hz, $J_{1'\text{-}2}$ = 5.0 Hz, 1H, H-1'), 2.19-2.05 (m, 2H, H-19), 1.92-1.84 (m, 2H, H-7), 1.53-1.45 (m, 2H, H-20), 1.30-1.22 (m, 26H, from H-8 to H-16 and from H-21 to H-24), 0.87 (t, $J_{CH3\text{-}CH2}$ = 6.8 Hz, 3H, CH_3), 0.86 (t, $J_{CH3\text{-}CH2}$ = 6.9 Hz, 3H, CH_3); **^{13}C NMR (400 MHz, $CDCl_3$)** δ in ppm: 175.9 (C-18), 149.3 (C-4), 122.7 (C-5), 71.8 (C-3), 62.4 (C-1), 56.5 (C-2), 50.8 (C-6), 36.5 (C-19), 32.0 (CH_2), 31.8 (CH_2), 30.3 (C-7), 29.8 (CH_2), 29.74 (CH_2), 29.67 (CH_2), 29.54 (CH_2), 29.47 (CH_2), 29.2 (CH_2), 29.13 (CH_2), 29.08 (CH_2), 26.6 (CH_2), 25.8 (C-20), 22.8 (CH_2), 22.7 (CH_2), 14.3 (CH_3), 14.2 (CH_3); **HRMS** (TOF ES+) for $[M+Na]^+$ $C_{25}H_{48}N_4O_3Na^+$ (m/z): calculated: 475.3624 found: 475.3620; **FT-IR (ATR)** ν in cm^{-1}: 3391, 3234, 3067, 2923, 2852, 1734, 1646, 1558, 1209, 1056, 773.

_N_-((1_S_,2_S_)-1-(1-dodecyl-1H-1,2,3-triazol-4-yl)-1,3-dihydroxypropan-2-yl)decanamide (1c)

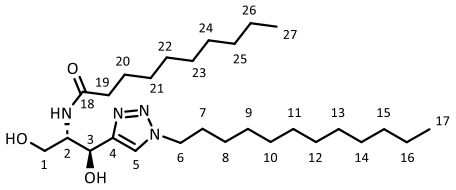

Decanoic acid (11.9 mg, 0.07 mmol), EDC (13.7 mg, 0.07 mmol) and HOBt (9.9 mg, 0.07 mmol) were dissolved in dry CH_2Cl_2 (3.5 mL) and stirred at room temperature for 30 min. The resulting mixture was added over a solution of aminodiol **10** (15.0 mg, 0.046 mmol) in dry CH_2Cl_2 (1.6 mL) and stirred at r.t. overnight. After this time water was added, both phases were separated, and the aqueous phase was extracted with CH_2Cl_2. The combined organic extracts were dried over anhydrous $MgSO_4$ and concentrated under vacuum to give a yellow oily residue which was purified by flash column chromatography on silica gel (CH_2Cl_2/MeOH, 96:4). Finally, ceramide analogue **1c** was obtained as a white solid (14.1 mg, 0.029 mmol, 63% yield).

R_f = 0.28 (CH_2Cl_2/MeOH, 96:4); α_D^{25} -20.8 (c 0.75, $CHCl_3$); **^{1}H NMR (400 MHz, $CDCl_3$)** δ in ppm: 7.59 (s, 1H, H-5), 6.51 (d, $J_{NH\text{-}2}$ = 6.2 Hz, 1H, NH), 5.08 (d, $J_{3\text{-}2}$ = 1.6 Hz, 1H, H-3), 4.37-4.26 (m, 3H, H-2, H-6), 4.18 (dd, $J_{1\text{-}1'}$ = 12.1 Hz, $J_{1\text{-}2}$ = 1.5 Hz, 1H, H-1), 3.80 (dd, $J_{1'\text{-}1}$ = 12.1 Hz, $J_{1'\text{-}2}$ = 5.1 Hz, 1H, H-1'), 2.19-2.05 (m, 2H, H-19), 1.92-1.85 (m, 2H, H-7), 1.53-1.45 (m, 2H, H-20), 1.31-1.17 (m, 30H, from H-8 to H-16 and from H-21 to H-26), 0.87 (t, $J_{CH3\text{-}CH2}$ = 6.7 Hz, 6H, H-17 and H-27); **^{13}C NMR (400 MHz, $CDCl_3$)** δ in ppm: 176.0 (C-18), 149.4 (C-4), 122.7 (C-5), 72.1 (C-3), 62.4 (C-1), 56.6 (C-2), 50.8 (C-6), 36.5 (C-19), 32.1 (CH_2), 32.0 (CH_2), 30.3 (C-7), 29.9 (CH_2), 29.8 (CH_2), 29.7 (CH_2), 29.58 (CH_2), 29.55 (CH_2), 29.48 (CH_2), 29.44 (CH_2), 29.43 (CH_2), 29.2 (CH_2), 29.1 (CH_2), 26.6 (CH_2), 25.9 (C-20), 22.83 (CH_2), 22.82 (CH_2), 14.3 (2 CH_3); **HRMS** (TOF ES+) for $[M+H]^+$ $C_{27}H_{52}N_4O_3Na^+$ (m/z): calculated: 503.3937 found: 503.3961; **FT-IR (ATR)** ν in cm^{-1}: 3409, 3236, 3056, 2921, 2850, 1731, 1645, 1569, 1210, 1057, 774.

1-Azidotridecane (38)[3]

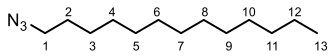

1-Bromotridecane, **36**, (2.5 mL, 9.78mmol) and sodium azide (1.926 g, 29.62mmol) were dissolved in dry DMF (30 mL). The resulting mixture was heated to 100 ºC and stirred at this temperature overnight.

After this time, the reaction mixture was cooled down to room temperature and diluted with Et_2O. Then, the organic solution was washed with brine to extract the DMF present in the reaction mixture. The organic phase was then dried over anhydrous $MgSO_4$ and concentrated under vacuum to give a yellowish oily residue. The residue was purified by flash column chromatography on silica gel (hexane) obtaining 1-azidodotridecane, **38**, as a colorless liquid (2.2978g, 8.99 mmol, 92%).

R_f = 0.26 (100 % hexane); **^{1}H NMR** (400 MHz, $CDCl_3$) δ in ppm: 3.25 (t, J_{1-2} = 7.0 Hz, 2H, H-1), 1.63-1.56 (m, 2H, H-2), 1.40-1.21 (m, 20 H, H-3 to H-12), 0.88 (t, *J*= 6.8 Hz, 3H, H-13) **^{13}C NMR** (100 MHz, $CDCl_3$) δ in ppm: 51.8 (C-1), 32.2 (CH_2), 30.0 (2 CH_2), 29.9 (CH_2), 29.9 (CH_2), 29.8 (CH_2), 29.8 (CH_2), 29.6 (C-2), 29.5 (C-3), 29.1(CH_2), 27.0 (CH_2), 23.0 (CH_2), 14.4 (C-13).

***tert*-butyl (*S*)-4-((*S*)-hydroxy(1-tridecyl-1H-1,2,3-triazol-5-yl)methyl)-2,2-dimethyloxazolidine-3-carboxylate (13)**

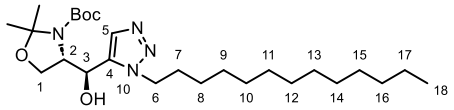

Cp*RuCl(COD) (29.0 mg, 0.076 mmol) was dissolved in dry and previously degassed toluene (9 mL, toluene was degassed for 1 h with nitrogen purge). A solution of terminal alkyne **14** (442.1 mg, 1.73 mmol) and 1-azidotridecane, **38**, (548.8 mg, 2.43 mmol) in dry and previously degassed toluene (5.6 mL) was added, the mixture was stirred at room temperature

[3] Full characterization: Liu, C.; Wang, X.; Li, Z.; Cui, L.; Li, C. *J. Am. Chem. Soc.* **2015**, *137*, 9820-9823.

overnight in which time the total consumption of the starting material was observed by TLC analysis.

Then, the reaction mixture was filtered through a short path of Celite followed by the evaporation of the solvent under reduced pressure. The residue was purified by flash column chromatography on silica gel (hexane/ethyl acetate, 7:3) and finally the desired product was obtained in form of a white oil (570.4 mg, 1.19 mmol, 69 %).

R_f = 0.33 (hexane/ethyl acetate, 8:2); α_D^{25} -10.4 (c 1.0, $CHCl_3$); **^{1}H NMR** (400 MHz, $CDCl_3$) δ in ppm: 7.53 (s, 1H, H-5), 5.16 (s, 1H, H-3), 4.48-4.34 (m, 2H, H-6), 4.25 (m, 1H, H-2), 4.08-4.04 (m, 1H, H-1), 4.00 (dd, $J_{1\text{-}1'}$= 9.6, $J_{1\text{-}2'}$=6.5 Hz, 1H, H-1'), 1.99-1.91 (m, 2H, H-7), 1.49-1.43 (m, 15H, 5H-isopropyldiene and 9H-Boc), 1.35-1.24 (m, 20H, from H-8 to H-17), 0.87 (t, $J_{18\text{-}17}$ = 6.7 Hz, 3H, H-18); **^{13}C NMR** (100.6 MHz, CDCl3) δ in ppm: 153.6 (Boc carbonyl), 136.9 (C-4), 131.6 (C-5), 94.7 (isopropylidene quaternary C), 81.7 (Boc quaternary C), 66.4 (C-3), 63.9 (C-1), 61.2 (C-2), 49.4 (C-6), 32.1 (CH_2), 30.3 (C-7), 29.8 (CH_2), 29.8 (CH_2), 29.8 (CH_2), 29.7 (CH_2), 29.6 (CH_2), 29.5 (CH_2), 29.2 (CH_2), 28.4 (Boc Me groups), 26.9 (isopropylidene Me group), 26.8 (CH_2), 24.0 (isopropylidene Me group), 22.8 (CH_2), 14.3 (C-18); **HRMS** (TOF ES+) for $[M+H]^+$ $C_{26}H_{49}N_4O_4^+$ (m/z): calculated: 481.3748 found: 481.3751; **FT-IR (ATR)** ν in cm^{-1}: 3.226, 2.923, 2.852, 1.698, 1.458, 1.364, 1.252, 1.170, 1.099, 1.067, 1.051, 847, 768, 605, 566, 526.

(1*S*,2*S*)-2-amino-1-(1-tridecyl-1H-1,2,3-triazol-5-yl)propane-1,3-diol (11)

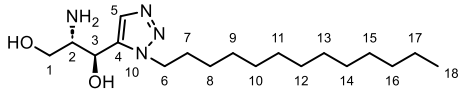

1,5-disubstituted triazole **13** (570.4 mg, 1.19 mmol) was dissolved in a H_2O/TFA (1:10, 12.2 mL) mixture and stirred at room temperature for 1h45min. After this time, the reaction mixture was slowly poured into a

saturated aqueous $NaHCO_3$ (250 mL) solution at -10 ºC. Bubbling was observed due to neutralization of the excess of TFA.

The resulting suspension was extracted with AcOEt, the combined organic extracts were dried over anhydrous $MgSO_4$ and concentrated under vacuum to give a white oily residue. The residue was purified by flash column chromatography on silica gel (CH_2Cl_2/MeOH/Et_3N, 9:1:0.1) and finally the desired aminodiol **11** was obtained as a white solid (294.1 mg, 0.86 mmol, 73 % yield).

R_f = 0.26 (CH_2Cl_2/MeOH/Et_3N, 9:1:0.1); α_D^{25} -4.0 (c 1.1, MeOH); **M.p.** 105-107 ºC; **^{1}H NMR** (400 MHz, $CDCl_3$) δ in ppm: 7.72 (s, 1H, H-5), 4.80 (d, $J_{3,2}$ = 7.3 Hz, 1H, H-3), 4.44 (m, 2H, H-6), 3.69 (d, $J_{1,2}$= 5.2 Hz, 2H, H-1), 3.16 (dt, $J_{6,7}$ = 7.3, $J_{2,1}$ = 5.2 Hz, 1H, H-2), 1.94 (m, 2H, H-7), 1.40-1.26 (m, 20H, from H-8 to H-17), 0.90 (t, $J_{18,17}$ = 6.7 Hz, H-18); **^{13}C NMR** δ in ppm: (100.6 MHz, $CDCl_3$) 139.3 (C-4), 133.1 (C-5), 66.0 (C-3), 62.8 (C-1), 57.5 (C-2), 49.8 (C-6), 33.1 (CH_2), 31.2 (C-7), 30.79 (CH_2), 30.76 (CH_2), 30.68(CH_2), 30.6 (CH_2), 30.5 (CH_2), 30.2 (CH_2), 27.7 (CH_2), 23.7 (CH_2), 14.44 (C-18), 8.46 (CH_2); **HRMS** (TOF ES+) for $[M+H]^+$ $C_{18}H_{37}N_4O_2^+$ (m/z): calculated: 341.2911 found: 341.2920; **FT-IR (ATR)** ν in cm^{-1}: 3.342, 3.276, 3.121, 2.954, 2.919, 2.848, 1.598, 1.468, 1.375, 1.303, 1.239, 1.123, 1.084, 1.032, 989, 956, 831, 721, 694, 619.

N-((1*S*,2*S*)-1,3-dihydroxy-1-(1-tridecyl-1H-1,2,3-triazol-5-yl)propan-2-yl)hexanamide (2a)

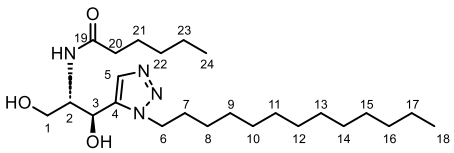

Hexanoic acid (62 μL, 0.50 mmol), EDC (93.9 mg, 0.49 mmol) and HOBt (66.0 mg, 0.49) were dissolved in dry CH_2Cl_2 (22 mL) and stirred at room temperature for 45 min. The resulting mixture was added over a solution of

aminodiol **11** (83.5 mg, 0.25 mmol) in dry CH_2Cl_2 (7.5 mL) and stirred at r.t. overnight.

After this time water was added, both phases were separated, and the aqueous phase was extracted with CH_2Cl_2. The combined organic extracts were dried over anhydrous $MgSO_4$ and concentrated under vacuum to give a yellow oily residue which was purified by flash column chromatography on silica gel (CH_2Cl_2/MeOH/NH_4OH, 97:3:1). Finally, ceramide **2a** analogue was obtained as a white solid (69.2 mg, 0.16 mmol, 64% yield).

R_f = 0.22 (CH_2Cl_2/MeOH/NH_4OH, 9:1:0.1); α_D^{25} +31,7 (c 1.1, CH_2Cl_2/MeOH (1:1)); **m.p.** 56-57 ºC; **^{1}H NMR** δ in ppm: (400 MHz, $CDCl_3$) **δ** 7.51 (s, 1H, H-5), 6.78 (d, $J_{NH,\,2}$ = 7.7 Hz, 1H, NH), 5.34 (d, $J_{OH\text{-}3}$ = 6.2 Hz, 1H, OH), 5.14-5.12 (m, 1H, H-3), 4.44-4.32 (m, 2H, H-6), 4.12-4.07 (m, 2H, H-2 and OH), 4.01 (d, $J_{1\text{-}1'}$ = 11.2 Hz, 1H, H-1), 3.69 (d, $J_{1'\text{-}1}$ = 11.2 Hz, 1H, H-1'), 2.20 (t, $J_{20\text{-}21}$ = 7.6 Hz, 2H, H-20), 1.93-1.86 (m, 2H, H-7), 1.59 (quint ap, *J* = 7.5 Hz, 2H, H-21), 1.34-1.24 (m, 24H, from H-8 to H-17 and from H-22 to H-23), 0.87 (*t*, J = 6.6 Hz, 6 H, H-18 and H-24); **^{13}C NMR** δ in ppm: (100.6 MHz, $CDCl_3$) 174.5 (C-19), 137.8 (C-4) , 132.0 (C-5), 66.6 (C-3), 61.4 (C-1), 53.8 (C-2), 49.1 (C-6), 36.7 (C-20), 32.1 (CH_2), 31.5 (CH_2), 30.4 (C-7), 29.82 ($2CH_2$), 29.79 (CH_2), 29.7 (CH_2), 29.6 (CH_2), 29.5 (CH_2), 29.3 (CH_2), 26.8 (CH_2), 25.4 (C-21), 22.8 (CH_2), 22.5 (CH_2), 14.3 (CH_3), 14.1 (CH_3); **HRMS** (TOF ES+) for $[M+Na]^+$ $C_{24}H_{46}N_4NaO_3$+ (m/z): calculated: 461.3462 found: 461.3465; **FT-IR (ATR)** ν in cm^{-1}: 3494, 3383, 3275, 3127, 2957, 2917, 2847, 1635, 1550, 1464, 1329, 1251, 1133, 1091, 1065, 1048, 878, 800, 756, 721, 634, 589, 527.

_N_-((1_S_,2_S_)-1,3-dihydroxy-1-(1-tridecyl-1H-1,2,3-triazol-5-yl)propan-2-yl)octanamide (2b)

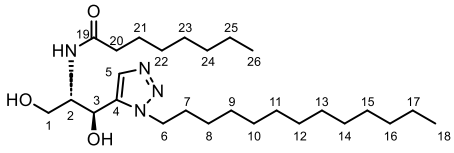

Octanoic acid (78 μL, 0.49 mmol), EDC (95.2 mg, 0.50 mmol) and HOBt (66.1 mg, 0.49 mmol) were dissolved in dry CH_2Cl_2 (22 mL) and stirred at room temperature for 45 min. The resulting mixture was added over a solution of aminodiol **11** (83.4 mg, 0.25 mmol) in dry CH_2Cl_2 (7.5 mL) and stirred at r.t. overnight.

After this time water was added, both phases were separated and the aqueous phase was extracted with CH_2Cl_2. The combined organic extracts were dried over anhydrous $MgSO_4$ and concentrated under vacuum to give a yellow oily residue which was purified by flash column chromatography on silica gel (CH_2Cl_2/MeOH/NH_4OH, 97:3:1). Finally, ceramide analogue **2b** was obtained as a white solid (80.0 mg, 0.17 mmol, 70% yield).

R_f = 0.23 (CH_2Cl_2/MeOH/NH_4OH, 9:1:0.1); α_D^{25} +24.7 (c 0.5, CH_2Cl_2/MeOH (1:1)); **m.p.** 67-68 ºC; **^{1}H NMR** δ in ppm: (400 MHz, $CDCl_3$) **δ** 7.50 (s, 1H, H-5), 6.74 (d, $J_{NH,2}$ = 7.7 Hz, 1H, NH), 5.23-5.22 (m, 1H, OH), 5.14-5.12 (m, 1H, H-3), 4.44-4.32 (m, 2H, H-6), 4.11-4.06 (m, 1H, H-2), 4.02-3.99 (m, 2H, H-1 and OH), 3.72-3.66 (m, 1H, H-1'), 2.21 (t, J_{20-21} = 7.7 Hz, 2H, H-20), 1.94-1.84 (m, 2H, H-7), 1.63-1.55 (m, 2H, H-21), 1.35-1.24 (m, 28H, from H-8 to H-17 and from H-22 to H-25), 0.87 (t, *J* = 6.6 Hz, 6H, H-18 and H-26); **^{13}C NMR** δ in ppm: (100.6 MHz, $CDCl_3$) 174.5 (C-19), 137.6 (C-4), 132.0 (C-5), 66.9 (C-3), 61.5 (C-1), 53.8 (C-2), 49.1 (C-6), 36.7 (C-20), 32.1 (CH_2), 31.8 (CH_2), 30.4 (C-7), 29.8 (CH_2), 29.8 ($2CH_3$), 29.7 (CH_2), 29.6 (CH_2), 29.5 (CH_2), 29.4 (CH_2), 29.3 (CH_2), 29.1 (CH_2), 26.8 (CH_2), 25.8 (C-21), 22.8 (CH_2), 22.8 (CH_2), 14.3 (CH_3), 14.2 (CH_3); **HRMS** (TOF ES+) for $[M+H]^+$ $C_{26}H_{51}N_4O_3$+ (m/z): calculated: 467.3956 found: 467.3961; **FT-IR (ATR)** ν in cm^{-1}: 3459, 3408, 3291, 3126, 3072, 2954, 2918, 2850, 1636, 1544, 1466, 1375, 1325, 1246, 1128, 1065, 1049, 1000, 869, 801, 758, 718, 680, 634, 549.

***N*-((1*S*,2*S*)-1,3-dihydroxy-1-(1-tridecyl-1H-1,2,3-triazol-5-yl)propan-2-yl)decanamide (2c)**

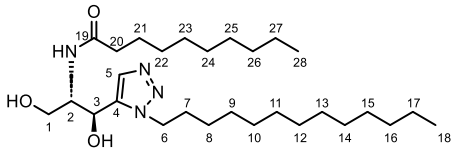

Decanoic acid (84.5 mg, 0.49 mmol), EDC (93.3 mg, 0.49 mmol) and HOBt (65.7 mg, 0.49 mmol) were dissolved in dry CH_2Cl_2 (22 mL) and stirred at room temperature for 45 min. The resulting mixture was added over a solution of aminodiol **11** (82.5 mg, 0.24 mmol) in dry CH_2Cl_2 (7.5 mL) and stirred at r.t. overnight.

After this time water was added, both phases were separated and the aqueous phase was extracted with CH_2Cl_2. The combined organic extracts were dried over anhydrous $MgSO_4$ and concentrated under vacuum to give a yellow oily residue which was purified by flash column chromatography on silica gel (CH_2Cl_2/MeOH/NH_4OH, 97:3:1). Finally, ceramide **2c** analogue was obtained as a white solid (86.3 mg, 0.17 mmol, 72% yield).

R_f = 0.27 (CH_2Cl_2/MeOH/NH_4OH, 9:1:0.1); α_D^{25} -10.3 (c 1.1, CH_2Cl_2/MeOH (1:1)); **m.p.** 79-80 ºC; **^{1}H NMR** (400 MHz, $CDCl_3$) δ in ppm: 7.57 (s, 1H, H-5), 6.54-6.52 (m, 1H, NH), 5.18 (d, $J_{3\text{-}2}$ = 4.0 Hz, 1H, H-3), 4.45-4.34 (m, 2H, H-6), 4.040 (bs, 1H, H-2), 4.035 (dd, $J_{1\text{-}1'}$ = 15.2 Hz, $J_{1\text{-}2}$ = 3.5 Hz, 1H, H-1), 3.72 (dd, $J_{1'\text{-}1}$ = 15.2, $J_{1'\text{-}2}$ = 3.5 Hz, 1H, H-1'), 2.24 (t, $J_{20\text{-}21}$ = 7.7 Hz, 2H, H-20), 1.92 (quint ap, $J_{7\text{-}6}$ = 7.2, $J_{7\text{-}8}$ = 7.2 Hz, 2H, H-7), 1.62 (quint ap, $J_{21\text{-}20}$ = 7.3, $J_{21\text{-}22}$ = 7.3, 2H, H-21), 1.33-1.25 (m, 32H, from H-8 to H-17 and from H-22 to H-27), 0.88 (t, J = 7.0 Hz, 6 H, H-18 and H-28); **^{13}C NMR** δ in ppm: (100.6 MHz, $CDCl_3$) 174.8 (C-19), 138.6 (C-4), 131.21 (C-5), 66.1 (C-3), 61.4 (C-1), 54.3 (C-2), 49.8 (C-6), 36.6 (C-20), 32.1 (CH_2), 32.0 (CH_2), 30.2 (C-7), 29.84 (CH_2), 29.80 ($2CH_2$), 29.75 (CH_2), 29.64 (CH_2), 29.61 (CH_2), 29.51 ($2CH_2$), 29.44 (CH_2), 29.41 (CH_2), 29.3 (CH_2), 26.8 (CH_2), 25.8 (C-21), 22.83 (CH_2), 22.81 (CH_2), 14.3 ($2CH_3$); **HRMS** (TOF ES+) for $[M+H]^+$ $C_{28}H_{55}N_4O_3^+$ (m/z): calculated: 495.4269 found: 495.4274;

FT-IR (ATR) ν in cm^{-1}: 3525, 3439, 3284, 3138, 2952, 2915, 2868, 2848, 1743, 1644, 1543, 1469, 1415, 1379, 1327, 1295, 1254, 1232, 1196, 1124, 1115, 1064, 1040, 1027, 865, 762, 718, 696, 614, 580, 526, 496.

2-dodecylfuran (17)

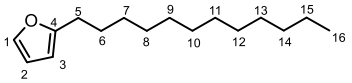

A solution of furan (0.91 mL, 12.5 mmol) in anhydrous THF (41.7 mL) was cooled down to -78 ºC. Then, butyllithium solution (2.5 M in hexanes, 4.7 mL, 11.8 mmol) was added dropwise and the resulting mixture was stirred at 0 ºC for 2h. After that time, the mixture was cooled down to -40 ºC and 1-bromododecae (2 mL, 8.3 mmol) dissolved in dry THF (2.3 mL) was added dropwise, the resulting mixture was stirred at room temperature overnight.

After this time, the reaction was quenched with the addition of saturated aqueous $NaHCO_3$, which caused the formation of two phases. Both phases were separated, the aqueous phase was diluted with saturated NaCl solution and extracted with AcOEt. The combined organic extracts were washed with saturated NaCl aqueous solution, dried over anhydrous Na_2SO_4 and concentrated under vacuum to give a yellowish oily residue. The residue was purified by flash column chromatography (dichloromethane) on silica gel and a yellow liquid was obtained, which was identified as the desired product 2-dodecylfuran (1.960 g, 8.34 mmol, 99%).

R_f = 0.77 (hexane/ethyl acetate, 8:2); **^{1}H NMR** (400 MHz, $CDCl_3$) **δ** 7.29 (dd, J_{1-2} = 1.85, J_{1-3} = 0.9 Hz, 1H, H-1), 6.27 (dd, J_{2-1} = 1.85, J_{2-3} = 3.1 Hz, 1H, H-2), 5.97 (m, 1H, H-3), 2.61 (t, J_{5-6} = 7.6 Hz, 2H, H-5), 1.66-1.61 (m, 2H, H-6), 1.35-1.26 (m, 18H, H-7 to H-15), 0.88 (t, J_{16-15} = 7 Hz, 3H, H-16). **^{13}C NMR** (100 MHz, CDCl3) δ in ppm: 156.8 (C-2), 140.7 (C-5), 110.2 (C-4), 104.6 (C-3), 32.1 (CH_2), 29.82 (CH_2), 29.79 (CH_2), 29.7 (CH_2), 29.52 (CH_2), 29.51 (CH_2), 29.3 (CH_2), 28.2 (CH_2), 28.1 (CH_2), 22.8 (CH_2), 14.3 (C-16); **HRMS** (TOF ES+) for $[M+H]^+$

$C_{16}H_{29}O^+$ (m/z): calculated: 237.2213 found: 237.2211; **FT-IR (ATR)** ν in cm^{-1}: 2953, 2922, 2852, 1597, 1507, 1465, 1146, 1007, 924, 885, 794, 723, 599 cm^{-1}.

***tert*-butyl (*S*)-4-((*S*)-(5-dodecylfuran-2-yl)(hydroxy)methyl)-2,2-dimethyloxazolidine-3-carboxylate (16)**

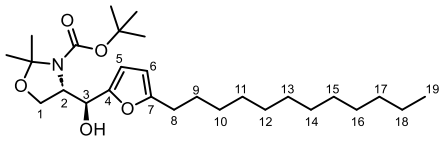

2-dodecylfuran, **17**, (412.4 mg, 1.59 mmol) was dissolved in anhydrous THF (8.3 mL). The resulting solution was cooled down to -78 ºC and BuLi solution (2.5 M in hexanes, 0.70 mL, 1.75 mmol) was added dropwise. After the addition, the mixture was warmed up to 0 ºC and stirred at this temperature. After 1 h dry HMPA (0.38 mL, 2.18 mmol) was added and the mixture was stirred an additional hour at 0 ºC. Afterwards, it was cooled down to -55 ºC and **(*S*)-Garner's aldehyde** (249.4 mg, 1.09 mmol) dissolved in dry THF (1 mL) was added. The resulting mixture was stirred at -55 ºC overnight. After this time NH_4Cl saturated aqueous solution was added, the two phases formed were separated and extractions of the aqueous phase with AcOEt were performed. The combined organic extracts were dried over anhydrous Na_2SO_4 and concentrated under vacuum to give a yellowish oily residue.

The residue was then dissolved in dry THF/MeOH solution (8 mL, 3:1). $NaBH_4$ (25.2 mg, 0.66 mmol) was added to the solution and the mixture was stirred at room temperature until the total consumption of the residual **(*S*)-Garner's aldehyde** was observed by TLC analysis. At this point, the mixture was diluted with aqueous NaCl saturated solution and extractions of the aqueous phase with AcOEt were performed. Finally, the combined organic extracts were dried over anhydrous Na_2SO_4 and concentrated under vacuum to give a yellowish oily residue. The residue was purified by flash column chromatography on silica gel (hexane/ethyl acetate, 8:2) and a yellow oil was

obtained, which was identified as a diastereomeric mixture of the desired product **16** (240. mg, 0.52 mmol, 60 % yield) in a 1:7 molar relation.

***R*f** = 0.31 (hexane/ethyl acetate, 8:2); Data shown for the major isomer (*trans*): **^{1}H NMR** (400 MHz, $CDCl_3$) δ in ppm: 6.15 (d, $J_{5\text{-}6}$ = 3.0 Hz, 1H, H-5), 5.91 (d, $J_{6\text{-}5}$ = 3.0 Hz, 1H, H-6), 4.89-4.85 (m, 1H, H-3), 4.64 (bs, 1H, OH), 4.35-4.32 (m, 1H, H-2), 4.07-4.05 (m, 2H, H-1), 2.56 (t, $J_{8\text{-}9}$ = 7.6 Hz, 2H, H-8), 1.66-1.47 (m, 17H, 2H-9 + 6H-isopropyldiene + 9H-*tert*-butyl), 1.34-1.26 (m, 18H, from H-9 to H-18), 0.88 (t, $J_{19\text{-}18}$ = 3.8 Hz, 3H, H-19); **^{13}C NMR** δ in ppm: 156.4 (C-7), 154.3 (Boc carbonyl), 151.9 (C-4), 107.9 (C-5), 105.3 (C-6), 94.7 (isopropylidene quaternary C), 81.3 (Boc quaternary C), 69.9 (C-3), 64.8 (C-1), 62.1 (C-2), 32.1 (CH_2), 29.9(CH_2), 29.82($2CH_2$), 29.79 ($2CH_3$), 29.7 (CH_2), 29.51 ($2CH_2$), 29.4 (CH_2), 28.5 ($3CH_3$), 28.2 (C-8), 22.8 ($2CH_2$), 14.3 (C-19); **HRMS** (TOF ES+) for $[2M+Na]^+$ $C_{54}H_{94}N_2NaO_{10}^+$ (m/z): calculated: 953.6801 found: 953.6798; **FT-IR (ATR)** ν in cm^{-1}: 3454, 2924, 2853, 1670, 1457, 1388, 1365, 1255, 1206, 1172, 1093, 1069, 1011, 949, 849, 781, 768, 721, 563, 524, 462.

(1*S*,2*S*)-2-amino-1-(5-dodecylfuran-2-yl)propane-1,3-diol (15)

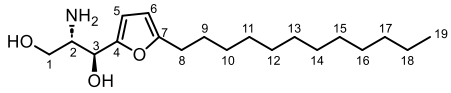

A diasteromeric mixture (1:7) of protected furan **17** (422.0 mg, 0.91 mmol) was dissolved in dry CH_2Cl_2 (9.1 mL), Et_3N (0.89 mL, 6.39 mmol) was added and the resulting mixture was stirred 20 minutes at room temperature. The mixture was cooled down to 0 ºC and TMSOTf (0.50 mL, 2.76 mmol) was added. The reaction mixture was stirred at 0 ºC for 3 h. After this time, the reaction was stopped with the addition of NH_4Cl saturated solution. Both phases were separated, the aqueous phase was extracted with CH_2Cl_2 and, afterwards, the combined organic extracts were washed up with $NaHCO_3$ saturated solution, dried over anhydrous $MgSO_4$ and concentrated under vacuum to give a yellow oily residue.

Without further purification, the previous crude was dissolved in anhydrous THF (9.1 mL), then, TBAF solution (1M in THF, 2.72 mL, 2.72 mmol) was added and the reaction mixture was stirred overnight at room temperature. After this time, the reaction was stopped with the addition of NH_4Cl saturated solution. Both phases were separated, the aqueous phase was extracted with AcOEt and the combined organic extracts were dried over anhydrous $MgSO_4$ and concentrated under vacuum to give a white oily residue which was purified by flash column chromatography on silica gel (CH_2Cl_2/MeOH/Et_3N, 95:5:1). Finally, a white solid was obtained, identified as a diasteromeric mixture (1:18) of the desired aminodiol (286.4 mg, 0.88 mmol, 97 %).

***R**f* = 0.26 (CH_2Cl_2/MeOH/NH_4OH, 9:1:0.1); Data shown for the major isomer (*trans*): **^{1}H NMR** (400 MHz, MeOD) δ in ppm: 6.23 (d, $J_{5\text{-}6}$ = 3.1, 1H, H-5), 5.99 (d, $J_{6\text{-}5}$ = 3.1 Hz, 1H, H-6), 4.52 (d, $J_{3\text{-}2}$ = 7.1 Hz, 1H, H-3), 3.72 (dd, $J_{1\text{-}1'}$ = 11.0, $J_{1\text{-}2}$ = 4.1 Hz, 1H, H-1), 3.59 (dd, $J_{1'\text{-}1}$ = 11.0, $J_{1'\text{-}2}$ = 6.5 Hz, 1H, H-1′), 3.12-3.08 (m, 1H, H-2), 2.61 (t, $J_{8\text{-}9}$ = 7.5 Hz, 2H, H-8), 1.67-1.60 (m, 2H, H-9), 1.34-1.27 (m, 18H, from H-10 to H-18), 0.90 (t, $J_{19\text{-}18}$ = 6.8 Hz, 3H, H-19); **^{13}C NMR** δ in ppm: (100.6 MHz, MeOD) 157.5 (C-4), 154.3 (C-7), 109.3 (C-5), 106.4 (C-6), 70.1 (C-3), 64.1 (C-1), 57.1 (C-2), 33.1 (CH_2), 30.81 (CH_2), 30.78 ($2CH_2$), 30.73 (CH_2), 30.5 ($2CH_2$), 30.3 (CH_2), 29.2 (C-9), 28.9 (C-8), 23.8 (CH_2), 14.47 (C-19); **HRMS** (TOF ES+) for $[M+Na]^+$ $C_{19}H_{35}NNaO_3^+$ (m/z): calculated: 348.2509 found: 348.2510; **FT-IR (ATR)** ν in cm^{-1}:3313, 2955, 2922, 2852, 1653, 1633, 1558, 1541, 1522, 1457, 1260, 1089, 1017, 798.

_N_-((1_S_,2_S_)-1-(5-dodecylfuran-2-yl)-1,3-dihydroxypropan-2-yl)hexanamide (3a)

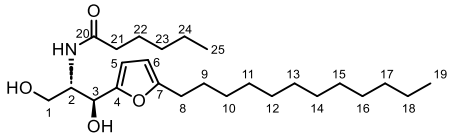

Hexanoic acid (62 μL, 0.50 mmol), EDC (94.6 mg, 0.49 mmol) and HOBt (66.0 mg, 0.49) were dissolved in dry CH_2Cl_2 (22 mL) and stirred at room temperature for 45 min. The resulting mixture was added over a solution of aminodiol **15** (79.2 mg, 0.24 mmol) in dry CH_2Cl_2 (7.5 mL) and stirred at r.t. overnight.

After this time water was added, both phases were separated and the aqueous phase was extracted with CH_2Cl_2. The combined organic extracts were dried over anhydrous $MgSO_4$ and concentrated under vacuum to give a yellow oily residue which was purified by flash column chromatography on silica gel (CH_2Cl_2/MeOH/NH_4OH, 96:4:1). Finally, ceramide analogue **3a** was obtained as a white solid (62.9 mg, 0.15 mmol, 61% yield).

R_f = 0.11 (CH_2Cl_2/MeOH/NH_4OH, 9.5:0.5:0.1); α_D^{25} -12.0 (c 1.1, $CHCl_3$); **m.p.** 58-59 ºC; **^{1}H NMR** δ in ppm: (400 MHz, $CDCl_3$) **δ** 6.31-6.30 (m, 1H, NH), 6.21 (d, $J_{5\text{-}6}$ = 3.0 Hz, 1H, H-5), 5.92 (d, $J_{6\text{-}5}$ = 3.0 Hz, 1H, H-6), 4.90 (d, $J_{3\text{-}2}$ = 4.4 Hz, 1H, H-3), 4.23 (m, 1H, H-2), 3.90 (dd, $J_{1\text{-}1'}$ = 11.5, $J_{1\text{-}2}$ =3.4 Hz, 1H, H-1), 3.70 (d, $J_{1'\text{-}1}$ = 11.5, $J_{1'\text{-}2}$ = 3.3 Hz, 1H, H-1'), 2.57 (t, $J_{8\text{-}9}$ = 7.7 Hz, 2H, H-8), 2.20 (t, $J_{21\text{-}22}$ = 7.6 Hz, 2H, H-21), 1.64-1.56 (m, 4H, H-9 and H-22), 1.34-1.22 (m, 22 H, from H-10 to H-18 and from H-23 to H-25), 0.88 (t, J = 6.9 Hz, 3 H, CH_3), 0.87 (t, J = 6.8 Hz, 3 H, CH_3); **^{13}C NMR** δ in ppm: (100.6 MHz, $CDCl_3$) 174.4 (C-20), 156.8 (C-7) , 151.7 (C-4), 108.2 (C-5), 105.5 (C-6), 69.9 (C-3), 62.8 (C-1), 54.5 (C-2), 36.9 (C-21), 32.1 (CH_2), 31.5 (CH_2), 29.81 (CH_2), 29.79 (CH_2), 29.78 (CH_2), 29.7 (CH_2), 29.5 (CH_2), 29.4 (CH_2), 28.2 (CH_2), 28.1 (C-8), 25.5 (CH_2), 22.8 (CH_2), 22.5 (CH_2), 14.3 (CH_3), 14.1 (CH_3); **HRMS** (TOF ES+) for $[M+Na]^+$ $C_{25}H_{45}NNaO_4$+ (m/z): calculated: 446.3241 found: 446.3234; **FT-IR (ATR)** ν in cm^{-1}:3288, 2954, 2923, 2852, 1651, 1636, 1541, 1456, 1418, 1376, 1302, 1259, 1218, 1189, 1057, 1013, 965, 784, 721, 669.

_N_-((1_S_,2_S_)-1-(5-dodecylfuran-2-yl)-1,3-dihydroxypropan-2-yl)octanamide (3b)

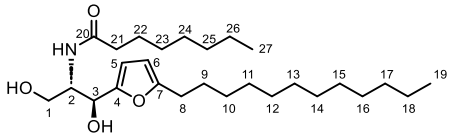

Octanoic acid (31 μL, 0.20 mmol), EDC (38.4 mg, 0.20 mmol) and HOBt (26.3 mg, 0.20) were dissolved in dry CH_2Cl_2 (8.7 mL) and stirred at room temperature for 45 min. The resulting mixture was additioned over a solution of aminodiol **15** (31.8 mg, 0.10 mmol) in dry CH_2Cl_2 (3.2 mL) and stirred at r.t. overnight.

After this time water was added, both phases were separated and the aqueous phase was extracted with CH_2Cl_2. The combined organic extracts were dried over anhydrous $MgSO_4$ and concentrated under vacuum to give a yellow oily residue which was purified by flash column chromatography on silica gel (CH_2Cl_2/MeOH/NH_4OH, 96:4:1). Finally, ceramide analogue **3b** was obtained as a white solid (26.5 mg, 0.06 mmol, 60 % yield).

R_f = 0.17 (CH_2Cl_2/MeOH/NH_4OH, 9.5:0.5:0.1); α_D^{25} -15.0 (c 1.0, $CHCl_3$); **m.p.** 46-47 ºC; **^{1}H NMR** δ in ppm: (400 MHz, $CDCl_3$) **δ** 6.24 (m, 1H, NH), 6.22 (d, $J_{5\text{-}6}$ = 3.3 Hz, 1H, H-5), 5.92 (d, $J_{6\text{-}5}$ = 3.3 Hz, 1H, H-6), 4.91 (t ap (dd), J = 4.60 Hz, 1H, H-3), 4.26-4.21 (m, 1H, H-2), 3.94-4.21 (m, 1H, H-1), 3.75-3.70 (m, 1H, H-1'), 3.39 (bs, 1H, OH), 2.72 (bs, 1H, OH), 2.58 (t, $J_{8\text{-}9}$ = 7.6 Hz, 2H, H-8), 2.22 (t, $J_{21\text{-}22}$ = 7.6 Hz, 2H, H-21), 1.65-1.57 (m, 4H, H-9 and H-22), 1.34-1.22 (m, 26 H, from H-10 to H-18 and from H-23 to H-26), 0.88 (t, J = 6.9 Hz, 6 H, H-19 and H-27); **^{13}C NMR** δ in ppm: (100.6 MHz, $CDCl_3$) 174.4 (C-20), 156.9 (C-7) , 151.7 (C-4), 108.3 (C-5), 105.6 (C-6), 70.1 (C-3), 63.0 (C-1), 54.5 (C-2), 36.9 (C-21), 32.1 (CH_2), 31.8 (CH_2), 29.82 (CH_2), 29.80 ($2CH_2$), 29.7 (CH_2), 29.5 (CH_2), 29.4 (CH_2), 29.3 (CH_2), 29.2 (CH_2), 28.2 (CH_2), 28.1 (C-8), 25.9 ($2CH_2$), 22.84 (CH_2), 22.76 (CH_2), 14.3 (CH_3), 14.2 (CH_3); **HRMS** (TOF ES+) for $[M+Na]^+$ $C_{27}H_{49}NNaO_4$+ (m/z): calculated: 474.3554 found: 474.3558; **FT-IR (ATR)** ν in cm^{-1}: 3301, 2955,

2922, 2851, 653, 1636, 1541, 1507, 1458, 1377, 1257, 1086, 1015, 858, 796, 724, 683, 668, 549.

***N*-((1*S*,2*S*)-1-(5-dodecylfuran-2-yl)-1,3-dihydroxypropan-2-yl)decanamide (3c)**

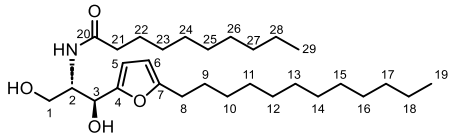

Decanoic acid (84.5 mg, 0.49 mmol), EDC (93.9 mg, 0.49 mmol) and HOBt (66.2 mg, 0.49) were dissolved in dry CH_2Cl_2 (22 mL) and stirred at room temperature for 45 min. The resulting mixture was additioned over a solution of aminodiol **15** (75.1 mg, 0.23 mmol) in dry CH_2Cl_2 (7.5 mL) and stirred at r.t. overnight.

After this time water was added, both phases were separated and the aqueous phase was extracted with CH_2Cl_2. The combined organic extracts were dried over anhydrous $MgSO_4$ and concentrated under vacuum to give a yellow oily residue which was purified by flash column chromatography on silica gel (CH_2Cl_2/MeOH/NH_4OH, 96:4:1). Finally, ceramide analogue **3c** was obtained as a white solid (81.2 mg, 0.17 mmol, 73% yield).

R_f = 0.20 (CH_2Cl_2/MeOH/NH_4OH, 9.5:0.5:0.1); α_D^{25} -14.0 (c 1.5, $CHCl_3$); **m.p.** 38-39 ºC; **^{1}H NMR** δ in ppm: (400 MHz, $CDCl_3$) **δ** 6.26 (d, $J_{NH\text{-}2}$ = 7.7 Hz, 1H, NH), 6.22 (d, $J_{5\text{-}6}$ = 3.1 Hz, 1H, H-5), 5.93 (d, $J_{6\text{-}5}$ = 3.1 Hz, 1H, H-6), 4.91 (d, $J_{3\text{-}2}$ = 4.4 Hz, 1H, H-3), 4.24 (m, 1H, H-2), 3.97 (dd, $J_{1\text{-}1'}$ = 11.5, $J_{1\text{-}2}$ =3.8 Hz, 1H, H-1), 3.71 (d, $J_{1'\text{-}1}$ = 11.5, $J_{1'\text{-}2}$ = 3.8 Hz, 1H, H-1'), 2.57 (t, $J_{8\text{-}9}$ = 7.7 Hz, 2H, H-8), 2.21 (t, $J_{21\text{-}22}$ = 7.6 Hz, 2H, H-21), 1.64-1.56 (m, 4H, H-9 and H-22), 1.33-1.25 (m, 30 H, from H-10 to H-18 and from H-23 to H-28), 0.87 (t, J = 6.8 Hz, 6 H, H-19 and H-29); **^{13}C NMR** δ in ppm: (100.6 MHz, $CDCl_3$) 174.4, 156.9, 151.7, 108.3 (C-5), 105.5 (C-6), 70.1 (C-3), 62.9 (C-1), 54.5 (C-2), 36.9 (C-21), 32.1 (CH_2), 32.0 (CH_2), 29.82 (CH_2), 29.80 ($2CH_2$), 29.7 (CH_2), 29.6 (CH_2), 29.5 ($2CH_2$), 29.4

(CH_2), 29.37 (CH_2), 29.36 (CH_2), 28.2 (CH_2), 28.1 (CH_2), 25.9 (CH_2), 22.84 (CH_2), 22.82 (CH_2), 14.27 (CH_3), 14.26(CH_3); **HRMS** (TOF ES+) for $[M+Na]^+$ $C_{29}H_{53}NNaO_4$+ (m/z): calculated: 502.3867 found: 474.3866; **FT-IR (ATR)** ν in cm^{-1}: 3383, 3310, 2918, 2849, 1644, 1620, 1557, 1466, 1378, 1262, 1234, 1102, 1051, 1013, 957, 787, 721, 651, 549, 427.

2-tridecylcycloprop-2-en-1-one (58)

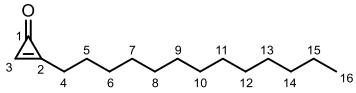

NaI (2.519 g, 16.80 mmol) and 1-pentadecyne (2 mL, 7.62 mmol) were dissolved in dry THF (10.2 mL) under argon atmosphere in a Schlenck pressure tube. $TMSCF_3$ (5.63 mL, 38.09 mmol) was added, the Schlenck pressure tube was sealed and the mixture was heated at 110 °C while vigorously stirring. After 21 hours the reaction was stopped with the addition of $NaHCO_3$ saturated aqueous solution. Both phases were separated, and the aqueous phase was extracted with Et_2O. The combined organic extracts were desiccated with anhydrous $MgSO_4$ and concentrated under vacuum to give a yellowish oily residue. The formation of the desired difluorocyclopropane was confirmed by ^1H NMR and ^{19}F NMR analysis.

The obtained difluorocyclopropane, **59**, was dissolved in a hexane/AcOH (99:1) mixture and treated with silice at room temperature overnight. Afterwards, the mixture was filtrated under vacuum through a filter plate and extracted with $NaHCO_3$ sat. sol. The organic phase was desiccated with anhydrous $MgSO_4$ and concentrated under vacuum to give a yellowish oily residue. The residue was purified by flash column chromatography on silica gel (gradient: hexane/ethyl acetate, from 7:3 to 6:4) and finally the desired cyclopropenone **58** was obtained in form of a white solid (1.5804 g, 6.69 mmol, 88 % yield).

***R*f** = 0.20 (hexane/ethyl acetate, 1:1); **M.p.** 41-42 ºC; **^{1}H NMR** (400 MHz, $CDCl_3$) δ in ppm: 8.40 (s, 1H, H-3), 2.64 (t, J_{4-5} = 7.3 Hz, 2H, H-4), 1.68 (q ap., *J* = 7.4 Hz, 2H, H-5), 1.40-1.33 (m, 2H, H-6), 1.30-1.17 (m, 20H, from H-7 to H-15), 0.84 (t, J_{16-15} = 6.6. Hz, 3H, H-16). **^{13}C NMR** (100.6 MHz, $CDCl_3$) δ in ppm: 170.3 (C-2), 158.0 (C-1), 148.2 (C-3), 32.0 (CH_2), 29.70 (CH_2), 29.68 ($2CH_2$), 29.6 (CH_2), 29.5 (CH_2), 29.4 (CH_2), 29.2 (CH_2), 29.0 (C-6), 27.5 (C-4), 25.7 (C-5), 22.7 (CH_2), 14.2 (C-16). **HRMS** (TOF ES+) for $[M+H]^+$ $C_{16}H_{29}O^+$ (m/z): calculated: 237.22129 found: 237.22124. **FT-IR (ATR)** ν in cm^{-1}: 3047, 2957, 2914, 2847, 1877, 1827, 1804, 1745, 1577, 1469, 1460, 1411, 1158, 1032, 886, 874, 715.

6,6-dimethyl-1-tridecyl-4,8-dioxaspiro[2.5]oct-1-ene (57)

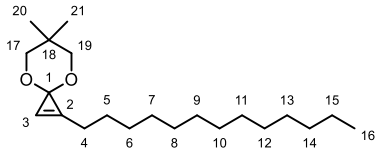

Tridecylcyclopropenone **58** (1.0053 g, 4.25 mmol) and BF_4OEt_3 (1.2146 g, 6.39 mmol) were dissolved in dry CH_2Cl_2 (7 mL) under argon atmosphere, the resulting mixture was vigorously stirred at room temperature for 30 min. Neopentylglycol (888.4 mg, 8.53 mmol) and Et_3N (1.18 mL, 8.47 mmol) dissolved in dry CH_2Cl_2 (2.3 mL) was added over the previous mixture dropwise. After the addition the reaction mixture was stirred at room temperature overnight.

After this time, the reaction was stopped with the addition of $NaHCO_3$ sat. sol. The organic phase was washed multiple times with $NaHCO_3$ sat. sol., then, desiccated with Na_2SO_4 and concentrated under reduced pressure. A brown oily residue was obtained, which was purified by flash column chromatography on silica gel (hexane/AcOEt, 9:1) to give the desired cyclopropenone acetal **57** in form of a yellow liquid (1.2181 g, 3.78mmol, 89 % yield).

R_f = 0.40 (hexane/ethyl acetate, 9:1); **^{1}H NMR** (400 MHz, $CDCl_3$) δ in ppm: 7.32 (t, $J_{3\text{-}4}$ = 1.2 Hz, 1H, H-3), 3.63 (d, J_{gem} = 10.4 Hz, 2H, H-17 and H-19), 3.59 (d, J_{gem} = 10.4 Hz, 2H, H-17′ and H-19′), 2.52 (td, $J_{4\text{-}5}$ = 7.3, $J_{4\text{-}3}$ = 1.2 Hz, 2H, H-4), 1.62 (q ap., J = 7.4 Hz, 2H, H-5), 1.40-1.25 (m, 22H,from H-6 to H-15), 1.06 (s, 3H, C-20), 1.00 (s, 3H, C-21), 0.88 (t, $J_{17\text{-}16}$ = 6.9 Hz, 3H, H-16). **^{13}C NMR** (100.6 MHz, $CDCl_3$) δ in ppm: 138.2 (C-2), 115.3 (C-3), 83.7 (C-1), 77.3 (C-17 and C-19), 32.1 (CH_2), 30.5 (C-18), 29.83 (CH_2), 29.81 (CH_2), 29.80 (CH_2), 29.76 (CH_2), 29.7 (CH_2), 29.5 (CH_2), 29.4 (CH_2), 29.3 (CH_2), 27.4 (C-5), 25.1 (C-4), 22.8 (CH_2), 22.6 (C-20/C-21), 22.3 (C-20/C-21), 14.3 (C-16). **HRMS** (TOF ES+) for $[M+H]^+$ $C_{16}H_{29}O^+$ (m/z): calculated: 323.29446 found: 323.29373. **FT-IR (ATR)** ν in cm^{-1}: 2952, 2924, 2852, 1729, 1467, 1393, 1362, 1279, 1217, 1076, 1024, 994, 935, 723.

tert-butyl (S)-4-((R)-(6,6-dimethyl-2-tridecyl-4,8-dioxaspiro[2.5]oct-1-en-1-yl)(hydroxy)methyl)-2,2-dimethyloxazolidine-3-carboxylate (56)

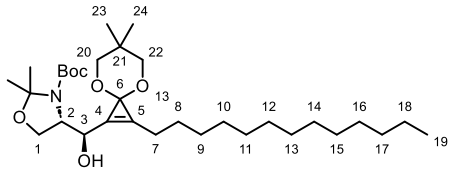

Cyclopropenone acetal **57** (609.5 mg, 1.89 mmol) and HMPA (0.66 mL, 3.79 mmol) were dissolved in dry THF (8.5 mL) under argon atmosphere. The solution was cooled down to -55 ˚C and BuLi (0.75 mL, 2.5 M in hexanes, 1.88 mmol) was added dropwise. The mixture was stirred for 30 min and then **(*S*)-Garner's aldehyde** (234.0 mg, 1.05 mmol) dissolved in dry THF (1.9 mL) was added. The resulting mixture was stirred at -55 ºC overnight.

After this time aqueous NH_4Cl sat. sol. was added, both phases were separated, and the aqueous phase was extracted with DCM. The combined organic extracts were dried over anhydrous Na_2SO_4, filtered and concentrated under vacuum to give a brownish residue which was purified by flash column

chromatography on silica gel (hexane/AcOEt, 8:2). Finally, the desired addition product **56** was obtained as a colourless liquid (438 mg, 76 % yield).

R_f = 0.17 Hexane/AcOEt (8:2); α_D^{25} -8,4 (c 1.3, $CHCl_3$); **^{1}H NMR** δ in ppm (400 MHz, $CDCl_3$, 50 °C): 5.04-5.03 (m, 1H, H-3), 4.16 (br s, 1H, H-2), 4.00-3.99 (m, 2H, H-1), 3.69-3.64 (m, 2H, H-20 and H-22), 3.56 (d, J_{gem} = 11.0 Hz, 2H, H-20' and H-22'), 2.47 (t, J_{7-8} = 7.5 Hz, 2H, H-7), 1.65-1.57 (m, 6H, isopropyldiene), 1.50 (s, 9H, *tert*-butyl), 1.37-1.26 (m, 22H, from H-8 to H-18), 1.06 (s, 3H, H-23), 0.94 (s, 3H, H-24), 0.88 (t, J_{19-18} = 6.7 Hz, 3H, H-19); **^{13}C NMR** δ in ppm (100.6 MHz, $CDCl_3$): 154.0 (Boc carbonyl), 130.1 (C-5), 128.7 (C-4), 95.0 (iopropylidene quaternary C), 84.9 (C-6), 81.3 (Boc quaternary C), 77.7 (C-20), 77.2 (C-22), 68.5 (C-3), 64.8 (C-1), 61.4 (C-2), 32.0 (CH_2), 30.4 (C-21), 29.8 (CH_2), 29.8 (CH_2), 29.8 (CH_2), 29.8 (CH_2), 29.7 (CH_2), 29.5 (CH_2), 29.5 (CH_2), 29.4 (CH_2), 28.5 (Boc Me groups), 27.7 (C-8), 26.2 (isopropyldiene Me groups), 24.5 (C-7), 22.8 (CH_2), 22.6 (C-23), 22.2 (C-24), 14.3 (C-19); **HRMS** (ESI+) for $[M+H]^+$ $C_{32}H_{58}NO_6^+$ (m/z): calculated: 552.42587, found: 552.42346; **FT-IR (ATR)** ν in cm^{-1}: 3424, 2952, 2923, 2850, 1807, 1702, 1467, 1370, 1365, 1256, 1171, 1072.

2-((1R,2S)-2-amino-1,3-dihydroxypropyl)-3-tridecylcycloprop-2-en-1-one (55)

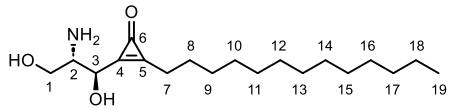

Addition product **56** (438 mg, 0.94 mmol) was dissolved in water (15.3 mL), cooled down to 0 °C and HCl (4.9 mL, 2M in Et2O, 9.8 mmol) was added dropwise. After the addition the reaction mixture was warmed up to room temperature and stirred for 3 h. After this time, it was concentred under vacuum to obtaining a brown solid residue. The residue was then dissolved in a CH_2Cl_2/MeOH/NH_4OH (9:1:1) mixture stirred for 30 min and concentrated again under vacuum.

The obtained brown solid was then purified by flash column chromatography on silica gel CH_2Cl_2/MeOH/NH_4OH (95:5:1) to furnish the desired aminodiol **55** as a white solid (159 mg, 62% yield).

R_f = 0.20 DCM/MeOH/NH_4OH (9:1:0.1); α_D^{25} +1.6 (c 1.1, MeOH); **M.p.** = 132-133 °C; **^{1}H NMR** δ in ppm (400 MHz, CD_3OD): 4.75 (dt, $J_{3\text{-}2}$ = 5.5 Hz, $J_{3\text{-}7}$ = 1.0 Hz, 1H, H-3), 3.66 (dd, J_{gem} = 11.0 Hz, $J_{1\text{-}2}$ = 5.5 Hz, 1H, H-1), 3.61 (dd, J_{gem} = 11.0 Hz, $J_{1'\text{-}2}$ = 5.5 Hz, 1H, H-1'), 3.09 (q ap, $J_{2\text{-}1}$ = $J_{2\text{-}3}$ = 5.5 Hz, 1H, H-2), 2.74 (td, $J_{7\text{-}8}$ = 7.2 Hz, $J_{7\text{-}3}$ = 1.0 Hz, 2H, H-7), 1.75 (p, $J_{8\text{-}7}$ = $J_{8\text{-}9}$ = 5.5 Hz, 2H, H-8), 1.46-1.26 (m, 20H, from H-9 to H-18), 0.90 (t, $J_{19\text{-}18}$ = 7.0 Hz, 3H, H-19); **^{13}C NMR** δ in ppm (100.6 MHz, CD_3OD): 162.8 (C-6), 162.0 (C-4), 161.2 (C-5), 71.3 (C-3), 63.6 (C-1), 57.6 (C-2), 33.1 (CH_2), 30.9 (CH_2), 30.8 (CH_2), 30.8 (CH_2), 30.8 (CH_2), 30.6 (CH_2), 30.5 (CH_2), 30.4 (CH_2), 30.3 (CH_2), 27.4 (C-8), 26.8 (C-7), 23.8 (CH_2), 14.5 (C-19); **HRMS** (ESI+) for $[M+H]^+$ $C_{19}H_{36}NO_3^+$ (m/z): calculated: 326,26897, found: 326,26923; **FT-IR (ATR)** ν in cm^{-1}: 3284, 2955, 291, 2850, 1843, 1617, 1464, 1045.

_N_-((1_R_,2_S_)-1,3-dihydroxy-1-(3-oxo-2-tridecylcycloprop-1-en-1-yl)propan-2-yl)hexanamide (45a)

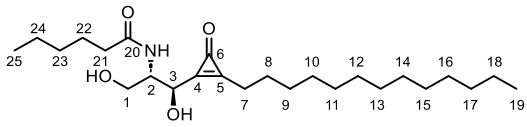

Hexenooic acid (21.5 μL, 0.17 mmol), EDC (33.2 mg, 0.17 mmol) and HOBt (23.3 mg, 0.17 mmol) were dissolved in dry CH_2Cl_2 (4.9 mL). The solution was stirred at room temperature for 45 min. The resulting mixture was added to a solution of aminodiol **56** (50.9 mg, 0.16 mmol) in dry CH_2Cl_2 (5.4 mL) and stirred at room temperature overnight.

After this time water was added, both phases were separated, and the aqueous phase was extracted with CH_2Cl_2. The combined organic extracts were dried over anhydrous Na_2SO_4, filtrated, and concentrated under vacuum to give a yellowish solid residue which was purified by flash column

chromatography on silica gel (DCM/MeOH/NH_4OH, 96:4:1). The resulting solid was recrystalized with pentane and finally the desired ceramide analog **45a** was obtained as a white solid (48.6 mg, 0.11 mmol, 73 % yield).

R_f = 0.37 DCM/MeOH/NH_4OH (9:1:0.1); α_D^{25} -33.9 (c 0.6, $CHCl_3$); **M.p.** = 121-122 ºC; **^{1}H NMR** δ in ppm (400 MHz, $CDCl_3$): 6.97 (d, J_{NH-2} = 5.9 Hz, 1H, NH), 5.94 (d, J_{OH-3} = 7.5 Hz, 1H, OH-3), 4.85-4.83 (m, 1H, H-3), 4.26-4.23 (m, 1H, OH-1), 4.22-4.17 (m, 1H, H-2), 3.99-3.93 (m, 1H, H-1), 3.90-3.84 (m, 1H, H-1') 2.66 (t, J_{7-8} = 7.4 Hz, 2H, H-7), 2.28-2.16 (m, 2H, H-21), 1.71 (p ap, J_{8-7} = J_{8-9} = 7.2 Hz, 2H, H-8), 1.59 (p ap, J_{22-21} = J_{22-23} = 7.3 Hz, 2H, H-22), 1.38-1.23 (m, 24 H, from H-9 to H-18, H-23 and H-24), 0.88 (t, J = 7.0 Hz, 3H, H-19/H-250.88 (t, J = 7.0 Hz, 3H, H-19/H-25); **^{13}C NMR** δ in ppm (100.6 MHz, $CDCl_3$): 176.5 (C-20), 162.2 (C-5), 160.6 (C-4), 159.5 (C-6), 72.1 (C-3), 61.5 (C-1), 56.5 (C-2), 36.3 (C-21), 32.1 (CH_2), 32.0 (CH_2), 29.82 (CH_2), 29.78 ($2CH_2$), 29.76 (CH_2), 29.6 (CH_2), 29.5 (CH_2), 29.4 (CH_2), 29.3 (CH_2), 26.6 (C-8), 26.2 (C-7), 25.4 (C-22), 22.8 (CH_2), 22.5 (CH_2), 14.3 (CH_3), 14.0(CH_3); **HRMS** (ESI+) for $[M+H]^+$ $C_{25}H_{46}NO_4^+$ (m/z): calculated: 424.34214, found: 424.34103; **FT-IR (ATR)** ν in cm^{-1}: 3303, 2953, 2851, 1838, 1645, 1577, 1547, 1466, 1457, 1417, 1376, 1326, 1289, 1254, 1217, 1120, 1071, 980, 952, 720, 695, 652, 620, 437.

_N_-((1_R_,2_S_)-1,3-dihydroxy-1-(3-oxo-2-tridecylcycloprop-1-en-1-yl)propan-2-yl)octanamide (45b)

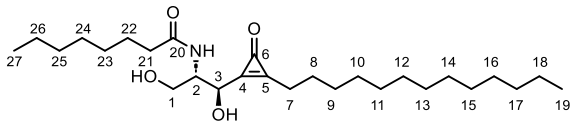

Octanoic acid (132 μL, 0.83 mmol), EDC (160 mg, 0.83 mmol) and HOBt (114 mg, 0.84 mmol) were dissolved in dry CH_2Cl_2 (24 mL). The solution was stirred at room temperature for 45 min. The resulting mixture was added to a solution of aminodiol **56** (150 mg, 0.46 mmol) in dry CH_2Cl_2 (16 mL) and stirred at room temperature overnight.

After this time water was added, both phases were separated, and the aqueous phase was extracted with CH_2Cl_2. The combined organic extracts were dried over anhydrous Na_2SO_4, filtrated, and concentrated under vacuum to give a yellowish solid residue which was purified by flash column chromatography on silica gel (DCM/MeOH/NH_4OH, 95:5:1). The resulting solid was recrystalized with pentane and finally the desired ceramide analog **45b** was obtained as a white solid (126 mg, 60 % yield).

R_f = 0.09 DCM/MeOH/NH_4OH (95:5:1); α_D^{25} -41.2 (c 0.5, $CHCl_3$); **M.p.** = 117-118 ºC; **^{1}H NMR** δ in ppm (400 MHz, $CDCl_3$): 6.81 (d, J_{NH-2} = 5.2 Hz, 1H, NH), 5.87 (d, J_{OH3-3} = 5.2 Hz, 1H, OH-3), 4.82 (d, J_{3-OH3} = 5.2 Hz, 1H, H-3), 4.2 (s, 1H, H-2), 4.02-3.98 (m, 2H, OH-1 and H-1), 3.94-3.89 (m, 1H, H-1'), 2.67 (t, J_{7-8} = 7.3 Hz, 2H, H-7), 2.29-2.17 (m, 2H, H-21), 1.75-1.68 (m, 2H, H-8), 1.59 (p, J_{22-21} = J_{22-23} = 7.3 Hz, 1H, H-22), 1.39-1.25 (m, 28H, from H-9 to H-18 and H-23 to H-26), 0.88 (t, J_{19-18} = J_{27-26} = 6.5 Hz, 6H, H-19 and H-27); **^{13}C NMR** δ in ppm (100.6 MHz, $CDCl_3$): 176.8 (C-20), 162.1 (C-5), 160.6 (C-4), 159.5 (C-6), 71.8 (C-3), 61.5 (C-1), 56.4 (C-2), 36.4 (C-22), 32.1 (CH_2), 31.8 (CH_2), 29.8 (CH_2), 29.8 (CH_2), 29.8 (CH_2), 29.8 (CH_2), 29.6 (CH_2), 29.5 (CH_2), 29.4 (CH_2), 29.3 (CH_2), 29.3 (CH_2), 29.1 (CH_2), 26.6 (C-8), 26.3 (C-7), 25.8 (C-22), 22.8 (CH_2), 22.8 (CH_2), 14.3 (CH_3), 14.3 (CH_3); **HRMS** (ESI+) for $[M+H]^+$ $C_{27}H_{50}NO_4^+$ (m/z): calculated: 452.37343, found: 452.37360; **FT-IR (ATR)** ν in cm^{-1}: 3307, 2956, 2919, 2852, 1840, 1647, 1578, 1548, 1459, 1073.

_N_-((1_R_,2_S_)-1,3-dihydroxy-1-(3-oxo-2-tridecylcycloprop-1-en-1-yl)propan-2-yl)decanamide (45c)

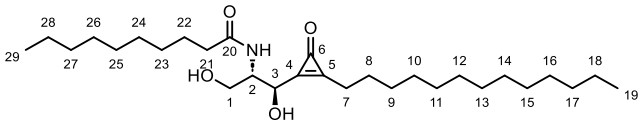

Decanoic acid (29.3 mg, 0.17 mmol), EDC (32.7 mg, 0.17 mmol) and HOBt (23.2 mg, 0.17 mmol) were dissolved in dry CH_2Cl_2 (4.9 mL). The solution was stirred at room temperature for 45 min. The resulting mixture was added to a

solution of aminodiol **56** (50.9 mg, 0.16 mmol) in dry CH_2Cl_2 (5.4 mL) and stirred at room temperature overnight.

After this time water was added, both phases were separated, and the aqueous phase was extracted with CH_2Cl_2. The combined organic extracts were dried over anhydrous Na_2SO_4, filtrated, and concentrated under vacuum to give a yellowish solid residue which was purified by flash column chromatography on silica gel (DCM/MeOH/NH_4OH, 96:4:1). The resulting solid was recrystalized with pentane and finally the desired desired ceramide analog **45b** was obtained as a white solid (49.6 mg, 0.10 mmol, 66 % yield).

R_f = 0.40 DCM/MeOH/NH_4OH (9:1:0.1); $\boldsymbol{\alpha_D^{25}}$ -10.6 (c 0.4, $CHCl_3$/MeOH, 1:1); **M.p.** = 132-133 ºC; **^{1}H NMR** δ in ppm (400 MHz, $CDCl_3$): 6.79 (d, $J_{NH\text{-}2}$ = 5.6 Hz, 1H, NH), 5.84 (bs, 1H, OH-3), 4.82 (bs, 1H, H-3), 4.22-4.18 (m, 1H, H-2), 4.00 (dd, $J_{1\text{-}1'}$ = 11.3, $J_{1\text{-}2}$ = 4.3 Hz, 1H, H-1), 3.90 (dd, $J_{1'\text{-}1}$ = 11.3, $J_{1'\text{-}2}$ = 5 Hz, 1H, H-1'), 2.67 (t, $J_{7\text{-}8}$ = 7.5 Hz, 2H, H-7), 2.29-2.17 (m, 2H, H-21), 1.75-1.68 (m, 2H, H-8), 1.59 (p ap, $J_{22\text{-}21}$ = $J_{22\text{-}23}$ = 7.3 Hz, 2H, H-22), 1.38-1.26 (m, 32H, from H-9 to H-18 and H-23 to H-8), 0.88 (t, $J_{19\text{-}18}$ = $J_{28\text{-}29}$ = 6.5 Hz, 6H, H-19 and H-27); **^{13}C NMR** δ in ppm (100.6 MHz, $CDCl_3$): 176.8 (C-20), 162.2 (C-5), 160.6 (C-4), 159.4 (C-6), 72.8 (C-3), 61.5 (C-1), 56.4 (C-2), 36.4 (C-21), 32.1 (CH_2), 32.0 (CH_2), 29.83 (CH_2), 29.80 ($2CH_2$), 29.78 (CH_2), 29.62 (CH_2), 29.60 (CH_2), 29.51 (CH_2), 29.49 (CH_2), 29.43 ($2CH_2$), 29.36 (CH_2), 29.3 (CH_2), 26.6 (C-8), 26.3 (C-7), 25.79 (C-22), 22.84 (CH_2), 22.81 (CH_2), 14.3 (CH_3), 14.2 (CH_3); **HRMS** (ESI+) for $[M+H]^+$ $C_{29}H_{54}NO_4^+$ (m/z): calculated: 480.40474, found: 480.40344; **FT-IR (ATR)** ν in cm^{-1}: 3306, 2955, 2919, 2851, 1838, 1647, 1577, 1547, 1467, 1417, 1389, 1330, 1292, 1259, 1230, 1200, 1117, 1073, 981, 944, 721, 695, 654, 621, 537.

_N_-((1_S_,2_S_)-1,3-dihydroxy-1-(3-oxo-4-tridecyl-3_H_-1,2-dithiol-5-yl)propan-2-yl)octanamide (80)

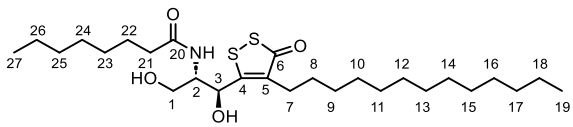

Cyclopropenone ceramide analog **45b** (22 mg, 0.049 mmol), KF (5.7 mg, 0.098 mmol) and S_8 (3.3 mg, 0.10 mmol) were dissolved in DMF (0.48 mL). The mixture was stirred overnight under air atmosphere at room temperature.

After this time NaCl sat. sol. was added, both phases were separated, and the aqueous phase was extracted with DCM. The combined organic extracts were washed with NaCl (sat. sol.), dried over anhydrous Na_2SO_4, filtered and concentrated under vacuum to give a yellowish residue that was purified by flash column chromatography on silica gel (hexane/AcOEt, 6:4). Finally, the desired product **80** was obtained as a brown liquid (12 mg, 50% yield).

R_f = 0.18 Hexane/AcOEt (6:4); $\boldsymbol{\alpha_D^{25}}$ 40.2 (c 1.0, $CHCl_3$); **^{1}H NMR** δ in ppm (400 MHz, $CDCl_3$): 6.51 (d, $J_{NH\text{-}2}$ = 7.5 Hz, 1H, NH), 5.36-5.34 (m, 1H, H-3), 4.73 (br s, 1H, OH-3), 4.08-4.02 (m, 2H, H-2 and H-1), 3.71 (d, $J_{1'\text{-}1}$ = 10.5 Hz, 1H, H-1'), 2.92 (s, 1H, OH-1), 2.54-2.49 (m, 2H, H-7) 2.27 (t, $J_{21\text{-}22}$ = 7.4 Hz, 2H, H-21), 1.65 (p, $J_{22\text{-}21}$ = $J_{22\text{-}23}$ = 7.4 Hz, 1H, H-22), 1.55-1.46 (m, 2H, H-8), 1.35-1.26 (m, 28H, from H-9 to H-18 and H-23 to H-26), 0.90-0.85 (m, 6H, H-19 and H-27); **^{13}C NMR** δ in ppm (100.6 MHz, $CDCl_3$): 196.0 (C-6), 174.3 (C-20), 167.2 (C-5), 131.3 (C-4), 73.8 (C-3), 61.6 (C-1), 53.7 (C-2), 36.8 (C-21), 32.1 (CH_2), 31.8 (CH_2), 29.9 (CH_2), 29.8 (CH_2), 29.8 (CH_2), 29.8 (CH_2), 29.7 (CH_2), 29.7 (CH_2), 29.6 (CH_2), 29.5 (CH_2), 29.4 (CH_2), 29.1 (CH_2), 28.4 (C-8), 27.9 (C-7), 25.8 (C-22), 22.8 (CH_2), 22.8 (CH_2), 14.3 (CH_3), 14.2 (CH_3); **HRMS** (ESI-) for $[M+Cl]^-$ $C_{27}H_{50}NO_4S_2Cl^-$ (m/z): calculated: 550.27970, found: 550.27991; **FT-IR (ATR)** ν in cm^{-1}: 3325, 2955, 2920, 2853, 1644, 1626, 1562, 1544, 1461, 1376, 1262, 1121, 1075, 600.

tert-butyl (S)-4-((R)-hydroxy(3-oxo-2-tridecylcycloprop-1-en-1-yl)methyl)-2,2-dimethyloxazolidine-3-carboxylate (107)

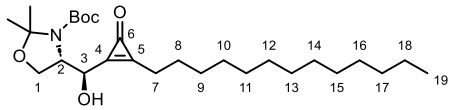

Cyclopropenone acetal **56** (1.21374 g, 2.19 mmol) was dissolved in $CDCl_3/CH_2Cl_2$ (30 mL) and stirred at 35 °C for 48 h.

After this time, the reaction was stopped with the addition of $NaHCO_3$ sat. sol. The organic phase was washed multiple times with $NaHCO_3$ sat. sol., then, desiccated with Na_2SO_4 and concentrated under reduced pressure. A light-yellow oily residue was obtained, which was purified by flash column chromatography on silica gel (hexane/AcOEt, 1:1) to give the desired cyclopropenone **107** in form of a colourless oil (989.2 mg, 2.12 mmol, 97 % yield).

R_f = 0.19 (hexane/ethyl acetate, 1:1); α_D^{25} -33.3 (c 1.0, $CHCl_3$); **^{1}H NMR** (400 MHz, $CDCl_3$) δ in ppm: 6.14 (d, $J_{OH\text{-}3}$ = 9.15 Hz, 1H, OH), 4.78 (d, $J_{3\text{-}OH}$ = 9.15 Hz, 1H, H-3), 4.30-4.26 (m, 1H, H-2), 4.20 (t ap, J =8.2 Hz, 1H, H-1), 4.03 (dd, J_{gem} = 9.19, $J_{1'\text{-}2}$ = 6.17 Hz, 1H,H-1'), 2.65 (dt, $J_{7\text{-}8}$ = 7.61, $J_{7\text{-}3}$ = 3.10 Hz, 2H, H-7), 1.75-1.67 (m, 2H, H-8), 1.48 (s, 5H, isopropyldiene), 1.47 (s, 9H, *tert*-butyl), 1.29-1.25 (m, 20H, from H-9 to H-18), 0.87 (t, $J_{19\text{-}18}$ = 6.7 Hz, 3H, H-19); **^{13}C NMR** δ in ppm: 163.1 (C-5), 160.1 (C-4), 157.9 (C-6), 155.3 (Boc carbonyl), 95.8 (iopropylidene quaternary C), 82.4 (Boc quaternary C), 72.0 (C-3), 65.1 (C-1), 62.0 (C-2), 32.1 (CH_2), 29.80 (CH_2), 29.77 (CH_2), 29.76 (CH_2), 29.73 (CH_2), 29.6 (CH_2), 29.48 (CH_2), 29.45 (CH_2), 29.2 (CH_2), 28.4 ($3CH_3$-Boc), 26.66 (CH_3-isopropylidene), 26.15 (CH_2), 26.13 (CH_2), 25.44 (CH_3-isopropylidene), 22.83 (CH_2), 14.3 (C-19); **HRMS** (TOF ES+) for $[M+Na]^+$ $C_{27}H_{47}NNaO_5^+$ (m/z): calculated: 488.33464 found: 488.33325; **IR** (neat): 3330, 2924, 2853, 1843, 1695, 1625, 1457, 1365, 1247, 1169, 1098, 1069, 846, 752, 665, 521, 461.

tert-butyl (S)-4-((R)-hydroxy(3-thioxo-2-tridecylcycloprop-1-en-1-yl)methyl)-2,2-dimethyloxazolidine-3-carboxylate (108)

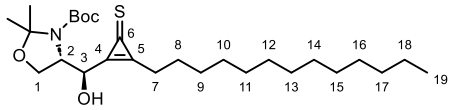

Cyclopropenone **107** (350.0 mg, 0.752 mmol) and Lawesson's reagent were dissolven in dry CH_2Cl_2. The mixture was stirred at room temperature for 2 h. The rection crude was concentrated under vacuum to obtain a brown oil,

which was purified by flash column chromatography on silica gel (hexane/AcOEt, from 8:n to 7:3) to give the desired cyclopropenethione **108** in form of a yellow oil (136.1 mg, 0.283 mmol, 38 % yield).

R_f = 0.43 (hexane/ethyl acetate, 7:3); α_D^{25} -34.7 (c 1.4, $CHCl_3$); **^{1}H NMR** (400 MHz, $CDCl_3$) δ in ppm: 5.03 (bs, 1H, H-3), 4.38-4.34 (m, 1H, H-2), 4.32-4.28 (m, 1H, H-1), 4.24-4.20 (m, 1H, H-1'), 2.82 (t, $J_{7\text{-}8}$ = 7.11, 2H, H-7), 1.84-1.76 (m, 2H, H-8), 1.47-1.44 (m, 15H, 5H-isopropyldiene + 9H-*tert*-butyl), 1.29-1.25 (m, 20H, from H-9 to H-18), 0.87 (t, $J_{19\text{-}18}$ = 6.7 Hz, 3H, H-19); **^{13}C NMR** δ in ppm: 184.8 (C-6), 170.3 (C-5), 167.4 (C-4), 155.3 (Boc carbonyl), 96.0 (iopropylidene quaternary C), 82.6 (Boc quaternary C), 71.7 (C-3), 64.k9 (C-1), 62.2 (C-2), 32.0 (CH_2), 29.82 ($2CH_2$), 29.78 (CH_2), 29.76 (CH_2), 29.74 (CH_2), 29.70 (CH_2), 29.53 (CH_2), 29.47 (CH_2), 29.2 (CH_2), 28.4 ($2CH_2$), 26.5 (CH_2), 26.12 (CH_2), 26.10 (CH_2), 25.5 (CH_2), 22.8 (CH_2), 14.3 (C-19); **HRMS** (TOF ES+) for $[M+Na]^+$ $C_{27}H_{47}NNaO_4S^+$ (m/z): calculated: 504.3123 found: 504.30692;

8.3 Biological evaluation

8.3.1 Materials

GT11, **XM462** and **dhCerC6NBD** were available in Gemma Fabria's laboratory (RUBAM, Department of Biological Chemistry, Institute for Advanced Chemistry of Catalonia, IQAC). Dulbecco's Modified Eagle Medium, Fetal bovine serum, penicillin and streptomycin, trypsin-EDTA and NADH were from Sigma-Aldrich/Merck.

8.3.2 Cell culture

Human glioblastoma cell lines T98G were cultured at 37 °C in 5% CO_2 in Dulbecco's Modified Eagle Medium supplemented with 10% fetal bovine serum and 100 ng/mL each of penicillin and streptomycin.

8.3.3 Des1 activity in intact cells

To determine the compounds activity on Des1 in intact cells, cells were seeded in 6 well plates at a density of 2.5×10^5 cells/mL. After incubation at 37 °C and 5 % CO_2, the medium was replaced with 1 mL of fresh complete medium containing the inhibitory candidates, positive control (**XM462** or **GT11**) or negative control (EtOH or DMSO) with a 10 μM final concentration. After incubation at 37 °C for 20 h, 1 ml of fresh complete medium containing **dhCerC6NBD** (fluorescent marked substrate) with a 10 μM concentration was added to the medium and incubated for an additional 4 h.

The media was then collected in an Eppendrof tube, cells were washed with PBS (400 μL/well) and the washing solution was combined with the collected media. After collecting the media, cells were detached by trypsinization (400 μL/well Trypsin-EDTA, 5 min. incubation at 37 °C, 5 % CO_2), 600 μL of medium was then added to the cell suspension and the solution was transferred to an Eppendorf tube. One millilitre of MeOH was added to each Eppendorf tube (medium and cell suspension) which was then vortexed and kept at 4 °C overnight. After centrifugation (10,000 rpm for 3 min), the supernatants were transferred to HPLC vials and either 25 μL (media) or 100 μL (cells) were injected in to HPLC.

Analyses were performed with an Alliance apparatus coupled to a fluorescence detector using a C18 reversed-phase column eluted with 15% H_2O and 8% acetonitrile, both with a 0.1% trifluoroacetic acid, flowing at 1 mL/min. The detector was set at an excitation wavelength of 470 nm and the emission wavelength at 530 nm. Each sample was run for up to 15 min.

8.3.4 Des1 activity in cell lysates

The needed volume (1×10^6 cells/sample) of a cell suspension in medium was transferred to a falcon tube and centrifugated at 400 g at 4 °C during 3 min, supernatant was discarded, and the obtained pellet was washed twice with PBS. Cellular lysates were obtained by suspending the previously obtained pellet with 0.25 M sacarose solution, applying a probe sonication (Branson Sonifier 150, 50% amplitude, microtip 2.4 mm) and centrifuging.

Then, 100 μL of the supernatant (1×10^6 cells) were transferred to an Eppendorf tube with 85 μL **dhCerNBD** solution (in PBS, final concentration: 10 μM), 85 μL inhibitor candidate solution (in DMSO or EtOH, final concentration: 10 μM), 35 μL NADH solution (in PBS, final concentration: 2.25 mM). The mixture was incubated for 4 h at 37 °C. After this time, one millilitre of MeOH was added to the Eppendorf tube, which was then vortexed and kept at 4 °C overnight. After centrifugation (10,000 rpm for 3 min), the supernatant was transferred to HPLC vials and 25 μL were injected in to HPLC.

Analyses were performed with an Alliance apparatus coupled to a fluorescence detector using a C18 reversed-phase column eluted with 15% H_2O and 8% acetonitrile, both with a 0.1% trifluoroacetic acid, flowing at 1 mL/min. The detector was set at an excitation wavelength of 470 nm and the emission wavelength at 530 nm. Each sample was run for up to 15 min.

8.3.5 IC_{50} in cell lysates determination

Cellular lysates were obtained by suspending the pellet with 0.25 M sacarose solution, applying a probe sonication (Branson Sonifier 150, 50% amplitude, microtip 2.4 mm) and centrifuging.

100 μL of the supernatant (1×10^6 cells) were transferred to an Eppendorf tube with 85 μL dhCerNBD solution (in PBS, final concentration: 10 μM), 85 μL inhibitor candidate solution (in DMSO or EtOH, final concentrations between 0.1 -10 μM), 30 μL NADH solution (in PBS, final concentration: 2.25

mM). The mixture was incubated for 4 h at 37 ˚C. After this time, 700 μL of MeOH was added to the Eppendorf tube, which was then vortexed and kept at 4 °C overnight. After centrifugation (10,000 rpm for 3 min), the supernatant was transferred to HPLC vials and 25 μL were injected in to HPLC.

Analyses were performed with an Alliance apparatus coupled to a fluorescence detector using a C18 reversed-phase column eluted with 15% H_2O and 8% acetonitrile, both with a 0.1% trifluoroacetic acid, flowing at 1 mL/min. The detector was set at an excitation wavelength of 470 nm and the emission wavelength at 530 nm. Each sample was run for up to 15 min.

The calculated **dhCerNBD** conversion at each PR280 concentration is presented in Table 8.1.

Table 8.1. concentration-dependence effect of PR280 in the conversion of dhCerNBD by Des1.

Entry	PR280 Concentration (μM)	dhCerNBD conversion(%DMSO)					
1	0.01	98.31	98.64	103.05	96.31	101.57	102.12
2	0.1	70.08	68.01	65.97	76.43	75.13	70.64
3	0.6	52.46	54.5	47.37			
4	1.2	45.32	36.72	37.5	46.86	51.6	51.4
5	2.5	32.1	25.19	33.19	33.88	35.75	38.87
6	5	14.72	14.53	21.05	17.21	20.02	21.78
7	10	15.1	14.57	8.96	13.97	9.87	9.4

8.4 Computational studies

8.4.1 Building of Fe_2O_2-Des1 system

There are no *apo* or *holo* X-ray crystal structures of human Sphingolipid delta(4)-desaturase (DES1) but a high-accuracy prediction of the 3D structure of the protein was achieved by AlphaFold2.[4] Des1 contains a non-heme dioxo-diiron prosthetic group which catalyses the desaturation of the natural substrate.[5] It is assumed that the iron atoms are coordinated by histidine residues located in the binding pocket.[6]

The AlphaFold DES1 structure was used to build the dioxo-diiron DES1 system. First, the histidine residues involved in the coordination of the prosthetic group must be identified, nine histidine residues were located at the end of a well-defined deep pocket. The Fe_2O_2 molecule was manually placed in the pocket with 5 histidine residues (His89, His93, His262, His128, His132 and His262) coordinating iron atom 1 and 4 histidine residues (His131, His233, His263, and His259) and a glutamine residue (Glu232) coordinating iron atom 2 (Figure 1). The Fe_2O_2-DES1 complex was then prepared for docking in MOE software using the Protein preparation protocol.[7]

---

[4] a) Jumper, J.; Evans, R.; Pritzel, A.; Green, T.; Figurnov, M.; Ronneberger, O.; Tunyasuvunakool, K.; Bates, R.; Žídek, A.; Potapenko, A.; Bridgland, A.; Meyer, C.; Kohl, S. A. A.; Ballard, A. J.; Cowie, A.; Romera-Paredes, B.; Nikolov, S.; Jain, R.; Adler, J.; Back, T.; Petersen, S.; Reiman, D.; Clancy, E.; Zielinski, M.; Steinegger, M.; Pacholska, M.; Berghammer, T.; Bodenstein, S.; Silver, D.; Vinyals, O.; Senior, A. W.; Kavukcuoglu, K.; Kohli, P.; Hassabis, D. *Nature* **2021**, *596*, 583–589. b) Varadi, M.; Anyango, S.; Deshpande, M.; Nair, S.; Natassia, C.; Yordanova, G.; Yuan, D.; Stroe, O.; Wood, G.; Laydon, A.; Žídek, A.; Green, T.; Tunyasuvunakool, K.; Petersen, S.; Jumper, J.; Clancy, E.; Green, R.; Vora, A.; Lutfi, M.; Figurnov, M.; Cowie, A.; Hobbs, N.; Kohli, P.; Kleywegt, G.; Birney, E.; Hassabis, D.; Velankar, S. *Nucleic Acids Res.* **2022**, *50*, 439-444. c) AlphaFold by EMBL-EBI. AlphaFold: O15121. https://alphafold.ebi.ac.uk/entry/O15121 (accessed December 1, 2023).

[5] Savile, C. K., Fabriàs, G.; Buist, P. H. *J. Am. Chem. Soc.* **2001**, *123*, 4382-4385.

[6] Nogueira, M. L. C.; Pastore, A. J.; Davidson, V. L. *Arch. Biochem. Biophys.* **2021**, *705*, 108917.

[7] Molecular Operating Environment (MOE), 2019.01; Chemical Computing Group ULC, 1010 Sherbooke St. West, Suite #910, Montreal, QC, Canada, H3A 2R7, 2021.

8.4.2 Molecular docking of ceramide analogs (dhCer, GT11, XM462, 1b, 2b, 3b, PR280, 46b, 124 and 124')

The specific active enantiomers ((R, S) or (S, R)) of inhibitors (GT11 and XM462), natural substrate (dhCer) and synthetized compounds (**1b**, **2b**, **3b**, **PR280**, **79**, **80** and **80'**) were drawn in MOE and underwent ligand preparation using Corina version 4.3.0 software,[8] openbabel 3 version 3.0.0[9] and ChemAxon software.[10] After the preparation steps, the rDock software[11] was used in Fe_2O_2-Des1 system for cavity generation and all molecules were docked in the generated binding pocket.

GT11, **XM462** and dhCer were subjected to exhaustive docking (50 independent genetic algorithm optimizations) using a free docking protocol. Each ligand's top 10 docking poses were visualised, from which the best scoring pose forming hydrogen bonds through the polar head was selected as the candidate-binding pose. This was necessary to compensate for the insufficient desolvation penalty of rDock's native scoring function. Compounds **1b**, **2b**, **3c**, **PR280**, **79**, **80** and **80'** were docked using a modified protocol that included pharmacophoric restraints to achieve the same effect. The restraints consisted of flat bottom potentials (2Å radius) for two hydrogen bond donors located near the Fe_2O_2 prosthetic group.

---

[8] Chemoinformatics ProgramPackage CORINA Classic, developed and distributed by Molecular Networks GmbH, Nuremberg, Germany and Altamira LLC, Columbus, OH, USA. www.mn-am.com.

[9] O'Boyle, N. M.; Banck, M.; James, C. A.; Morley, C.; Vandermeersch, T.; Hutchison, G. R. *J. Cheminform.* **2011**, *33*, 1-14.

[10] ChemAxon software was used for drawing, displaying and characterizing chemical structures, ChemAxon (https://www.chemaxon.com).

[11] Ruiz-Carmona, S.; Álvarez-García, D.; Foloppe, N.; Garmendia-Doval, A. B.; Juhos, S.; Schmidtke, P.; Barril, X.; Hubbard, R. E.; Morley, S. D. *PLoS Comput. Biol.* **2014**, *10*, e1003571.

8.4.3 Proposal of a second generation PR280 ceramide analogues via *in silico* optimization using Fe_2O_2-Des1 system 3D model.

PR280 analogs were docked using the same docking protocol as previously synthesized ceramide analogs (**1b**, **2b**, **3c**, **PR280**, **79**, **80**, and **80'**), but with the addition of tethering corresponding to the rigid scaffold and polar head of the reference docking pose obtained for the reference ligand **PR280**.

Table 8.2. Top 45 ranked PR280-analogs in the virtual screening of cyclopropenone containing ceramide analogs virtual library.

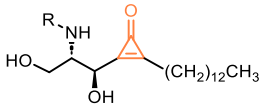

PR280-X

Rank	R	Score	Observed interactions
1	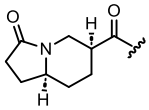	-23.164	
2	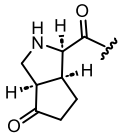	-22.925	
3	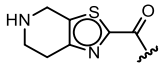 **PR280-1**	-22.612	- Parallel displaced π-stacking (Tyr170) - H-bond: NH-carbonyl backbone
4	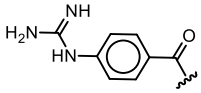 **PR280-2**	-22.548	- Parallel displaced π-stacking (Tyr170) - H-bond: NH-carbonyl backbone
5	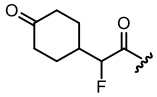	-21.420	- H-bond: NH-Carbonyl (amide backbone) - Fluor in non-polar environment
6	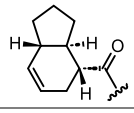	-21.376	

7	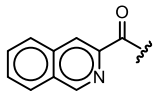 PR280-3	-21.199	- Parallel displaced π-stacking (Tyr170)
8	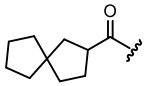 PR280-8	-20.955	- Aliphatic compound in a in a non-polar environment.
9	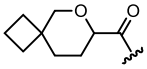 PR280-5	-20.887	- H-bond: OH-O (Tyr 120)
10	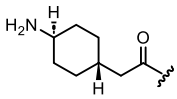	-20.743	- Weak H-bond: NH_2-aromatic ring (Tyr120)
11	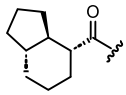	-20.515	
12	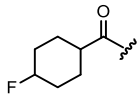	-20.506	- Fluor in non-polar environment
13	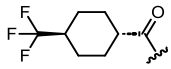 PR280-9	-20.383	- Aliphatic groups in a in a non-polar environment.
14	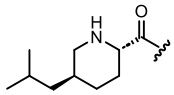	-20.205	- H-bond: OH-N (Tyr120)
15	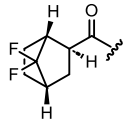	-20.178	- H-bond: OH-F (Tyr120) - CF_2 in an apolar enviroment
16	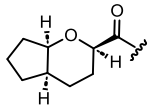	-20.090	- H-bond: OH-O (Tyr120)
17	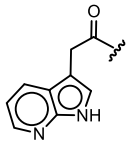	-20.090	- Weak H-bond: NH - carbonyl backbone
18	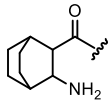	-20.044	- Weak H-bond: NH - carbonyl backbone
19	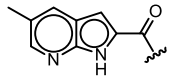	-19.931	

20	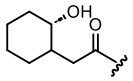	-19.895	
21	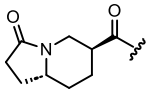 PR280-6	-19.856	
22	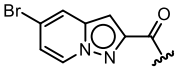	-19.843	
23	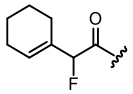	-19.842	
24	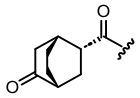	-19.806	
25	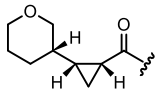	-19.781	
26	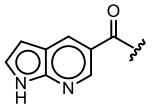 PR280-4	-19.697	- Parallel displaced π-stacking (Tyr170) - H-bond: NH-carbonyl backbone
27	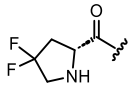 PR280-7	-19.687	- Weak H-bond: NH-π (Tyr170) - *gem*-difluoro group in a non-polar environment.
28	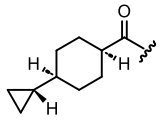	-19.675	
29	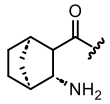	-19.625	
30	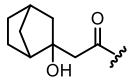	-19.603	
31	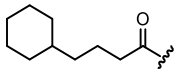 PR280-10	-19.512	- Aliphatic compound in a in a non-polar environment.
32	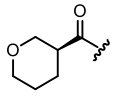	-19.511	
33	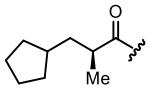	-19.454	

34	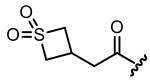	-19.408	
35	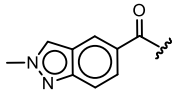	-19.398	
36	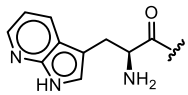	-19.343	- H-bond: NH (pyrrole)-carbonyl backbone
37	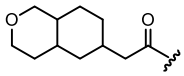	-19.219	
38	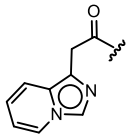	-19.185	- H-Bond: OH-N (Tyr120) - π-stacking interaction
39	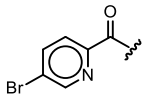	-19.087	
40	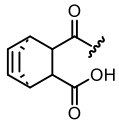	-19.078	
41	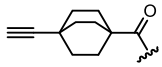	-19.073	
42	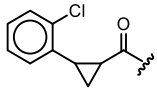	-19.029	- π-stacking interaction
43	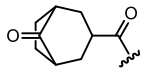	-19.023	
44	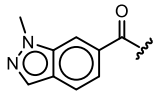	-19.007	
45	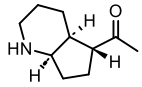	-18.932	

8.5 X-ray crystallographic data.

8.5.1 Data collection

Crystal structure determination for samples 2c and PR280 were carried out using an Apex DUO Kappa 4-axis goniometer equipped with an APPEX II 4K CCD area detector, a Microfocus Source E025 IuS using $Cu_{K\alpha}$ radiation, Quazar MX multilayer Optics as monochromator and an Oxford Cryosystems low temperature device Cryostream 700 plus (T = –173 °C). Full-sphere data collection was used with ω and ϕ scans. Programs used: Data collection APEX-2,[12] data reduction Bruker Saint[13] V/.60A and absorption correction SADABS.[14]

8.5.2 Structure solution and refinement

Crystal structure solution was achieved using the computer program SHELXT.[15] Visualization was performed with the program SHELXle.[16] Missing atoms were subsequently located from difference Fourier synthesis and added to the atom list. Least-squares refinement on F2 using all measured intensities was carried out using the program SHELXL 2015.[17] All non-hydrogen atoms were refined including anisotropic displacement parameter.[18]

---

[12] Data collection with APEX II version v2013.4-1. Bruker (**2007**). Bruker AXS Inc., Madison, Wisconsin, USA.

[13] Data reduction with Bruker SAINT version V8.30c. Bruker (**2007**). Bruker AXS Inc., Madison, Wisconsin, USA

[14] SADABS: V2012/1 Bruker (**2001**). Bruker AXS Inc., Madison, Wisconsin, USA. *Blessing, R. H. Acta Cryst.* **1995**, A51, 33–38.

[15] SHELXT; V2014/4 (Sheldrick 2014). Sheldrick, G. M. *Acta Cryst.* **2015**, A71, 3-8.

[16] SHELXle; Huebschle, C. B.; Sheldrick, G. M.; Dittrich B. J. *Appl. Cryst.* **2011**, *44*, 1281-1284.

[17] SHELXL; SHELXL-2014/7 (Sheldrick 2014). Sheldrick, G. M. *Acta Cryst.* **2015**, C71, 3-8.

[18] Flack H.D., Acta Cryst. A39 (1983) 876, Parsons S., Flack H., Acta Cryst. A39 (2004) S61, Parson, Flack and Wagner, Acta Cryst. B69 (2013) 249-259; E.C. Escudero-Adán, J. Benet-Buchholz, P. Ballester; Acta Cryst. (2014) B70, 660-668.

***N*-((1*S*,2*S*)-1,3-dihydroxy-1-(1-tridecyl-1H-1,2,3-triazol-5-yl)propan-2-yl)undecanamide (2c)**

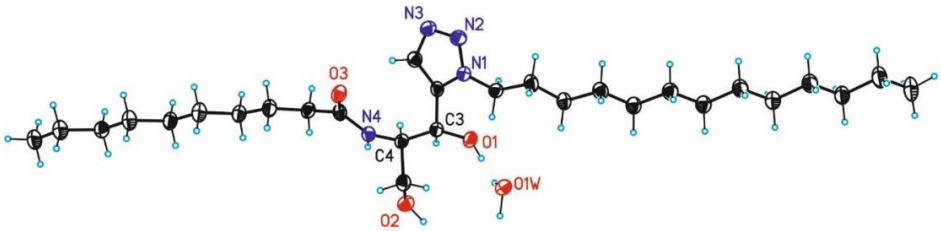

Figure 8.1. Ortep-Drawing (thermal ellipsoids draw at 50% level) showing the structure of **2c**.

Comments on the structure (2c): This compound crystallizes in the orthorhombic chiral space group $P2_12_12_1$. The asymmetric unit contains one molecule of the organic compound and one water molecule (hydrate). Although the crystal measured was of extremely small dimensions (0.01 x 0.02 x 030 $Å^3$), the structure was of enough quality for the absolute structure determination. The absolute structure could be determined reliable based on two methodologies. Since one of the two chiral centers has a known absolute configuration, the absolute configuration of the second chiral center was determined relatively to the first one. Also, the direct assignment of the absolute structure using the Flack value based on Parsons' quotients, confirmed the right stereochemistry, obtaining a value of -0.001(13) (Flack X determined using 1539 quotients [(I+)-(I-)]/[(I+)+(I-)]). The Flack (Parsons) parameter value for the correct absolute structure determination should be 0; the inverted structure would give 1; always taking in account the standard deviation which should be below 0.1. In this case of the measured structure, the standard deviation is 0.13, but having confirmation in respect to the relative configuration, the Flack parameter based on Parsons' Quotients was considered good enough to confirm the stereochemistry. The absolute configuration based on the relative assignment and the absolute structure of the measured crystal based of the Flack Parameter, was determined as: ***S*(C3),*S*(C4)**. The CIF-file was submitted with a commented B-alert related to the low data completeness which reached 94.3 %.

***N*-((1*R*,2*S*)-1,3-dihydroxy-1-(3-oxo-2-tridecylcycloprop-1-en-1-yl)propan-2-yl)octanamide (PR280)**

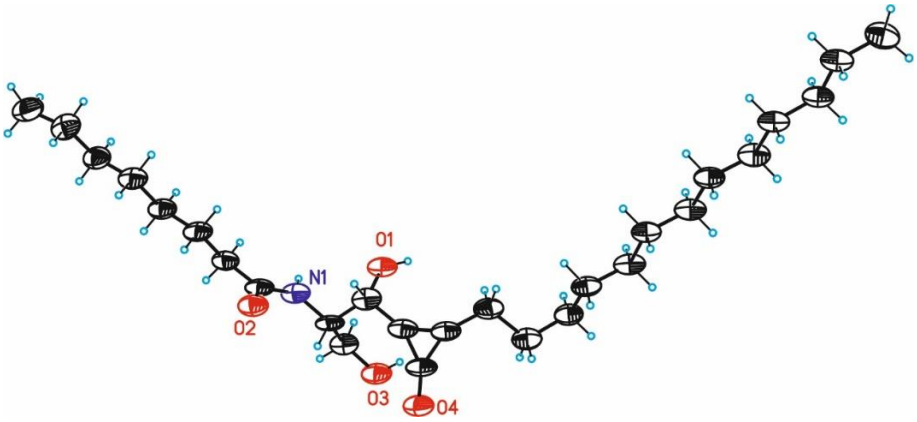

Figure 8.2. Ortep-Drawing (thermal ellipsoids draw at 50% level) showing the structure of **PR280**.

Comments on the structure (PR280): This sample was very difficult to measure, since the crystals were extremely thin and bended in a curved manner. We measured several crystals until, after sticking a fragment of a crystal on Kapton-foil, we could obtain a dataset of acceptable quality to obtain the structure. Due to the bending of the crystals and the resulting deformation of the reflections collected, it was impossible to determine the absolute configuration of the molecule. The structure was considered is of acceptable quality for publication. The CIF-file was submitted with a commented B-alert related to the low precision on C-C bonds.

SECTION 2: Development of a Ru-catalyzed RCM reaction on CPG-coupled DNA for the Synthesis of DNA-encoded Macrocyclic Library

8.6 General considerations

Unless otherwise noted, chemicals were purchased from abcr, Acros Organics, Alfa Aesar, Fisher Scientific, Merck, Sigma Aldrich, TCI and VWR and were used as provided without further purifications. Dry solvents (DMA, DMF, DMSO, toluene) were used as commercially available.

5'-Aminolinker-modified DNA oligonucleotides on controlled pore glass solid support (CPG, 1000 Å porosity) were synthesized by IBA (Göttingen, Germany). CPG with oligonucleotide-small molecule conjugates were filtered and washed through synthesis columns using a vacuum manifold (Vac-Man®) from Promega.

Semi-preparative ion pair RP-HPLC. Compound purification was performed on a Shimadzu Prominence HPLC System equipped with a C18 stationary phase (Phenomenex, Gemini, 5 μm, C18, 110 Å, 100 x 4.6 mm). A gradient from 100 mM aqueous triethylammonium acetate (pH = 8.0, eluent A) to MeOH (eluent B) was used at a flow rate of 5 mL/min. Fractions containing the desired product were pooled and concentrated.

Method: Step gradient of 20% to 70% B within 13 min, then 70% to 100% B within 1 min followed by 100% B for 3 min using 100 mM aqueous triethylammonium acetate (pH = 8.0, eluent A) and MeOH (eluent B) at a flow rate of 5 mL/min.

Analytical RP-HPLC. HPLC analysis was performed on an Agilent 1100 series chromatograph equipped with 1100 Quaternary Pump (G1311A), a 1100 Multi-Wavelength Detector (G1365B) and an Agilent Eclipse Plus C18

(4.6 x 100 mm, 3.5 μm) column. The purity of DNA conjugates were determined by integration of peaks recorded at 254 nm wavelength.

Method: Step gradient of 10% to 70% B within 10 min, then 70% to 100% B within 2 min followed by 100% B for 2 min using 10 mM aqueous triethylammonium acetate (pH = 8.0, eluent A) and MeOH (eluent B) at a flow rate of 0.6 mL/min.

MALDI-TOF. Mass analysis was performed on a MALDI TOF/TOF MS from Bruker Daltonicsusing 2′,4′,6′-trihydroxyacetophenone (THAP) matrix (Dichrom). Incubation experiments of Ru-catalysts with CPG-DNA.

8.7 Synthetic procedures

DMT deprotection (GP1)

DMT-protecting group of CPG-bound oligonucleotide (250 nmol, 9-10 mg of solid phase material) was removed by addition of 200 μL 3% trichloroacetic acid in CH_2Cl_2 for 1 min. Orange colouring of the solution is observed during the reaction and indicated successful removal of protecting group. The deprotection was repeated 3-5 times until no further coloring of the solution was observed. CPG-bound deprotected DNA was washed three times with each 200 μL of 1% TEA in ACN, DMF, MeOH, ACN and CH_2Cl_2 and dried *in vacuo*.

Amide coupling (GP2)

CPG-coupled oligonucleotide, carboxylic acid and HATU were dried *in vacuo* for 30 min. Stock solutions of all reactants in dry DMF were prepared before the reaction was started. To the solution of the acid (40 μmol,100 equiv.) in dry DMF (120 μL), HATU (40 μmol, 100 equiv.) dissolved in dry DMF (120 μL) and DIPEA (100 μmol, 250 equiv.) were added. The mixture was shaken for 15 min and added to the solid support-bound DNA (20 mg, 400 nmol) suspended in dry DMF (240 μL). The amide coupling reaction was

shaken at ambient temperature for 2 hours. Then, the CPG-bound conjugate was filtered over a filter column and washed three times with each 200 μL of DMF, MeOH, ACN and CH_2Cl_2 and dried in vacuo. Amide coupling was repeated a total of three times.

Fmoc derotection (GP3)

The Fmoc-protecting group of the CPG-bound oligonucleotide (400 nmol, 20 mg) was cleaved off by addition of 400 μL 20% piperidine in dry DMF and shaking for 20 min at room temperature. Afterwards, the CPG-bound deprotected oligonucleotide was washed three times with each 200 μL of DMF, MeOH, ACN and CH_2Cl_2 and then dried *in vacuo*.

Boc deprotection (GP4)

The CPG-bound DNA conjugate was dried *in vacuo* for 15 minutes. Then it was treated with a solution of TFA (75 % in DCM) for 30 seconds. The process was repeated for a total of 8 times. Then, the CPG-bound conjugate was filtered over a filter column and washed three times with each 200 μL of DMF, MeOH, ACN and CH_2Cl_2 and dried *in vacuo*.

Ring closing metathesis (GP5)

The CPG-bound DNA conjugate was dried *in vacuo* for 15 minutes. Reaction was set up inside a golve-bag under argon atmosphere. Dry and previously degassed toluene was used in the reaction, DA catalyst (200 nmol, 10 equiv.) suspended in toluene (10 μL) was additioned over the CPG-bound DNA (20 nmol, 1 equiv.) suspended in toluene (40 μL). The resulting mixture was stirred outside the Glove-bag for 30 min at r.t.

Afterwards, the CPG-bound oligonucleotide was washed three times with each 200 μL of DMF, MeOH, ACN and CH_2Cl_2 and then dried *in vacuo*. Then, the CPG-bound DNA was suspended in KTP solution in THF (0.5 M) and stirred at r.t. overnight. After this time, reaction mixture was washed

three times with each 200 μL of DMF, MeOH, ACN and CH_2Cl_2 and then dried *in vacuo*.

8.8 Synthesis of CPG-DNA diene conjugates

Synthesis of CPG-DNA diene conjugates 5-8.

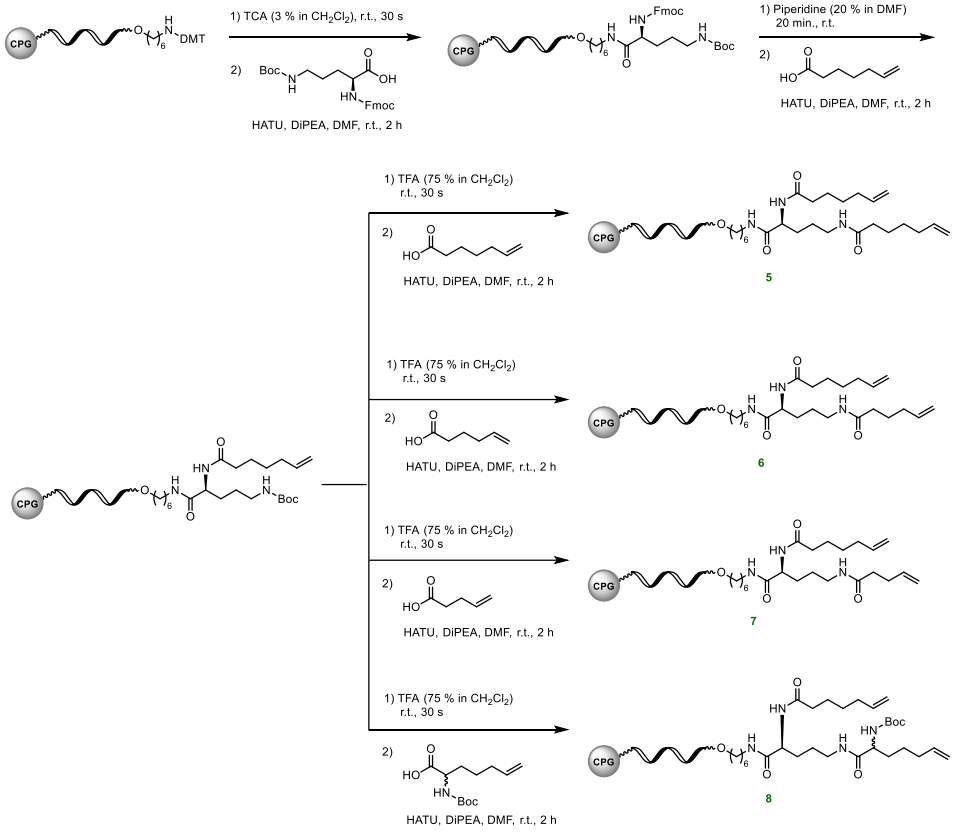

Synthesis of CPG-DNA diene conjugate 9

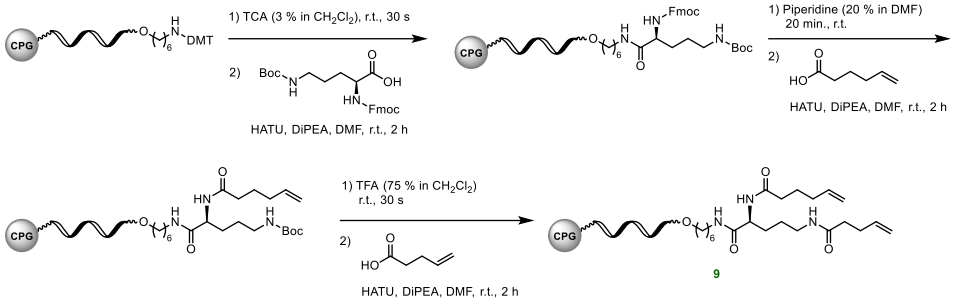

Synthesis of CPG-DNA diene conjugate 10

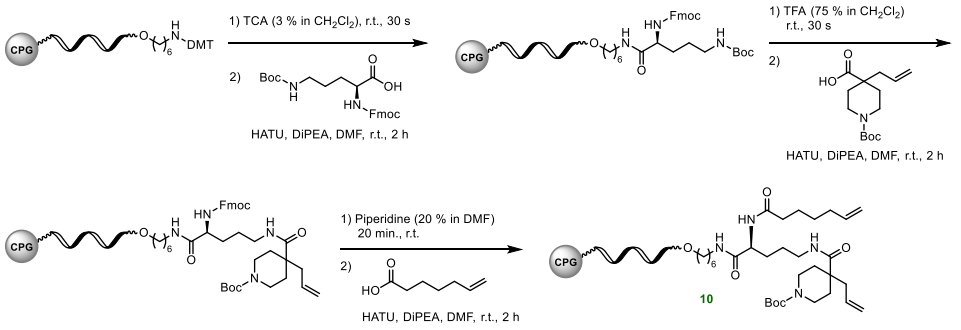

Synthesis of CPG-DNA diene conjugate 11

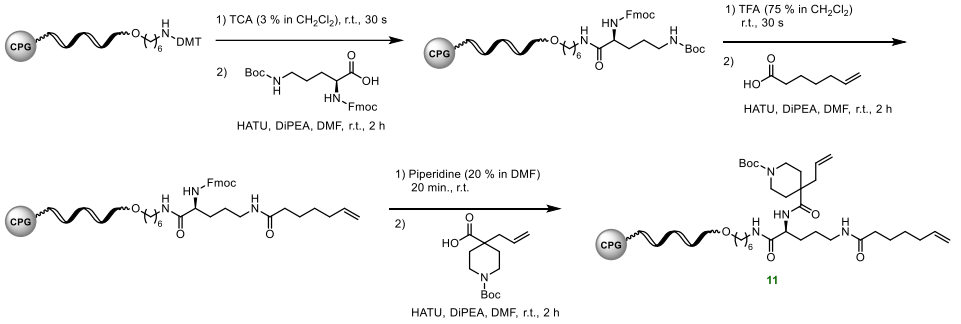

Synthesis of CPG-DNA diene conjugate 12

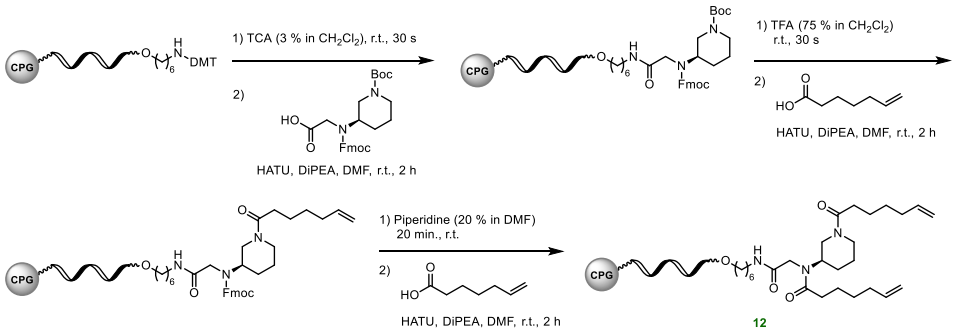

Synthesis of CPG-DNA diene conjugate 13

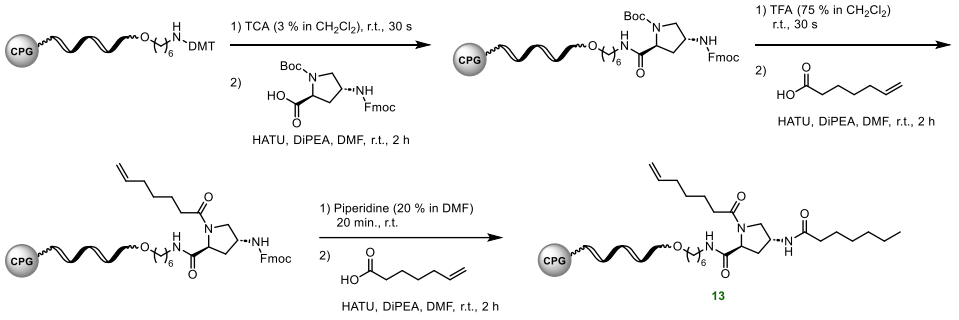

8.9 Compound identification

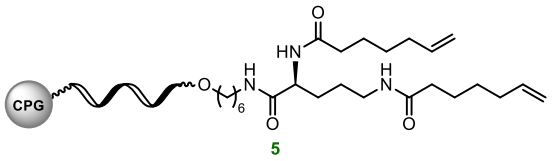

M calculated: 3420,24
$[M+H]^+$ found: 3419.622

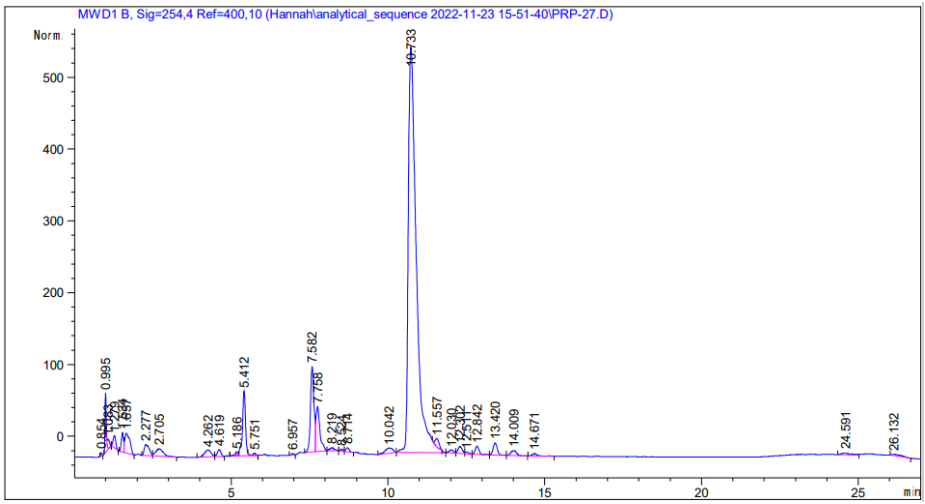

HPLC trace of crude reaction mixture **5**.

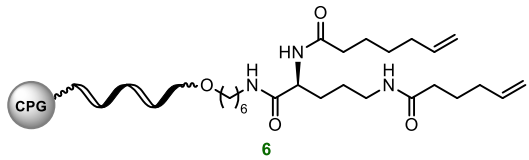

6

M calculated: 3406,22
$[M+H]^+$ found: 3409.610

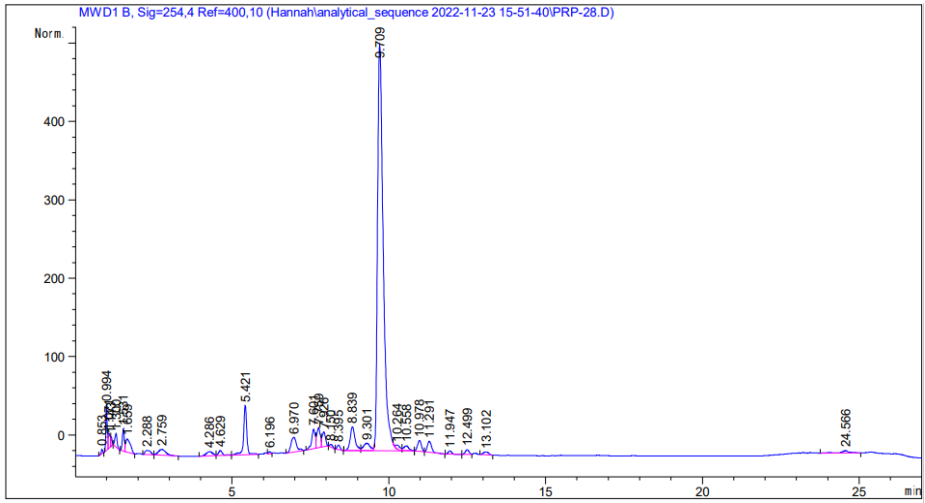

HPLC trace of crude reaction mixture **6**

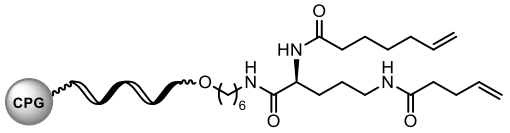

7

M calculated: 3392,2
$[M+H]^+$ found: 3392.314

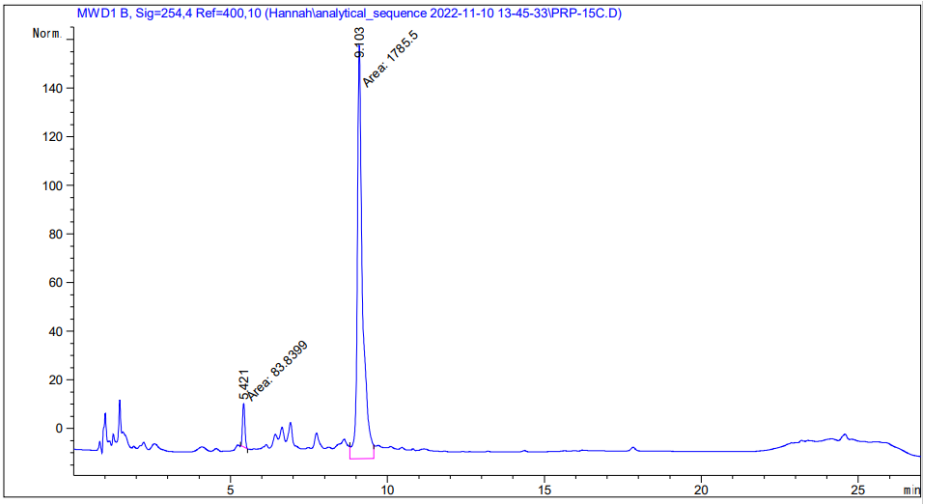

HPLC trace of crude reaction mixture **7**

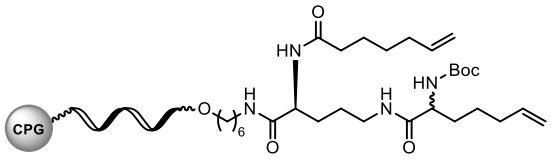

8

M calculated: 3535,3
$[M+H]^+$ found: 3535.007

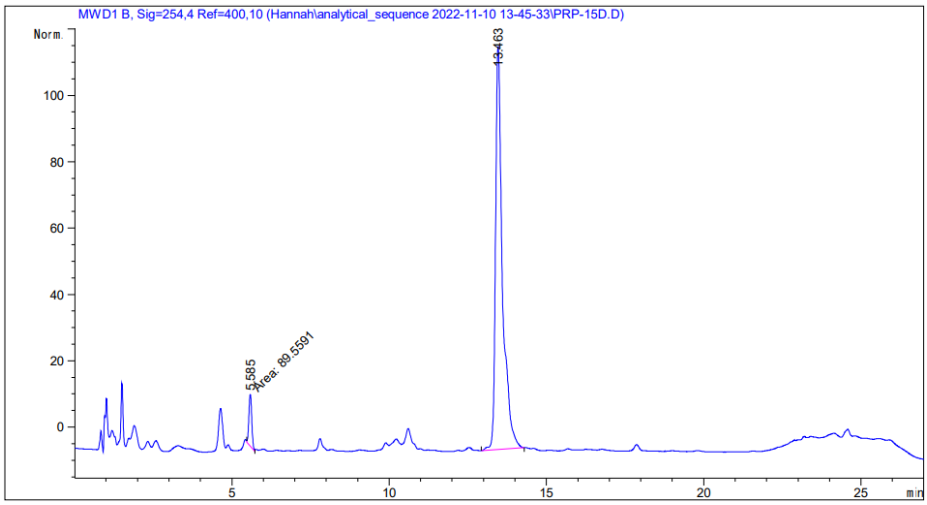

HPLC trace of crude reaction mixture **8**

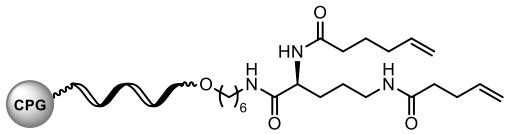

9

M calculated: 3378,19
$[M+H]^+$ found: 3377.411

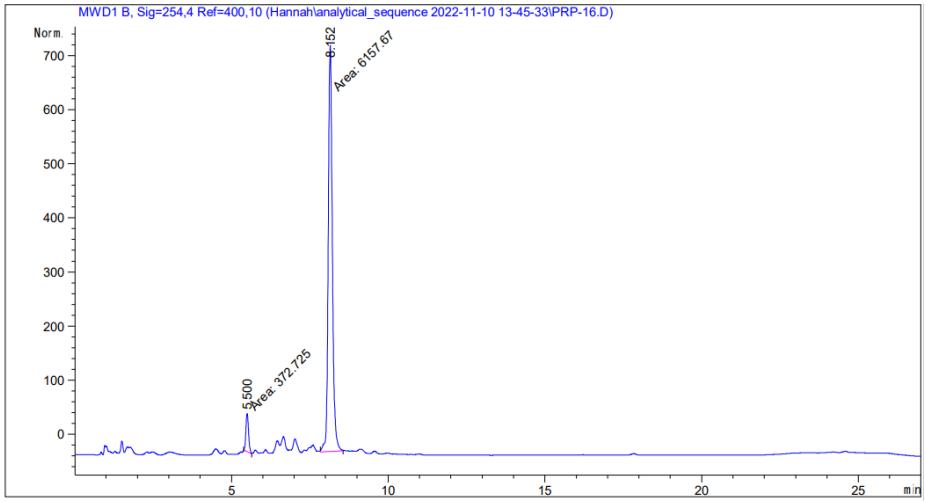

HPLC trace of crude reaction mixture **9**

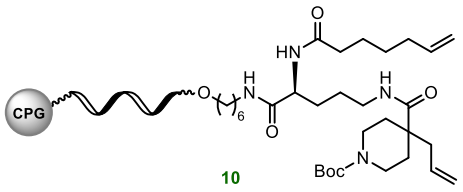

10

M calculated: 3561,32
$[M+H]^+$ found: 3564.436

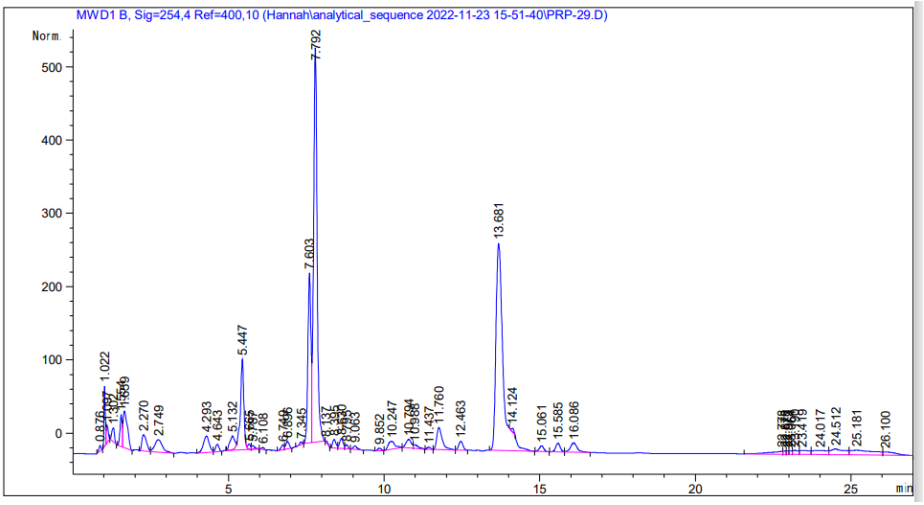

HPLC trace of crude reaction mixture **10**.

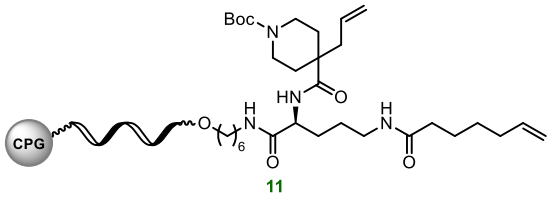

11

M calculated: 3561,32
$[M+H]^+$ found: 3561.311

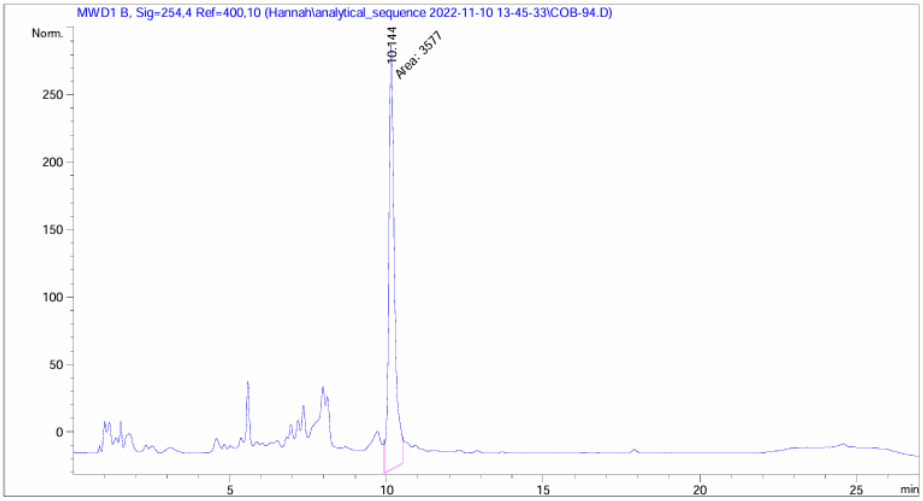

HPLC trace of crude reaction mixture **11**.

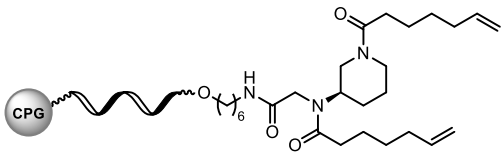

12

M calculated: 3446,25
$[M+H]^+$ found: 3445.730

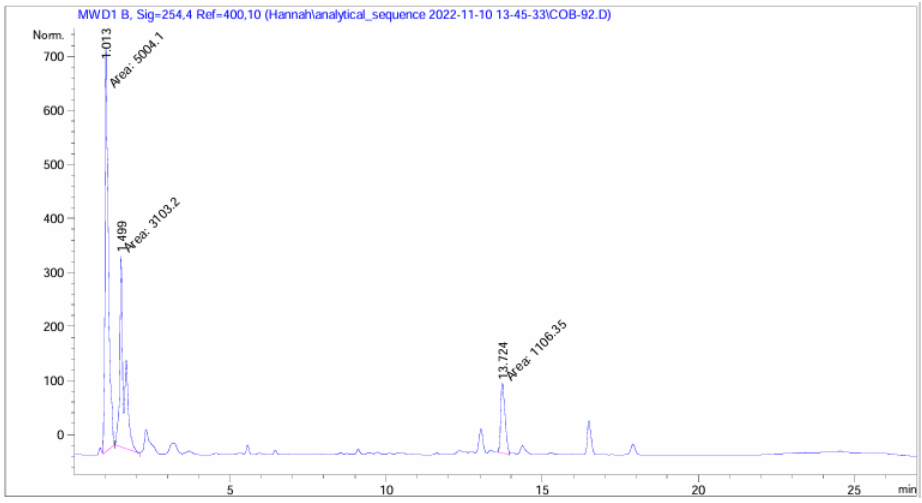

HPLC trace of crude reaction mixture **12**.

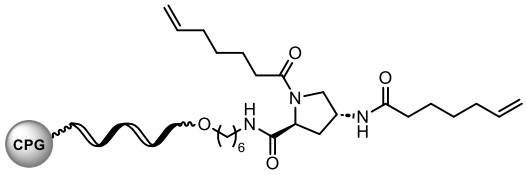

13

M calculated: 3418,22
$[M+H]^+$ found: 3417.694

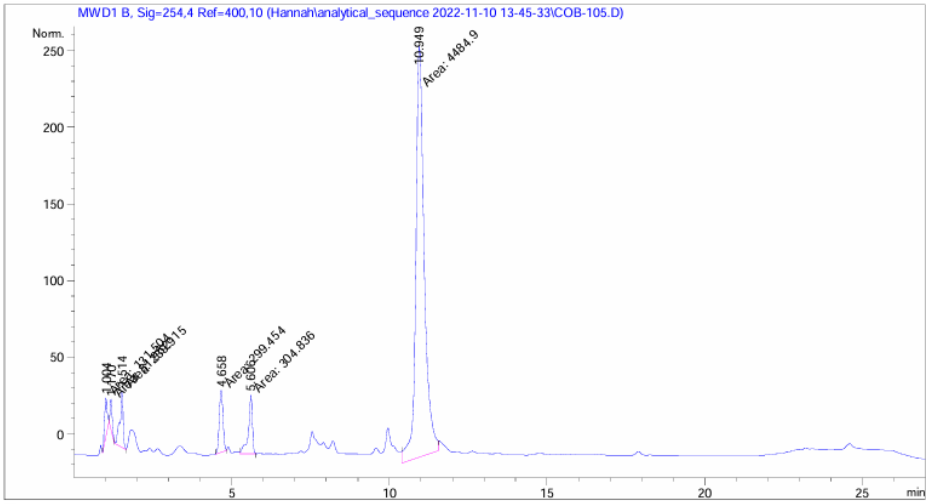

HPLC trace of crude reaction mixture **13**.

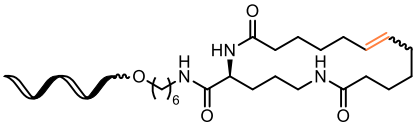

14

M calculated: 3390.4

M found: 3391.742

37.748 µM

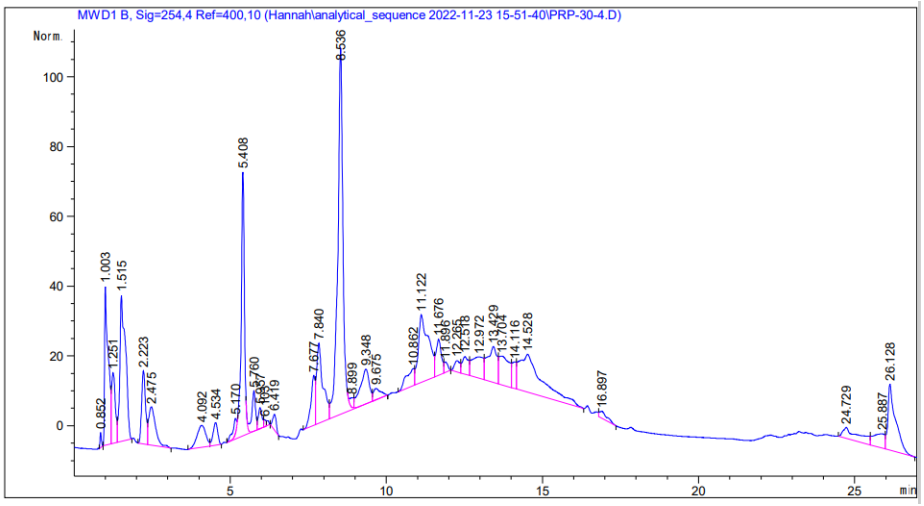

HPLC trace of crude reaction mixture **14**

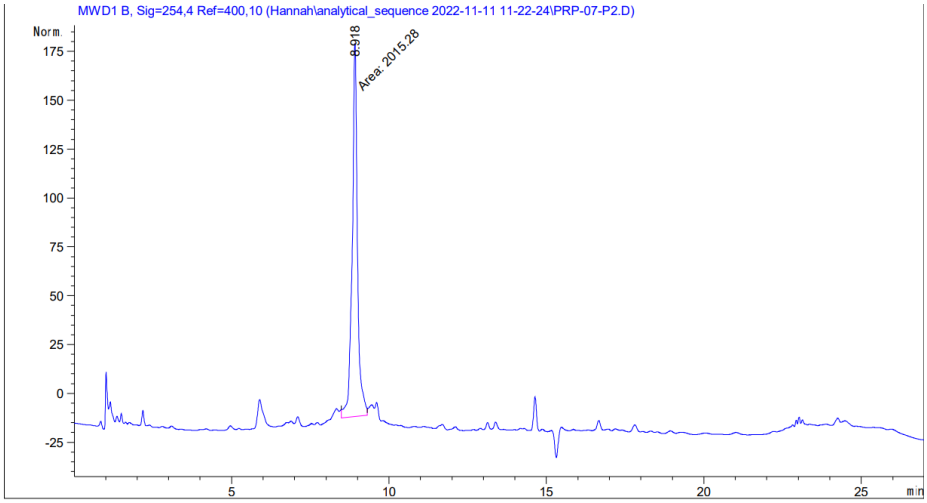

HPLC trace of isolated product **14**

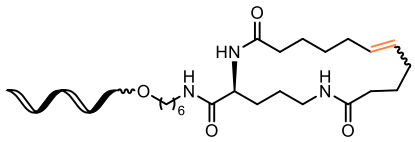

15

M calculated: 3376.4

M found: 3378.575

56.168 µM

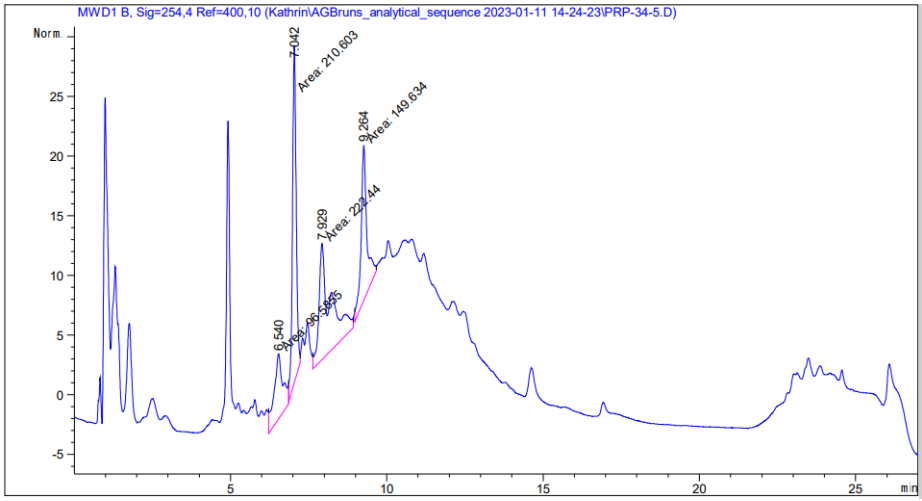

HPLC trace of crude reaction mixture **15**

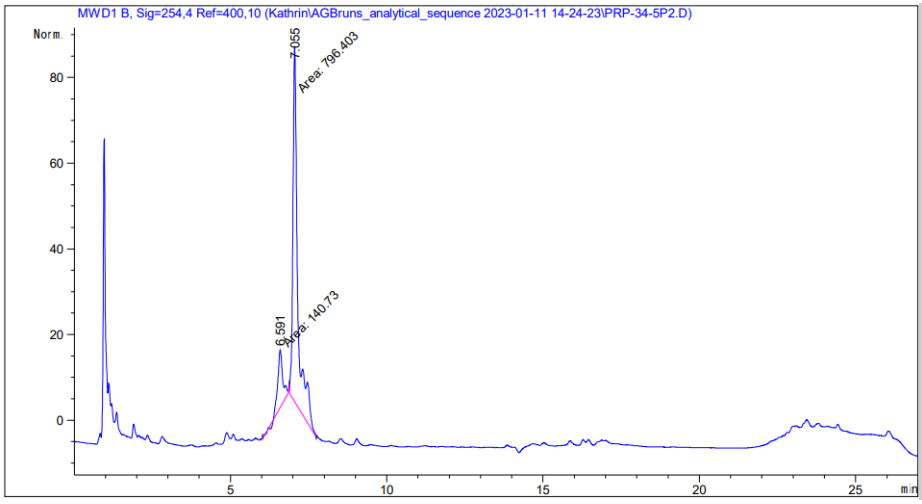

HPLC trace of isolated product **15**

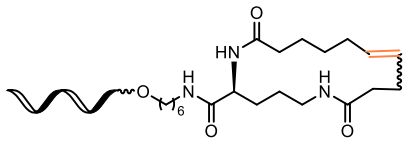

16

M calculated: 3362.4

M found: 3364.287

34.718 µM

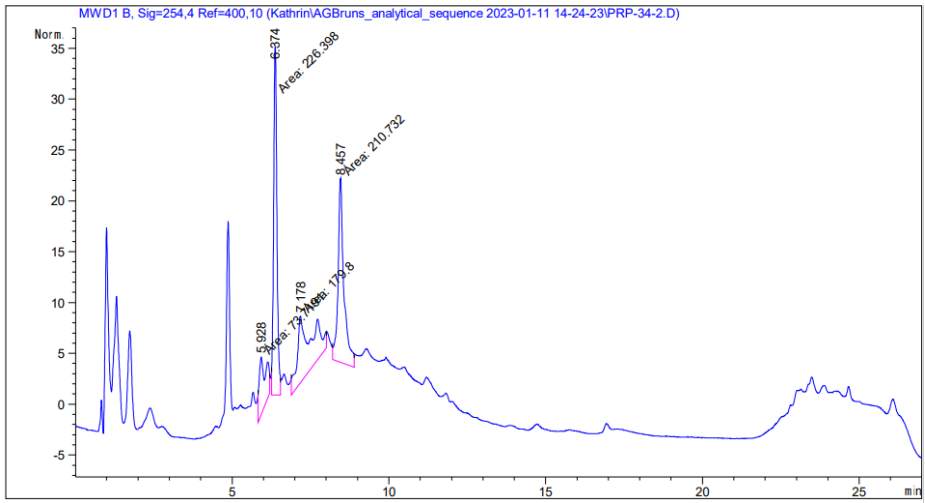

HPLC trace of crude reaction mixture **16**

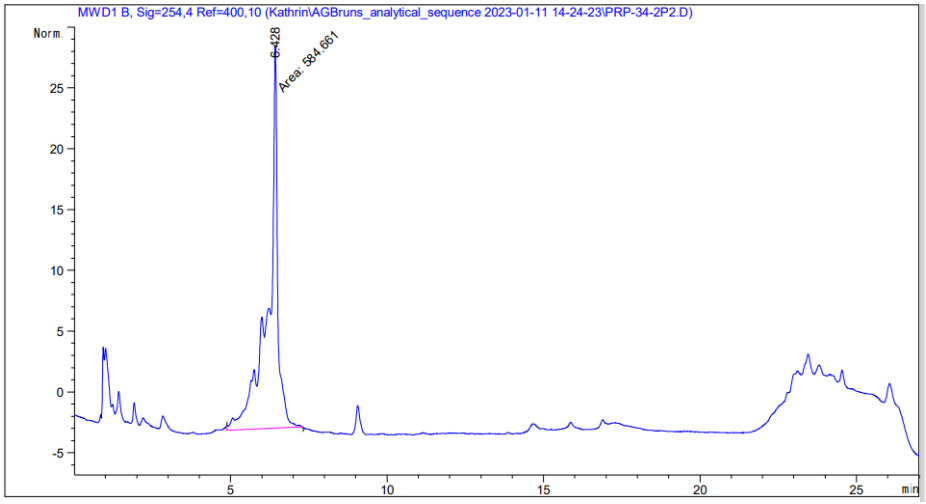

HPLC trace of isolated product **16**

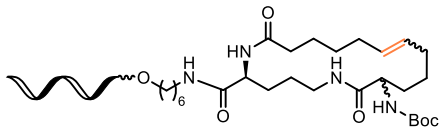

17

M calculated: 3505.6 g/mol

M found: 3506.535

66.058 µM

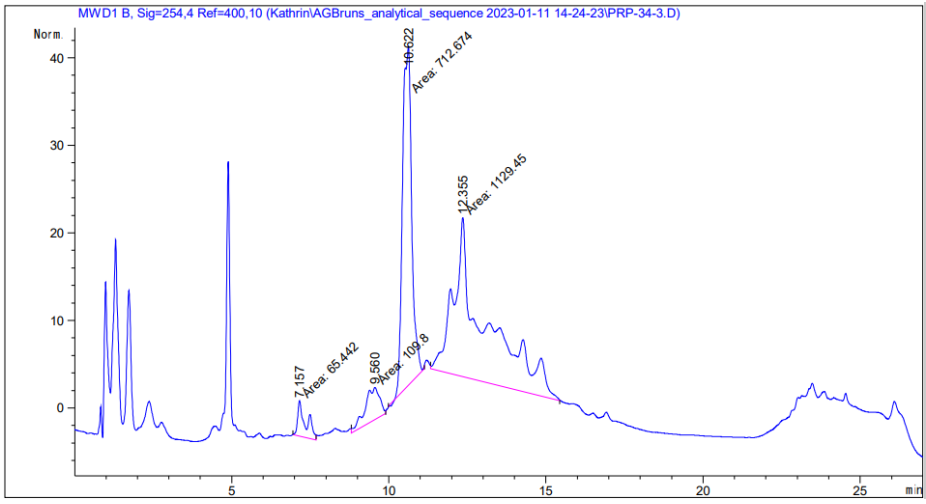

HPLC trace of crude reaction mixture **17**

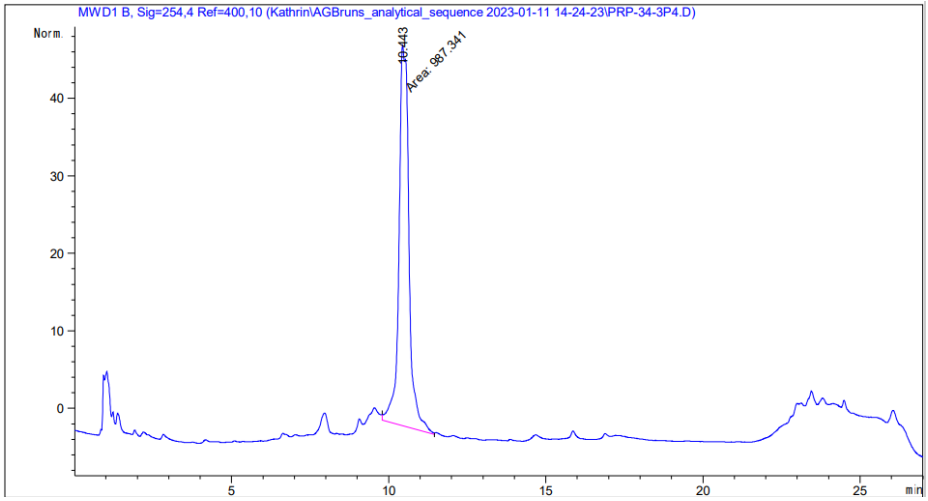

HPLC trace of isolated product **17**

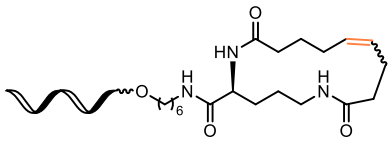

18

M calculated: 3348.3

M found: 3381.551

44.945 µM

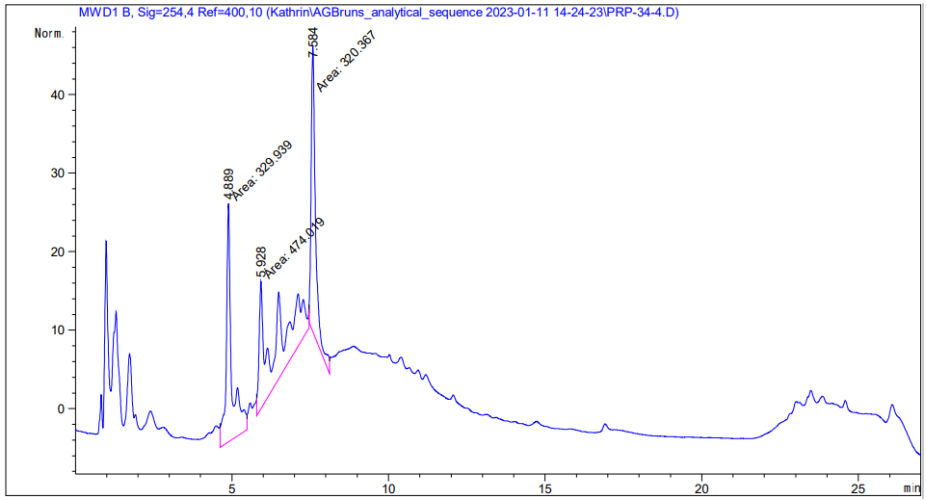

HPLC trace of crude reaction mixture **18**

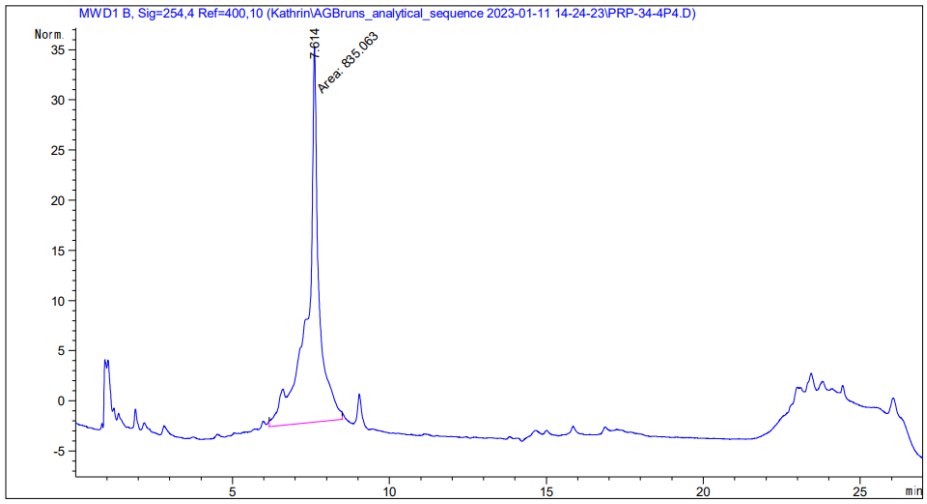

HPLC trace of isolated product **18**

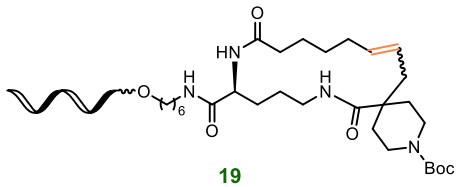

19

M calculated: 3531.6

M found: 3531.474

103.586 µM

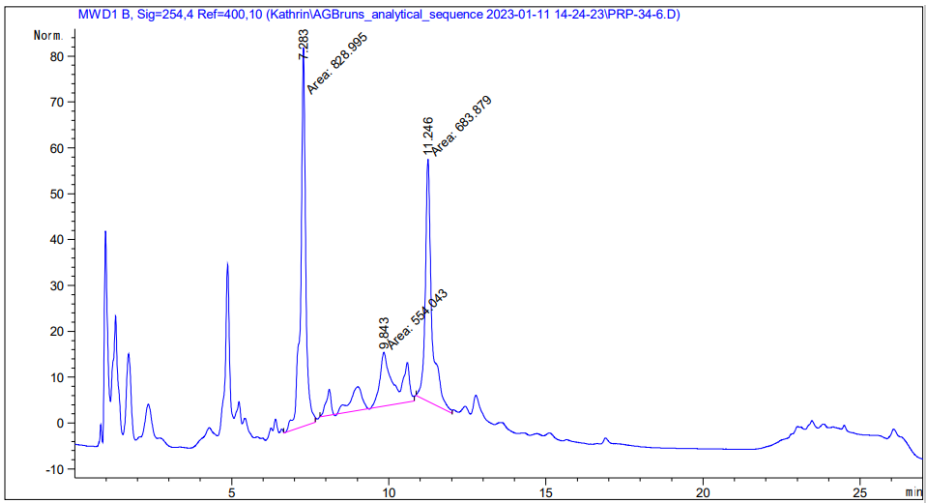

HPLC trace of crude reaction mixture **19**

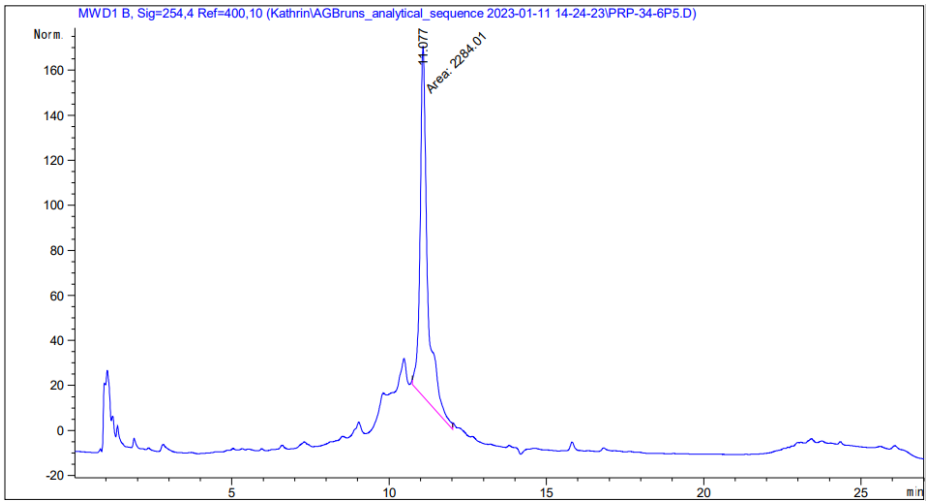

HPLC trace of isolated product **19**

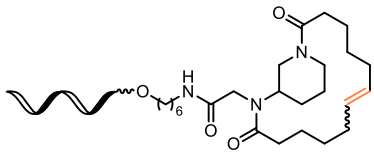

20

M calculated: 3416.5

M found: 3416.98

Not detected after purification

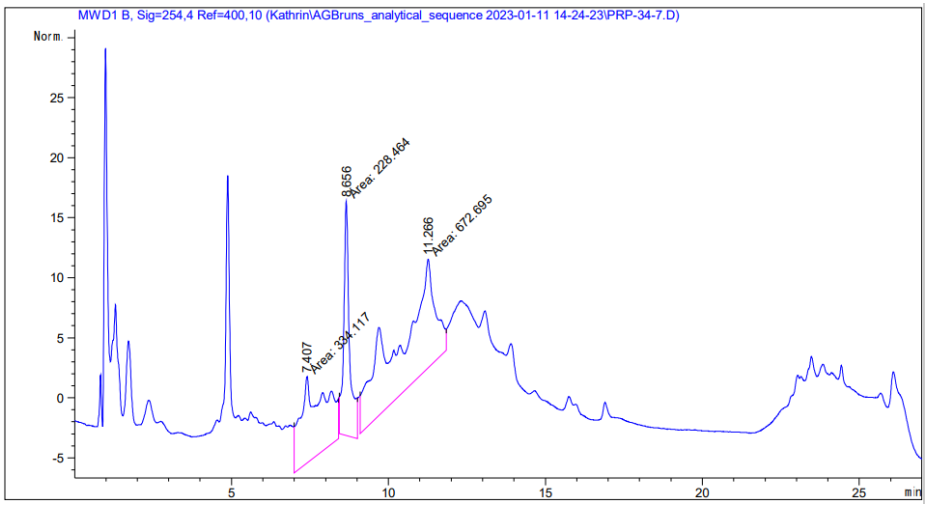

HPLC trace of crude reaction mixture **20**

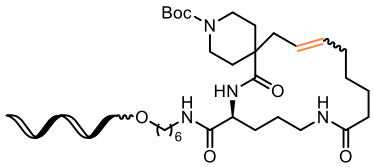

21

M calculated: 3531.6

M found: 3532.098

Not detected after purification

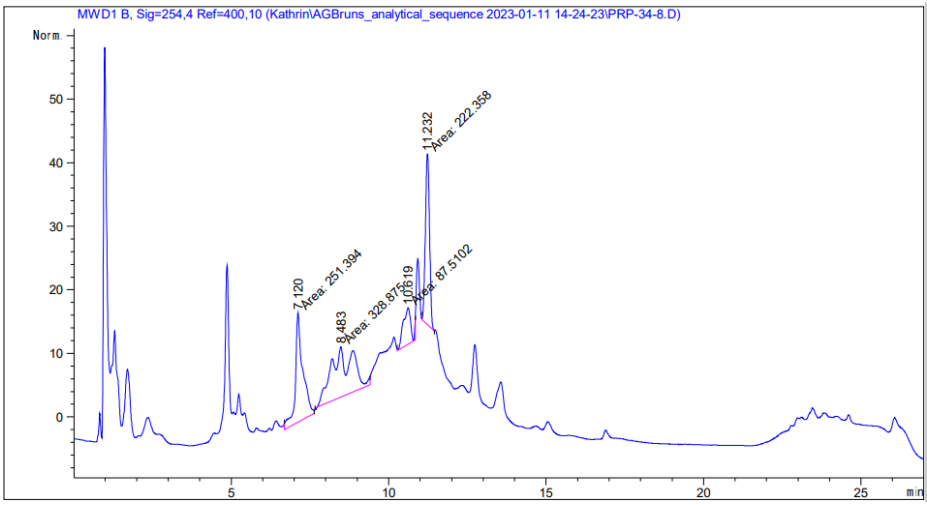

HPLC trace of crude reaction mixture **21**

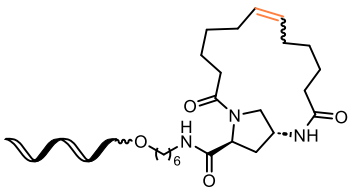

22

Mcalculated: 3388.4

$[M+H]^+$ found: 3389.569

17.191 µM

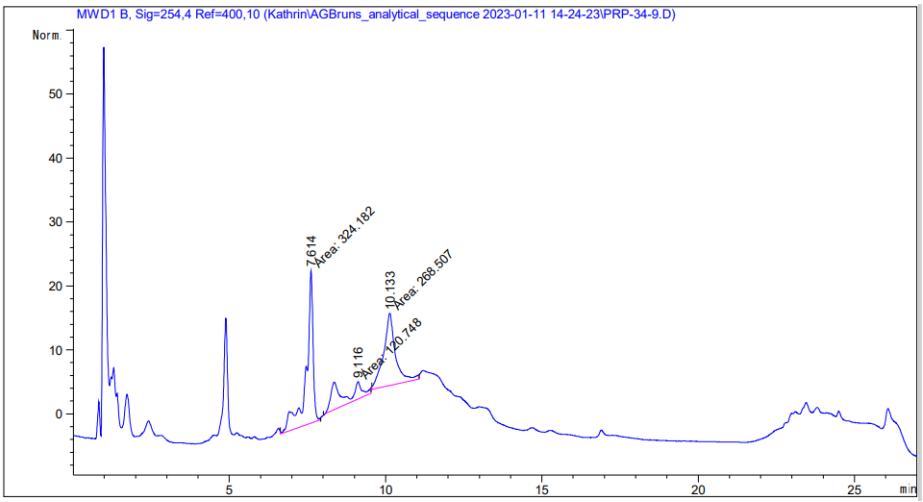

HPLC trace of crude reaction mixture **22**

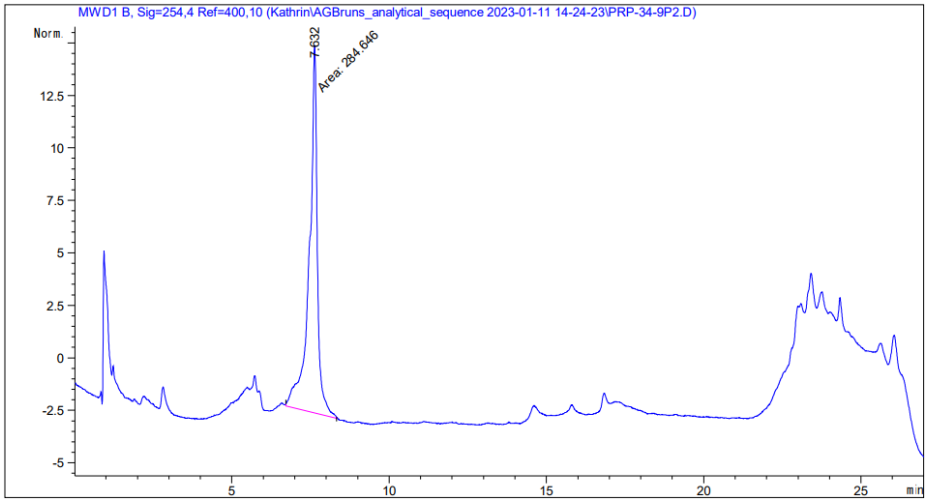

HPLC trace of isolated product **22**

UNIVERSITAT ROVIRA I VIRGILI
TARGETING DES1: SYNTHESES OF CERAMIDE ANALOGUES WITH A RIGID SCAFFOLD, INHIBITORY ASSAYS, AND AF2-ASSISTED STRUCTURAL INSIGHTS REVEAL PR280 AS A POTENT INHIBITOR
Pablo Rivero Prieto

ANNEX

UNIVERSITAT ROVIRA I VIRGILI
TARGETING DES1: SYNTHESES OF CERAMIDE ANALOGUES WITH A RIGID SCAFFOLD, INHIBITORY ASSAYS, AND AF2-ASSISTED STRUCTURAL INSIGHTS REVEAL PR280 AS A POTENT INHIBITOR
Pablo Rivero Prieto

NMR spectra

(S)-*tert*-butyl 4-((*R*)-1-hydroxyprop-2-yn-1-yl)-2,2-dimethyloxazolidine-3-carboxylate (14)

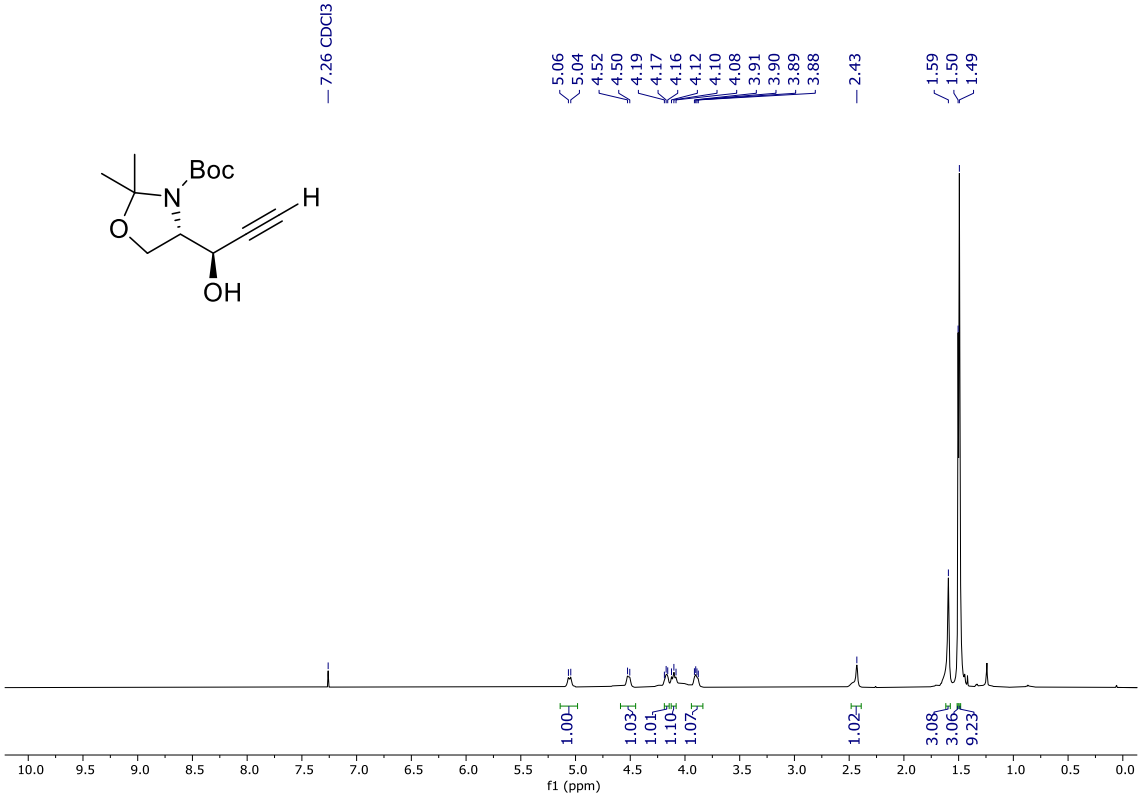

^{1}H NMR (400 MHz, $CDCl_3$) of **14**.

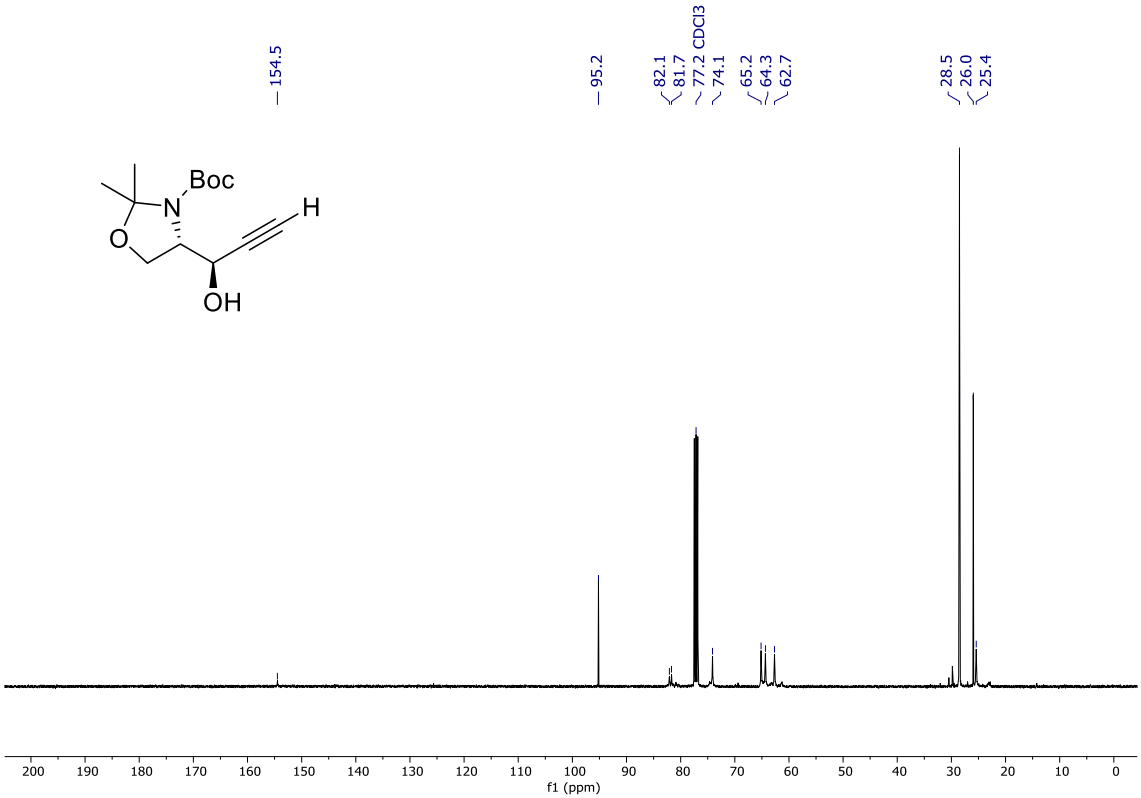

^{13}C NMR (100.6 MHz, $CDCl_3$) of **14**

***Tert*-butyl (4*S*,1'*R*)-2,2-dimethyl-4-[1'-hydroxy-3'-(trimethylsilyl)-2'-propynyl]oxazolidine-3-carboxylate (31).**

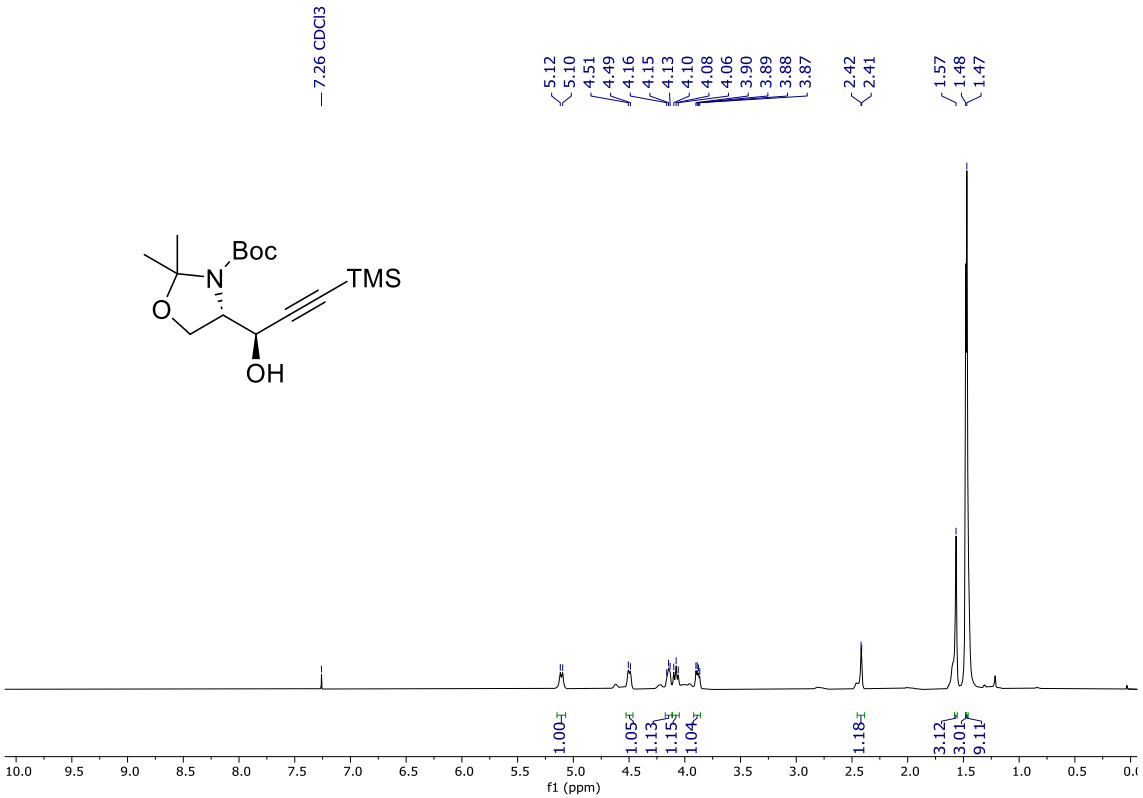

^{1}H NMR (400 MHz, $CDCl_3$) of **31**.

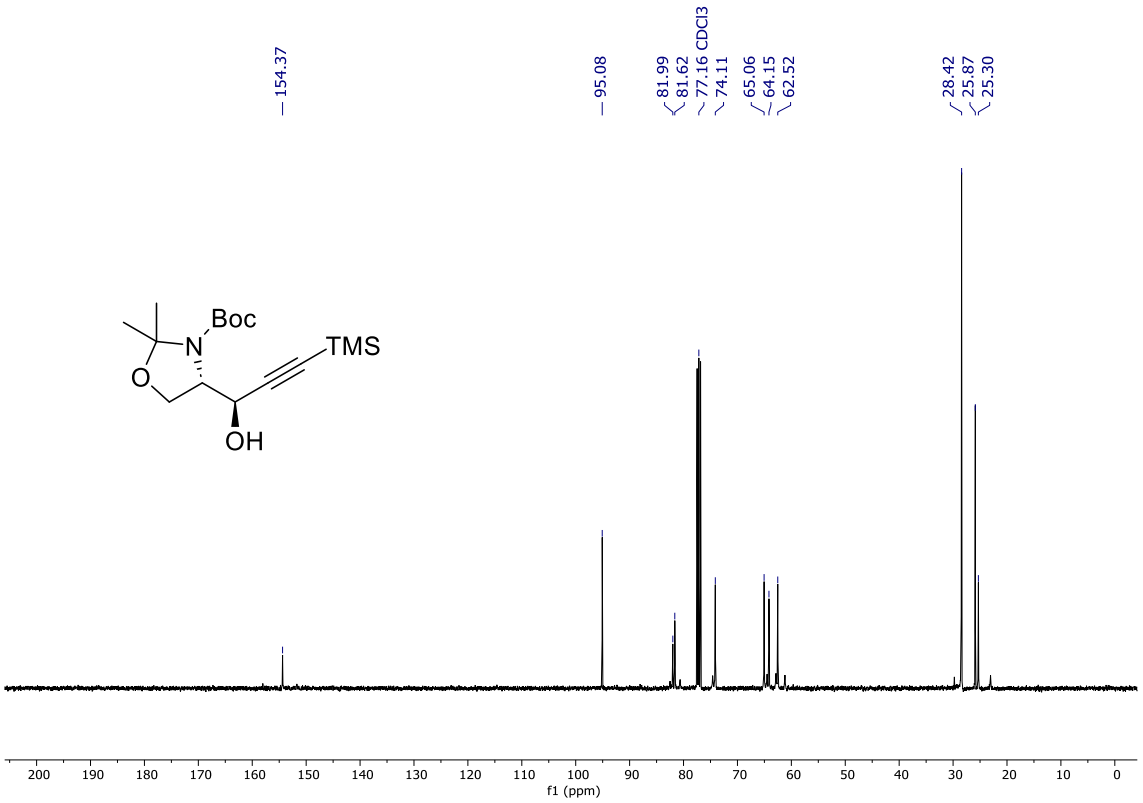

^{13}C NMR (100.6 MHz, $CDCl_3$) of **31**

1-Azidododecane (37)

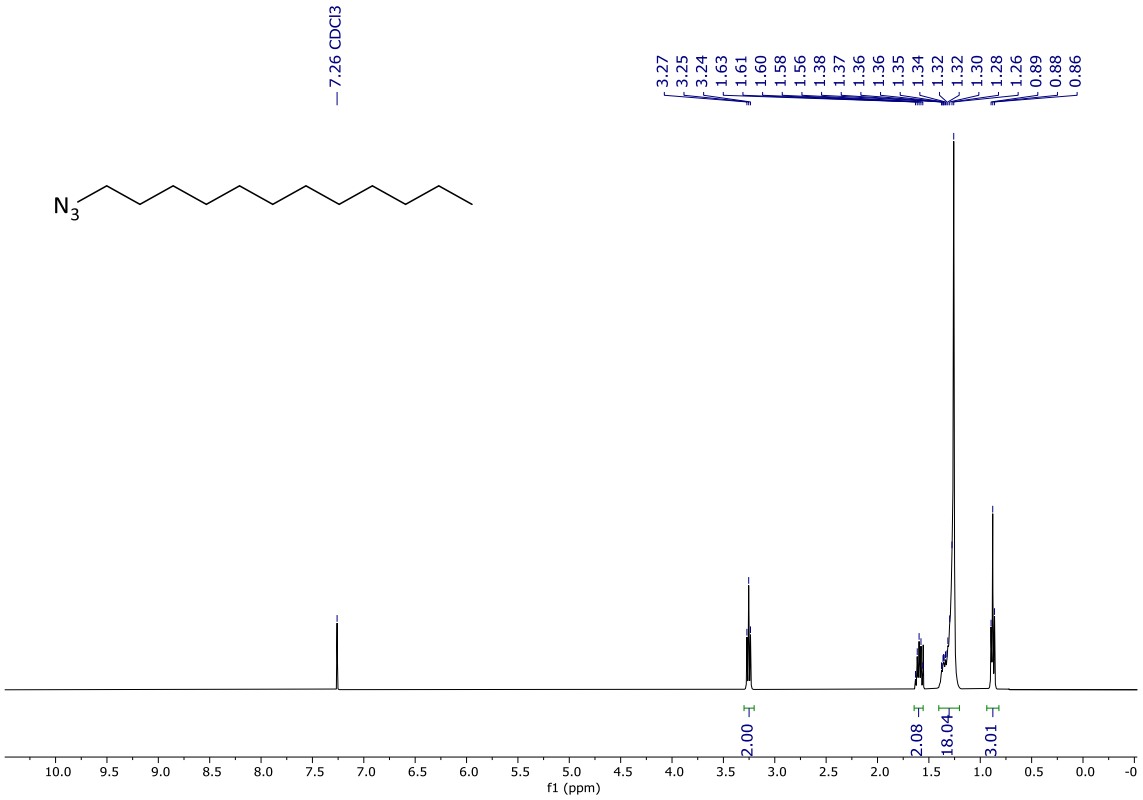

^{1}H NMR (400 MHz, $CDCl_3$) of **37**.

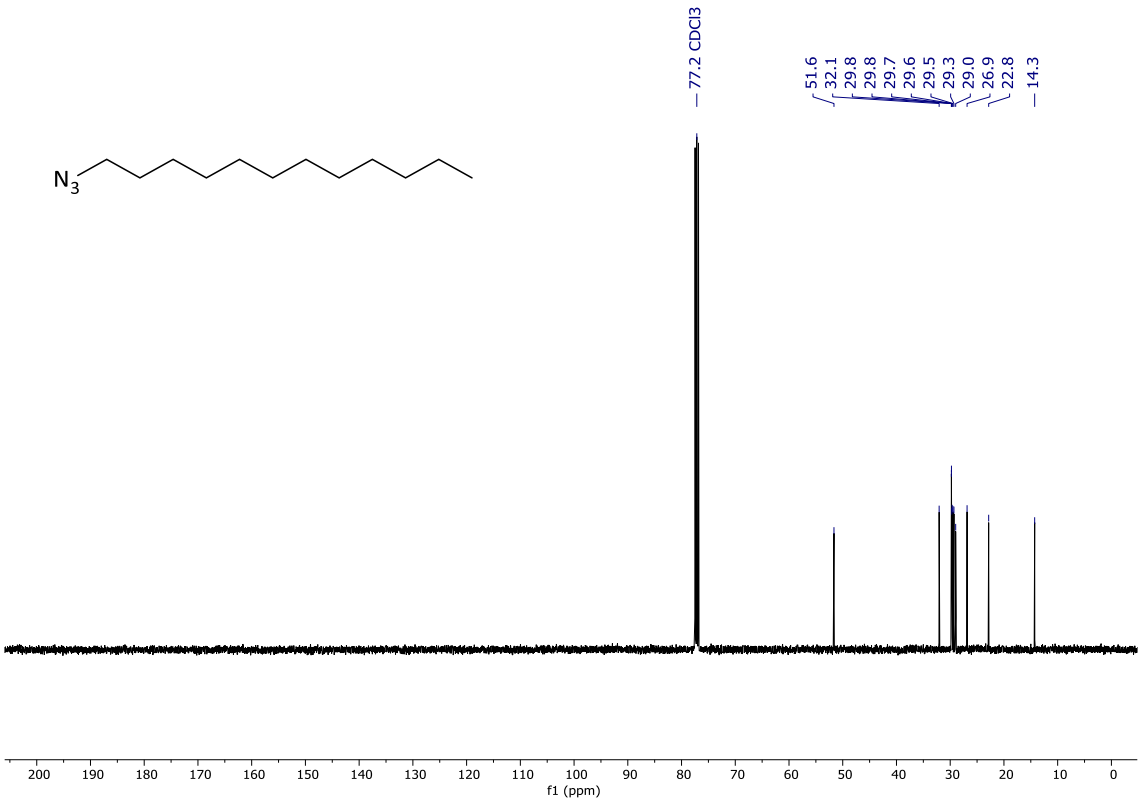

^{13}C NMR (100.6 MHz, $CDCl_3$) of **37**.

tert-butyl (_S_)-4-((_S_)-(1-dodecyl-1H-1,2,3-triazol-4-yl)(hydroxy)methyl)-2,2-dimethyloxazolidine-3-carboxylate (12)

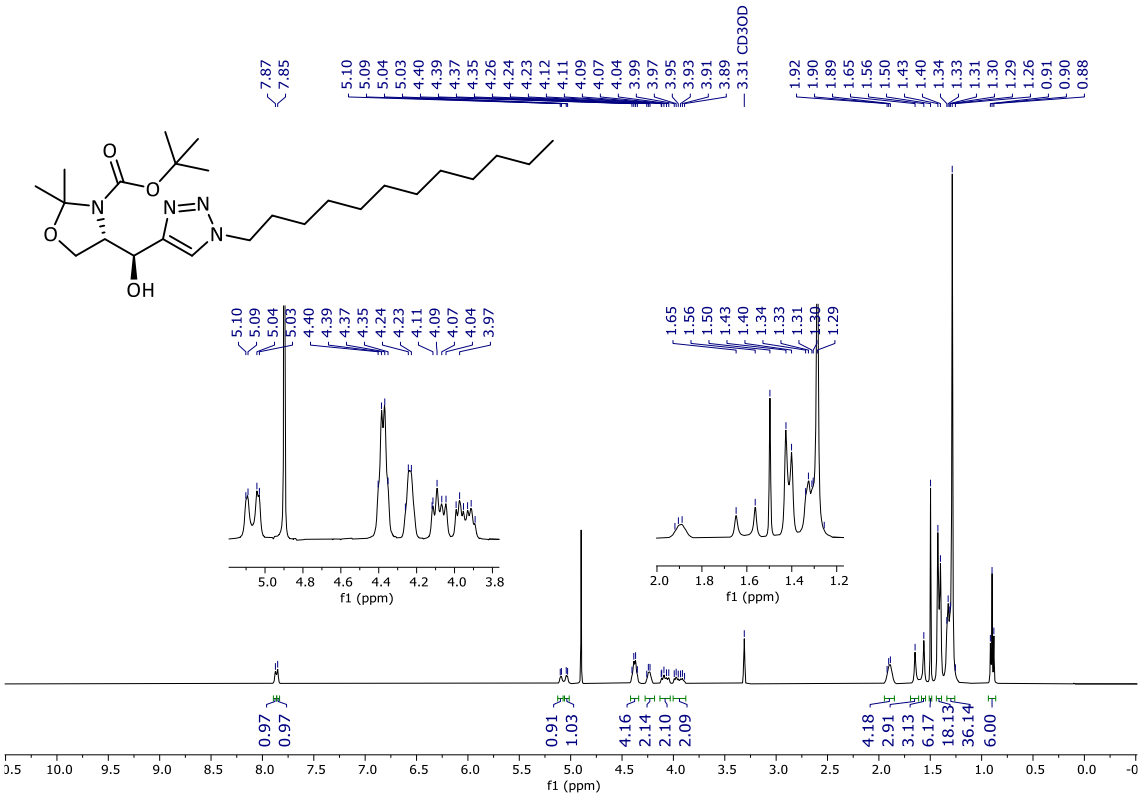

^{1}H NMR (400 MHz, $CDCl_3$) of **12**.

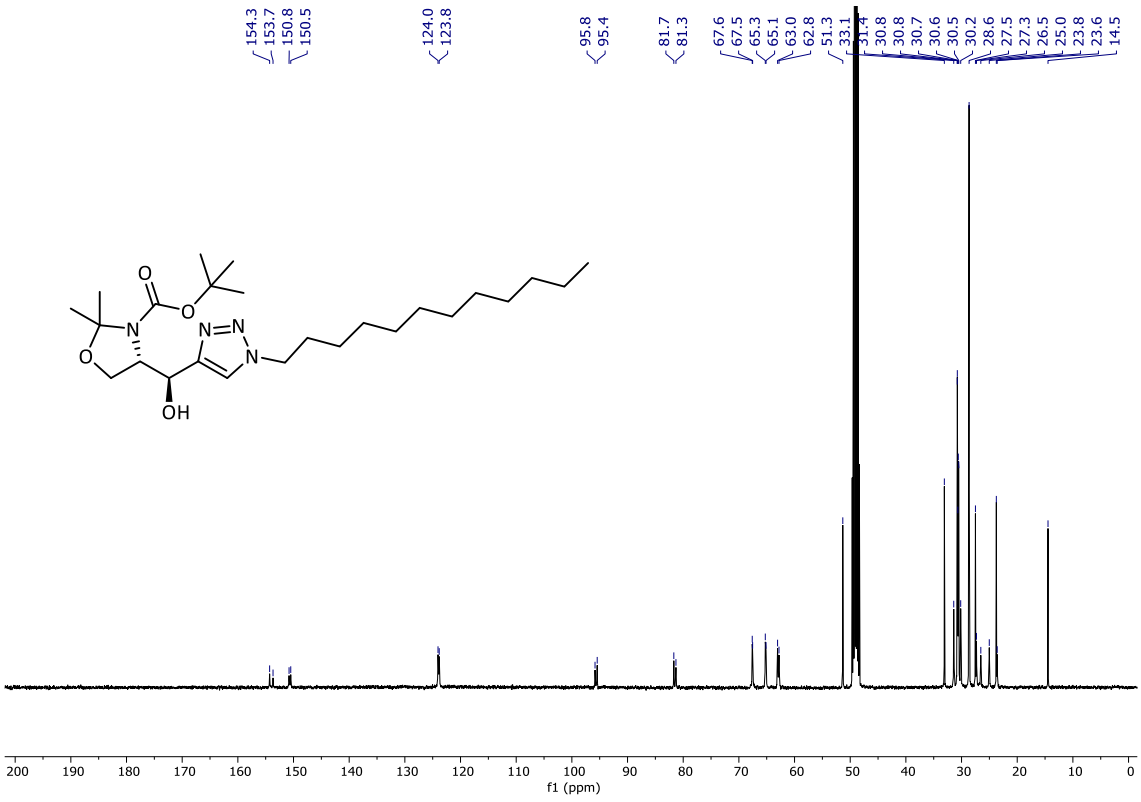

^{13}C NMR (100.6 MHz, $CDCl_3$) of **12**.

(1*S*,2*S*)-2-amino-1-(1-tridecyl-1H-1,2,3-triazol-5-yl)propane-1,3-diol (10)

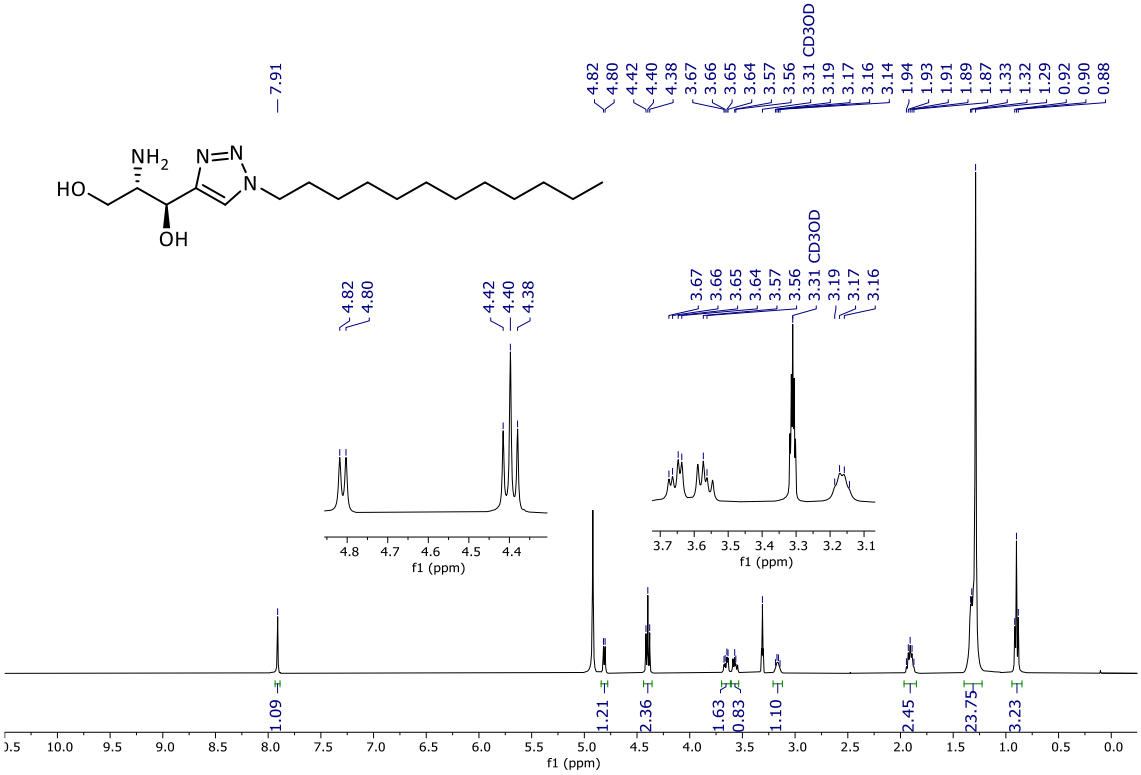

^{1}H NMR (400 MHz, CD_3OD) of **10**.

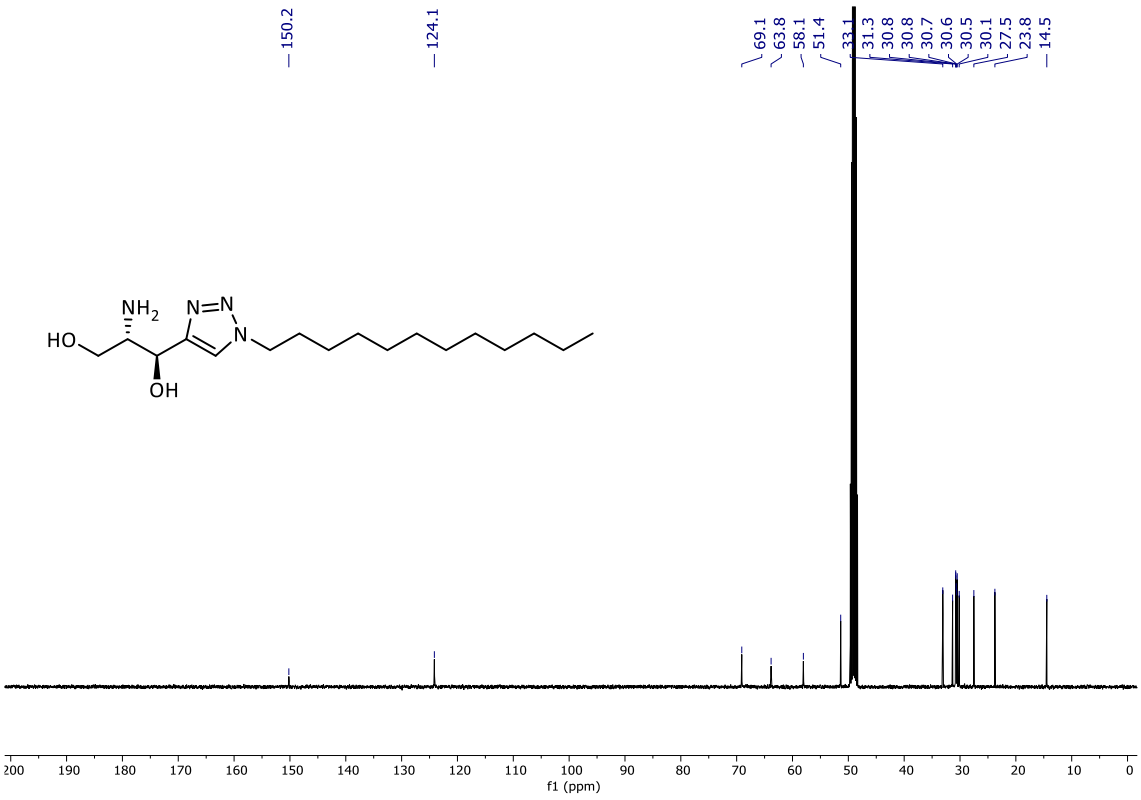

^{13}C NMR (100.6 MHz, CD_3OD) of **10**.

N-((1*S*,2*S*)-1-(1-dodecyl-1H-1,2,3-triazol-4-yl)-1,3-dihydroxypropan-2-yl)hexanamide (1a)

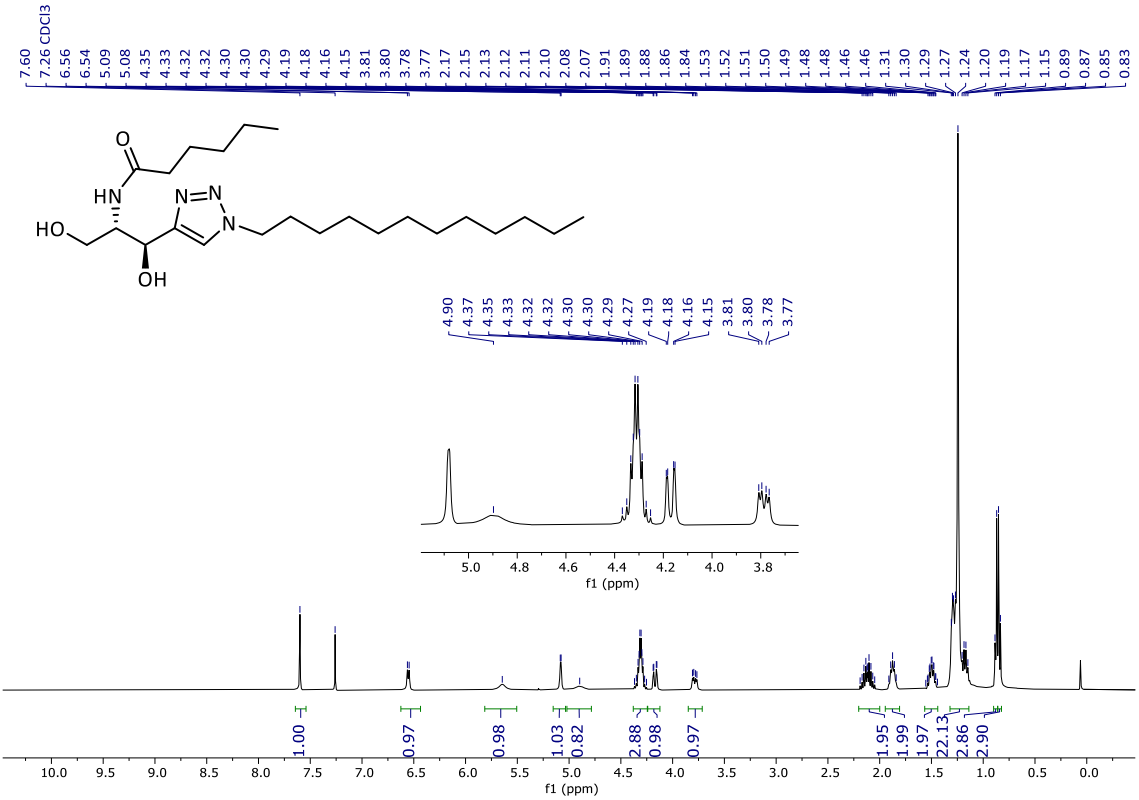

^{1}H NMR (400 MHz, $CDCl_3$) of **1a**.

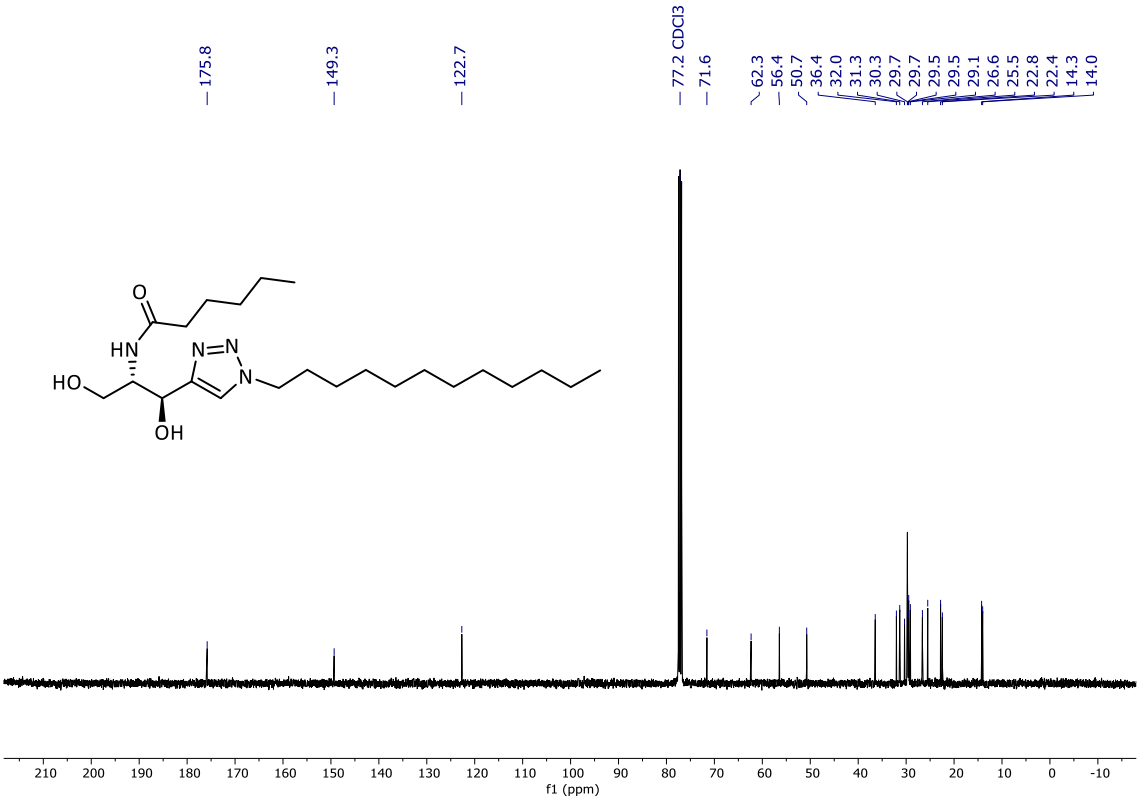

^{13}C NMR (100.6 MHz, $CDCl_3$) of **1a**.

N-((1*S*,2*S*)-1-(1-dodecyl-1H-1,2,3-triazol-4-yl)-1,3-dihydroxypropan-2-yl)octanamide (1b)

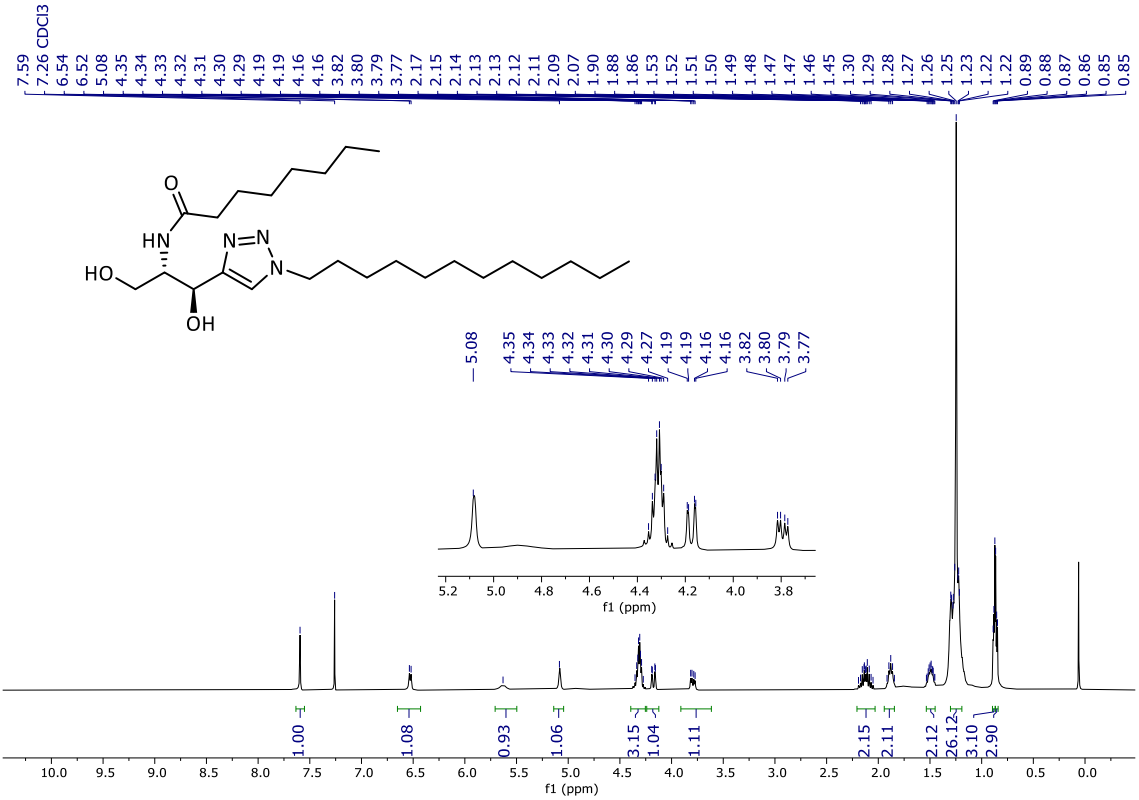

^{1}H NMR (400 MHz, $CDCl_3$) of **1b**.

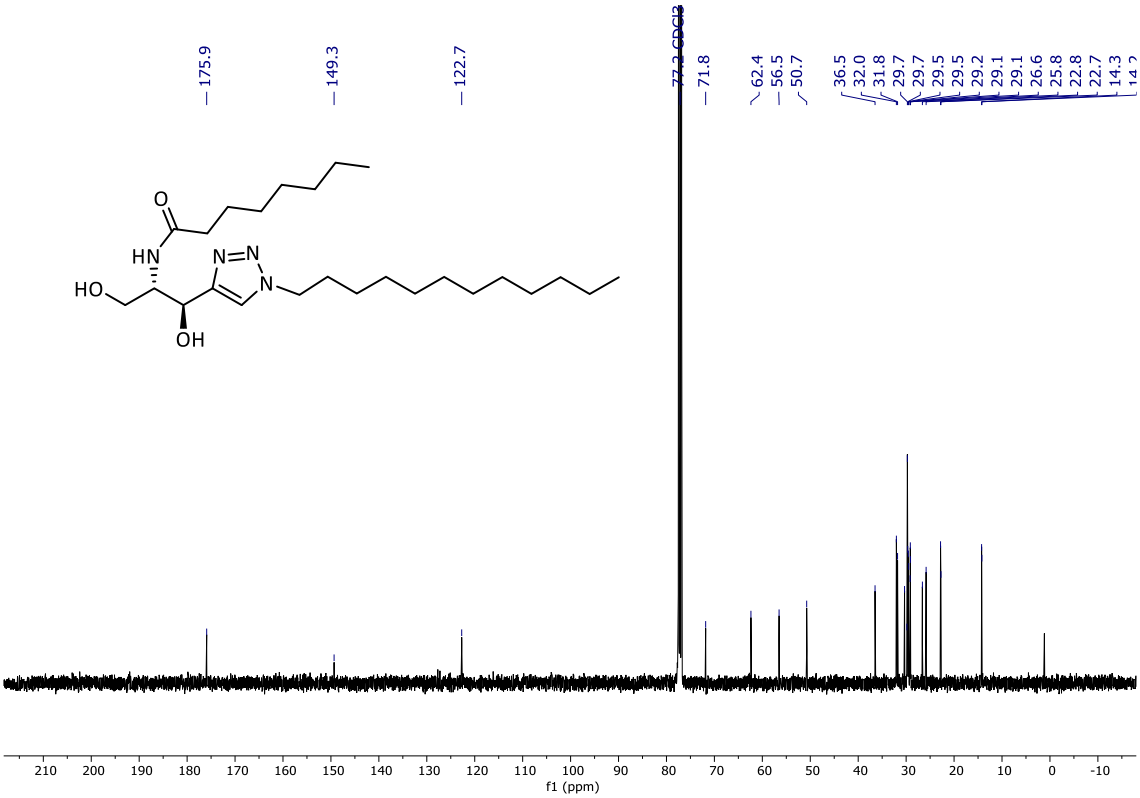

^{13}C NMR (100.6 MHz, $CDCl_3$) of **1b**.

N-((1*S*,2*S*)-1-(1-dodecyl-1H-1,2,3-triazol-4-yl)-1,3-dihydroxypropan-2-yl)decanamide (1c)

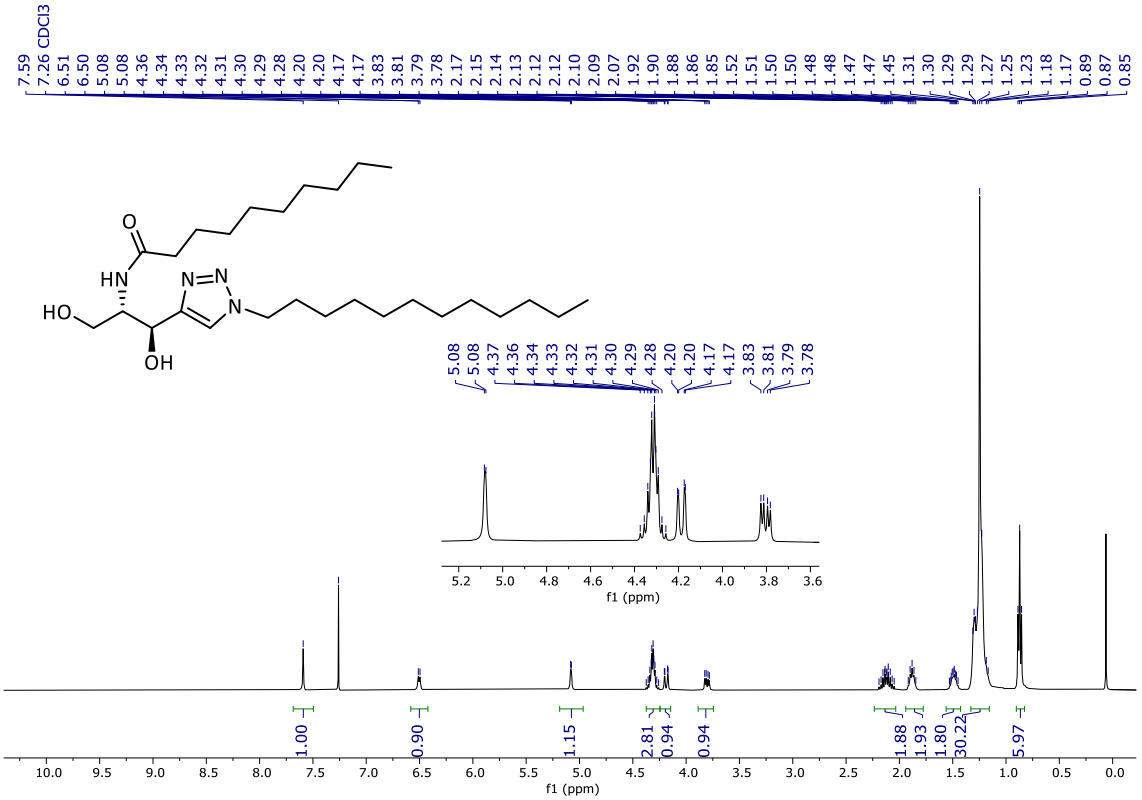

^{1}H NMR (400 MHz, $CDCl_3$) of **1c**.

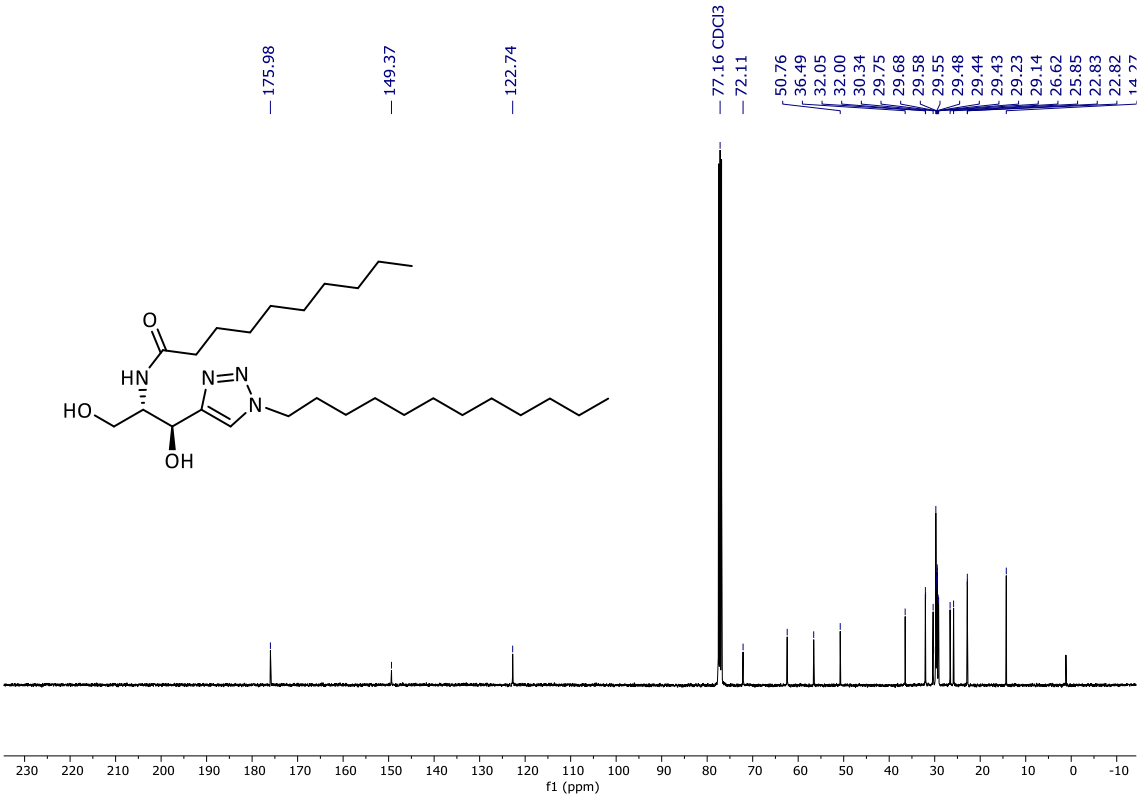

^{13}C NMR (100.6 MHz, $CDCl_3$) of **1c**.

1-Azidotridecane (38)

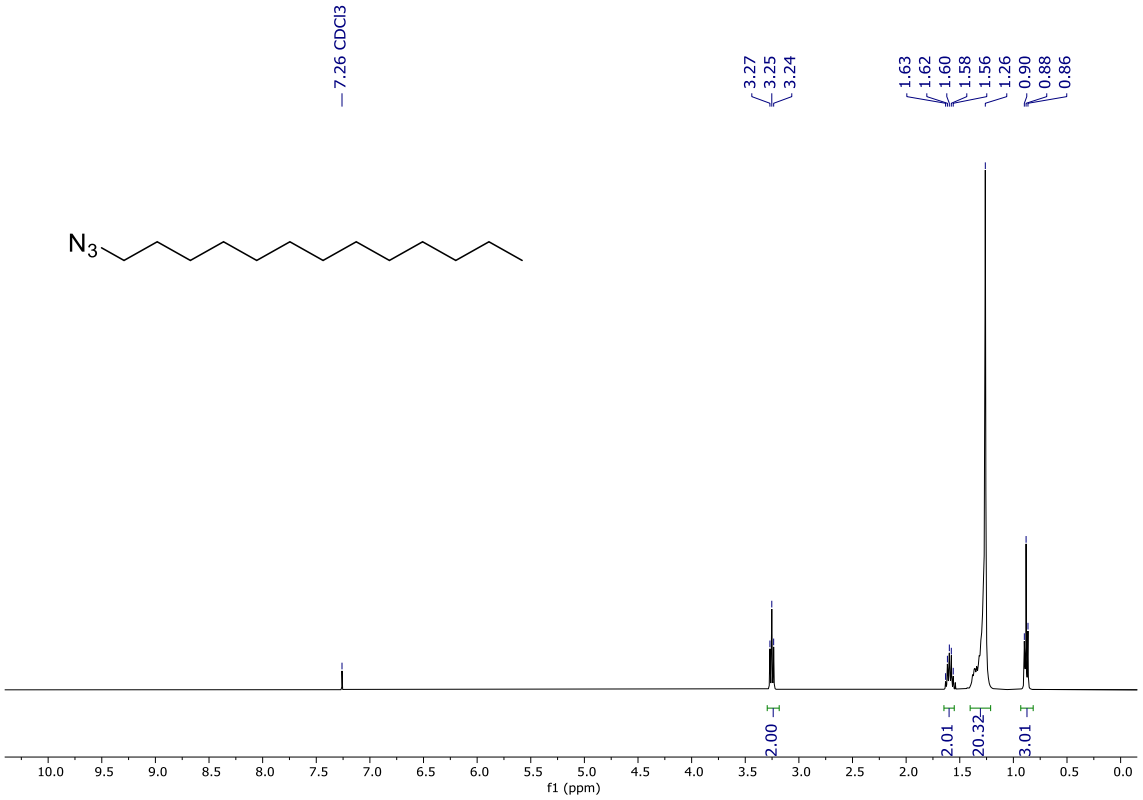

^{1}H NMR (400 MHz, $CDCl_3$) of **38**.

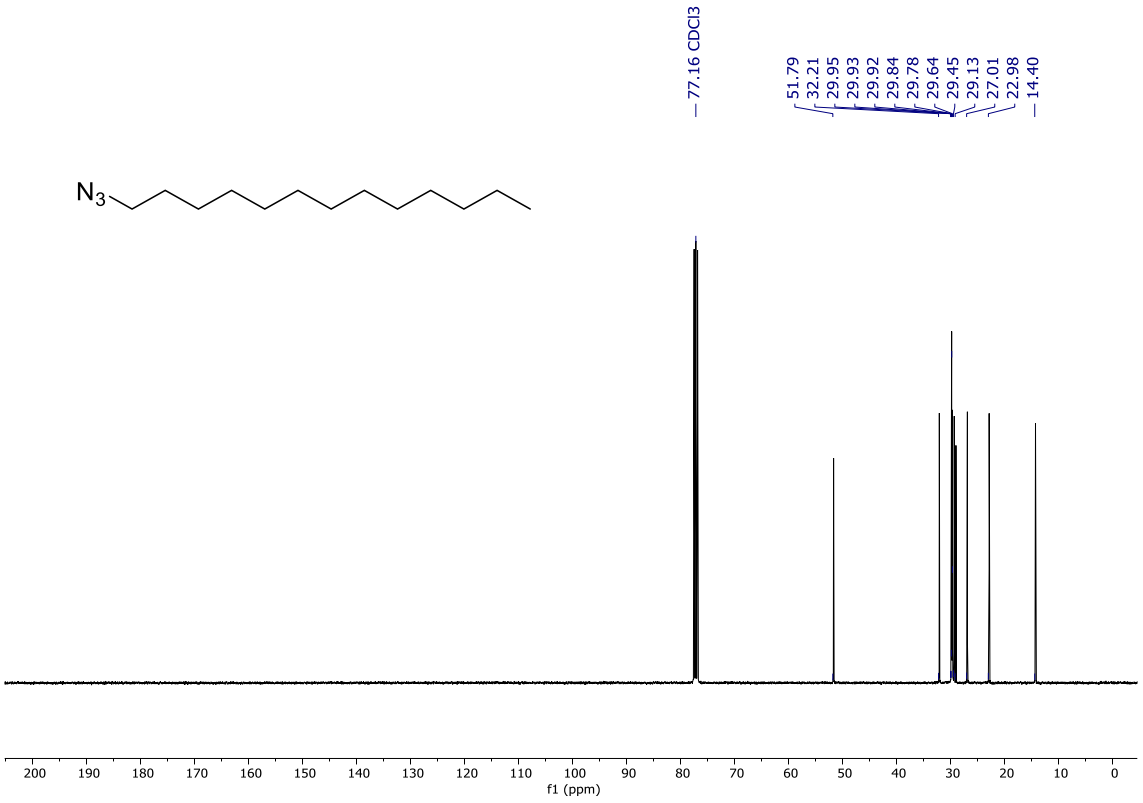

^{13}C NMR (100.6 MHz, $CDCl_3$) of **38**.

tert-butyl (_S_)-4-((_S_)-hydroxy(1-tridecyl-1H-1,2,3-triazol-5-yl)methyl)-2,2-dimethyloxazolidine-3-carboxylate (13)

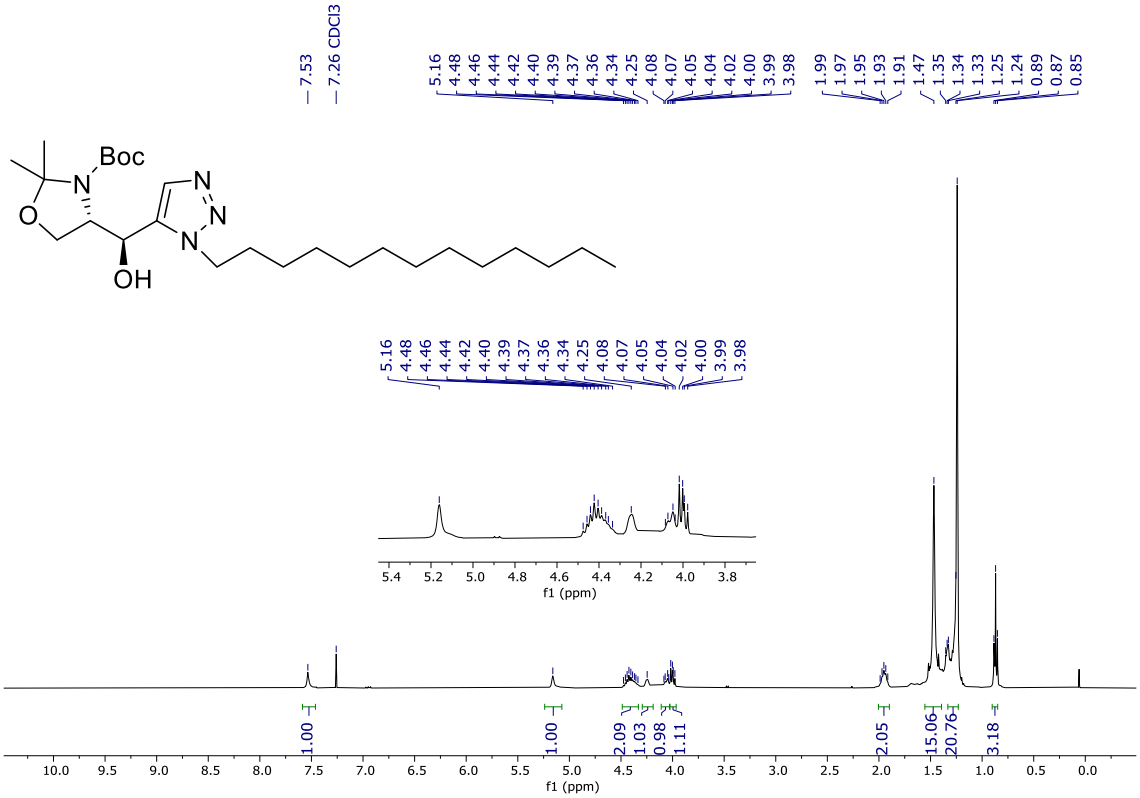

^{1}H NMR (400 MHz, $CDCl_3$) of **13**.

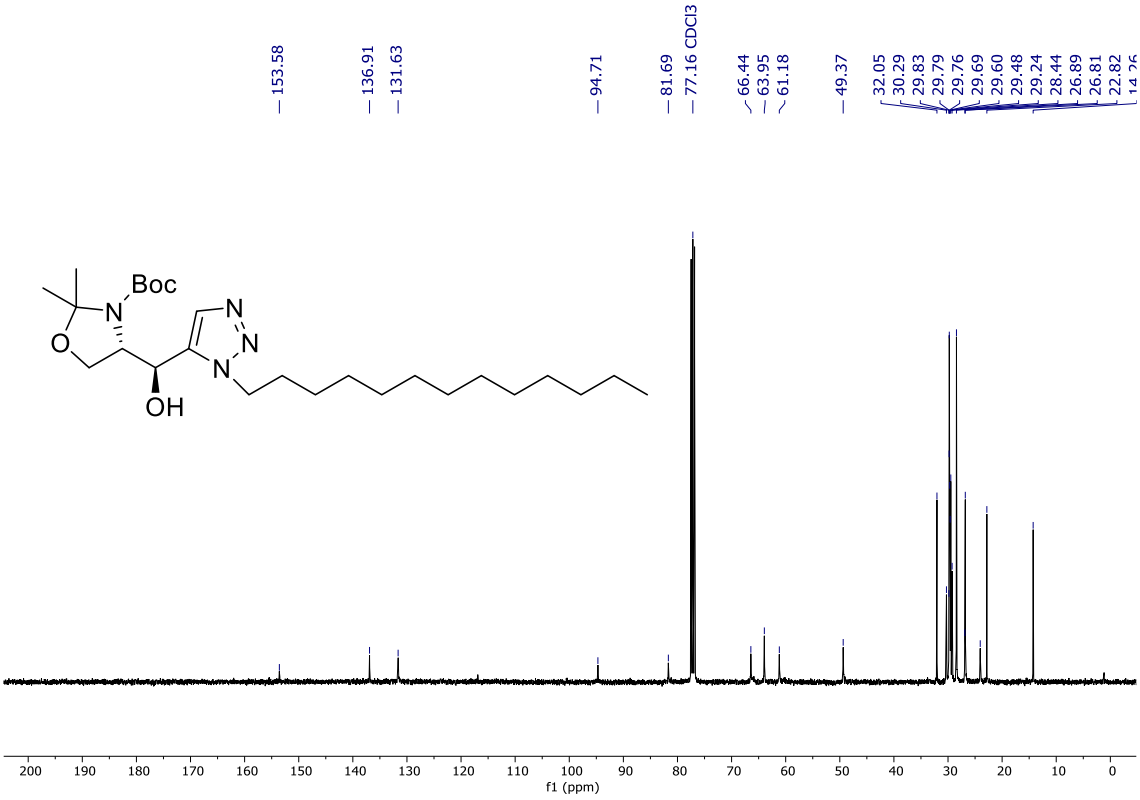

^{13}C NMR (100.6 MHz, $CDCl_3$) of **13**.

(1*S*,2*S*)-2-amino-1-(1-tridecyl-1H-1,2,3-triazol-5-yl)propane-1,3-diol (11)

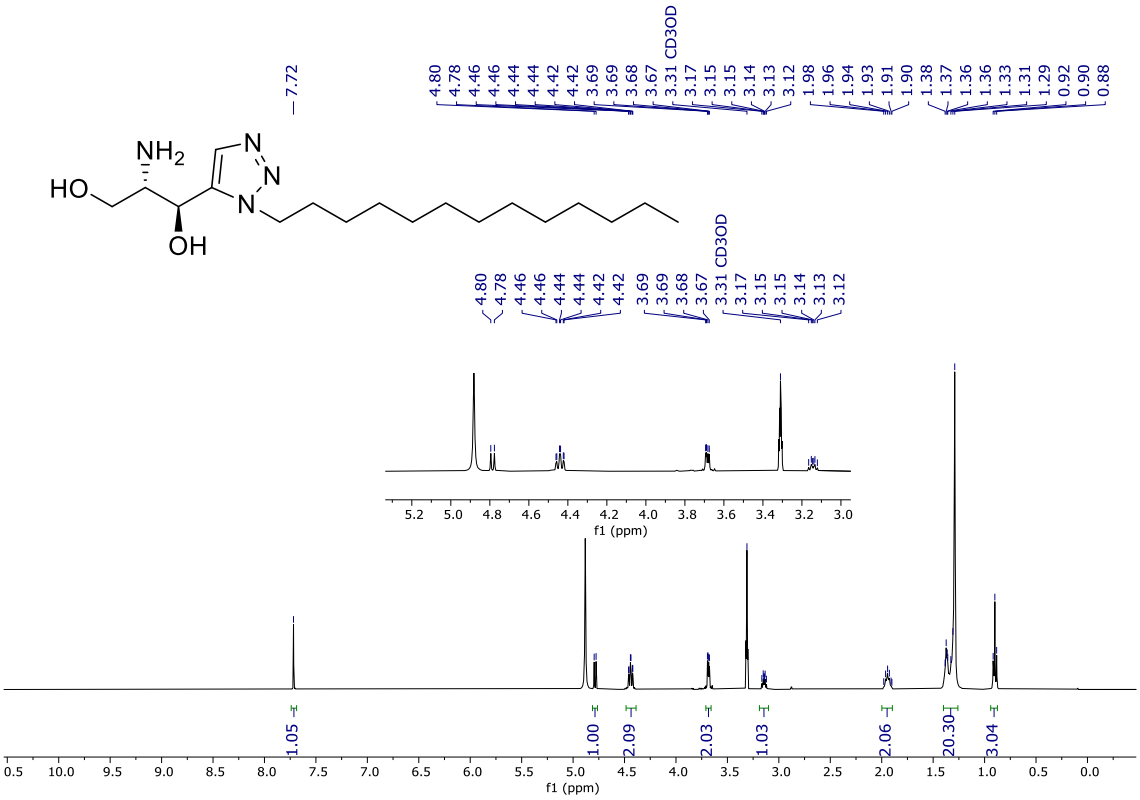

^{1}H NMR (400 MHz, CD_3OD) of **11**.

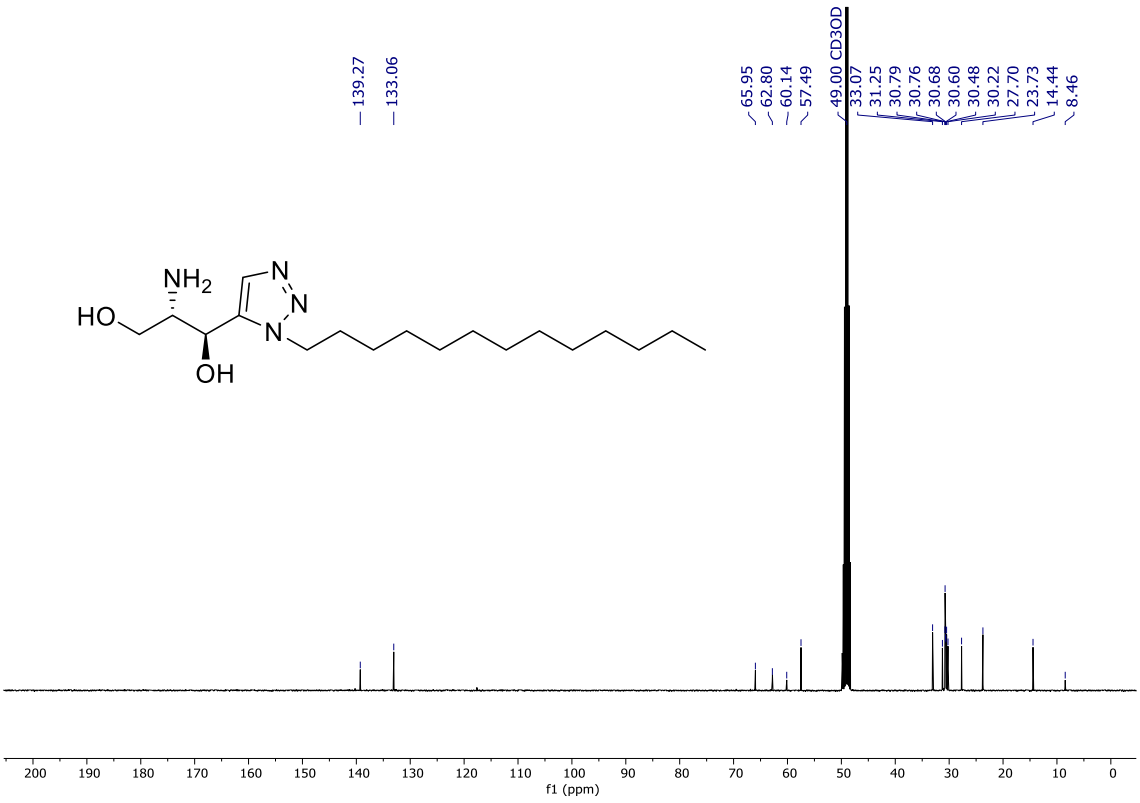

^{13}C NMR (100.6 MHz, CD_3OD) of **11**.

_N_-((1_S_,2_S_)-1,3-dihydroxy-1-(1-tridecyl-1H-1,2,3-triazol-5-yl)propan-2-yl)hexanamide (2a)

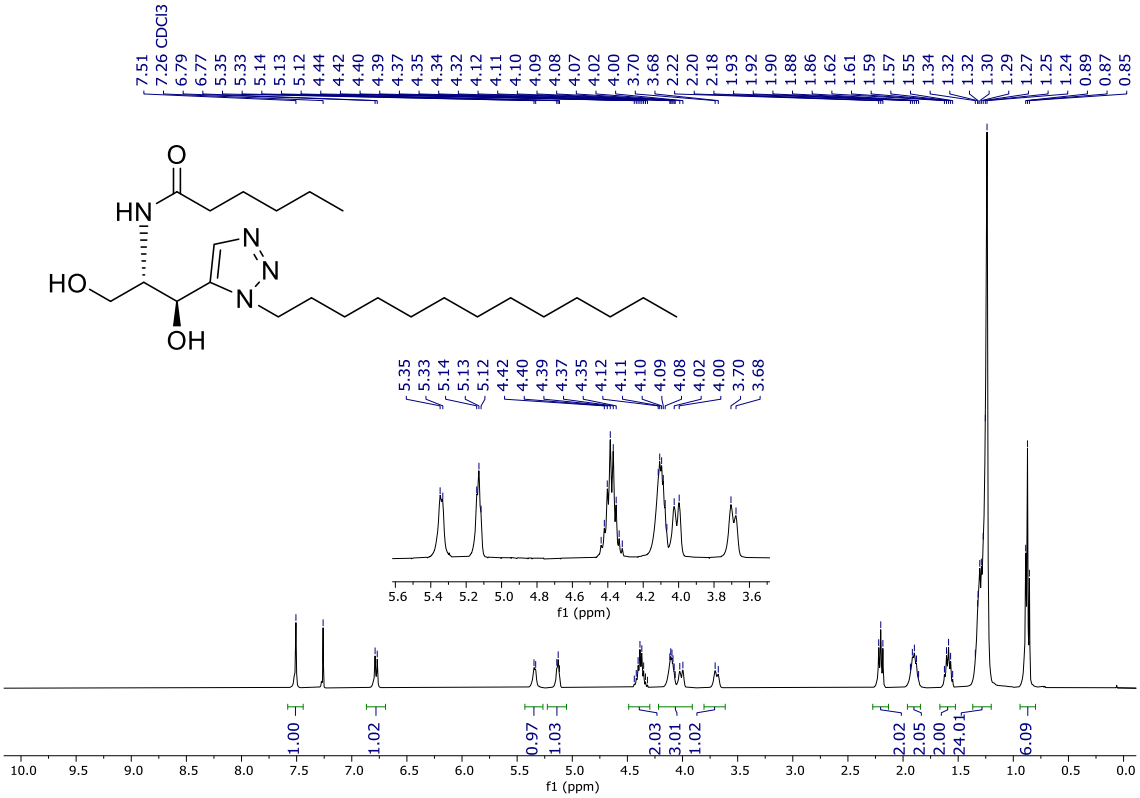

^{1}H NMR (400 MHz, $CDCl_3$) of **2a**.

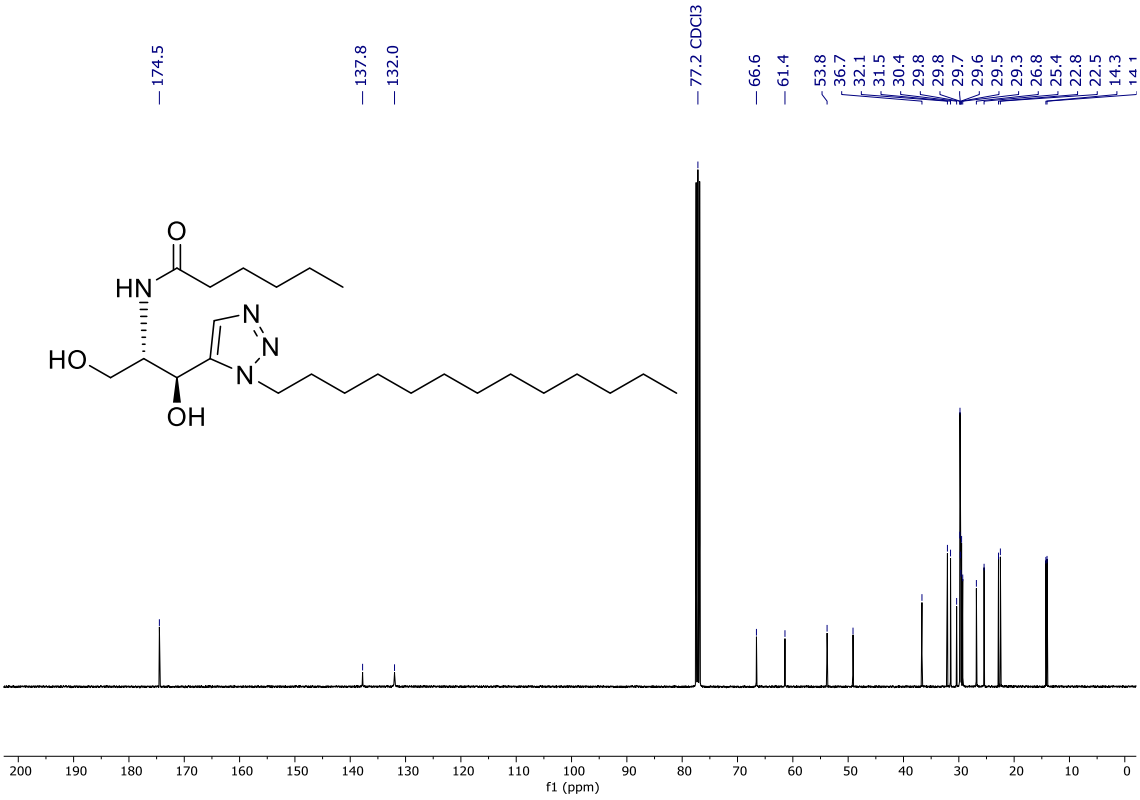

^{13}C NMR (100.6 MHz, $CDCl_3$) of **2a**.

N-((1*S*,2*S*)-1,3-dihydroxy-1-(1-tridecyl-1H-1,2,3-triazol-5-yl)propan-2-yl)octanamide (2b)

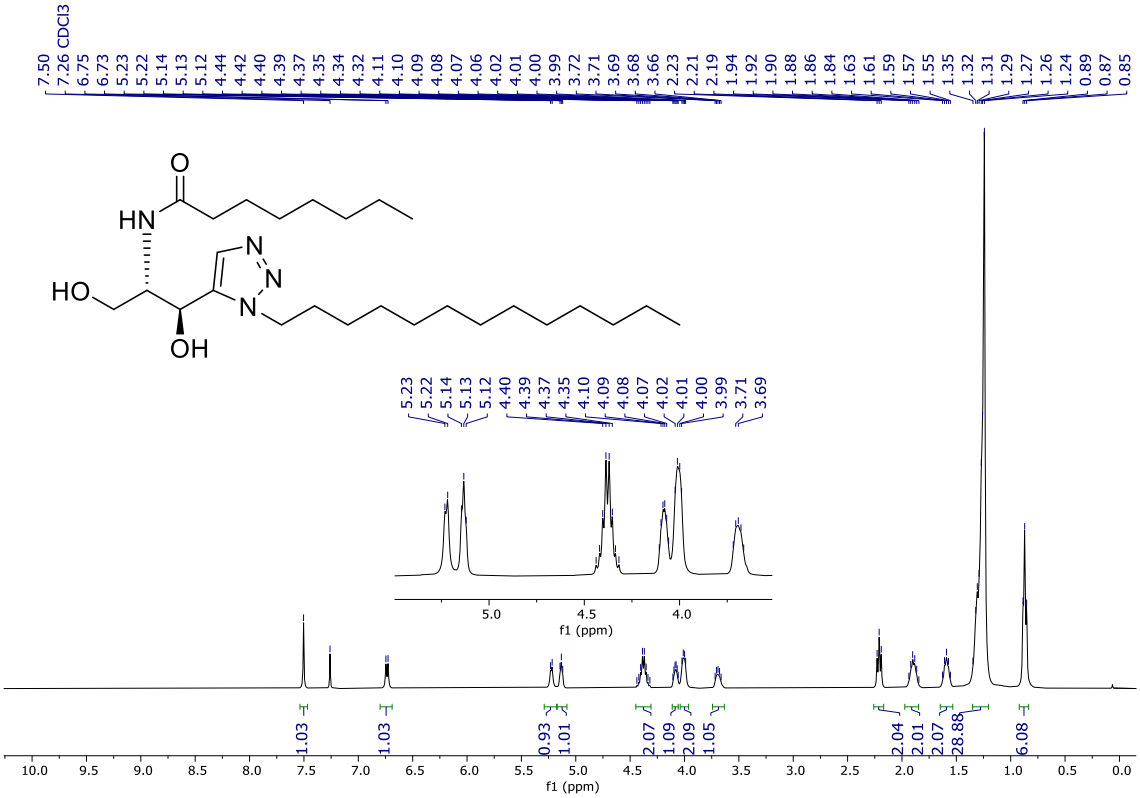

^{1}H NMR (400 MHz, $CDCl_3$) of **2b**.

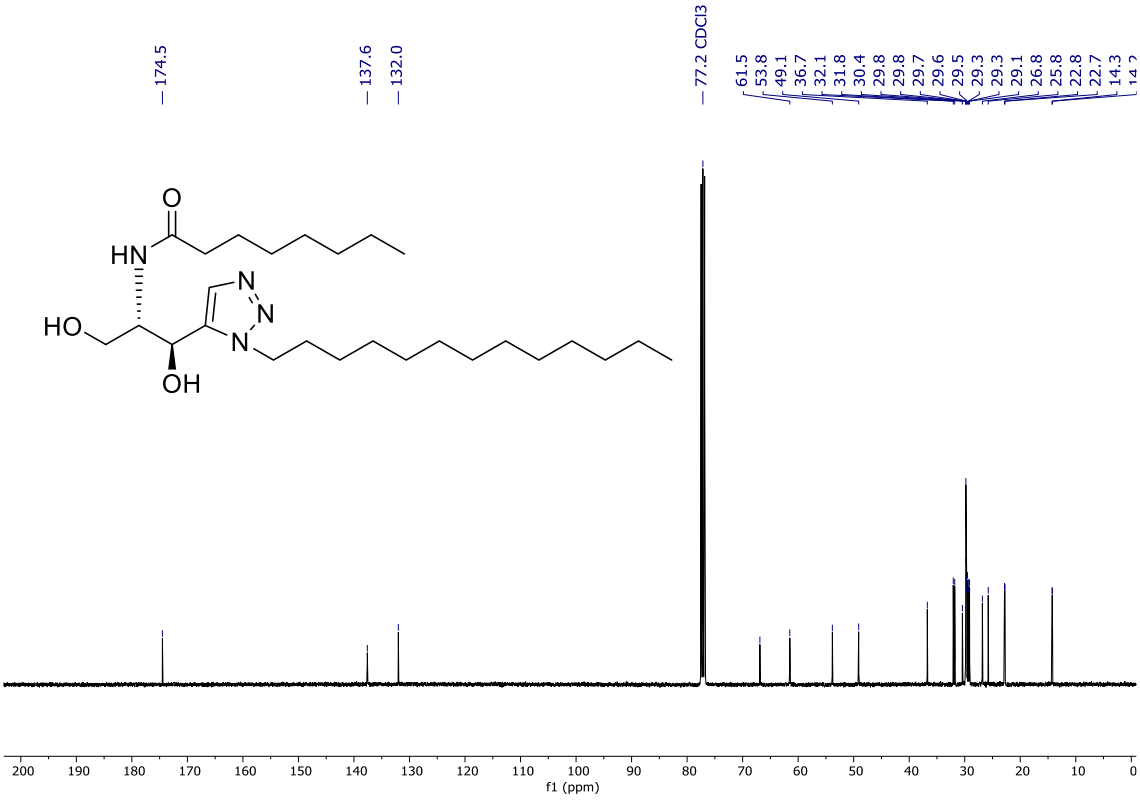

^{13}C NMR (100.6 MHz, $CDCl_3$) of **2b**.

N-((1*S*,2*S*)-1,3-dihydroxy-1-(1-tridecyl-1H-1,2,3-triazol-5-yl)propan-2-yl)decanamide (2c)

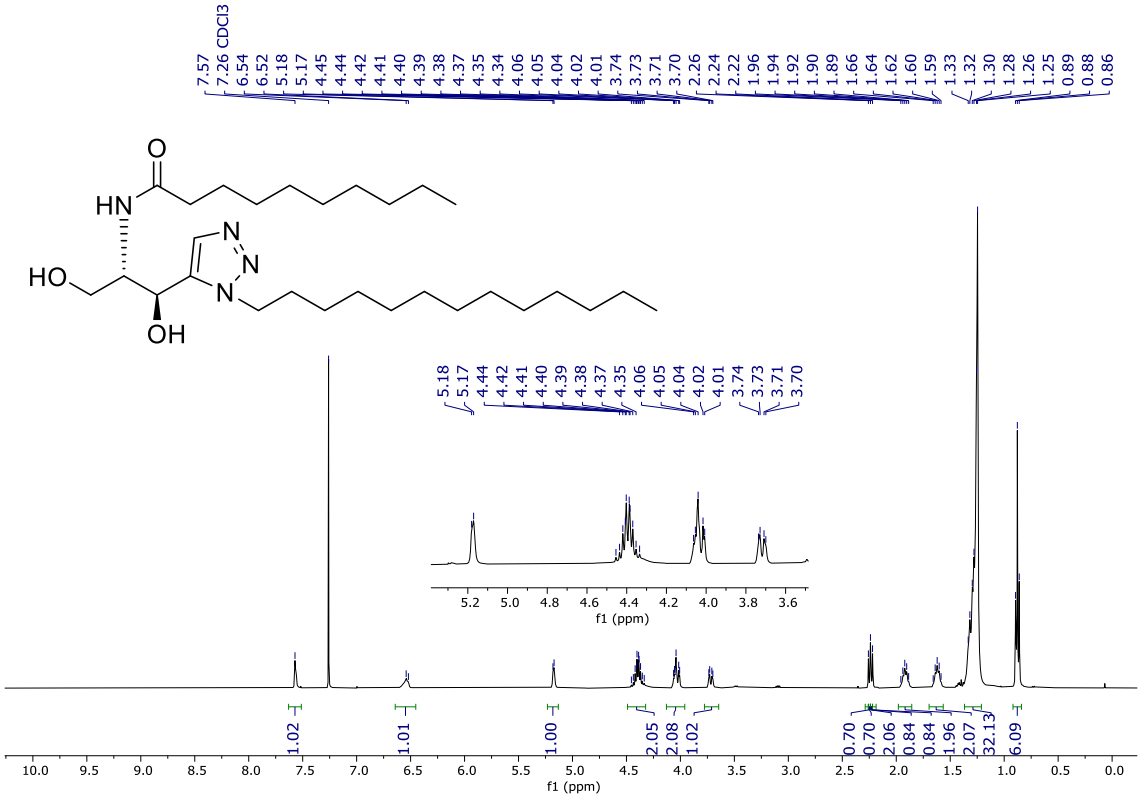

^{1}H NMR (400 MHz, $CDCl_3$) of **2c**.

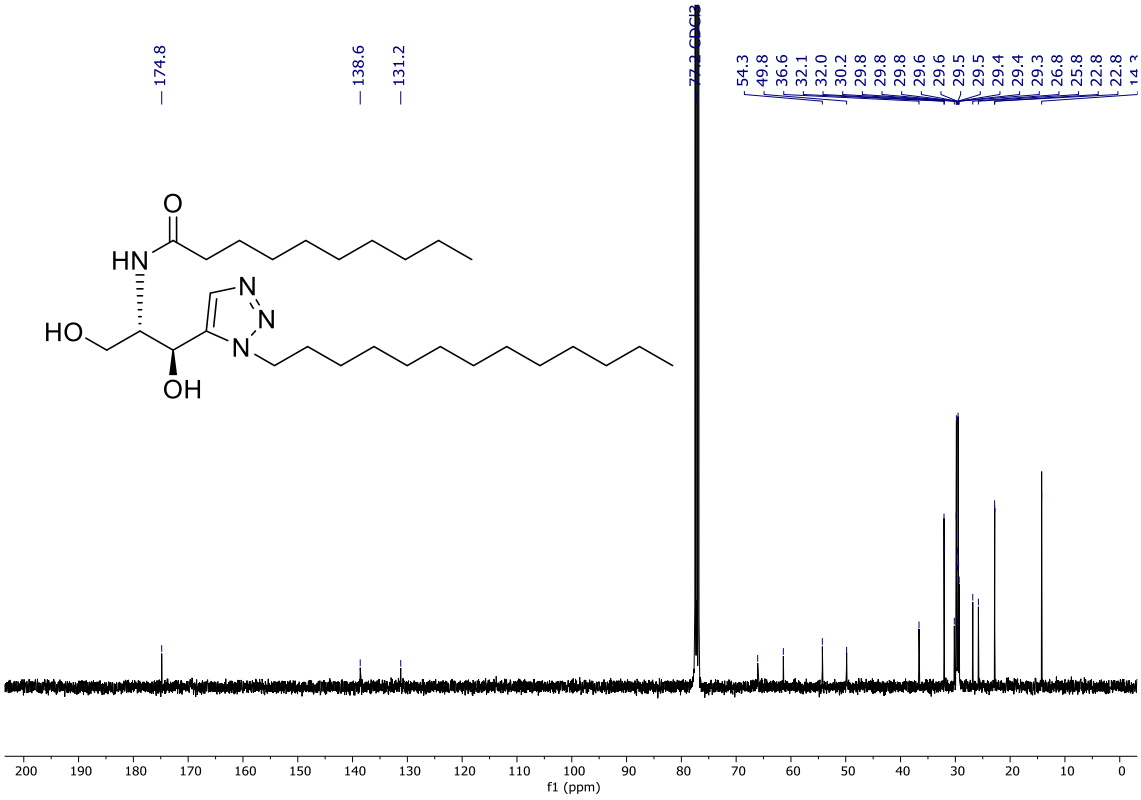

^{13}C NMR (100.6 MHz, $CDCl_3$) of **2c**.

2-dodecylfuran (17)

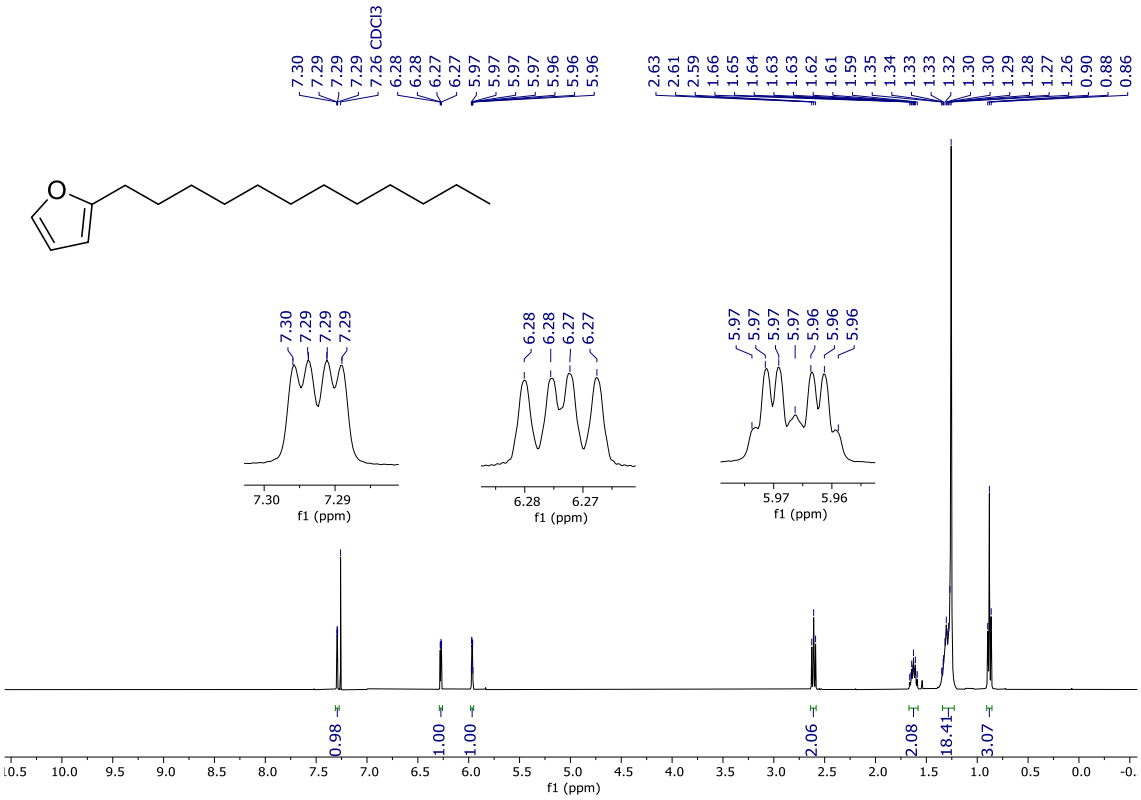

^{1}H NMR (400 MHz, $CDCl_3$) of **17**.

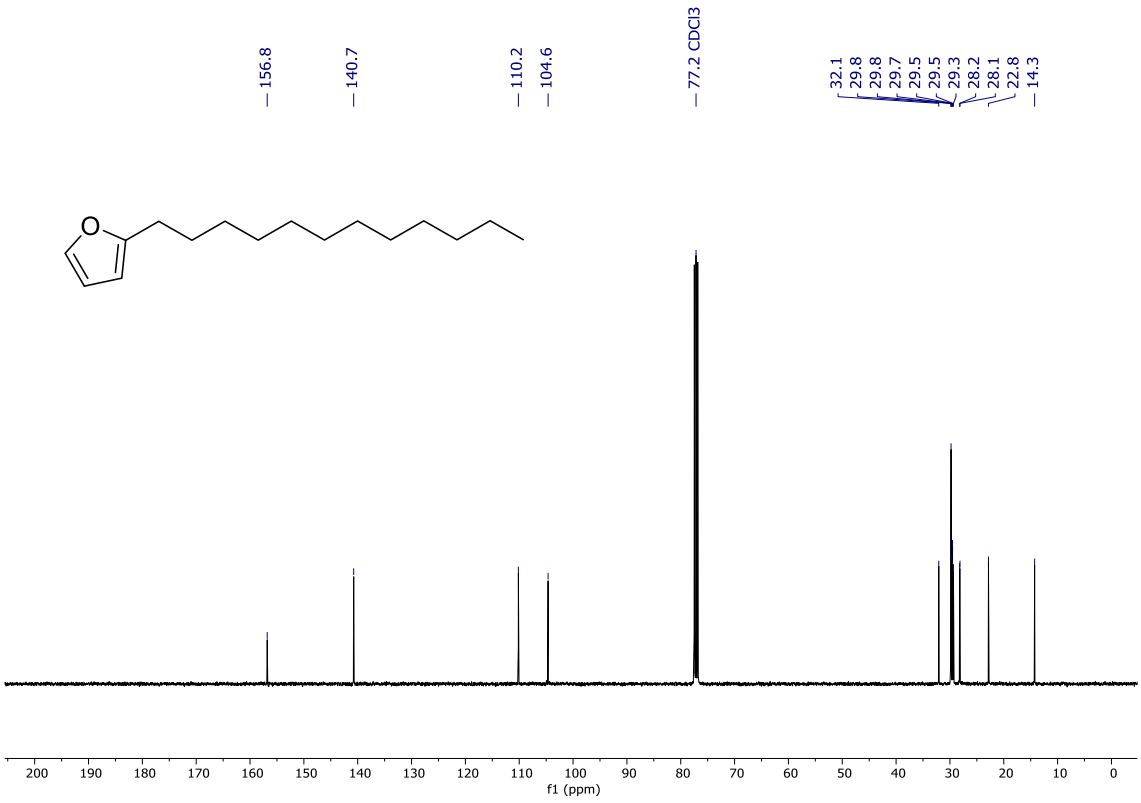

^{13}C NMR (100.6 MHz, $CDCl_3$) of **17**.

tert-butyl (*S*)-4-((*S*)-(5-dodecylfuran-2-yl)(hydroxy)methyl)-2,2-dimethyloxazolidine-3-carboxylate (16)

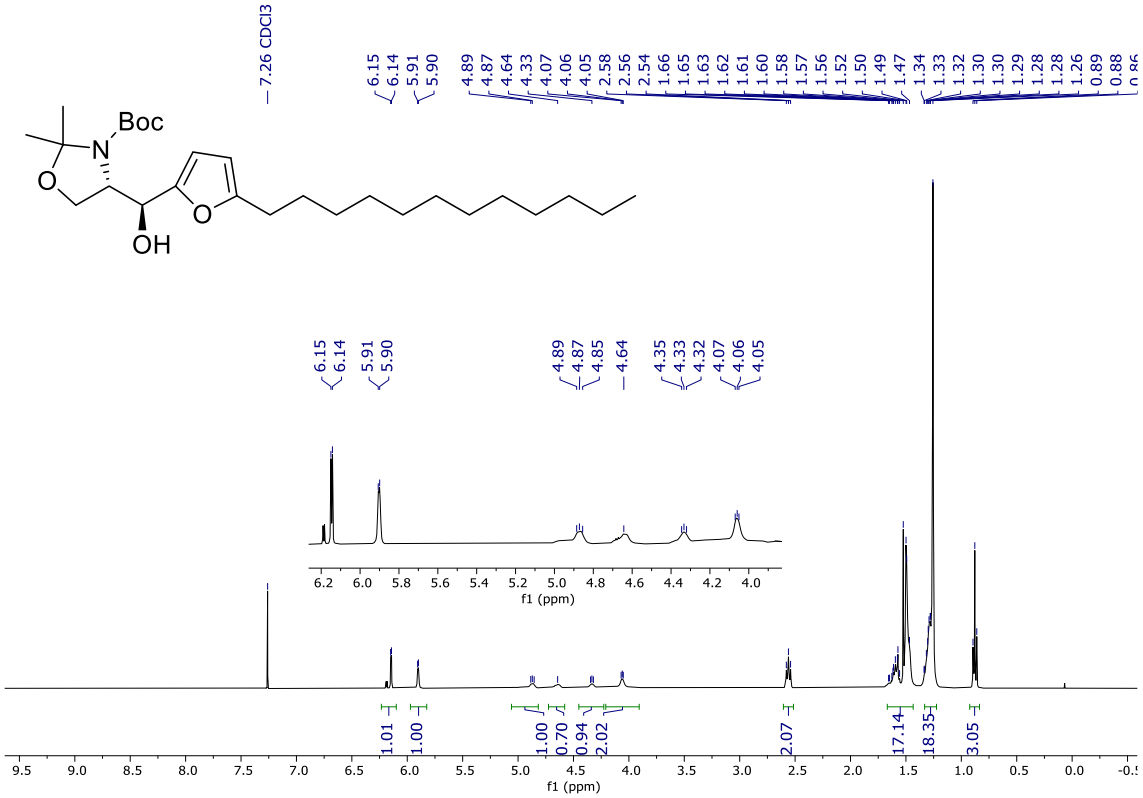

^{1}H NMR (400 MHz, $CDCl_3$) of **16**.

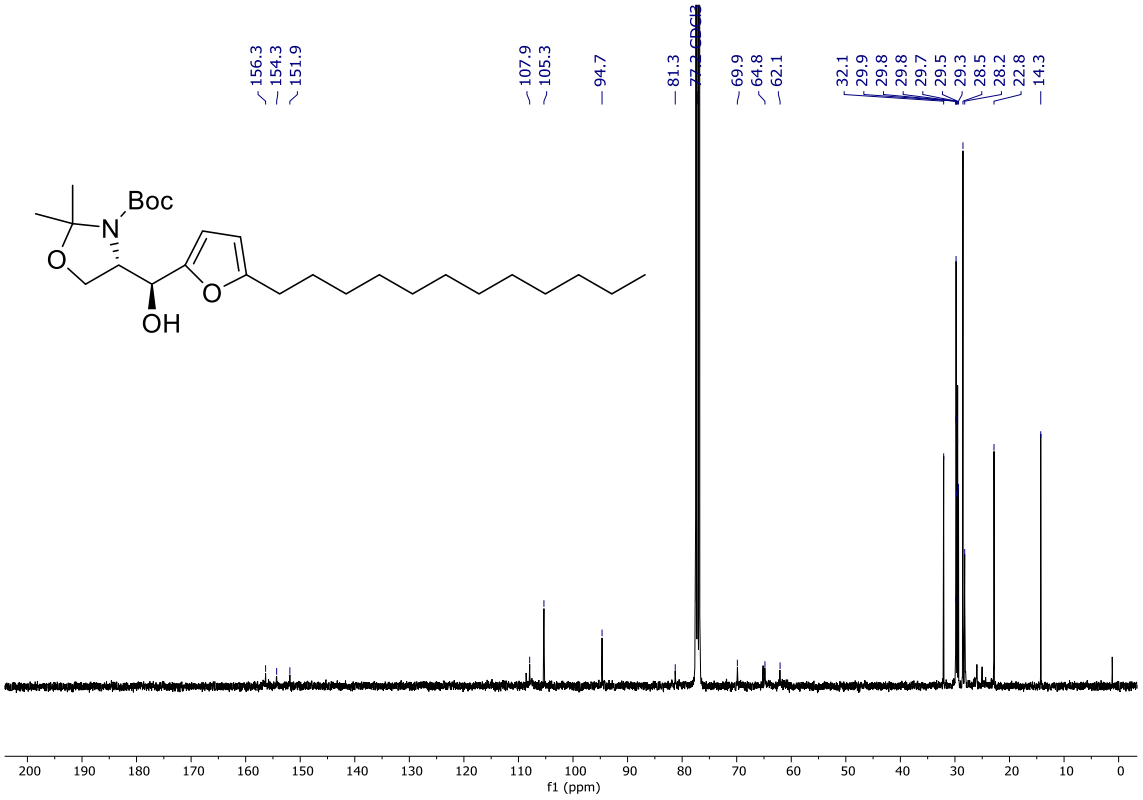

^{13}C NMR (100.6 MHz, $CDCl_3$) of **16**.

(1*S*,2*S*)-2-amino-1-(5-dodecylfuran-2-yl)propane-1,3-diol (15)

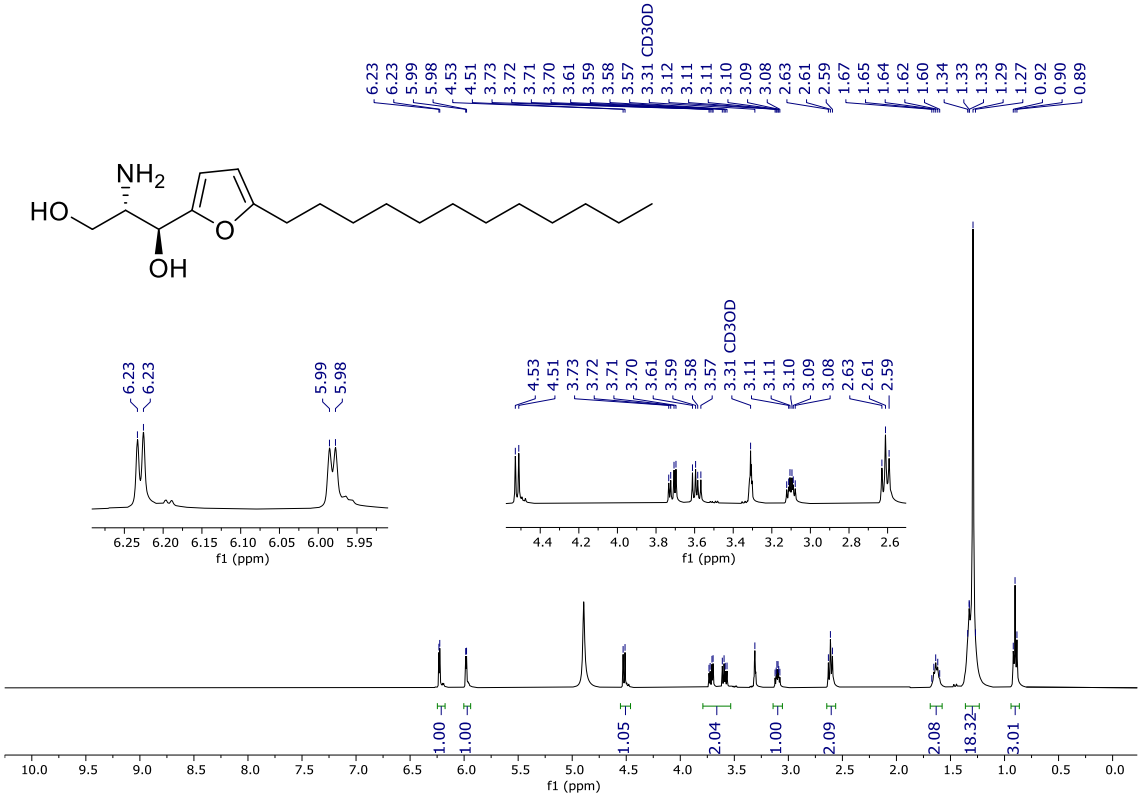

^{1}H NMR (400 MHz, CD_3OD) of **15**.

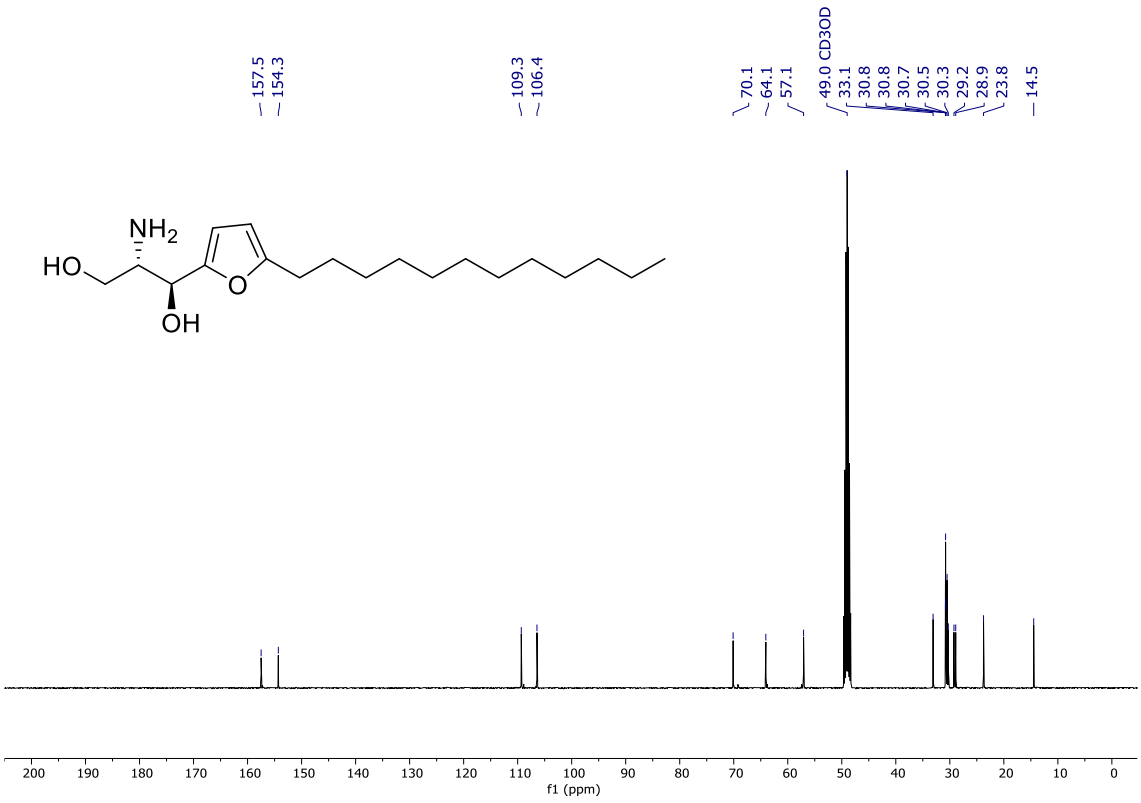

^{13}C NMR (100.6 MHz, CD_3OD) of **15**.

N-((1*S*,2*S*)-1-(5-dodecylfuran-2-yl)-1,3-dihydroxypropan-2-yl)hexanamide (3a)

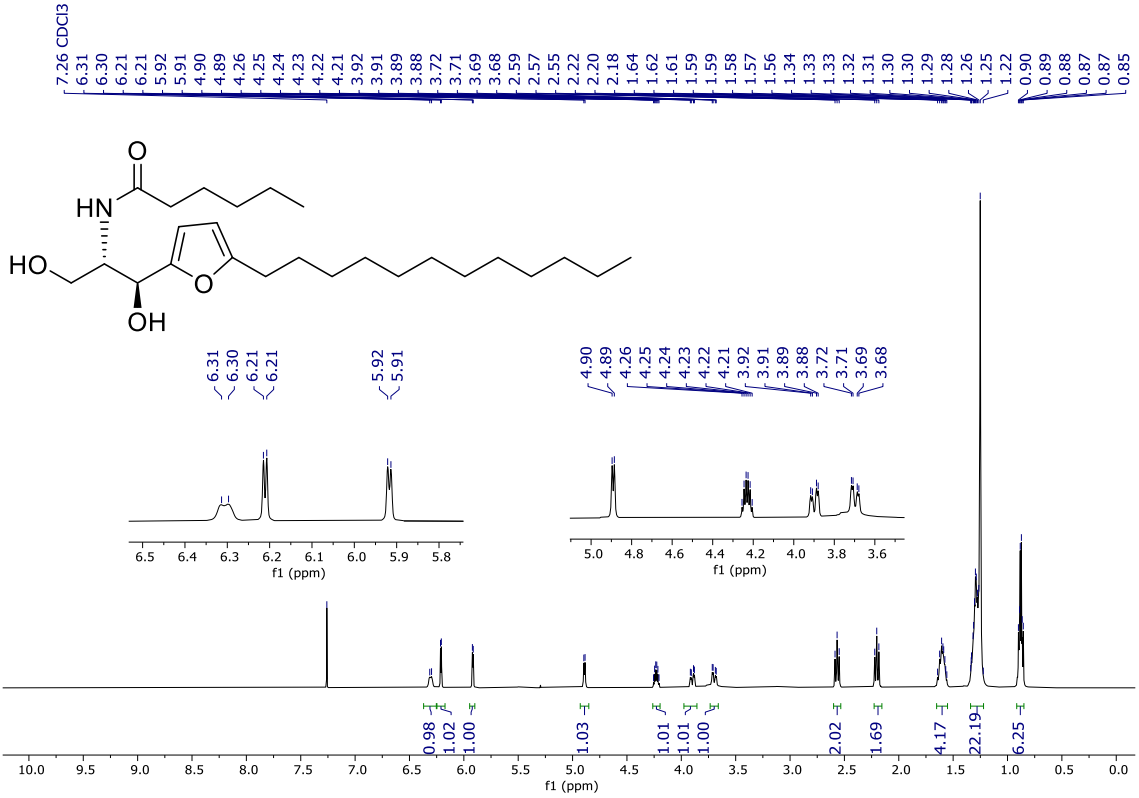

^{1}H NMR (400 MHz, $CDCl_3$) of **3a**.

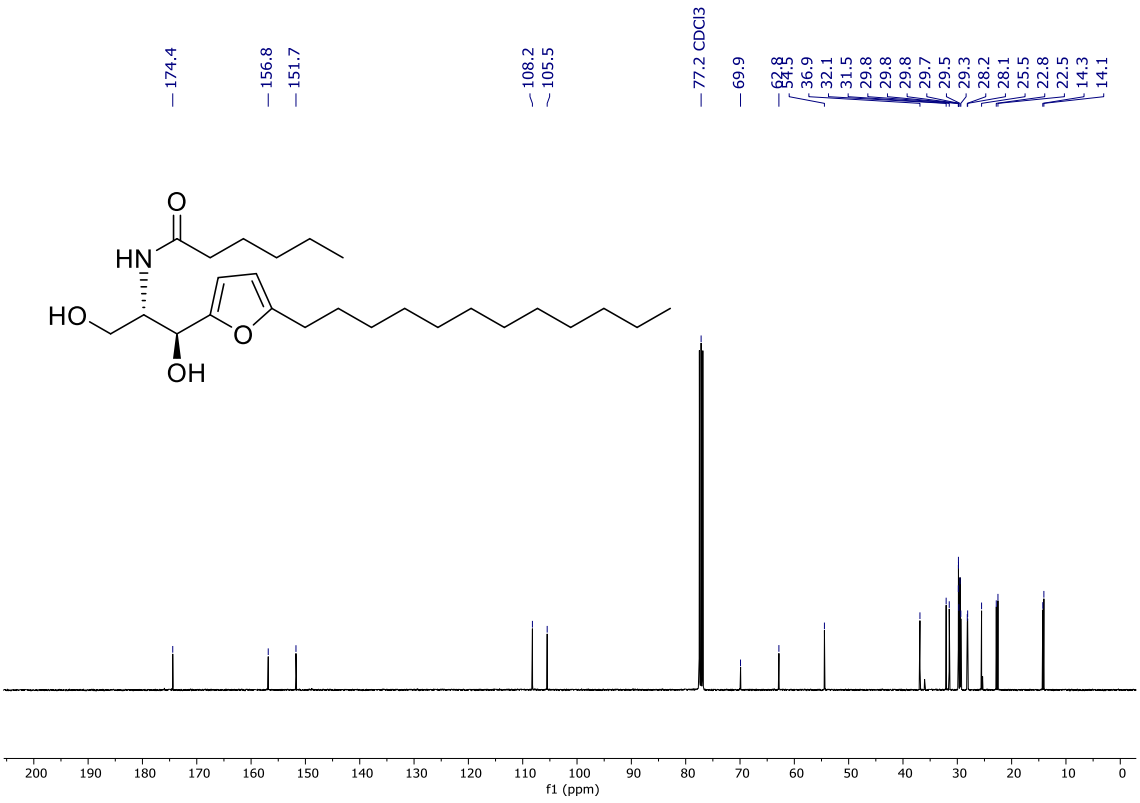

^{13}C NMR (100.6 MHz, $CDCl_3$) of **3a**.

N-((1*S*,2*S*)-1-(5-dodecylfuran-2-yl)-1,3-dihydroxypropan-2-yl)octanamide (3b)

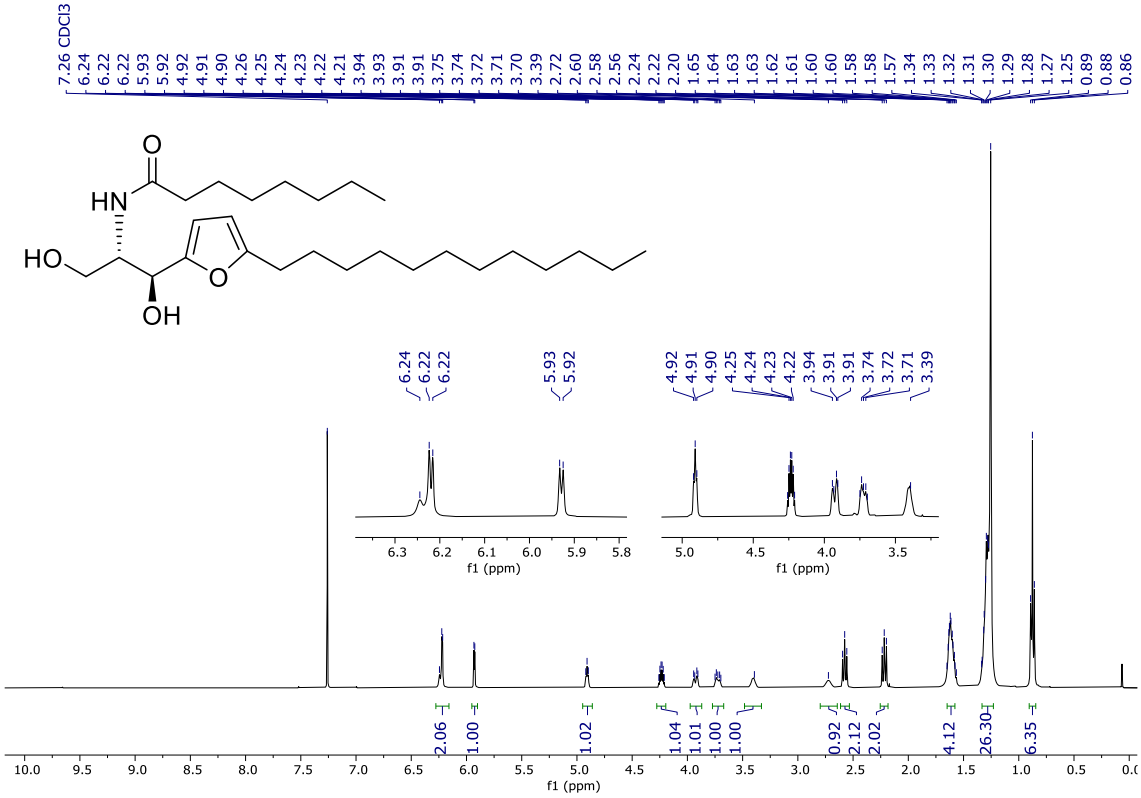

^{1}H NMR (400 MHz, $CDCl_3$) of **3b**.

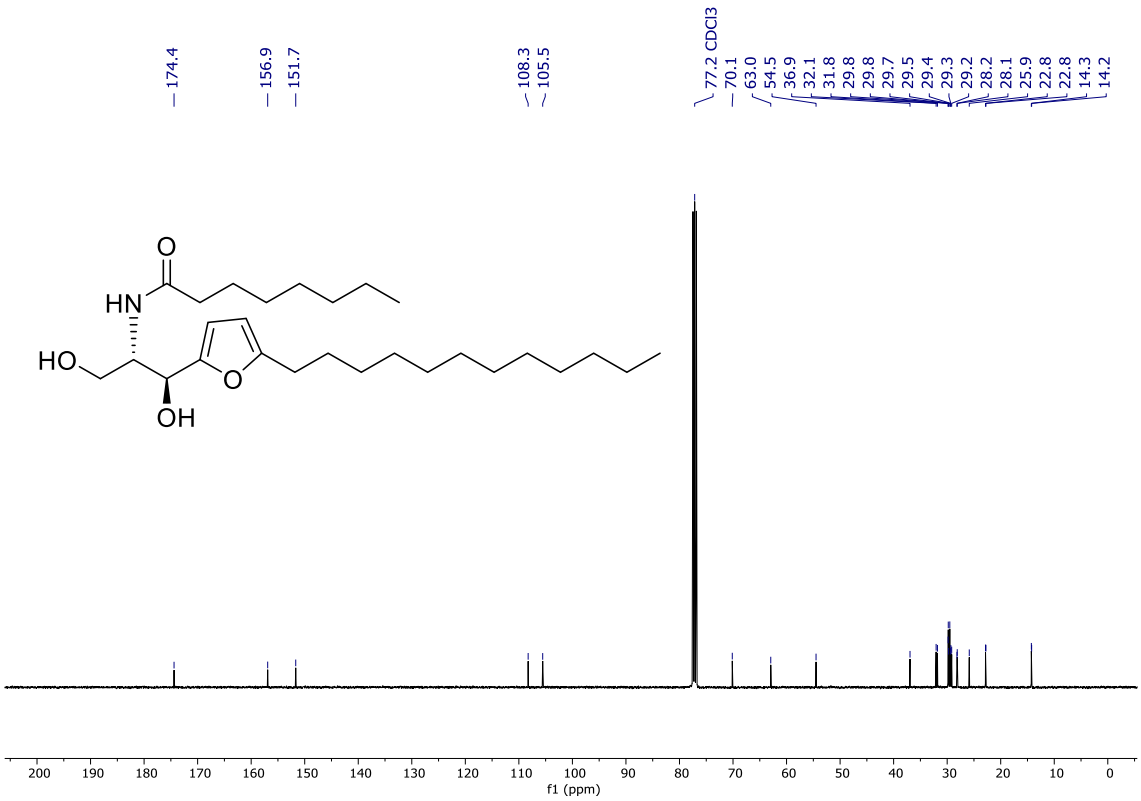

^{13}C NMR (100.6 MHz, $CDCl_3$) of **3b**.

N-((1*S*,2*S*)-1-(5-dodecylfuran-2-yl)-1,3-dihydroxypropan-2-yl)decanamide (3c)

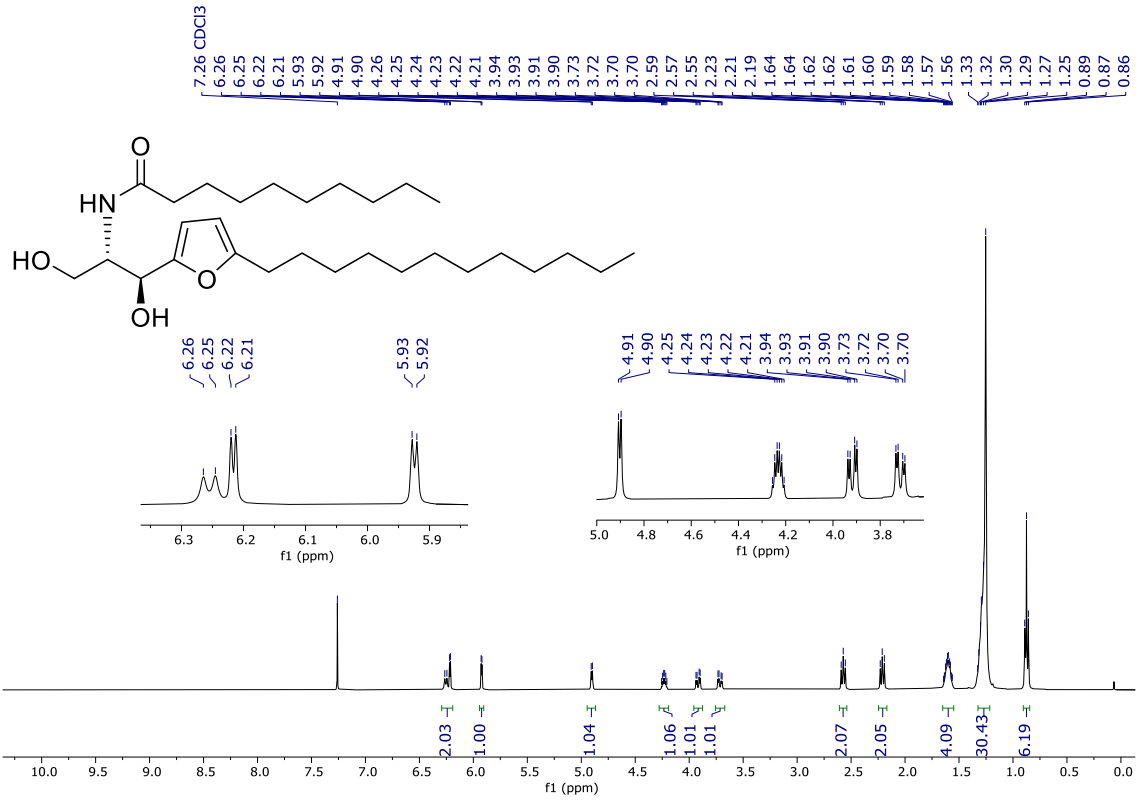

^{1}H NMR (400 MHz, $CDCl_3$) of **3c**.

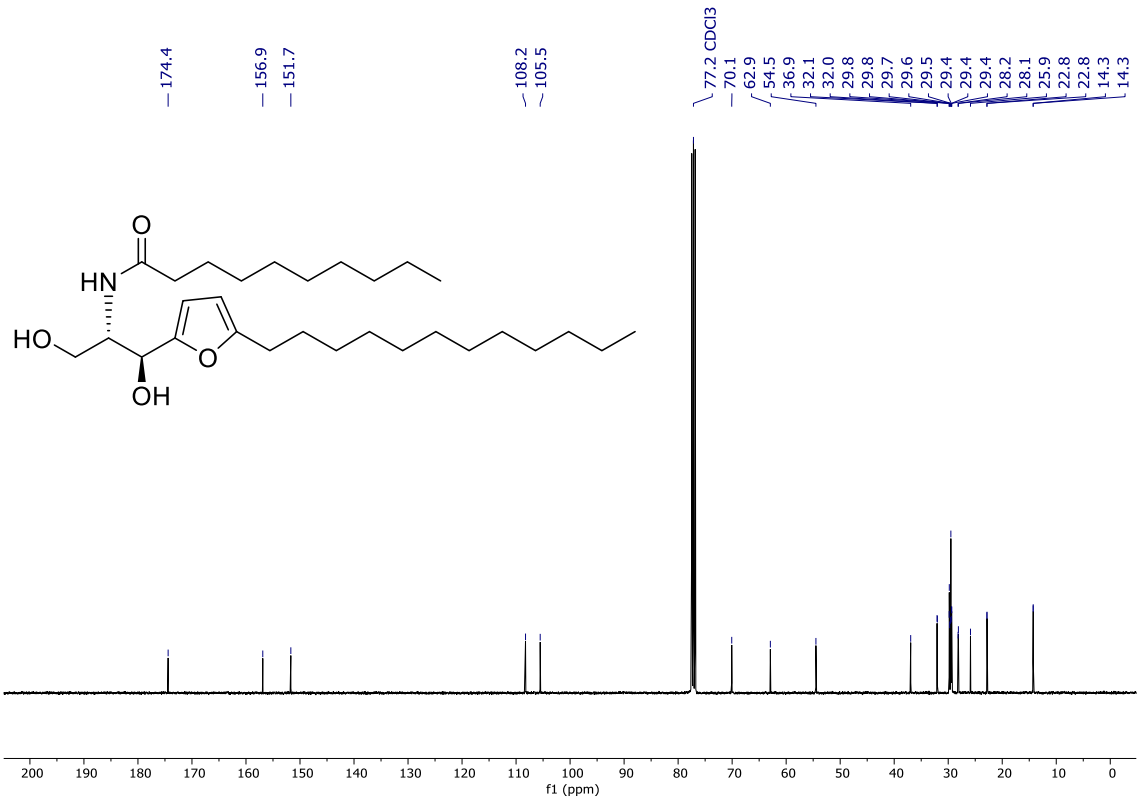

^{13}C NMR (100.6 MHz, $CDCl_3$) of **3c**.

2-tridecylcycloprop-2-en-1-one (59)

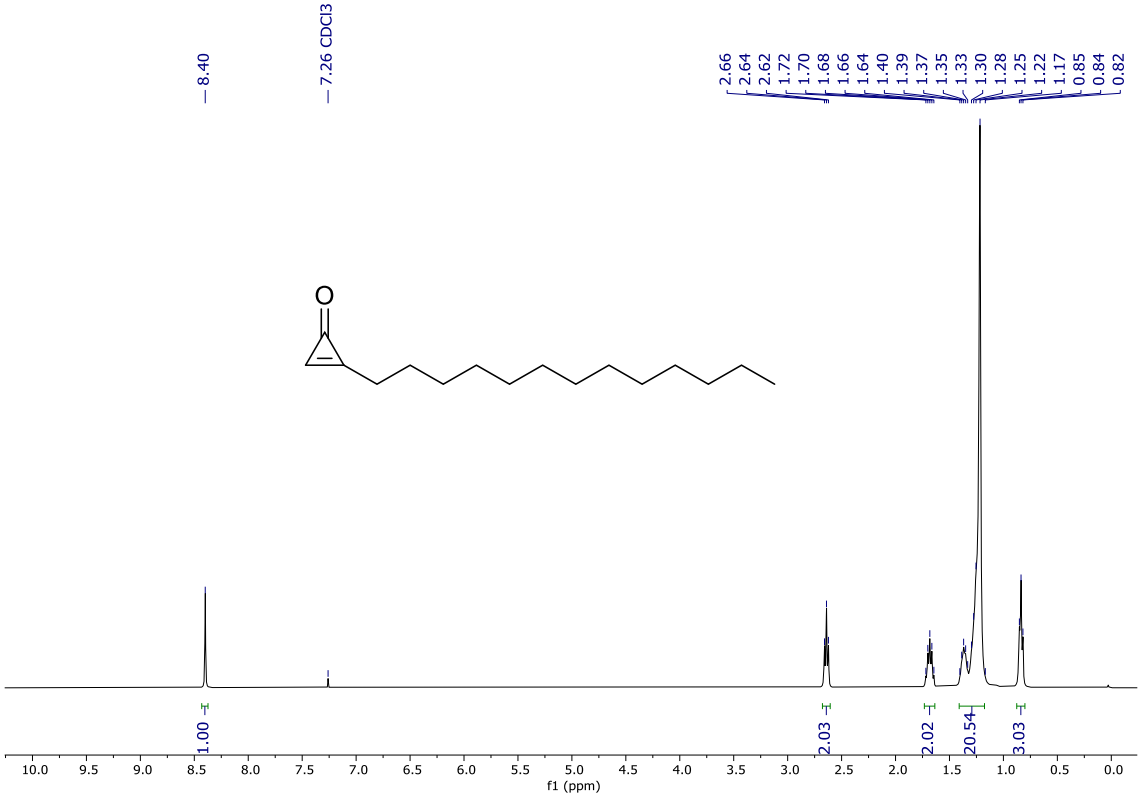

^{1}H NMR (400 MHz, $CDCl_3$) of **59**.

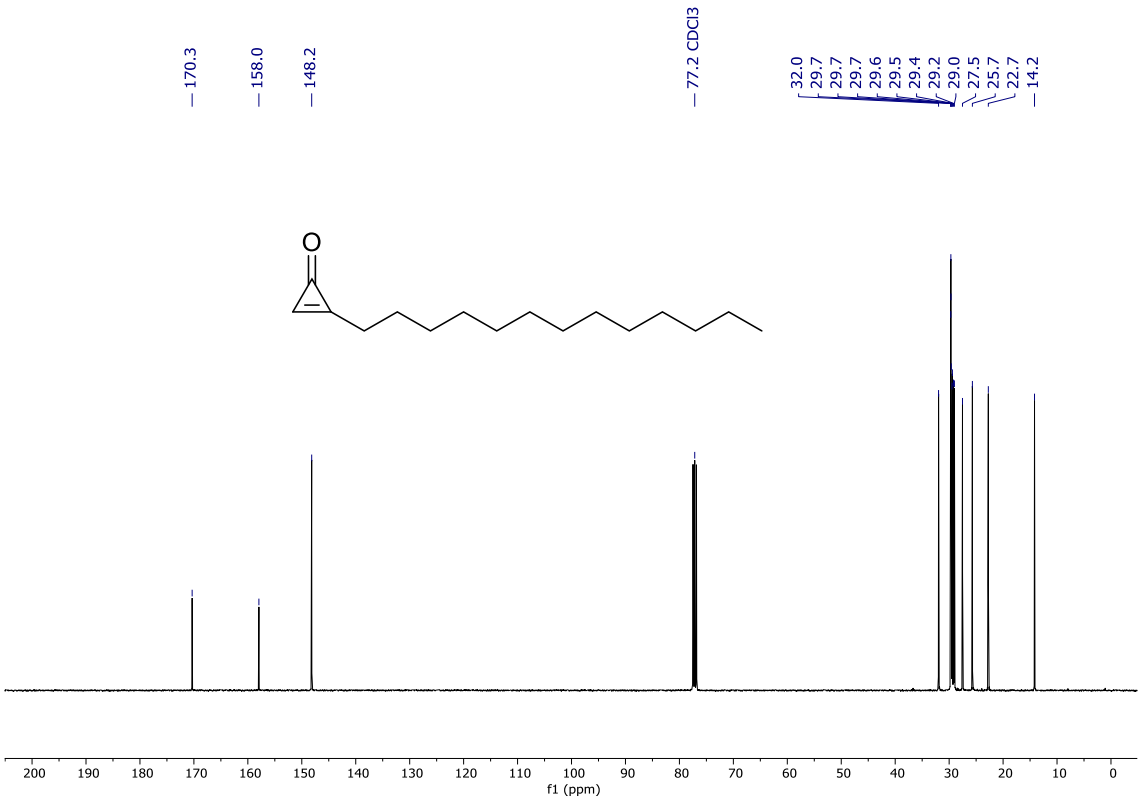

^{13}C NMR (100.6 MHz, $CDCl_3$) of **59**.

6,6-dimethyl-1-tridecyl-4,8-dioxaspiro[2.5]oct-1-ene (58)

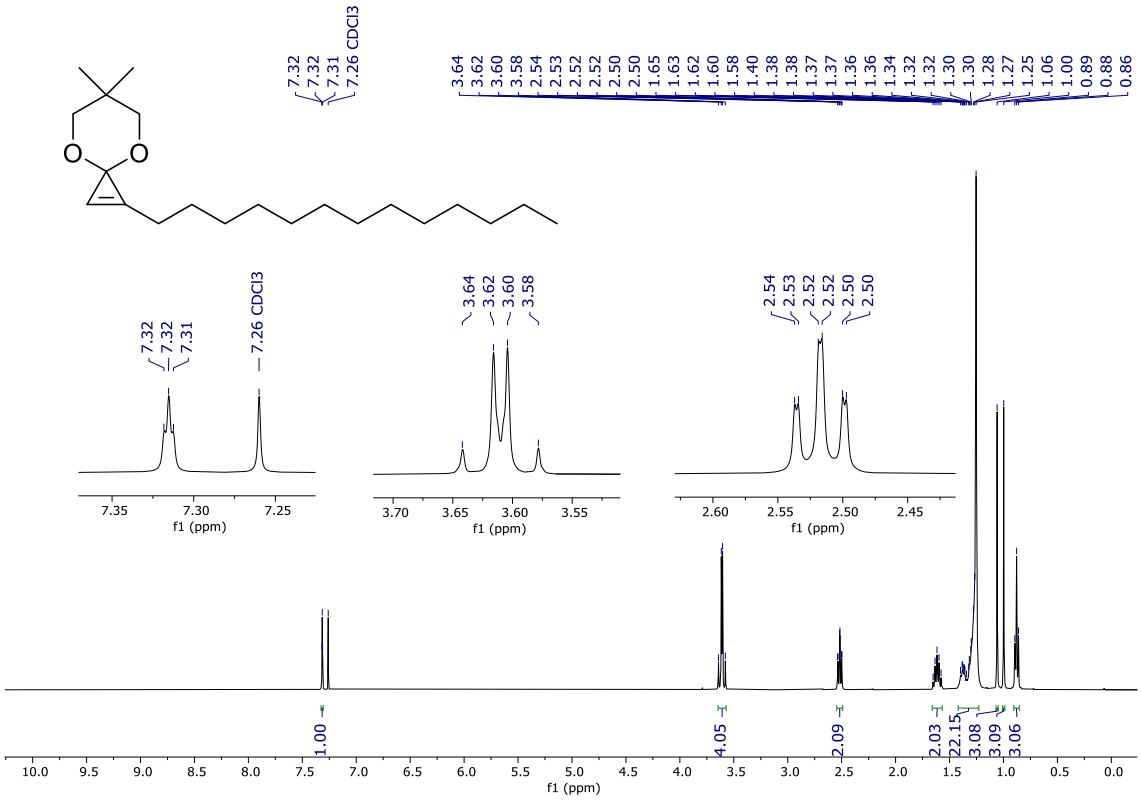

^{1}H NMR (400 MHz, $CDCl_3$) of **58**.

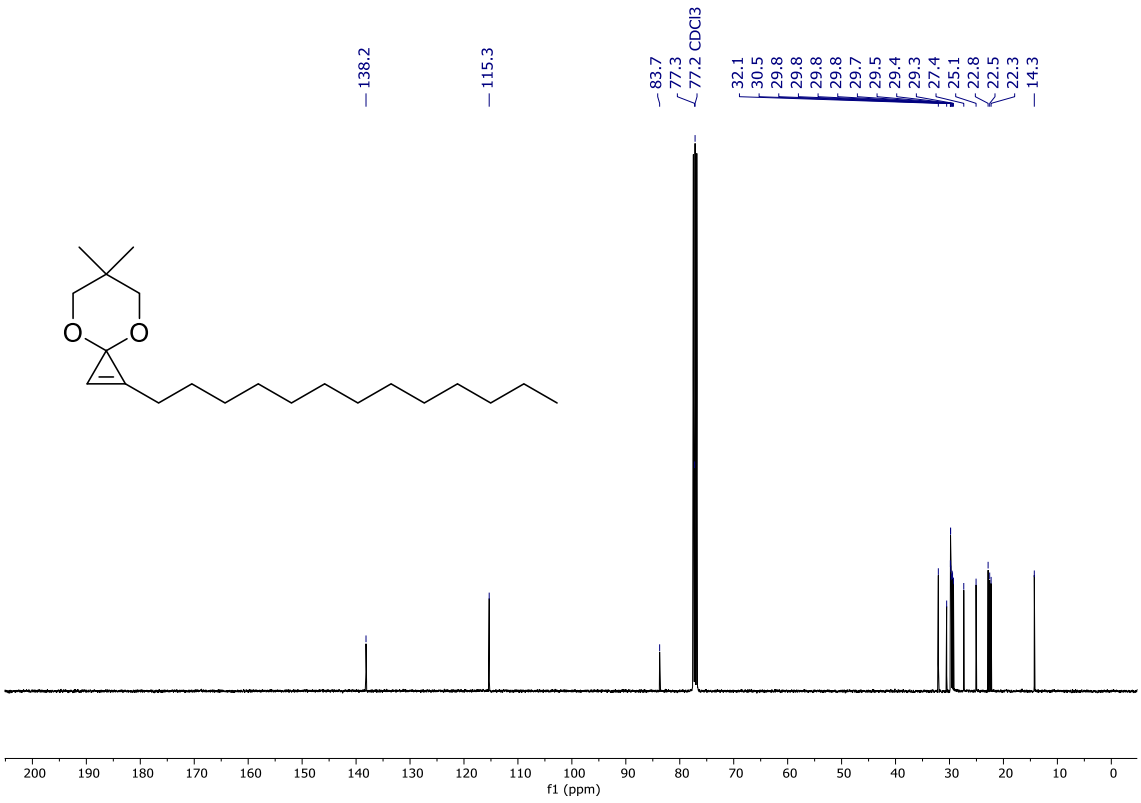

^{13}C NMR (100.6 MHz, $CDCl_3$) of **58**.

tert-butyl (S)-4-((R)-(6,6-dimethyl-2-tridecyl-4,8-dioxaspiro[2.5]oct-1-en-1-yl)(hydroxy)methyl)-2,2-dimethyloxazolidine-3-carboxylate (57)

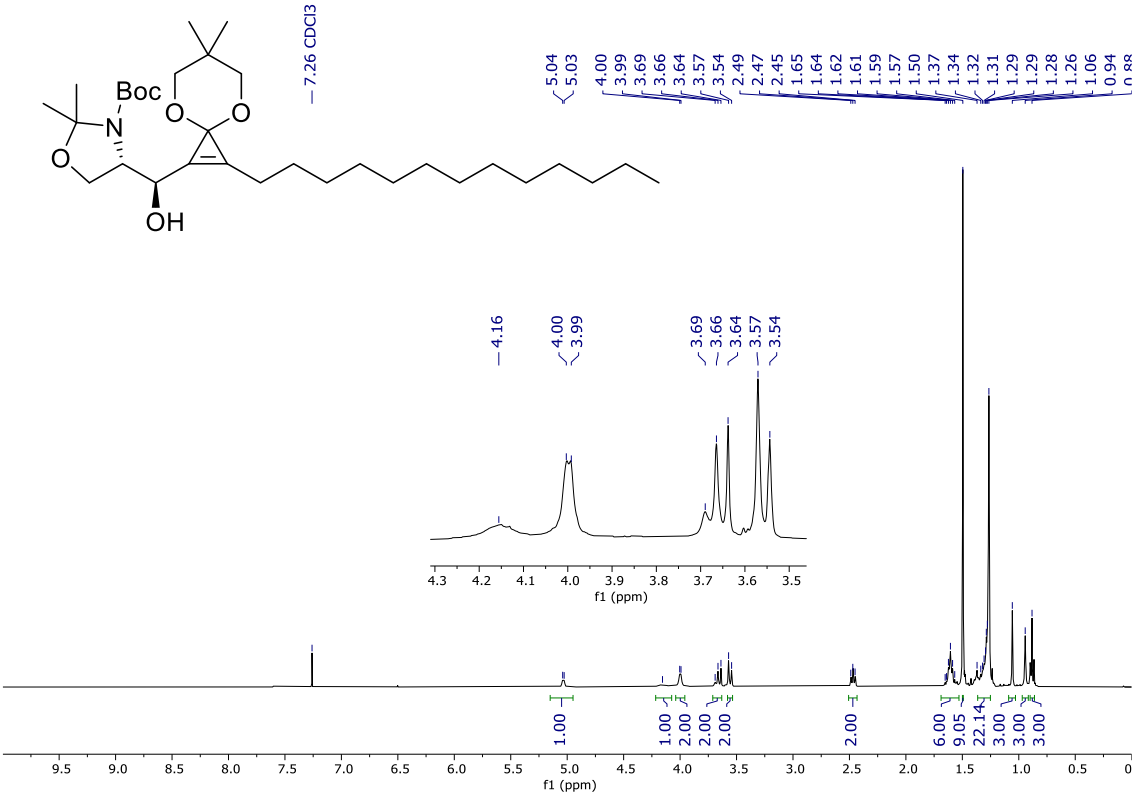

^{1}H NMR (400 MHz, $CDCl_3$) of **57**.

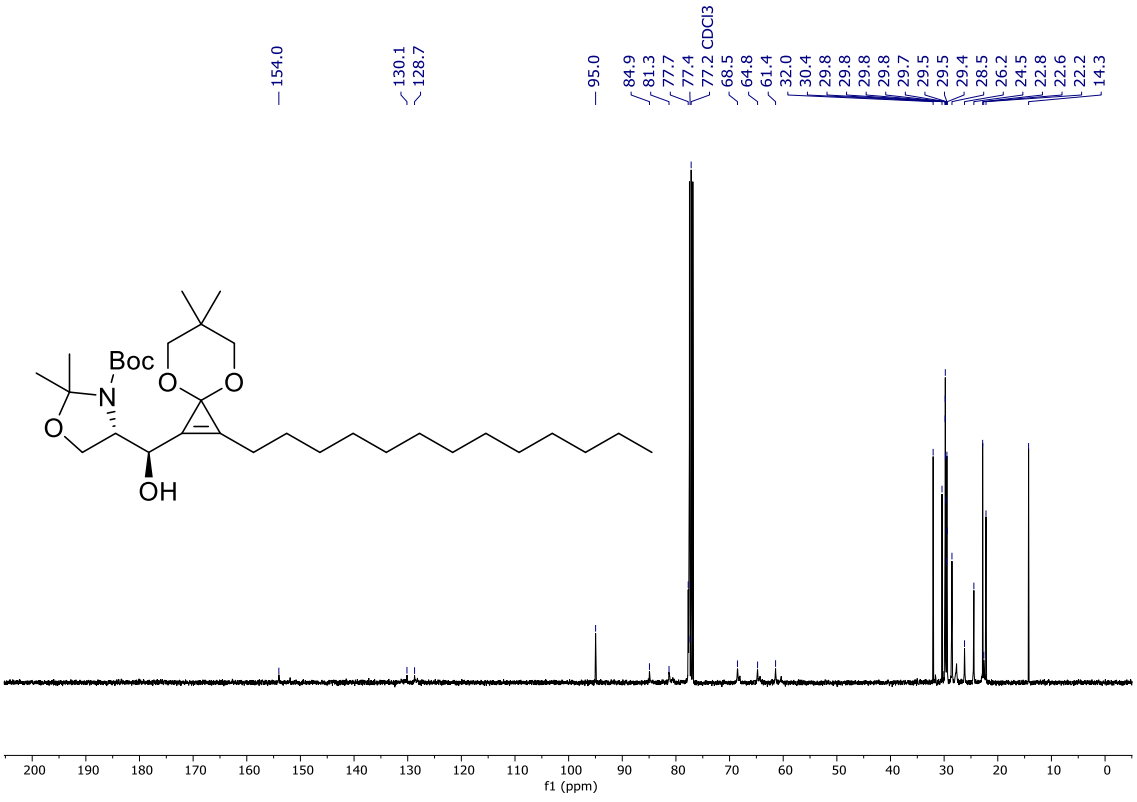

^{13}C NMR (100.6 MHz, $CDCl_3$) of **57**.

2-((1R,2S)-2-amino-1,3-dihydroxypropyl)-3-tridecylcycloprop-2-en-1-one (56)

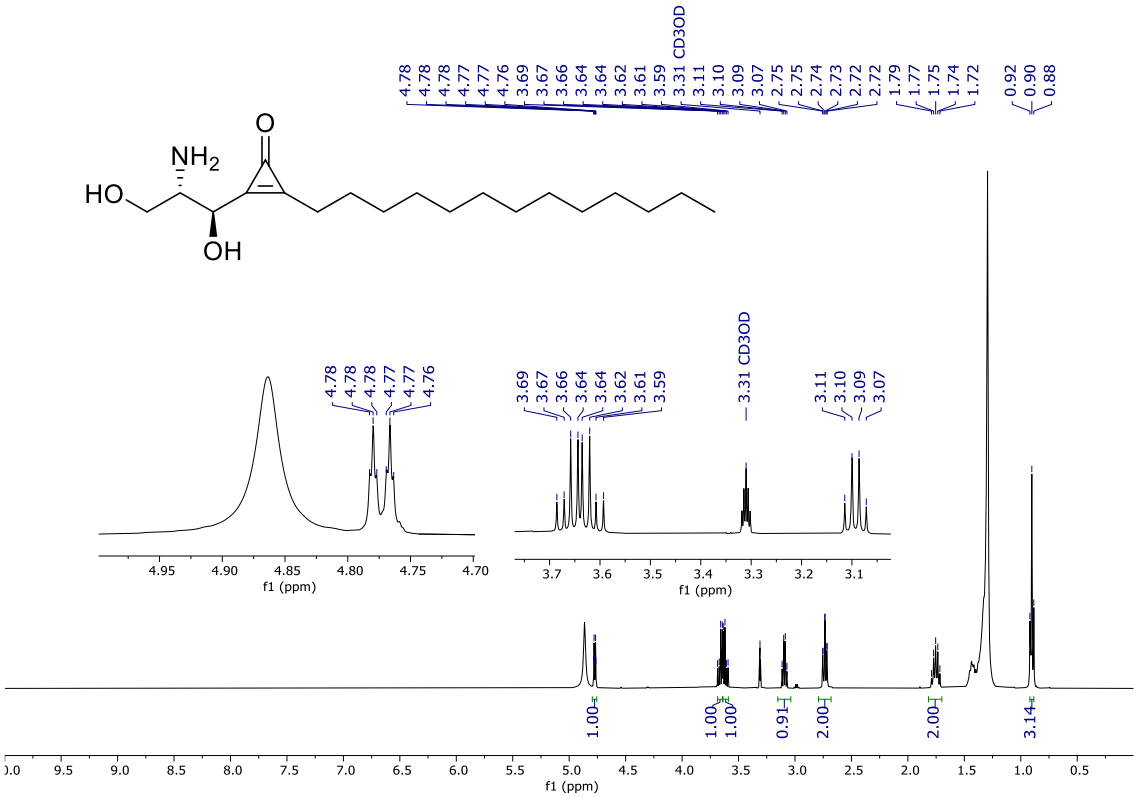

^{1}H NMR (400 MHz, CD_3OD) of **56**.

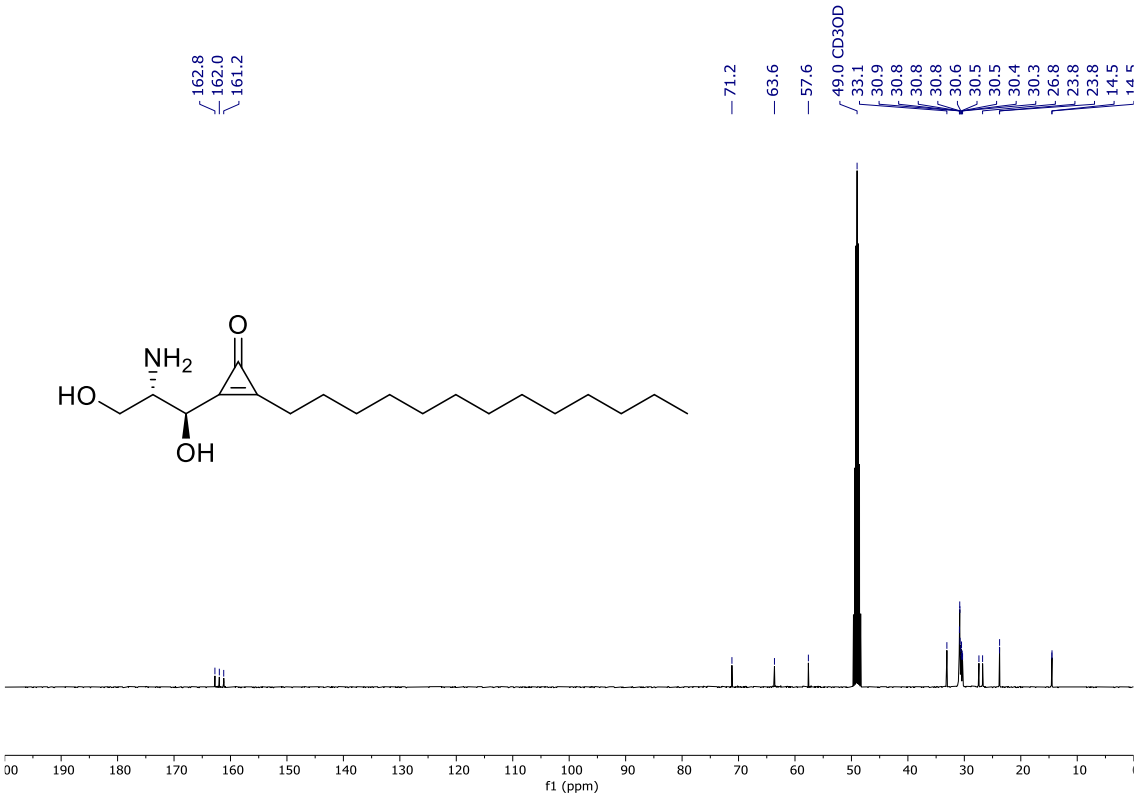

^{13}C NMR (100.6 MHz, $CDCl_3$) of **56**.

N-((1*R*,2*S*)-1,3-dihydroxy-1-(3-oxo-2-tridecylcycloprop-1-en-1-yl)propan-2-yl)hexanamide (45a)

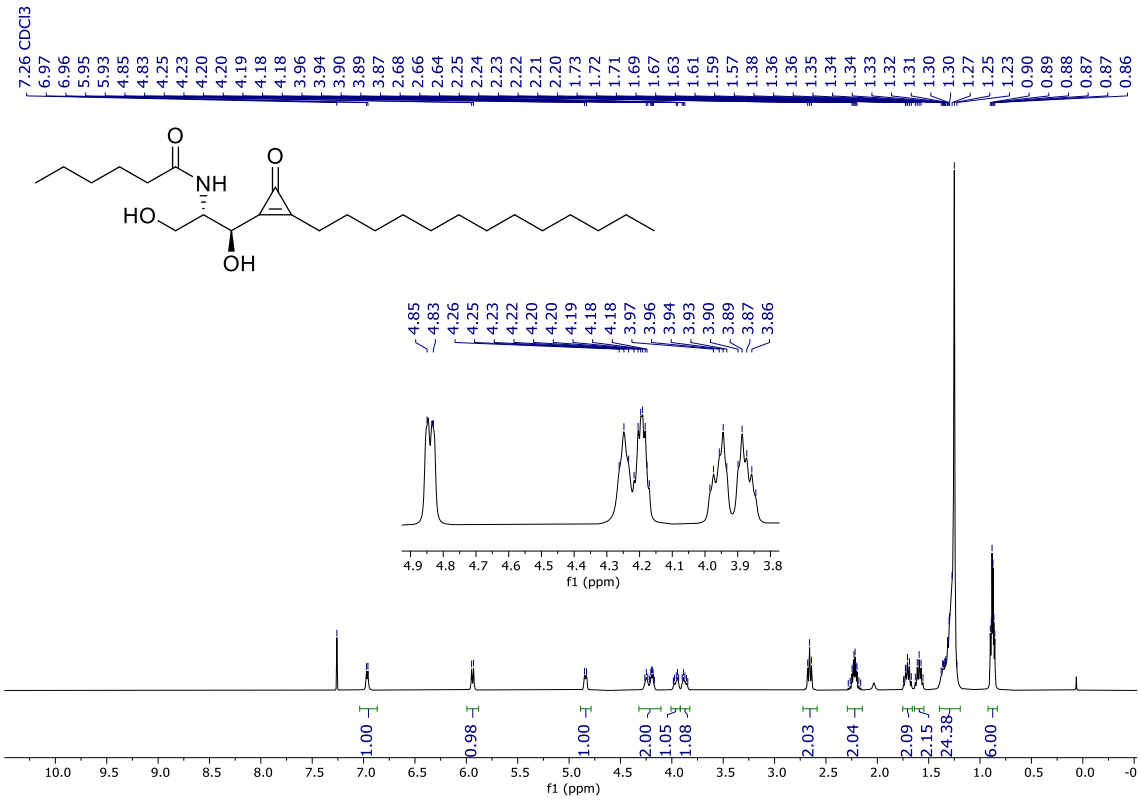

^{1}H NMR (400 MHz, $CDCl_3$) of **45a**.

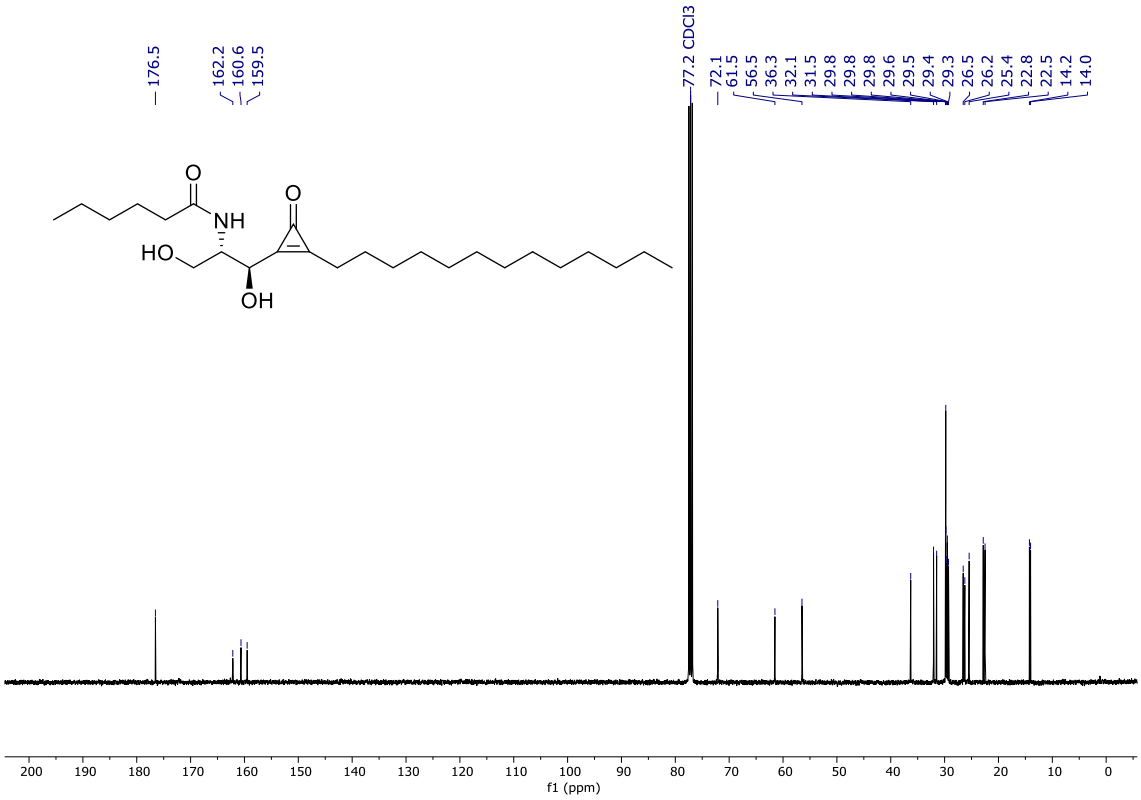

^{13}C NMR (100.6 MHz, $CDCl_3$) of **45a**.

N-((1*R*,2*S*)-1,3-dihydroxy-1-(3-oxo-2-tridecylcycloprop-1-en-1-yl)propan-2-yl)octanamide (PR280)

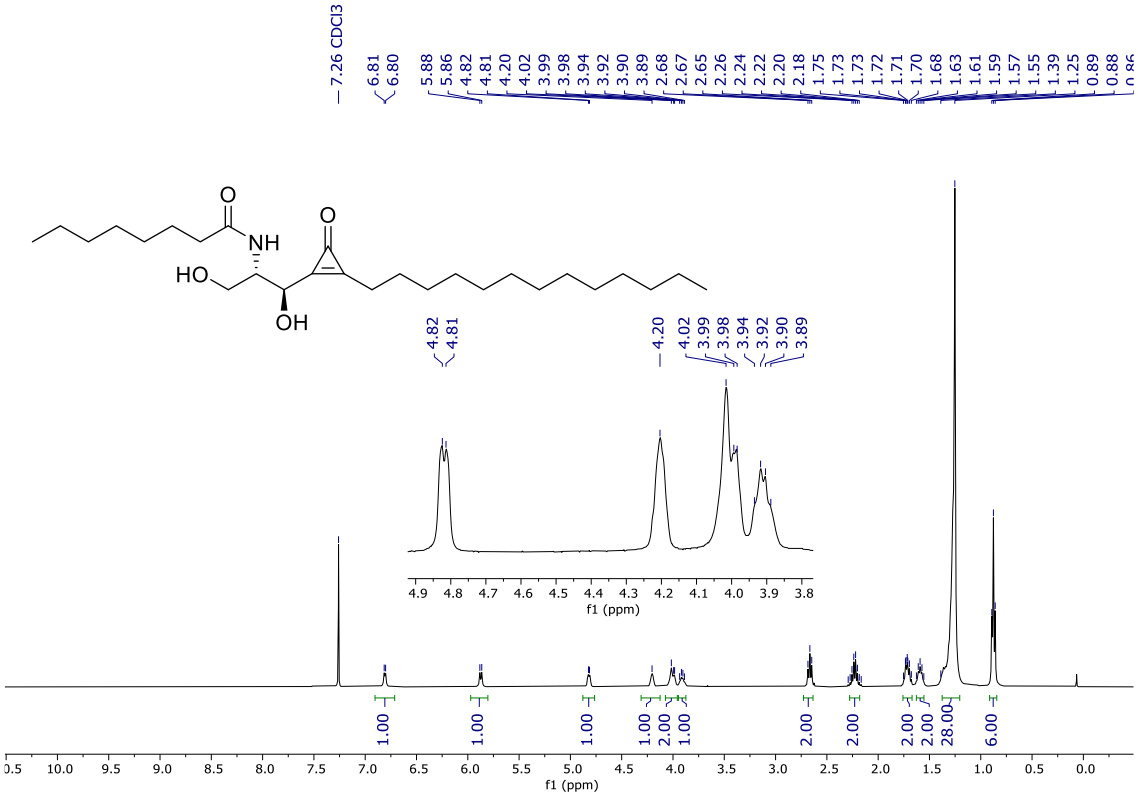

^{1}H NMR (400 MHz, $CDCl_3$) of **PR280**.

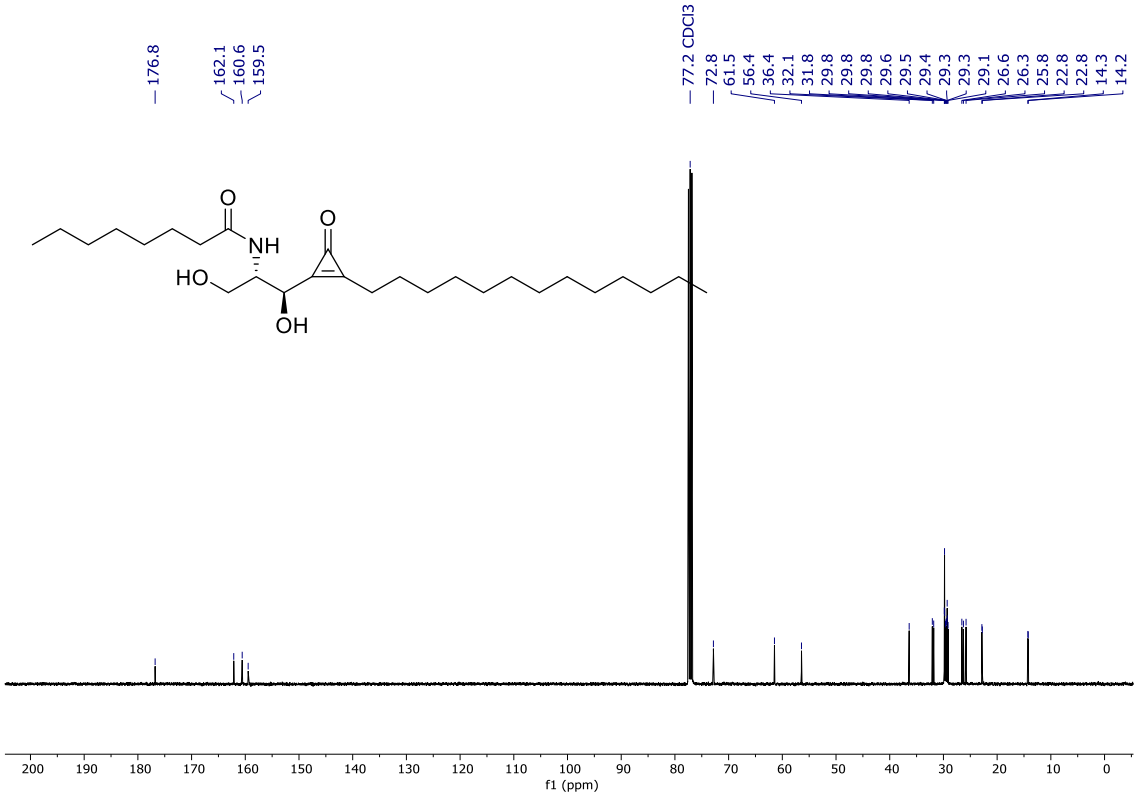

^{13}C NMR (100.6 MHz, $CDCl_3$) of **PR280**.

***N*-((1*R*,2*S*)-1,3-dihydroxy-1-(3-oxo-2-tridecylcycloprop-1-en-1-yl)propan-2-yl)decanamide (45c)**.

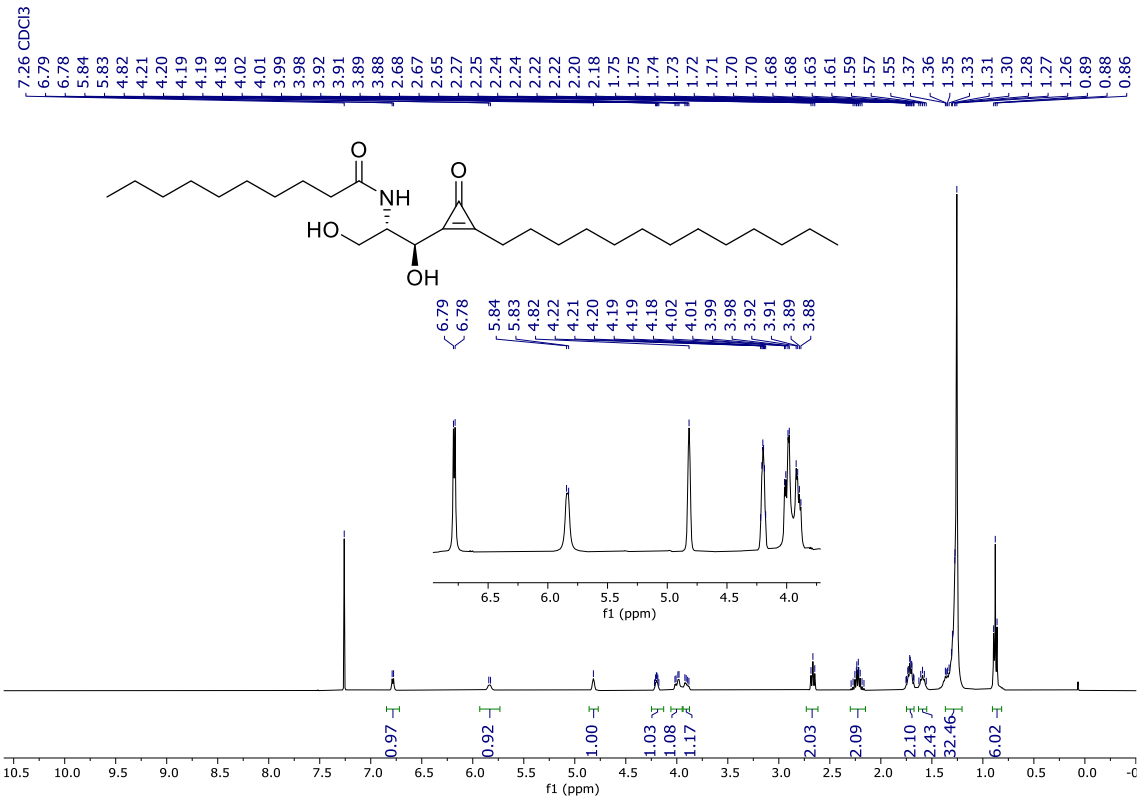

^{1}H NMR (400 MHz, $CDCl_3$) of **45c**.

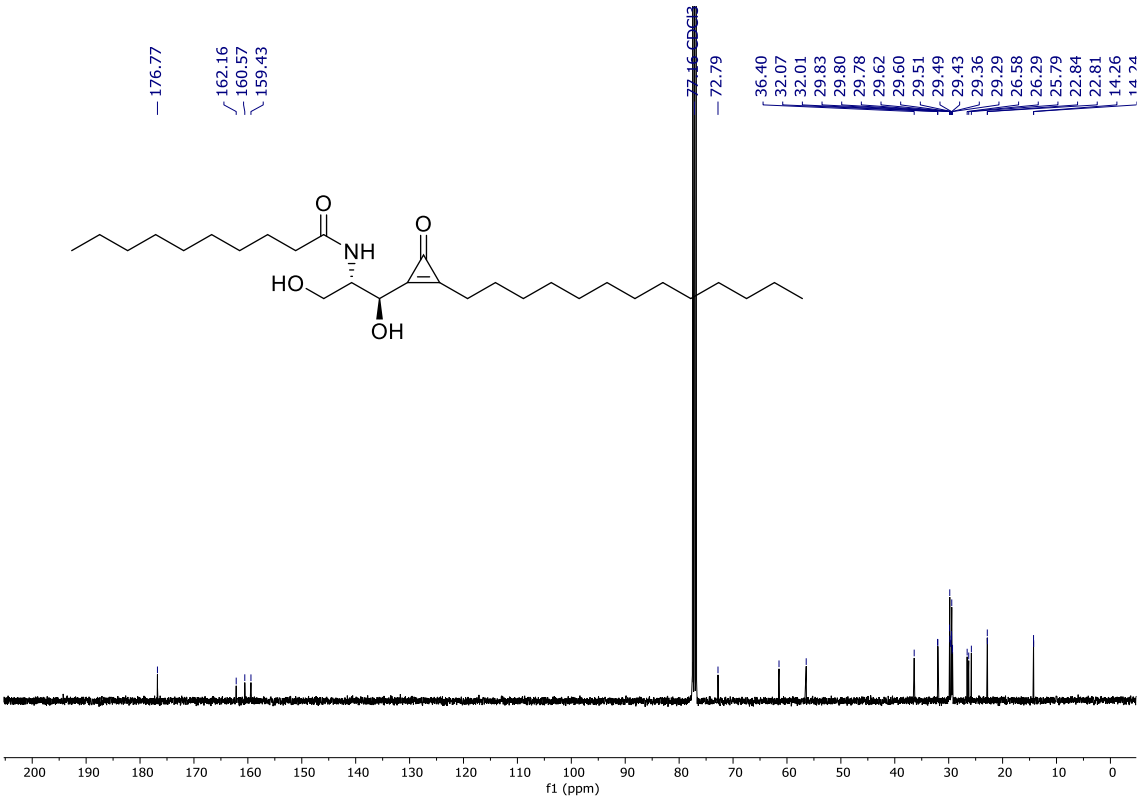

^{13}C NMR (100.6 MHz, CDCl3) of **45c**.

N-((1*S*,2*S*)-1,3-dihydroxy-1-(3-oxo-4-tridecyl-3*H*-1,2-dithiol-5-yl)propan-2-yl)octanamide (124)

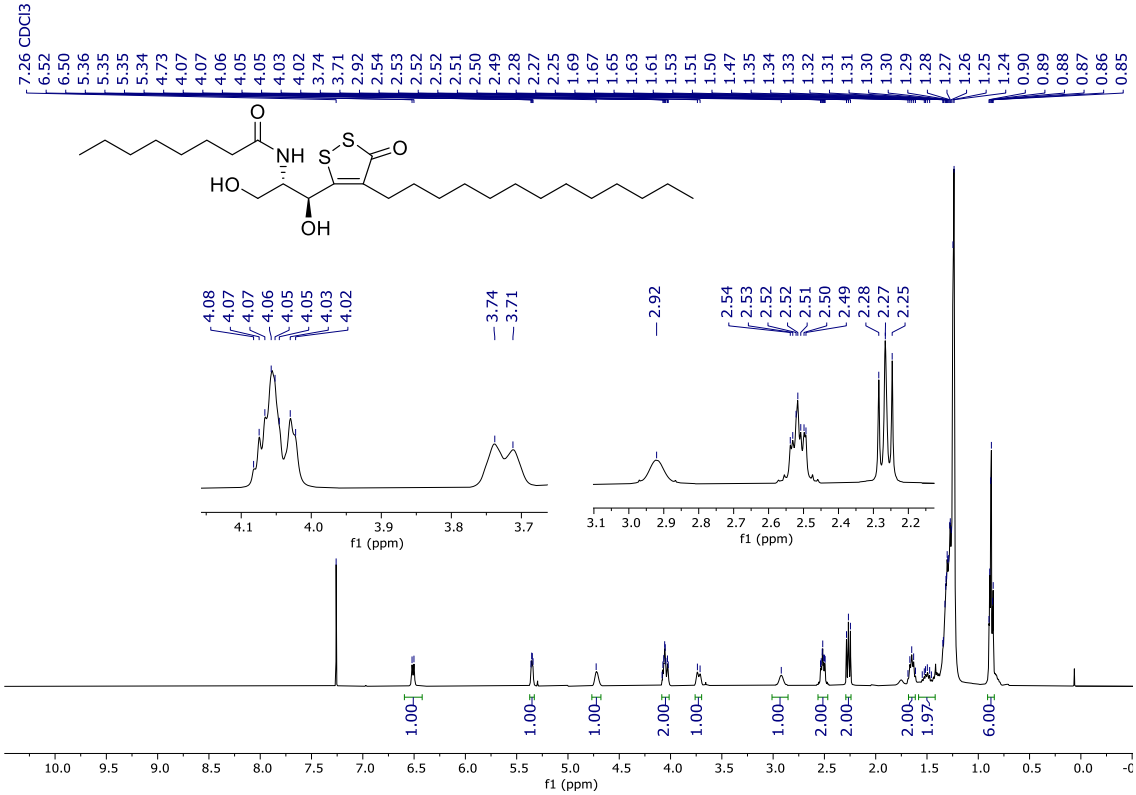

^{1}H NMR (400 MHz, $CDCl_3$) of **124**

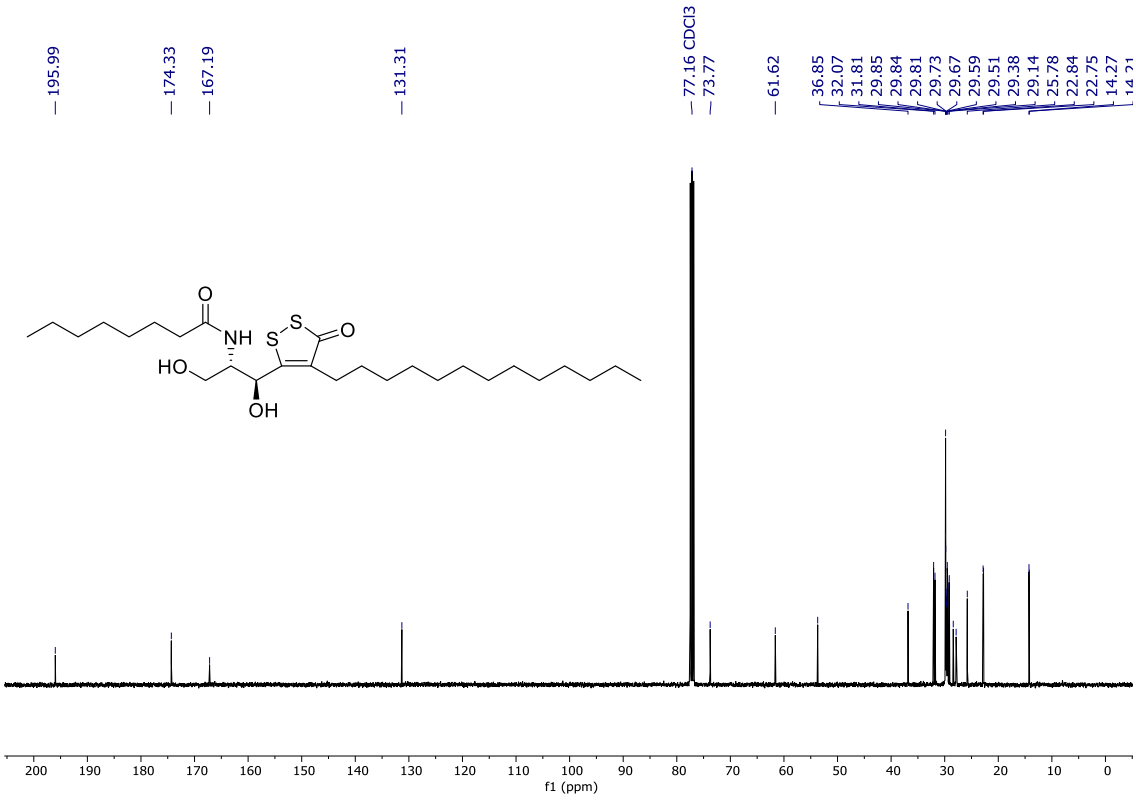

^{13}C NMR (100.6 MHz, CDCl3) of **124**

Crystal data and structure refinement

N-((1*S*,2*S*)-1,3-dihydroxy-1-(1-tridecyl-1H-1,2,3-triazol-5-yl)propan-2-yl)decanamide (2c)

CCDC	2252494	
Empirical formula	C28 H56 N4 O4	
Formula weight	512.76	
Temperature	100(2)K	
Wavelength	1.54178 Å	
Crystal system	orthorhombic	
Space group	P 21 21 21	
Unit cell dimensions	a = 4.7196(4)Å	a= 90°.
	b = 15.7304(18)Å	b = 90°.
	c = 41.331(4)Å	g = 90°.
Volume	3068.4(5) $Å^3$	
Z	4	
Density (calculated)	1.110 Mg/m^3	
Absorption coefficient	0.582 mm^{-1}	
F(000)	1136	
Crystal size	0.300 x 0.020 x 0.010 mm^3	
Theta range for data collection	2.138 to 67.852°.	
Index ranges	-2<=h<=5,-14<=k<=18,-48<=l<=47	
Reflections collected	15457	
Independent reflections	5021[R(int) = 0.0301]	
Completeness to theta =67.852°	94.7%	
Absorption correction	Multi-scan	
Max. and min. transmission	0.75 and 0.55	
Refinement method	Full-matrix least-squares on F^2	
Data / restraints / parameters	5021/ 0/ 336	
Goodness-of-fit on F^2	1.139	
Final R indices [I>2sigma(I)]	R1 = 0.0629, wR2 = 0.1626	
R indices (all data)	R1 = 0.0679, wR2 = 0.1662	
Flack parameter	x =0.00(13)	
Largest diff. peak and hole	0.252 and -0.280 e.$Å^{-3}$	

_N_-((1_R_,2_S_)-1,3-dihydroxy-1-(3-oxo-2-tridecylcycloprop-1-en-1-yl)propan-2-yl)octanamide (PR280)

CCDC	2252495	
Empirical formula	C54 H98 N2 O8	
Formula weight	903.34	
Temperature	100(2)K	
Wavelength	1.54178 Å	
Crystal system	orthorhombic	
Space group	P 21 21 21	
Unit cell dimensions	a = 4.8812(5)Å	a= 90°.
	b = 9.7966(8)Å	b = 90°.
	c = 55.962(4)Å	g = 90°.
Volume	2676.1(4) $Å^3$	
Z	2	
Density (calculated)	1.121 Mg/m^3	
Absorption coefficient	0.575 mm^{-1}	
F(000)	1000	
Crystal size	0.500 x 0.200 x 0.200 mm^3	
Theta range for data collection	3.159 to 68.141°.	
Index ranges	-2<=h<=5,-11<=k<=11,-65<=l<=65	
Reflections collected	18986	
Independent reflections	4588[R(int) = 0.0604]	
Completeness to theta =68.141°	95.6%	
Absorption correction	Multi-scan	
Max. and min. transmission	0.75 and 0.45	
Refinement method	Full-matrix least-squares on F^2	
Data / restraints / parameters	4588/ 0/ 293	
Goodness-of-fit on F^2	1.051	
Final R indices [I>2sigma(I)]	R1 = 0.1077, wR2 = 0.2997	
R indices (all data)	R1 = 0.1111, wR2 = 0.3018	
Flack parameter	x =-0.13(14)	
Largest diff. peak and hole	0.569 and -0.292 $e.Å^{-3}$	

UNIVERSITAT ROVIRA I VIRGILI
TARGETING DES1: SYNTHESES OF CERAMIDE ANALOGUES WITH A RIGID SCAFFOLD, INHIBITORY ASSAYS, AND AF2-ASSISTED STRUCTURAL INSIGHTS REVEAL PR280 AS A POTENT INHIBITOR
Pablo Rivero Prieto

UNIVERSITAT ROVIRA I VIRGILI
TARGETING DES1: SYNTHESES OF CERAMIDE ANALOGUES WITH A RIGID SCAFFOLD, INHIBITORY ASSAYS, AND AF2-ASSISTED STRUCTURAL INSIGHTS REVEAL PR280 AS A POTENT INHIBITOR
Pablo Rivero Prieto

UNIVERSITAT ROVIRA I VIRGILI
TARGETING DES1: SYNTHESES OF CERAMIDE ANALOGUES WITH A RIGID SCAFFOLD, INHIBITORY ASSAYS, AND AF2-ASSISTED STRUCTURAL INSIGHTS REVEAL PR280 AS A POTENT INHIBITOR
Pablo Rivero Prieto

UNIVERSITAT
ROVIRA i VIRGILI